Environment and Natural Resources Journal

AIMS AND SCOPE

The Environment and Natural Resources Journal is a peer-reviewed journal, which provides insight scientific knowledge into the diverse dimensions of integrated environmental and natural resource management. The journal aims to provide a platform for exchange and distribution of the knowledge and cutting-edge research in the fields of environmental science and natural resource management to academicians, scientists and researchers. The journal accepts a varied array of manuscripts on all aspects of environmental science and natural resource management. The journal scope covers the integration of multidisciplinary sciences for prevention, control, treatment, environmental clean-up and restoration. The study of the existing or emerging problems of environment and natural resources in the region of Southeast Asia and the creation of novel knowledge and/or recommendations of mitigation measures for sustainable development policies are emphasized.

The subject areas are diverse, but specific topics of interest include:
- Biodiversity
- Climate change
- Detection and monitoring of polluted sources e.g., industry, mining
- Disaster e.g., forest fire, flooding, earthquake, tsunami, or tidal wave
- Ecological/Environmental modelling
- Emerging contaminants/hazardous wastes investigation and remediation
- Environmental dynamics e.g., coastal erosion, sea level rise
- Environmental assessment tools, policy and management e.g., GIS, remote sensing, Environmental Management System (EMS)
- Environmental pollution and other novel solutions to pollution
- Remediation technology of contaminated environments
- Transboundary pollution
- Waste and wastewater treatments and disposal technology

Schedule

Environment and Natural Resources Journal (EnNRJ) is published 6 issues per year in January-February, March-April, May-June, July-August, September-October, and November-December.

Publication Fees

There is no cost of the article-processing and publication.

Ethics in publishing

EnNRJ follows closely a set of guidelines and recommendations published by Committee on Publication Ethics (COPE).

CONTENT

Minimum Requirement to Improve Quality before Discharging from Hybrid Red Tilapia Intensive Cage-Culture in Earthen Ponds to the Environment

Wara Taparhudee[1], Jesada Is-haak[2], and Roongparit Jongjaraunsuk[1*]

[1]*Department of Aquaculture, Faculty of Fisheries, Kasetsart University, Bangkok 10900, Thailand*
[2]*Department of Fisheries Science, Faculty of Agricultural Technology and Agro-Industry, Rajamangala University of Technology Suvarnabhumi, Ayutthaya Campus, Ayutthaya 13000, Thailand*

ARTICLE INFO

* Corresponding author:
E-mail: roongparit.jo@ku.th

ABSTRACT

This study determined a practical method to reduce environmental pollution by wastewater from fish ponds. Water quality in three hybrid red tilapia ponds (0.24 ha) was examined before and during harvest at five water depths of 10, 20, 50, 100, and 150 cm, as well as at the water surface and pond bottom. All water samples were analyzed for BOD, TN, TP, TAN, TS, TSS, and SS, with results compared with the Thailand control standard for freshwater aquaculture effluent. All quality parameters of the seven water samples showed statistical significance (p<0.05) that increased with water depth. Degradation was highest in the bottom 50 cm of the fish pond. Limiting drainage to a depth of 50 cm was achieved by tilting the drainage pipe, and the resulting effluent met all water quality parameter standards. At a water depth of 50 cm, the remaining water was drained using a water pump, and all water quality parameters failed to meet the required standards. When this water was allowed to settle for 24 h, BOD, TN, TP, TAN, and TSS reduced to 21.06%, 2.42%, 11.68%, 5.47%, and 43.36% of full pond values, respectively. Results suggested sedimentation as a practical technique requiring a smaller pond area to reduce environmental pollution.

1. INTRODUCTION

Aquaculture farms release discharge water from fish ponds to 1) improve water quality during the culture period and 2) drain water during harvesting. The main inputs to aquaculture systems are feed and seston. These are transformed to fish biomass or released in the water as feed waste and excreta in the form of suspended organic solids or dissolved nutrients, including nitrogen and phosphorus (Feng et al., 2004; Li et al., 2011), and are often discharged without treatment (Li et al., 2011). Dissolved inorganic nutrients such as ammonia, urea and phosphate are readily taken up by phytoplankton and macroalgae to stimulate their growth (Troell et al., 2003; Feng et al., 2004; Newell, 2004), leading to hypoxia and harmful algal blooms (Alonso-Rodríguez et al., 2003; Troell et al., 2003; Feng et al., 2004; Cao et al., 2007; Mohamed and Al-Shehri, 2012). In many countries, aquaculture farm effluents cause major ecological impacts on the environment through habitat destruction and water pollution (Teichert-Coddington, 1995; Coldebella et al., 2018; Sampantamit et al., 2020).

In 2007, the Thailand Pollution Control Department enacted a wastewater control standard to reduce water pollution from aquaculture ponds impacting the environment. This standard suggested a requirement for sedimentation ponds of the same size as the cultivation ponds; however, farmers considered this to be a burden on production. Reducing the amount of discharge wastewater requiring treatment would reduce sedimentation pond size and lessen the burden on farmers. This research assessed the minimum water level sedimentation requirement to improve wastewater quality before discharge from intensive cage-culture earthen ponds to the environment.

Two ways to reduce the impact of wastewater on the environment include reducing the amount of discharge wastewater or improving the discharge water quality. Intensive cultivation of hybrid red tilapia requires a large quantity of feed, leading to high accumulation of organic matter in ponds from left over feed and fish excretion. Cole and Boyd (1985) reported that excessive nutrients in fish ponds result in poor water quality and slow growth rate. Intensive culture ponds require frequent water changes. Therefore, improving discharge water quality is a more practical alternative to reducing discharge water quantity.

A wetlands technique is widely used for improving wastewater quality. Plants in wetlands absorb soluble nutrients and filter solids, thereby improving polluted wastewater quality (Turcios and Papenbrock, 2014). This technique is very effective but limitations include a large land area for water treatment of 0.7-2.7 times the size of the culture ponds (Schwartz and Boyd, 1995). Shpigel et al. (2013) applied 10,000 m^2 of wetland with *Salicornia* spp. for the removal of nitrogen and total suspended solids produced from 900 kg of 45% crude protein fish feed (11 m^2/kg of feed) during one year. However, biotreatment investment costs are high (Gutierrez-Wing and Malone, 2006). Solid precipitation is another technique commonly used in aquaculture farms, with wastewater drained to sedimentation ponds, dried under the sun and removed as fertilizer in solid form. This method requires a smaller area than the wetland technique but is more labor-intensive.

Recently, reports have shown that the nutrients and solids in aquaculture ponds are highly concentrated in the last 5-20% of the discharge volume (Schwartz and Boyd, 1994; Teichert-Coddington et al., 1995; Teichert-Coddington et al., 1999; Coldebella et al., 2018). Thus, the quality of the upper water pond layers may qualify for discharge into the environment, and the common process of treatment of all drained water after harvest may not be necessary. Precipitation treatment performed only on the lower pond layers would reduce sedimentation pond size and treatment costs, while increasing land efficiency. Previous research investigated channel catfish and shrimp in the USA and Honduras under lower temperatures and humidity values than experienced in Thailand. A tropical environment stimulates biological activity and increases the concentration of sewage; therefore, volumes of discharge water needing treatment will be

different. If farmers know the level of sewage in the pond that does not meet the water quality standard, then this will reduce the volume of water requiring treatment. Hybrid red tilapia in Thailand are raised in highly intensive systems that create large amounts of nutrients and wastewater.

This research studied the quality of water at different depths in hybrid red tilapia ponds before and during harvesting, and compared water quality parameters at each depth to the Thailand control standard of wastewater from freshwater aquaculture farms. The Thai standard requires biochemical oxygen demand (BOD) <20 mg/L, total nitrogen (TN) <4.0 mg/L, total phosphorus (TP) <0.5 mg/L, total ammonia nitrogen (TAN) <1.1 mg/L, and total suspended solids (TSS) <80.0 mg/L (TECAC, 2008). The first drained water level that did not reach all the standard parameters was considered as the minimum water level required to improve water quality before discharge into the environment.

2. METHODOLOGY
2.1 Ponds cultivation and water management
The commercial hybrid red tilapia culture ponds used in this study were located at Jittiporn Farm, Klong 13, Pathum Thani Province in the central region of Thailand. Three rectangular ponds (0.24 ha, 150 cm deep and 1:1 inner dike slope) were tested for the experiment. In each pond, fish were raised in six 7.5×15×1.2 m^3 cages. The fish (weight 100 g) were stocked at 1,200 fish per cage (9 fish/m^3) and fed at 2-3% of their body weight per day with 30% protein pellet feed divided into three meals at 07:00, 11:30, and 17:00 h. Two 3-h.p. aerators were operated to maintain water circulation. These were turned off during each feeding time for about 45 min. The fish were raised for four months to reach a harvestable size of 800 to 1,000 g. Fish harvesting was performed by lifting the cage out of the water. The out-cage fish were seined when the water was drained to a depth of 50 cm.

Water exchange at a rate of 10 to 20% of total pond water volume began three weeks after stocking by adding fresh water and draining the wastewater through a ten-inch diameter PVC drain pipe installed 50 cm above the bottom of the pond (Figure 1). The pond was drained by lowering this pipe to reduce the water level to 50 cm depth. Wastewater was pumped out by a twelve-inch diameter pump installed at the bottom of the pond.

Figure 1. PVC pipe installed

Most of the wastewater and sewage from the pond are discharged during fish harvesting. This creates an environmental problem. Fortunately, the lifting cage harvest method does not disturb the sewage at the bottom of the pond. The upper drained water does not mix with the sewage and may qualify under Thai control standards to allow discharge into the environment. However, this has not yet been scientifically proven. The lower part of the wastewater, with high concentrations of organic matter, becomes disturbed during the seining of the out-cage fish and electrical pumping. Research to determine the required time for the solids to precipitate and the water to qualify for discharge was therefore undertaken, comprising three experiments.

2.2 Sampling and testing

2.2.1 Water quality at different water depths before harvesting

This experiment was conducted on the day of harvesting. After shutting down all the aerators for 30 min and before draining water out of the pond, a technician collected water samples using a 20 cm diameter PVC water sampling pipe. Three water samples were taken at five water depths of 10, 20, 50, 100, and 150 cm and also from the water surface and the pond bottom.

All water samples were analyzed for BOD, TN, TP, TAN, total solids (TS), TSS, and settleable solids (SS) by the methods shown in (Table 1). Water volume in the pond is shown in Table 2 and calculated using equation 1.

$$\text{Water volume (m}^3) = (\tfrac{1}{2} \times (\text{water surface area} + \quad (1)$$
$$\text{pond bottom area, m}^2))$$
$$\times \text{water depth (m)}$$

• *Data analysis*

Water quality parameters from the three experimental ponds were averaged, with water quality data at different water depths analyzed for variance by one-way ANOVA. Comparison of mean differences between treatments was performed using Duncan's New Multiple Range Test at 95% confidence interval ($p<0.05$). Each parameter was averaged, with results reported as standard deviation by SPSS 24.0. Water quality data at different depths were then compared with the Thai standards of wastewater drainage from freshwater aquaculture farms (TECAC, 2008), as shown in Table 1.

Table 1. Water quality analysis methods and Thailand control standards.

Water quality parameter (mg/L)	Analysis method	Thailand standard
BOD	APHA et al. (2005)	<20.0 mg/L
TN	Raveh and Avnimelech (1979)	<4.0 mg/L
TP	Raveh and Avnimelech (1979)	<0.5 mg/L
TAN	APHA et al. (2005)	<1.1 mg/L
TS	APHA et al. (2005)	-
TSS	APHA et al. (2005)	<80.0 mg/L
SS	APHA et al. (2005)	-

2.2.2 Water quality at different water depths during harvesting

This experiment investigated water quality discharge from red tilapia ponds during harvesting using two steps of draining according to pond depth. First, water was drained by lowering the drainage pipe from the surface (150 cm total water depth) until the water depth was 50 cm. The remaining water was then pumped out by a 20 cm diameter water pump. Three water samples were collected at the tip of the drainage pipe or the pump outlet at 0, 50, 100, 130, 140, and 150 cm water depths and at the pond bottom.

Before water quality analysis, the three samples taken at each water depth were mixed and measured using the method shown in Table 1. Data analysis was performed as followed in experiment 1.

2.2.3 Wastewater quality changes after settling for different times

This experiment investigated the precipitation of solids and nutrients inside the ponds. From the results of the second experiment, only water samples that did not pass the control standard were studied for sedimentation. The substandard samples were allowed to stand in test tubes at room temperature, with samples taken at sedimentation times 1, 3, 6, 12, 24, 48, 72, and 96 h. Water quality analysis methods are shown in Table 1. Changes in sedimentation percentages were recorded from 0 h.

Before water quality analysis, the three samples taken at each sedimentation time were mixed and measured using the methods shown in Table 1. Data analysis followed the procedures used in experiment 1.

3. RESULTS
3.1 Water quality at different water depths before harvesting

Results of calculated water volume and analyzed water quality at different water depths before the discharge was drained from the pond are shown in Tables 2 and 3. The total volume of the water in the pond was 3,097 m^3 and 50 cm of the last part of pumped water was 31% of that volume. All water quality parameters of the seven water samples were statistically significant ($p<0.05$) and increased at each water depth.

Table 2. Water volume in the hybrid red tilapia pond at different water depths

Water depth (cm)	Water volume (m^3)	Water volume (%)
150	3,097	100.0
100	2,017	65.1
50	985	31.8
20	389	12.5
10	193	6.2
5	96	3.1

Table 3. Water quality in the hybrid red tilapia pond before drainage

Water depth (cm from surface)	BOD (mg/L)	TN (mg/L)	TP (mg/L)	TAN (mg/L)	TS (mg/L)	TSS (mg/L)	SS (mg/L)
10	7.80±0.29[e]	0.26±0.04[e]	0.156±0.021[d]	0.051±0.013[d]	204.50±6.36[e]	57.50±0.71[d]	0[d]
20	11.40±0.28[d]	0.61±0.02[d]	0.220±0.028[c]	0.085±0.007[d]	225.50±2.12[d]	63.10±0.57[cd]	0.15±0.04[cd]
50	12.60±0.34[c]	0.73±0.08[cd]	0.265±0.007[c]	0.120±0.014[d]	233.00±4.24[d]	67.00±0.85[cd]	0.24±0.07[bcd]
100	15.00±0.28[b]	0.89±0.06[bc]	0.320±0.014[b]	0.245±0.007[c]	246.50±2.12[c]	75.55±1.34[c]	0.36±0.04[bc]
150	15.80±0.28[b]	0.97±0.01[b]	0.360±0.014[b]	0.525±0.064[b]	278.00±2.83[b]	97.90±1.63[b]	0.47±0.04[b]
Pond bottom	28.80±0.57[a]	1.48±0.16[a]	0.425±0.035[a]	2.486±0.014[a]	1309.50±113.40[a]	369.50±12.02[a]	3.38±0.23[a]

Mean±standard deviations with different superscript letters in the same column are significantly different ($p<0.05$).

3.2 Water quality at different water depths during harvesting

All water quality parameters in the three ponds sampled at different water depths during harvest draining were statistically significantly different ($p<0.05$). Results in Table 4 showed that at a depth of 100 cm from the surface BOD, TN, TP, TAN, and TSS contents in the water were lower than the control standard. However, at over 100 cm depth, the BOD, TP, and TSS contents exceeded the control standard, while the TN and TAN contents exceeded the standard at the pond bottom and at depths over 150 cm.

During the harvest period, water quality in the ponds deteriorated with increasing depth. The last 50 cm of water recorded the highest deterioration (31.80% of the final volume of water in the pond), as shown in Table 4. Using the PVC drain pipe to reduce the pond water level did not stir up the sediment at the

pond bottom. When the water depth reduced to 50 cm, the water was drained using the pump head placed on the bottom of the pond. When pumping started, the sediment at the bottom of the pond was disturbed. During this period the remaining fish in the ponds were also harvested by seining.

Table 4. Water quality parameters at different water depths during pond drainage

Water depth (cm from surface)	BOD (mg/L)	TN (mg/L)	TP (mg/L)	TAN (mg/L)	TS (mg/L)	TSS (mg/L)	SS (mg/L)
Surface	8.20 ± 0.49^f	0.38 ± 0.04^f	0.160 ± 0.014^d	0.052 ± 0.012^d	191.50 ± 2.12^e	65.70 ± 0.71^f	0.13 ± 0.02^d
50	11.10 ± 0.42^e	0.83 ± 0.04^e	0.205 ± 0.007^d	0.088 ± 0.011^c	224.50 ± 4.95^d	66.80 ± 1.06^f	0.17 ± 0.02^d
100	12.70 ± 0.28^d	1.06 ± 0.03^d	0.240 ± 0.014^d	0.096 ± 0.010^{bc}	238.00 ± 2.83^d	79.00 ± 1.41^e	0.53 ± 0.05^d
130	23.70 ± 0.42^c	1.73 ± 0.04^c	0.560 ± 0.014^c	0.110 ± 0.019^b	474.00 ± 2.83^c	264.80 ± 5.91^d	57.05 ± 2.69^c
140	27.80 ± 1.56^c	1.85 ± 0.04^c	0.605 ± 0.007^c	0.144 ± 0.017^b	487.50 ± 12.02^c	282.20 ± 2.35^c	60.14 ± 7.88^c
150	48.60 ± 6.79^b	2.16 ± 0.09^b	0.730 ± 0.042^b	0.206 ± 0.011^b	633.00 ± 8.49^b	448.20 ± 2.35^b	140.34 ± 1.07^b
Pond bottom	94.10 ± 4.81^a	4.89 ± 0.16^a	2.130 ± 0.099^a	4.150 ± 0.410^a	1324.50 ± 16.36^a	1027.40 ± 12.02^a	403.40 ± 1.61^a
Average (mg/L)	32.31 ± 30.53	1.84 ± 1.48	0.660 ± 0.680	0.690 ± 1.530	510.43 ± 395.24	319.16 ± 343.56	94.54 ± 145.34

Mean±standard deviations with different superscript letters in the same column are significantly different ($p<0.05$).

3.3 Comparison of discharge quality changes in the hybrid red tilapia ponds at harvest and after settling at different times

Precipitation of the discharge from the hybrid red tilapia ponds during harvest resulted in significant differences in water quality parameters for all time periods ($p<0.05$), as shown in Table 5. Sedimentation times to meet the standard drainage controls for freshwater aquaculture ponds of BOD, TP and TSS in the water were 3 h, 1 h, and 24 h, respectively showing decreases of 37.4%, 38.5%, and 85.0%.

Table 5. Average concentrations of nutrients and solids from the last 50 cm of water left in the hybrid red tilapia ponds after sedimentation at different times compared with initial concentrations

Sedimentation time	BOD (mg/L)	TN (mg/L)	TP (mg/L)	TAN (mg/L)	TSS (mg/L)
Pumping	31.30 ± 0.25^a (100%)	1.74 ± 0.06^a (100%)	0.578 ± 0.016^a (100%)	0.386 ± 0.023^a (100%)	511.80 ± 12.30^a (100%)
1 h	23.50 ± 0.21^b (75.0%)	1.71 ± 0.04^{ab} (98.0%)	0.355 ± 0.008^b (61.5%)	0.292 ± 0.013^b (75.6%)	258.10 ± 9.80^b (50.4%)
3 h	19.60 ± 0.29^c (62.6%)	1.70 ± 0.04^{ab} (97.4%)	0.348 ± 0.007^{bc} (60.3%)	0.286 ± 0.005^b (74.0%)	194.80 ± 12.11^c (38.1%)
6 h	14.70 ± 0.23^d (47.0%)	1.64 ± 0.06^{abc} (94.0%)	0.342 ± 0.006^{bc} (59.2%)	0.281 ± 0.004^b (72.7%)	123.50 ± 8.50^d (24.1%)
12 h	11.40 ± 0.11^e (36.5%)	1.62 ± 0.08^{bc} (92.8%)	0.337 ± 0.007^{bcd} (58.4%)	0.268 ± 0.002^{bc} (69.3%)	115.70 ± 4.60^d (22.6%)
24 h	9.90 ± 0.18^f (31.7%)	1.60 ± 0.06^{bcd} (91.7%)	0.335 ± 0.011^{bcd} (57.9%)	0.267 ± 0.004^{bc} (69.2%)	76.70 ± 5.80^e (15.0%)
48 h	9.50 ± 0.11^f (30.3%)	1.52 ± 0.01^{cde} (87.4%)	0.322 ± 0.016^{cde} (55.8%)	0.247 ± 0.007^{cd} (64.0%)	48.40 ± 10.20^f (9.5%)
72 h	6.30 ± 0.17^g (20.3%)	1.49 ± 0.03^{de} (85.6%)	0.314 ± 0.008^{de} (54.3%)	0.236 ± 0.010^{de} (61.1%)	22.60 ± 6.70^g (%4.4)
96 h	3.90 ± 0.30^h (12.6%)	1.47 ± 0.05^e (84.5%)	0.303 ± 0.015^e (52.4%)	0.212 ± 0.015^e (54.8%)	15.00 ± 4.70^g (2.9%)

Mean±standard deviations with different superscript letters in the same column are significantly different ($p<0.05$).

As shown in Table 6, average totals of BOD, TN, TP, TAN, and TSS in the full ponds were 100.08, 5.71, 2.05, 2.14, and 988.43 kg, respectively. When the final 50 cm of harvest effluent (31% of pond water volume, 985 m^3) was pumped and left to sediment for 24 h, BOD, TN, TP, TAN, and TSS reduced by 21.08, 0.14, 0.24, 0.12, and 428.57 kg or 68.37%, 8.05%, 42.04%, 30.83%, and 85.01%, respectively. This technique gave waste reduction in total pond water as 21.06% of BOD, 2.42% of TN, 11.68% of TP, 5.47% of TAN, and 43.36% of TSS.

Table 6. Average mass nutrient and total suspended solids in full ponds and reduction after settling the last 50 cm of effluent for 24 h

Exposition	BOD	TN	TP	TAN	TSS
Average concentration of waste in the pond (mg/L)	32.31	1.84	0.66	0.69	319.16
Total water volume (m^3)	3,097	3,097	3,097	3,097	3,097
Total waste in the pond (kg)	100.08	5.71	2.05	2.14	988.43
Concentration of waste during pumping the last 50 cm (mg/L)	31.30	1.74	0.58	0.39	511.80
Concentration of waste after 24 h of settling (mg/L)	9.90	1.60	0.34	0.27	76.70
Water volume of the last 50 cm of effluent (m^3)	985	985	985	985	985
Total waste in the last 50 cm of effluent (kg)	30.80	1.70	0.60	0.40	504.10
Total waste after 24 h of settling (kg)	9.75	1.58	0.33	0.26	75.55
Total waste reduction after 24 h of settling (kg)	21.08	0.14	0.24	0.12	428.57
Total waste reduction after 24 h of settling (%)	68.37	8.05	42.04	30.83	85.01
Total waste reduction in total pond water (%)	21.06	2.42	11.68	5.47	43.36

4. DISCUSSION

4.1 Water quality at different water depths before harvesting

Comparing the results to the standard for wastewater drainage from freshwater aquaculture farms (TECAC, 2008) the BOD, TN, TP, and TAN values from all depths did not exceed the control levels, while only TSS exceeded the control standard at 150 cm depth. This one parameter exceeding the control standard made the water at 150 cm unqualified for discharge. Therefore, before harvesting, the caged tilapia pond water qualified for discharge into the environment to up to 100 cm depth from the surface. Boyd (1995), Teichert-Coddington et al. (1995) and Assan et al. (2021) reported that factors contributing to feed intake directly affected the concentration of nutrients in the pond as organic and inorganic substances derived from excess food and the release of fish waste in the form of feces and urine. These substances are deposited as sediment on the bottom of the pond, causing high BOD levels (Islam, 2005). Here, total nitrogen, total phosphorus and ammonia contents on the bottom of the pond were less than recorded by Teichert-Coddington et al. (1999) who studied intensive shrimp pond cultivation. In red tilapia ponds, total nitrogen, total phosphorus and total ammonia contents were 1.480, 0.425, and 2.486 mg/L, respectively while in shrimp ponds they were 4.15, 1.67, and 2.40 mg/L, respectively. The feed given to red tilapia in this study comprised only 30% protein, while shrimp farming uses a diet containing 40 to 45% protein. Higher protein feed results in higher organic and inorganic contents, particularly at the pond bottom (Halver and Hardy, 2002).

4.2 Water quality at different water depths during harvesting

During harvest, the fish are in a small volume of water. This increases density and encourages water agitation, leading to increased suspension of solids (Coldebella et al., 2018). Therefore, harvesting causes a significant increase in all water quality parameters. TN increased by 63.21% or 0.63 times, TP increased 133.33% or 1.33 times, TAN increased by 14.58% or 0.15 times, and TSS increased by 235.19% or 2.35 times. These concentrations were higher in water near the bottom of the pond. Schwartz and Boyd (1994) reported that pond nutrient concentration was inversely related to the depth of water within the pond. Concentrations of BOD, TN, TP, TAN, TSS, and TS in the water were significantly different ($p<0.05$) at different water depths. The concentration of nutrients was highest in the last 20 cm of water, or 12.5% of pond volume. This result concurred with Munsiri et al. (1996), Teichert-Coddington et al. (1999) and Coldebella et al. (2018) who reported that concentrations of nutrients and solids in the discharge increased, with highest values in the last 5 to 20% of discharge from the pond.

Results showed that disturbance of the pond bottom by the water pump as the last process of harvesting mostly affected TSS in the water followed by TP, BOD, and TN. The bottom of the pond was a sink of accumulated sludge (Ayub et al., 1993). Phosphorus is usually accumulated at the pond bottom in the form of total phosphorus, thereby increasing BOD levels (Islam, 2005). TN level showed little increase as nitrogen in the pond evaporated into the atmosphere in the form of nitrogen and ammonia by nitrification and/or denitrification processes (Funge-Smith and Briggs, 1998).

4.3 Comparison of discharge water quality changes in hybrid red tilapia ponds at harvest and after settling for different times

Total nitrogen and total ammonia both passed the standard from the beginning of water precipitation. These results differed from Teichert-Coddington et al. (1999) who found that sedimentation time of total nitrogen and total phosphorus from shrimp ponds was about 6 h. In their experiment, water quality data were analyzed at 0, 6, 12, 24, and 48 h, while in our study the frequency of data collection was 1, 3, 6, 12, 24, 48, 72, and 96 h, giving more detailed sedimentation measurements. Sedimentation time for suspended solids in our study was 24 h, similar to Teichert-Coddington et al. (1999).

Our study results showed that sedimentation was most efficient for TSS reduction, while removal of nitrogen, BOD and phosphorus by sedimentation was less effective. Nitrogen loss in ponds occurs mainly by nitrification and denitrification processes. Most phosphorus was adsorbed by the pond bottom sediment. Sedimentation removes BOD in the short term but it may later increase because of autochthonous organic matter production in the settling ponds (Teichert-Coddington et al., 1999). Therefore, this technique is another option to reduce the waste from the lowest water levels of harvest effluent with high concentrations of BOD, TN, TP, and TSS that are generally greater than the Thailand control standard of wastewater from freshwater aquaculture farms. This technique removed 21.08 kg of BOD, 0.14 kg of TN, 0.24 kg of TP, 0.12 kg of TAN, and 428.57 kg of TSS in a 0.24 ha pond in one culture crop or 87.83 kg of BOD, 0.58 kg of TN, 1.0 kg of TP, 0.50 kg of TAN, and 1,785.71 kg of TSS in a 1 ha pond.

Numerous techniques have been applied to reduce waste from aquatic animal ponds including wetland establishment (Turcios and Papenbrock, 2014 and Marques et al., 2019), biological treatment with duckweed (*Lemna minor*) and *Bacillus* sp. (Omitoyin et al., 2017), green microalgae (*Coelastrum morum*) (Adekanmi et al., 2020), and a co-culture system (Attasat et al., 2013). Most of these methods treat all the wastewater and require time, large wastewater treatment areas and additional treatment systems to achieve satisfactory results.

The results of this study can be used as an effective discharge treatment from hybrid red tilapia ponds. Water quality in the ponds should be monitored according to depth ranges. Water depths that do not meet the standard of control for drainage from freshwater aquaculture should be settled in a sedimentation pond before release. This method reduces the size of sedimentation ponds. If it is not easy to measure water quality at depth periodically, farmers can apply the results of this study by settling water from a depth of 50 cm to the bottom of the pond for at least 24 h. The upper water can be released or recycled. This will reduce the environmental impact. Pond sediment contains high levels of organic matter, organic carbon and nitrogen as well as phosphorus and potassium. These can be used as fertilizers for many types of plants (Haque et al., 2016; Eymontt et al., 2017; Dróżdż et al., 2020) and for construction of dams, roads, embankments and landfills (Maj and Koszelnik, 2016).

5. CONCLUSION

Uncontrolled draining of fish ponds significantly impacts the environment. Drainage from the water surface to a depth of 100 cm by lowering a drainage pipe can meet the standard of wastewater drainage for freshwater aquaculture. When the water depth reaches 50 cm, a water pump is used and all water quality parameters do not meet the standard. If this water is allowed to settle for 24 hours, all parameters meet the standard. However, before finally draining the water, the quality should first be measured because different management techniques give diverse results.

ACKNOWLEDGEMENTS

REFERENCES

Adekanmi AA, Adekanmi SA, Adekanmi OS. Biological treatment of fish pond waste water by *Coelastrum morum*, a green microalgae. International Journal of Engineering and Information Systems 2020;4(4):62-77.

Alonso-Rodríguez R, Paez-Osuna F. Nutrients, phytoplankton and harmful algal blooms in shrimp ponds: A review with special reference to the situation in the Gulf of California. Aquaculture 2003;219:317-36.

American Public Health Association, American Water Works Association and Water Pollution Control Federation (APHA). Standard Methods of the Examination of Water and Wastewater. Maryland, USA: United Book Press; 2005.

Assan D, Huang Y, Mustapha UF, Addah MN, Li G. Chen H. Fish feed intake, feeding behavior, and the physiological response of apelin to fasting and refeeding. Frontiers in Endocrinology 2021;12:Article No. 798903.

Attasat S, Wanichpongpan P, Ruenglertpanyakul W. Design of integrated aquaculture of the pacific white shrimp, tilapia and green seaweed. Journal of Sustainable Energy and Environment 2013;4:9-14.

Ayub M, Boyd CE, Teichert-Coddington DR. Effects of urea application, aeration, and drying on total carbon concentrations in pond bottom soils. The Progressive Fish-Culturist 1993;55(3):210-3.

Boyd CE. Bottom Soils, Sediment and Pond Aquaculture. New York, USA: Chapman and Hall; 1995.

Cao L, Wang W, Yang Y, Yang C, Yuan Z, Xiong S, et al. Environmental impact of aquaculture and countermeasures to aquaculture pollution in China. Environmental Science and Pollution Research International 2007;14:452-62.

Coldebella A, Piana PA, Coldebella PE, Boscolo WR, Feiden A. Effluents from fish farming ponds: A view from the perspective of its main components. Sustainability 2018;10(1):Article No. 3.

Cole BA, Boyd CE. Feeding rate, water quality, and channel catfish production in ponds. The Progressive Fish-Culturist 1985;48(1):25-9.

Dróżdż D, Malińska K, Mazurkiewicz J, Kacprzak M, Mrowiec M, Szczypiór A, et al. Fish pond sediment from aquaculture production–current practices and the potential for nutrient recovery: A review. International Agrophysics 2020;34:33-41.

Eymontt A, Wierzbicki K, Brogowski Z, Burzyńska I, Rossa L. A new technology for removal of bottom sediments from ditches located in fish farms and the application of bottom sediments in agriculture. Komunikaty Rybackie 2017;2(157):7-13. (in Polish)

Feng YY, Hou LC, Ping NX, Ling TD. Development of mariculture and its impacts in Chinese coastal waters. Reviews in Fish Biology and Fisheries 2004;14:1-10.

Funge-Smith SJ, Briggs MRP. Nutrient budgets in intensive shrimp ponds: Implications for sustainability. Aquaculture 1998;164:117-33.

Gutierrez-Wing MT, Malone RF. Biological filters in aquaculture: Trends and research directions for freshwater and marine applications. Aquacultural Engineering 2006;34:163-70.

Halver JE, Hardy RW. Fish Nutrition. San Diego, USA: Academic Press; 2002.

Haque MM, Belton B, Alam MM, Ahmed AG, Alam MR. Reuse of fish pond sediments as fertilizer for fodder grass production in Bangladesh: Potential for sustainable intensification and improved nutrition. Agriculture, Ecosystems and Environment 2016;216:226-36.

Islam MS. Nitrogen and phosphorus budget in coastal and marine cage aquaculture and impacts of discharge loading on ecosystem: review and analysis towards model development. Marine Pollution Bulletin 2005;50:48-61.

Li X, Li J, Wang Y, Fu L, Fu Y, Li B, et al. Aquaculture industry in China: Current state, challenges, and outlook. Reviews in Fisheries Science 2011;19:187-200.

Maj K, Koszelnik P. Methods for management of bottom sediments. Czasopismo Inżynierii Lądowej, Środowiska i Architektury 2016;63:157-69. (in Polish)

Marques EATM, Filho GQDL, Oliveira CRDe, Cunha MCC, Calado SCDS, Sobra MDCM. Improving wastewater quality of a fish farm in Itacuruba, Northeastern Brazil. Advances in Oceanography and Marine Biology 2019;1(3):Article No. 000515.

Mohamed ZA, Al-Shehri AM. The link between shrimp farm runoff and blooms of toxic *Heterosigma akashiwo* in Red Sea coastal waters. Oceanologia 2012;54:287-309.

Munsiri P, Boyd CE, Teichert-Coddington DR, Hajek BF. Texture and chemical composition of soils from shrimp ponds near Choluteca, Honduras. Aquaculture International 1996;4:157-68.

Newell RIE. Ecosystem influences of natural and cultivated populations of suspension-feeding bivalve molluscs: A review. Journal of Shellfish Research 2004;23(1):51-62.

Omitoyin BO, Ajani EK, Okeleye OI, Akpoilih BU, Ogunjobi AA. Biological treatments of fish farm effluent and its reuse in the culture of Nile tilapia (*Oreochromis niloticus*). Journal of Aquaculture Research and Development 2017;8(2):Article No. 1000469.

Raveh A, Avnimelech Y. Total nitrogen analysis in water, soil and plant material with persulphate oxidation. Water Research 1979;13:911-2.

Sampantamit T, Ho L, Lachat C, Sutummawong N, Sorgeloos P, Goethals P. Aquaculture production and its environmental sustainability in Thailand: Challenges and potential solutions. Sustainability 2020;12:Article No. 2010.

Schwartz MF, Boyd CE. Channel catfish pond discharges. The Progressive Fish-Culturist 1994;56(4):273-81.

Schwartz MF, Boyd CE. Constructed wetlands for treatment of channel catfish pond effluents. The Progressive Fish-Culturist 1995;57:255-66.

Shpigel M, Ben-Ezra D, Shauli L, Sagi M, Ventura Y, Samocha T, et al. Constructed wetland with Salicornia as a biofilter for mariculture effluents. Aquaculture 2013;412-413:52-63.

Teichert-Coddington DR. Estuarine water quality and sustainable shrimp culture in Honduras. Thirteenth Annual Report [Internet]. 1995 [cited 2020 May 9]. Available from: http://pdacrsp.oregonstate.edu/pubs/Technical/13Techpdf/2.b.1.pdf.

Teichert-Coddington DR, Rouse DB, Potts A, Boyd CE. Treatment of harvest discharge from intensive shrimp ponds by settling. Aquacultural Engineering 1999;19:147-67.

Thai Environmental Compliance Assistance Center (TECAC). Standard for the control of drainage from freshwater aquaculture farms [Internet]. 2008 [cited 2021 Sep 10]. Available from: http://cac.pcd.go.th/index.php/ourservices/knowledgebased-law/cac-menu-law-fisheries/cac-menu-law-freshwater-fisheries/262-2535-39.

Troell M, Halling C, Neori A, Chopin T, Buschmann AH, Kautsky N, et al. Integrated mariculture: Asking the right question. Aquaculture 2003;226:69-90.

Turcios AE, Papenbrock J. Sustainable treatment of aquaculture effluents: What can we learn from the past for the future? Sustainability 2014;6:836-56.

Sources and Distribution of Organic Matter in Coastal Area of Muang Chonburi District, Eastern Thailand: Using Carbon and Nitrogen Stable Isotopes

Namthip Boonkwang[1] and Thanomsak Boonphakdee[1,2*]

[1]*Graduate Program in Environmental Science, Faculty of Science, Burapha University, Chonburi 20131, Thailand*
[2]*Department of Aquatic Science, Faculty of Science, Burapha University, Chonburi 20131, Thailand*

ARTICLE INFO

* Corresponding author:
E-mail: nuiosk@yahoo.com

ABSTRACT

The sources and spatial distribution of organic matter were investigated in the nearshore area receiving untreated urban wastewater and offshore areas containing bivalve mariculture in Muang Chonburi District. Content, elemental, carbon, and nitrogen isotopic analyses in particulate organic matter (POM) and surface sediments were performed. We found particulate organic carbon (POC), δ^{13}C, and δ^{15}N of POM ranging from 435.0-5,247.7 µg/L, -27.7 to -22.0‰ , and 1.7-8.6‰ , respectively, whereas total organic carbon (TOC), total nitrogen (TN), δ^{13}C and δ^{15}N in sediment were 3.5-76.9 µg/g, 0.8-8.3 µg/g, -25.7 to -22.9 ‰ and 2.6-6.0 ‰, respectively. These values show significant differences between nearshore and offshore sampling stations wherein accumulation of organic matter was high in the nearshore and decreased with greater distance offshore, with some retained in the bivalve farming area. The results from a mixing model indicated that organic matter in POM and sediment were initially derived from anthropogenic organic matter. In contrast to the offshore water which had organic matter derived from marine organic matter. This study highlights the distribution of anthropogenic organic waste released to coastal waters with plenty of bivalve farms such as green mussels and oysters. The results can be used to advise national strategies regarding bivalve aquaculture zoning and seafood safety policies going forward.

1. INTRODUCTION

Shallow coastal waters are where the biotic and abiotic components of the marine and terrestrial environments interact to form complex ecological and economic resources systems. These area are highly influenced by human activities, including housing developments, commercial industries, as well as recreation (Nordstrom, 2000). Consequently, these areas have been affected by various anthropogenic pollutants in sewage. Among the existing pollutants, the accumulation and distribution of organic matter in the shallow waters that receive urban wastewater, such as the inner Gulf of Thailand, has not been well understood.

Chonburi Province is situated on the east coast of the Inner Gulf of Thailand, covering 4,363 km² with a current population of more than 1.6 million. Muang Chonburi District is one of the most densely populated areas in Thailand, with more than 400,000 residents (1,490 people/km²) (Official Statistics Registration Systems, 2021). Consequently, these vast expanses of man-made activities cause a potential risk to the survival, growth, and ecological relationship of sessile and intertidal bivalves (Thushari et al., 2017). Coastal area of the district has become a significant economic ecosystem for tourism, industry, human settlement, and bivalve shellfish farms covering 197 ha with a production of 4,200 tons per year (Department of Fisheries, 2020). Oysters, green mussels, and bloody cockle have high commercial values because they are popular seafood sources for residents and tourists in this area and nationwide.

However, coastal water along Muang Chonburi District receives untreated wastewater from several communities via small canals (Boonkhwang et al., 2010). Therefore, massive amount of anthropogenic

pollutants, for instance, organic matter (Onpankoon et al., 2010), nutrients (Boonphakdee et al., 2008), microbial contaminants (Bussi et al., 2017), persistent organic pollutants (POPs) (Beyer et al., 2017), household chemicals and emerging contaminants of concern (Ocharoen et al., 2018) have been discharged to the coastal water of Muang Chonburi District. Organic matter and nutrient substances may cause eutrophication and eventually a red tide (Lassauque et al., 2010; Nijole et al., 2017), which creates a severe deterioration of the coastal environment and bivalve farming due to excessive oxygen consumption during the microbial respiration of the dead phytoplankton cells (Andrews et al., 1998). The low oxygen conditions may, in turn, kill fish and invertebrates, with severe consequences for the marine ecosystem (Boyer et al., 2009). Microbial contaminants, persistent organic pollutants (POPs), household chemicals, and emerging contaminants of concern may accumulate in bivalves and impact human health via consumption (Webber et al., 2021).

This study is focused on the distribution and sources of organic matter in the coastal area with an abundance of bivalve mariculture, and are receiving urban wastewater by using the stable carbon (δ^{13}C) and nitrogen (δ^{15}N) isotopes. Distribution of organic matter and its origin are essential approaches for understanding the movement and accumulation of organic matter in a coastal area. The results from this study can assist in improving a national policy for mariculture zoning and seafood safety.

2. METHODOLOGY

2.1 Study area and sampling sites

We took samples from three canals located in Muang Chonburi District, Chonburi Province; Sungkep (SK) (N13º22.437' E100º58.690'), Bangplasoy (BPS) (N13º21.697' E100º58.383') and Bangprong (BPR) (N13º18.856' E100º55.078') canals (Figure 1). These three canals receive municipal wastewater from densely populated communities in Muang Chonburi District (Sangmanee et al., 2017) before emptying into the east coast of the inner Gulf of Thailand. Stn. SK1, BPS1, and BPR1 were located at the mouth of each canal. We classified Stn. SK1-4, BPS1-4, and BPR1-4 as nearshore areas with shallow areas (depth <3.0 m). In contrast to Stn. SK5, BPS5, and BPR5 located >1,500 m. from the coastline and deeper water (>5.0 m) were determined as offshore stations. The sampling stations were approximately 300 m interval in the seaward direction along the

discharging plume from the canals (Boonkhwang et al., 2010).

The bivalve mariculture area along the coast of Muang Chonburi District is shown in Figure 1, covering 197 ha with a production of 4,200 tons per year (Department of Fisheries, 2020). Bivalves cultured in this area are mainly green mussel (*Perna veridis*) in Sungkeb and Bangplasoy sites and oyster (*Saccostrea cucullate*) Bangprong site Figure 1 (a) and (b).

2.2. Sample collection and pretreatment

Water samples for marine organic matter, mangrove leaves, sewage, particulate organic matter (POM) and sediment samples were taken at Sungkep (Stn. SK1-SK5), Bangplasoy (Stn. BPS1-BPS5), and Bangprong (Stn. BPR1-BPR5) sites during 10-14 January 2016. This period is classified as a dry season (Boonphakdee et al., 2008). Water samples were collected at a depth of 0.5 m using the Kitahara water sampler. Surface sediments samples were taken by an acrylic core sampler at a depth of 0-3 cm. After sample collection, water samples were stored in labelled plastic bottles and then frozen at -4°C. Sediment samples were stored in labelled plastic bags and then transported to the laboratory for further process.

Mangrove leaves were sampled from the reserved mangrove area in Muang Chonburi District (Figure 1), whereas sewage samples were collected at sewer outlets discharging into the three canals. Marine phytoplankton samples were vertically taken by using 60 µm mesh size plankton net at Stn. SK5, BPS5, and BPR5 where salinity was >33 and used as marine organic matter (OM).

After being transferred to the laboratory, water samples were filtered through pre-combusted (550°C, 2 h) GF/F Whatman glass fiber. The filtered samples were dried in an oven at 60°C for 24 h and decarbonated by HCl fumes for 6 h. After that, samples were rinsed with distilled water and stored at -20°C for elemental and isotopic analysis. The sediment samples were dried at 60°C for 48 h and then ground to a fine powder and homogenized. Powder sediment samples were acidified with 5 N HCl to remove inorganic carbon and washed with distilled water. Finally, sediment samples were dried at 60°C for 48 h and kept in a desiccator for further elemental and isotopic determination (Boonphakdee et al., 2008). Total organic matter was determined using the ignition loss procedure (Verardo et al., 1990). The organic carbon and nitrogen contents were determined using a CHN elemental analyzer. We

conducted a t-test using SPSS software (Version 20) to check the differences in $\delta^{13}C$, $\delta^{15}N$, and C/N ratio values among samples.

The contents of organic carbon and nitrogen were determined using a CHN elemental analyzer. We conducted a t-test using SPSS software (Version 20) to check the differences in $\delta^{13}C$, $\delta^{15}N$, and C/N ratio values among samples.
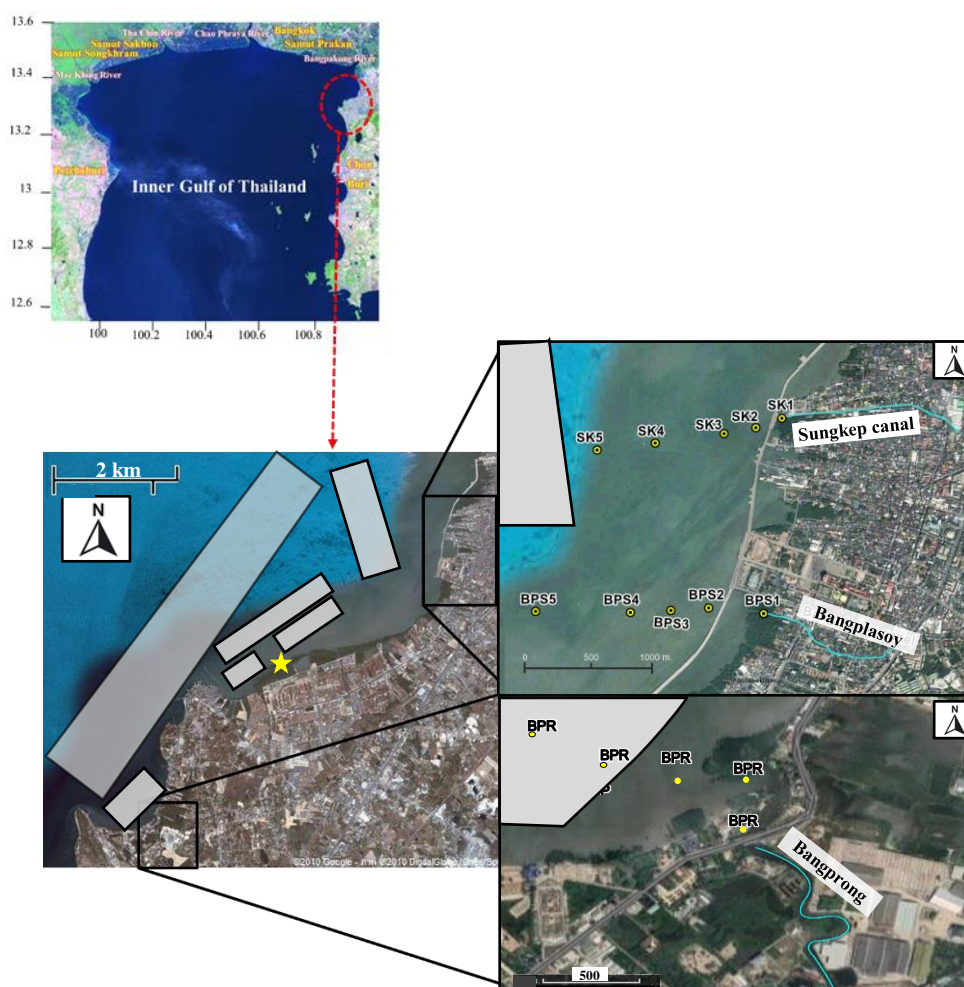
Figure 1. Map of sampling sites and stations in (a) Sungkep (Stn. SK1-5) and Bangplasoy (Stn. BPS1-5) and (b) Bangprong (Stn. BPR1-5) canals in Muang Chonburi District, Eastern Thailand. A star symbol indicates a sampling point for mangrove leaves. Grey areas illustrate bivalve mariculture in Muang Chonburi District (Department of Fisheries, 2021).

2.3 Stable isotope analysis

Stable isotopes were analyzed by a Thermo Finnigan Delta V advantage Isotope Ratio Mass Spectrometer Analyzer at Cornell Isotope Laboratory, Cornell University, USA. Carbon and nitrogen isotopic signatures were expressed as the relative differences between the isotopic ratio in the sample and conventional standards ($^{13}C/^{12}C$ or $^{15}N/^{14}N$), using the standard equation:

$$\delta^{13}C \text{ or } \delta^{15}N \text{ (‰)} = [(R_{sample}/R_{reference}) - 1] \times 1,000$$

In this expression, R_{sample} and $R_{reference}$ are the isotopic ratios of the sample and reference, respectively. The carbon standard is Peedee Belemnite (PDB), and the nitrogen standard is atmospheric N_2. All samples were analyzed twice. Reproducibility was better than ±0.1‰ of absolute difference for both $\delta^{13}C$ and $\delta^{15}N$.

3. RESULTS AND DISCUSSION
3.1 Compositions of organic matter in POM and sediment
3.1.1 Particulates organic matter (POM)

The values of particulate organic carbon (POC), particulate organic nitrogen (PON), C:N ratio, $\delta^{13}C$ and $\delta^{15}N$ of POM ranged from 435.0-5,247.4 µg/L, 85.1 to 927.5 µg/L, 2.6-10.1, -27.7 to -22.0 ‰, and 1.7-8.6 ‰, respectively (Table 1). Concentrations of POC and PON were significantly different ($p<0.05$)

among the three sampling sites. Spatial variations in PON and POC were observed with a similar pattern showing the high values in nearshore, especially in canal mouth stations (Stn. SK1, BPS1, and BPR1) and decreased seaward to low values at offshore stations (Stn. SK5, BPS5 and BPR5) (Table 1 and Figure 2(a)).

Table 1 . Compositions of organic matter in coastal waters of Muang Chonburi District.

Sites/stations	$\delta^{13}C_{POM}$ (‰)	$\delta^{15}N_{POM}$ (‰)	POC (µg/L)	C:N_{POM}	$\delta^{13}C_{sed}$ (‰)	$\delta^{15}N_{sed}$ (‰)	TOC_{sed} (mg/g)	TN_{sed} (mg/g)	C:N_{Sed}
Sungkep									
SK1	-27.0	3.4	6,352.0	10.1	-25.2	4.6	76.9	8.3	7.9
SK2	-26.0	2.3	5,114.5	8.9	-23.6	5.0	33.4	4.5	6.4
SK3	-24.5	2.5	3,970.7	7.2	-23.4	5.5	13.3	2.7	6.7
SK4	-23.4	3.0	3,734.2	6.7	-23.2	5.3	19.4	2.5	6.2
SK5	-23.3	3.0	1,849.8	5.7	-22.4	5.8	23.5	3.2	5.6
Bangplasoy									
BPS1	-27.7	2.5	3,887.2	9.7	-25.7	6.0	33.3	2.8	9.3
BPS2	-27.4	5.7	2,897.8	8.8	-24.3	2.7	8.3	1.1	7.9
BPS3	-26.9	4.7	1,414.7	6.2	-23.4	4.5	6.2	0.9	7.6
BPS4	-24.9	5.3	1,289.9	6.0	-23.6	2.6	3.5	0.8	6.0
BPS5	-23.2	5.9	1,479.4	6.1	-23.0	5.3	7.7	2.1	5.9
Bangprong									
BPR1	-24.7	1.7	5,247.4	5.7	-23.9	5.3	34.2	3.2	9.2
BPR2	-23.2	8.6	1,021.4	5.5	-22.8	4.5	8.4	1.0	7.2
BPR3	-22.9	8.5	925.4	5.5	-22.3	5.0	4.3	0.5	7.4
BPR4	-22.9	7.2	492.9	5.5	-22.0	5.9	28.4	2.6	6.4
BPR5	-22.5	7.0	436.0	5.4	-20.9	5.8	4.1	0.5	6.0

This indicates organic matter released from the municipal communities contributing to coastal water and was influenced by resuspension of bottom sediment in shallow water (Lamb and Swart, 2008). The values of POC:Chla at the canal mouth (SK1, BPS1, and BPR1) and nearshore stations of Sunkep and Bangplasoy canals (Stn.SK2-4 and BPS2-4) were higher (>200) than those of the offshore stations (<100) (Figure 2(b)), indicating a strong distribution of anthropogenic organic matter (Maksymowska et al., 2000; Boonphakdee et al., 2008; Nijole et al., 2017). This coincides with the lowest $\delta^{13}C$ at all canal mouth stations (-27.0, -27.7, and -24.7‰ for Stn. SK1, BPS1, and BPR1, respectively). The low $\delta^{13}C$ values (approx. -27‰) were close to that of sewage (Wu et al., 2003; Rumolo et al., 2011), indicating high anthropogenic input at Stn. SK1 and BPS1. Higher $\delta^{13}C$ value at BPR1 implies more contribution of marine OM at this station (Table 1). Values of $\delta^{13}C$ increased in seaward direction with the highest values (lower negative) at offshore stations (SK5, BPS5, and BPR5) (Figure 2(c)), which are close to -21.5‰ determining marine OM (Boonphakdee et al., 2008).

The values of $\delta^{13}C$, $\delta^{15}N$, total organic carbon (TOC), total nitrogen (TN) and C:N ratio of sediment ranged from -25.7 to -22.9 ‰, 2.6-6.0 ‰, 3.5-76.9 mg/g, 0.8-8.3 mg/g and 1.0-9.3, respectively (Table 1). Comparing with TOC and TN concentrations in sediments from worldwide coastal waters (Gu et al., 2017 and references therein), we found TOC and TON in this study were comparable to those from Bohai Bay, China. The spatial distribution of TOC and TN showed similar patterns (Figures 3(a-b)) to those in POM, with higher concentrations at the canal mouth and lower values in nearshore and offshore stations.

The values of TOC and TN in sediment were high at the canal mouth and nearshore stations and decreased with an increase in seaward distance (Figures 3(a-b)). These results imply that an increased organic matter falls to the bottom, and the benthic environment is transformed from one of oxidation to reducibility, leading to decreased benthic diversity and increased adverse biological effects on marine organisms (MPI, 2013). Fine-grained sediment in the nearshore also provides good binding for organic matter adsorbed on fine particles (Onpankoon and Boonpakdee, 2012; Gu et al., 2017). Generally, sedimentary organic matter is closely associated with fine-grained sediments undistubed by human activities (Gao et al., 2012).

The relationship between TOC and TN in sediment was high with $R^2=0.85$ (Figure 4(b)), showing a single source of organic matter in sediment (Pastene et al., 2019). The values of $\delta^{13}C$ in sediment showed similar patterns to $\delta^{13}C$ in POM. The low values of $\delta^{13}C$ in sediment were at the canal mouth and nearshore (-23.5 to -25.7‰), whereas the higher values were found in samples from the offshore stations at all sampling sites (-21 to -23‰) (Figure 3(c)). This suggests that the distribution of sediment organic matter in this study area was influenced by large amounts of organic waste from human waste.
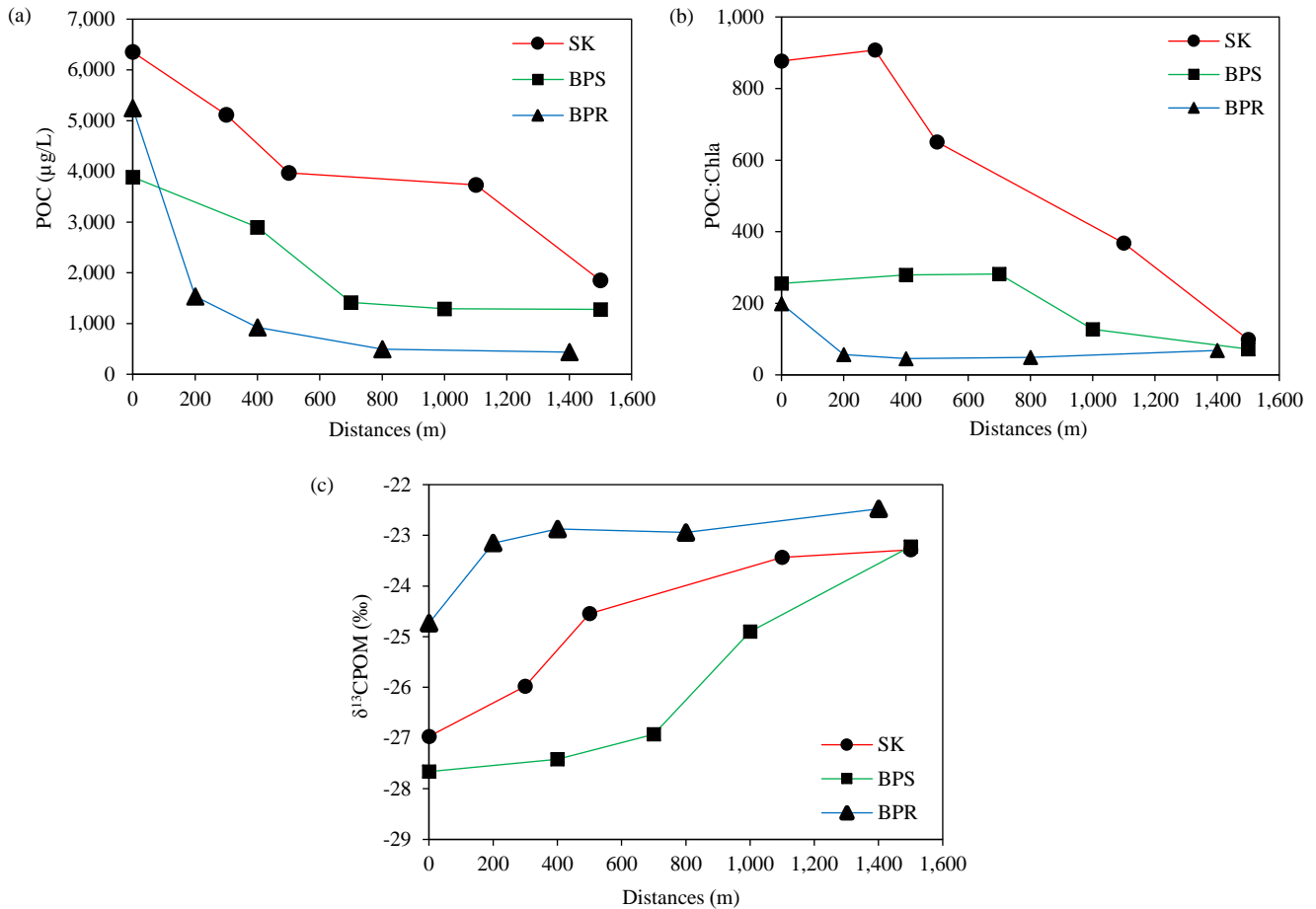

Figure 2. Values of (a) POC, (b) POC:Chla ratio, and (c) $\delta^{13}C$ in POM of SK, BPS, and BPR sampling sites. Positive distances indicate seaward direction.
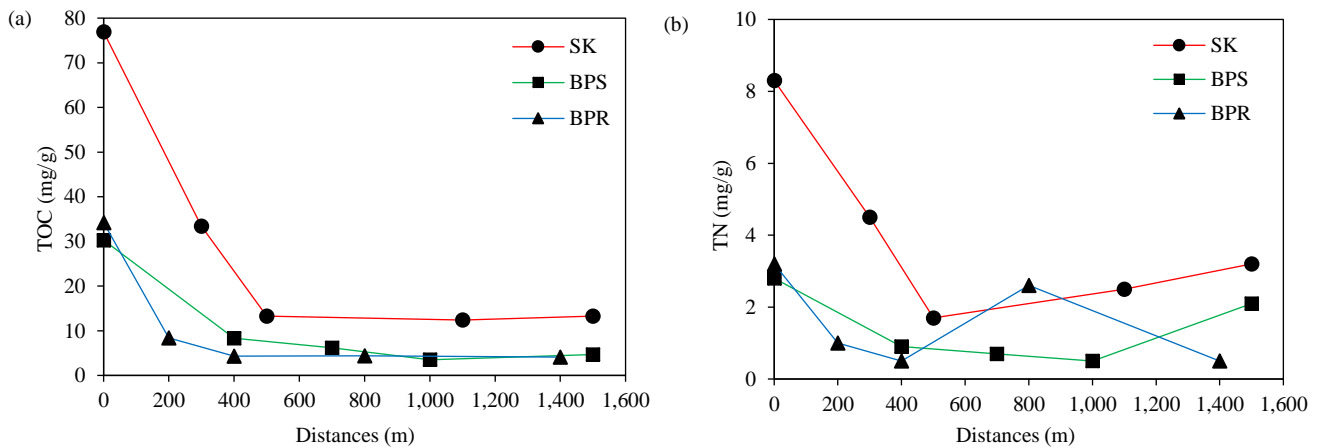

Figure 3. Values of (a) TOC, (b) TN, and (c) $\delta^{13}C$ in surface sediments of SK, BPS, and BPR sampling sites. Positive distances indicate seaward direction.

Figure 3. Values of (a) TOC, (b) TN, and (c) $\delta^{13}C$ in surface sediments of SK, BPS, and BPR sampling sites. Positive distances indicate seaward direction (cont.).
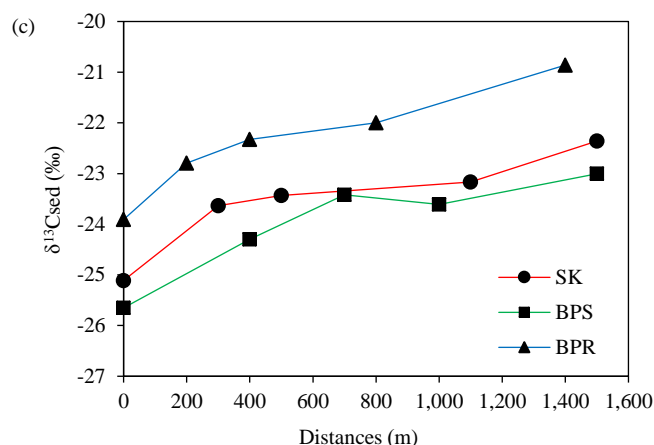
3.2 Sources of organic matter in POM and sediment

Significant linear relationships (r^2=0.75, p<0.001) between POC and PON were observed (Figure 4(a)) with highly strong correlation (r^2>0.95, p<0.001) at each study site (Table 1), suggesting they are derived from the same source (Gu et al., 2017). C/N ratios, $\delta^{13}C$, and $\delta^{15}N$ values have been widely used as markers to effectively discriminate sources of organic matter in aquatic ecosystems (Boonphakdee et al., 2008; Holtgrieve et al., 2011; Kikumoto et al., 2014; Li et al., 2016). Marine phytoplankton derived organic matter typically has C/N ratios between 4 and 7 (Gu et al., 2010), whereas terrestrial C_3 plants have C/N ratios typically higher than 12 (Ogrinc et al.,

2005; Boonphakdee et al., 2008). In this study, C/N ratios in POM and sediment varied from 5.4 to 10.1 and from 5.6 to 9.3 with an average of 6.8±1.7 and 7.0±1.2, respectively. These results indicate a mix of terrigenous or anthropogenic and marine sources. To confirm the source of organic matter in our study, we, therefore, analyzed $\delta^{13}C$ and $\delta^{15}N$ values. The $\delta^{13}C$ and $\delta^{15}N$ values derived from marine organic matter ranging from -22‰ to -18‰, and 3‰ to 12‰, respectively (Boonphakdee et al., 2008; Gao et al., 2012). Terrestrial C_3 and C_4 plants generally have $\delta^{13}C$ values ranging from -33‰ to -21‰ and -17‰ to -9‰, respectively. (Lamb et al., 2006; Boonphakdee et al., 2008; Yu et al., 2010).
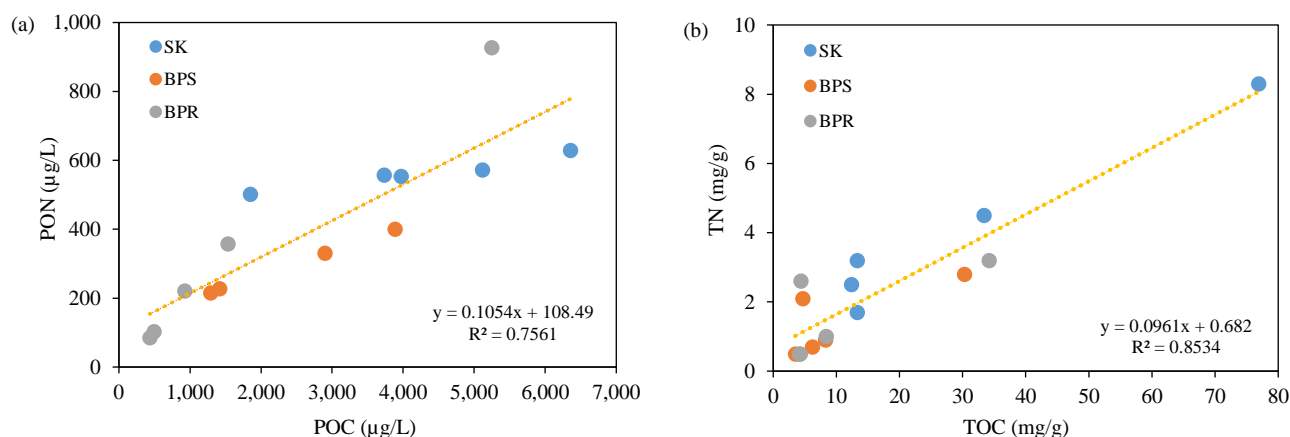
Figure 4. The relationships of (a) POC vs. PON and (b) TN vs. TOC in surface sediment of SK, BPS, and BPR sampling sites.

The $\delta^{15}N$ values in terrestrial organic matter varied from -10‰ to 10‰ (Li et al., 2016), and from 0.67‰ to 7.67‰ in terrestrial vegetations (Wei et al., 2010). The elevated $\delta^{15}N$ signature of untreated sewage (0-5‰) distinguished it from other nitrogen

sources (e.g., inorganic fertilizers 0 ‰) and treated sewage (10-15‰) (Anderson and Cabana, 2006; Finlay and Kendall, 2007). However, identifying sources of nitrogen to aquatic ecosystems, some

overlap may exist in isotope values of sewage and terrestrial organic matter (Diebel and Zanden, 2009).

The δ^{13}C and δ^{15}N distribution (Figures 3(c) and Figure 5) show that POM and sediment in the nearshore stations, located within 800 m from the shore, were close to those in sewage. In contrast, stations located further than 1,000 m. from the shoreline had values of δ^{13}C and δ^{15}N similar to those in marine OM. This suggests that organic matter in POM and sediment represents a mixture of continentally derived sewage and marine material (Figure 2(c) and Figure 3(c)). However, higher values of δ^{13}C of POM and sediment in the BPR site indicate low sewage origin contribution (Ogrinc et al.,2005). We measured values of δ^{13}C, δ^{15}N, and C:N ratio of potential organic matter sources, as shown in Table 2. However, low values of $\delta15$N (<3‰) in some POM and sediment samples (Figures 5(a-b)) indicate the possibility of another source, which may be autochthonous organic matter such as benthic diatom (Sugimoto et al., 2006) or detritus derived organic matter (Sampaio et al., 2010). Therefore, further investigation is needed.

Table 2. Values of δ^{13}C, δ^{15}N, and C:N ratios of potential sources in coastal waters of Muang Chonburi District

Potential sources	δ^{13}C (‰)		δ^{15}N (‰)		C:N	
	Mean±SD	Range	Mean±SD	Range	Mean±SD	Range
Sewage	-28.6±0.3	-28.3 to -28.8	5.2±1.2	4.6-5.7	10.6±0.8	10.0-11.2
Marine POM	-19.5±0.6	-19.0 to -21.4	7.0±0.6	5.2-9.4	5.4±1.0	4.2-6.5
Mangrove leaves	-30.7±2.5	-21.9 to -32.9	7.2±1.7	3.7-9.5	15.4±3.3	14.9-19.8

3.3 Contribution of sewage and marine organic matter

To understand the sources of organic matter in the POM and sediment in this coastal environment, we applied a mixing model based on two end-member of δ^{13}C. This two-end-member mixing model was applied to quantify the portion of organic origin considered terrigenous (sewage) and marine OM. This model has been demonstrated to effectively assess the relative proportions of terrigenous and marine organic matter in coastal waters (Goni et al., 2003; Boonphakdee et al., 2008; Gu et al., 2017; Sasmito et al., 2020).

In this study, we used δ^{13}C values of -19.5‰ and 26.80 ‰ for marine end-member (δ^{13}C$_{marine}$) and sewage end-member (δ^{13}C$_{sewage}$), respectively. Even though our previous works implemented terrigenous C$_3$ plants (mangrove leaves) as a potential source of organic matter in larger and open waters such as the Banpakong river estuary (Boonphakdee et al., 2008) and the inner Gulf of Thailand (Onpankoon et al., 2010) where terrigenous C$_3$ plant was the main contributor of organic matter. However, in our study sites, mangroves were available in narrow patches along the coastline and there was no terrestrial organic input from other water sources during the dry season. This coincides with values of δ^{15}N and C:N ratios of sewage that are closer to POM and sediment than those of mangrove (Figure 5(b) and Tables (1-2)). Therefore, in this study, we determined sewage as the main potential source of terrigenous organic matter.

We took sewage samples from the main sewer outlets flowing to the three canals. The value of -26.80‰ was close to that of untreated raw sewage reported by Anderson and Cabana (2006) and Finlay and Kendall (2007). The relative percentage contributions of sewage organic matter (SOM) and marine OM in POM and sediment samples were calculated using Equations (1) and (2).

$$SOM(\%) = \frac{\delta^{13}C_{marine} - \delta^{13}C_{sample}}{\delta^{13}C_{marine} - \delta^{13}C_{sewage}} \times 100 \qquad (1)$$

$$\text{Marine OM (\%)} = 100 - SOC \qquad (2)$$

The estimated contributions of sewage and marine OM indicate spatial variation in organic sources in all sampling sites (Figure 6). Accumulation of derived anthropogenic organic from the municipal wastewater was the majority in canal mouth stations with $>80\%$ and $>60\%$ for POM and sediment, respectively, decreasing with greater distance in a seaward direction (Ogrinc et al., 2005). In contrast to the offshore station, marine OM was the main contributor (Sampaio et al., 2010). However, we found that the percentage of the anthropogenic OM was higher in POM than that in sediment. This was due to the high biodegradation rate of anthropogenic POM, which typically occurs in shallow water (Zhou et al., 2021). In addition, marine OM mainly derived from marine phytoplankton has short lifetimes, and the heavier isotopic carbon weight could accumulate.
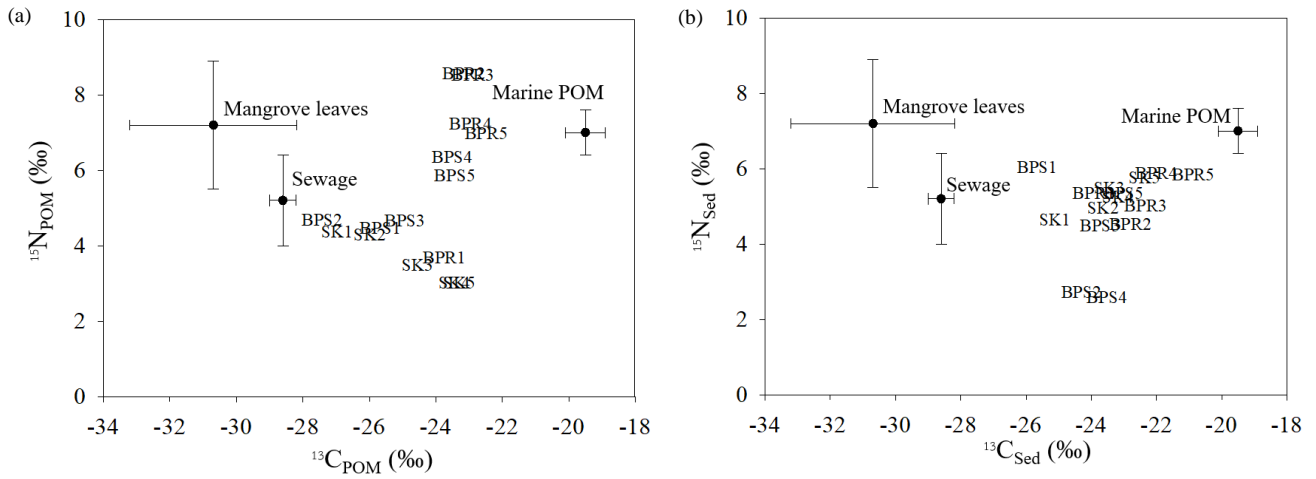
Figure 5. Scatter plots of δ¹³C vs. δ¹⁵N in (a) POM and (b) surface sediment samples, and their potential sources (mangrove leaves, marine POM and sewage).

Figure 6. The relative percentage of sewage and marine OM in (a) POM and (b) surface sediment based on δ¹³C two end-member mixing model

A higher percentage of marine OM was observed in the bivalve farming area (Stn. BPR 4-5), as shown in Figures 2 and 6. In this area, the primary farmed bivalve species was oysters that preferentially makes use of benthic diatoms (Richard et al., 1997). Uneaten natural food and cultivated bivalve feces can contribute to the accumulation of marine OM in the surface sediments of Oyster farming areas. In addition, Peng et al. (2014) and Gu and Lin (2016) reported that relatively higher nutrient levels in the seawater of the mariculture area promote algal blooms. As algae blooms subside, their major components are retained in the sediments.

3.4 Sewage and bivalve mariculture

This study demonstrates that sewage derived organic matter can reach bivalve mariculture area, such as the BPR site. This is particularly the case with filter feeding bivalves, which can accumulate significant amounts of contaminants from the water. Many chemical contaminants in sewage include persistent organic pollutants (Beyer et al., 2017) endocrine disrupting chemicals (Ocharoen et al., 2018), metals (Green et al., 2021), biocides, pesticides (Watts et al., 2017), veterinary and human medicines (Webber et al., 2021) all of which can be bio-transformed and bio-magnified to human via bivalves. Therefore, to assess the sustainability of the shellfish farming industry and/or seafood safety policy, we have to identify a range of future aquaculture management scenarios pertinent to future development and the sustainability of bivalve mariculture in Thailand.

4. CONCLUSION

This study has revealed the distribution of organic matter in coastal waters receiving municipal wastewater. It clearly shows that anthropogenic organic matter released from the coastal municipality accumulates in the nearshore with a decrease in a seaward direction. A mixing model indicated that the POM and organic matter in the nearshore sediment were initially derived from anthropogenic organic matter whist the source of offshore organic matter was marine phytoplankton. These results can be used to inform policies regarding bivalve mariculture zoning as well as general seafood safety regulations on a regional and national level.

ACKNOWLEDGEMENTS

REFERENCES

Anderson C, Cabana G. Does delta N-15 in river food webs reflect the intensity and origin of N loads from the watershed. Science of the Total Environment 2006;367:968-78.

Andrews JE, Greenaway AM, Dennis PF. Combined carbon isotope and C/N ratios as indicators of source and fate of organic matter in a poorly flushed, tropical estuary: Hunts Bay, Kingston Harbour, Jamaica. Estuarine, Coastal and Shelf Science 1998;46:743-56.

Beyer J, Green NW, Brooks S, Allan IJ, Ruus A, Gomes T, et al. Blue mussels (*Mytilus edulis* spp.) as sentinel organisms in coastal pollution monitoring: A review. Marine Environmental Research 2017;130:338-65.

Boonkhwang N, Sutthasom N, Boonphakdee T. Role of small rivers in nitrogen transport to the Inner Gulf of Thailand. Proceedings of the 8th Conference of Science and Technology and Technology for Development Social Happy; 2010 Mar 19; Thammasat University, Rangsit Campus: Thailand; 2010.

Boonphakdee T, Kasai A, Fujiwara T, Sawangwong P. Combined stable carbon isotope and C/N ratios as indicators of source and fate of organic matter in the Bangpakong River estuary, Thailand. EnvironmentAsia 2008;1:28-36.

Boyer JN, Kelble CR, Ortner PB, Rudnick DT. Phytoplankton bloom status: Chlorophyll a biomass as an indicator of water quality condition in the southern estuaries of Florida, USA. Ecological Indicators 2009;9:56-67.

Bussi G, Whitehead PG, Thomas ARC, Masante D, Jones L, Jack Cosby B, et al. Climate and land use change impact on fecal indicator bacteria in a temperate maritime catchment (the River Conwy, Wales). Journal of Hydrology 2017;553:248-61.

Department of Fisheries. Statistics of Marine Shellfish Culture Report Number 14/2020. Bangkok, Thailand: Ministry of Agriculture and Cooperatives; 2020. (in Thai).

Department of Fisheries. Map of controlled shellfish mariculture area [Internet]. 2021 [cited 2022 Feb 20]. Available from: https://gisportal.fisheries.go.th/portal/apps/webappviewer/index.html?id=61050ffe668b408bb9e8e39f4e187a4a.

Diebel MW, Zanden MJV. Nitrogen stable isotopes in streams: Effects of agricultural sources and transformations. Ecological Applications 2009;19:1127-34.

Finlay JC, Kendall C. Stable isotope tracing of temporal and spatial variability in organic matter sources to freshwater ecosystems. In: Michener R, Lajtha K, editors. Stable Isotope in Ecology and Environmental Science. New Jersey, USA: Blackwell Publishing; 2007.

Gao XL, Yang YW, Wang CY. Geochemistry of organic carbon and nitrogen in surface sediments of coastal Bohai Bay inferred from their ratios and stable isotopic signatures. Marine Pollution Bulletin 2012;64:1148-55.

Goni M, Teixeira M, Perkey D. Sources and distribution of organic matter in a river-dominated estuary (Winyah Bay, SC, USA). Estuarine Coastal and Shelf Science 2003;57:1023-48.

Green N, Pettersen R, Ruus A, Beyer J, Green NW. Proposed Environmental Quality Standards (EQSs) for blue mussel (*Mytilus edulis*) [internet]. 2021 [cited 2022 Feb 8]. Available from: https://niva.brage.unit.no/niva-xmlui/handle/11250/2731548.

Gu YG, Wang ZH, Lv SH, Yang YF, Feng J, Fang J, et al. Distribution of biogenic elements and potential contamination assessment in surface sediments from western Guangdong coasts. Journal of Shenzhen University Science and Engineering 2010;27:347-53.

Gu YG, Lin Q. Trace metals in a sediment core from the largest mariculture base of the eastern Guangdong coast, South China: Vertical distribution, speciation, and biological risk. Marine Pollution Bulletin 2016;113:520-5.

Gu YG, Ouyang J, Ning JJ, Wang ZH. Distribution and sources of organic carbon, nitrogen and their isotopes in surface sediments from the largest mariculture zone of the eastern Guangdong coast, South China. Marine Pollution Bulletin 2017;120:286-91.

Holtgrieve GW, Schindler DE, Hobbs WO, Leavitt PR, Ward EJ, Bunting L, et al. A coherent signature of anthropogenic nitrogen deposition to remote watersheds of the northern hemisphere. Science 2011;334:1545-8.

Kikumoto R, Tahata M, Nishizawa M, Sawaki Y, Maruyama S, Shu D, et al. Nitrogen isotope chemostratigraphy of the Ediacaran and Early Cambrian platform sequence at Three Gorges, South China. Gondwana Research 2014;25:1057-69.

Lamb AL, Wilson GP, Leng MJ. A review of coastal palaeoclimate and relative sea-level reconstructions using $\delta^{13}C$ and C/N ratios in organic material. Earth-Science Reviews 2006;75:29-57.

Lamb K, Swart PK. The carbon and nitrogen isotopic values of particulate organic material from the Florida Keys: A temporal and spatial study. Coral Reefs 2008;27:351-62.

Lassauque J, Lepoint G, Thibaut T, Francour P, Meinesz A. Tracing sewage and natural freshwater input in a Northwest Mediterranean Bay: Evidence obtained from isotopic ratios in marine organisms. Marine Pollution Bulletin 2010;60:843-51.

Li Y, Zhang HB, Tu C, Fu CC, Xue Y, Luo YM. Sources and fate of organic carbon and nitrogen from land to ocean: Identified by coupling stable isotopes with C/N ratio, Estuarine. Coastal and Shelf Science 2016;181:114-22.

Maksymowska D, Richard P, Piekarek-Jankowska H, Riera P. Chemical and isotopic composition of the organic matter source in the Gulf of Gdansk (Southern Baltic sea). Estuarine, Coastal and Shelf Science 2000;51:585-98.

Ministry for Primary Industries (MPI). Overview of Ecological Effects of Aquaculture. New Zealand: Ministry for Primary Industries; 2013.

Nijole RN, Galina L, Vitalijus M, Ruta B, Mindaugas Z, Irma VL, et al. Assessing nature and dynamics of POM in transitional environment (the Curonian Lagoon, SE Baltic Sea) using a stable isotope approach. Ecological Indicators 2017;82: 217-26.

Nordstrom KF. Beaches and Dunes on Developed Coasts. Cambridge, UK: Cambridge University Press; 2000.

Ocharoen Y, Boonphakdeea C, Boonphakdee T, Shinn AP, Moonmangmee S. High levels of the endocrine disruptors bisphenol-A and 17β-estradiol detected in populations of green mussel, *Perna viridis*, cultured in the Gulf of Thailand. Aquaculture 2018;497:348-56.

Official Statistics Registration Systems. Population and house statistics report [Internet]. 2021 [cited 2021 Oct 10]. Available from: http://stat.bora.dopa.go.th/stat/statnew /statTDD /views/showDistrictData.php?rcode=20&statType=1&year=63.

Ogrinc N, Fontolan G, Faganeli J, Covelli S. Carbon and nitrogen isotope composition of organic matter in coastal marine sediment (the Gulf of Trieste, N Adriatic Sea): Indicators of sources and preservation. Marine Chemistry 2005;95:163-81.

Onpankoon S, Sutthasom N, Boonphakdee T. An importance of small rivers on phosphorus and suspended solid transportation from Chonburi Municipality to the Inner Gulf of Thailand. Proceedings of the 8th Conference on Science and Technology and Technology for Development Social Happy; 2010 Mar 19; Thammasat University, Rangsit Campus: Thailand; 2010. (in Thai).

Onpankoon S, Boonphakdee T. Chemical and sources of organic matter in sediment from the Inner Gulf of Thailand. Proceedings of the Marine Sciences Conference; 2012 Oct 17-19; The Tawanna Bangkok Hotel: Thailand; 2012. (in Thai).

Pastene M, Quirogab E, Hurtadob CF. Stable isotopes and geochemical indicators in marine sediments as proxies for anthropogenic impact: A baseline for coastal environments of central Chile (33°S). Marine Pollution Bulletin 2019;142:76-84.

Peng X, Ma SW, Chen HG, Zhang Z, Zhou YB, Cai WG. Spatial distribution and assessment of nutrients in marine ranching in Zhelin Bay-Nanao Island in summer, South China. Fisheries Science 2014;10:27-35.

Richard P, Riera P, Galois R. Temporal variations in the chemical and carbon isotope compositions of marine and terrestrial organic inputs in the Bay of Marennes-Oleron (France). Journal of Coastal Research 1997;13(3):879-89.

Rumolo P, Barra M, Gherardi S, Marsella E, Sprovieri M. Stable isotopes and C/N ratios in marine sediments as a tool for discriminating anthropogenic impact. Journal of Environmental Monitoring 2011;13:3399-408.

Sampaio L, Freitas R, Mangus C, Rodringues A, Quintino V. Coastal sediments under the influence of multiple organic enrichment sources: An evaluation using carbon and nitrogen stable isotopes. Marine Pollution Bulletin 2010;60:272-82.

Sangmanee P, Boonphakdee T, Boonkhwang, N. An application of geographic information systems for wastewater management based on land use characteristic in Chonburi Province. EnvironmentAsia 2017;1:626-35.

Sasmito SD, Kuzyakov Y, Lubis AA, Murdiyarso D, Hutley LB, Bachri S, et al. Organic carbon burial and sources in soils of coastal mudflat and mangrove ecosystems. Catena 2020; 87:104-14.

Sugimoto R, Kasai A, Yamao S, Fujiwara T, Kimura T. Short-term variation in behavior of allochthonous particulate organic matter accompanying changes of river discharge in Ise Bay, Japan. Estuarine, Coastal and Shelf Science 2006;66:267-79.

Thushari GGN, Senevirathna JDM, Yakupitiyage A, Chavanich S. Effects of microplastics on sessile invertebrates in the eastern coast of Thailand: An approach to coastal zone conservation. Marine Pollution Bulletin 2017;124:349-55.

Verardo JD, Froelich PN, McIntyre A. Determination of organic carbon and nitrogen in marine sediments using the Carlo Erba NA-1500 analyzer. Deep Sea Research 1990;37:157-65.

Watts JEM, Schreier HJ, Lanska L, Hale MS. The rising tide of antimicrobial resistance in aquaculture: Sources, sinks and solutions. Marine Drugs 2017;15(6):Article No. 158.

Webber JL, Tyler CR, Carless D, Jackson B, Tingley D, Stewart-Sinclair P, et al. Impacts of land use on water quality and the viability of bivalve shellfish mariculture in the UK: A case study and review for SW England. Environmental Science and Policy 2021;126:122-31.

Wei XG, Zhuo MN, Guo ZX, Zhu LA. Carbon and nitrogen stable isotope composition of soil, vegetation and suspended

sediment in Dongjiang River Basin. International Journal of Ecology and Environmental Sciences 2010;19:1186-90.

Wu Y, Zuang J, Li DJ, Wei H, Lu RX. Isotope variability of particulate organic matter at the PN Section in the East China Sea. Biologeochemistry 2003;65:31-49.

Yu FL, Zong YQ, Lloyd JM, Huang GQ, Leng MJ, Kendrick C, et al. Bulk organic $\delta^{13}C$ and C/N as indicators for sediment

sources in the Pearl River delta and estuary, southern China, Estuarine. Coastal and Shelf Science 2010;87:618-30.

Zhou B, Yuan H, Song J, Li X, Li N, Duan L, et al. Source, transformation and degradation of particulate organic matter and its connection to microbial processes in Jiaozhou Bay, North China. Estuarine, Coastal and Shelf Science 2021;260:Article No. 107501.

Anatomical and Histochemical Responses of Vetiver Grass (*Chrysopogon zizanioides* L. Roberty) to Phytoremediation Ability of Liquid Batik Waste

Alfera Linggawati*, Maryani, Andhika Puspito Nugroho, and Diah Rachmawati

Faculty of Biology, Universitas Gadjah Mada, Special Region of Yogyakarta, Indonesia

ARTICLE INFO

ABSTRACT

Due to poor management of Indonesian batik waste, pollutants are discharged directly into rivers and absorbed from soil, causing environmental pollution. A phytoremediation strategy was chosen as one of the environmentally friendly and community-implementable solutions. Vetiver grass (*Chrysopogon zizanioides* L. Roberty) is a type of Poaceae plant that is suitable for the phytoremediation process of batik waste. This study analyzed the anatomical responses, distribution of secondary metabolites as defense compounds, and the ability to absorb heavy metals contained in liquid batik waste. Liquid batik waste was applied as plants irrigation at various concentration (0%, 25%, 50%, 75%, and 100%) for 60 days. Vetiver grass was able to grow well in the applied concentrations range. The results showed that vetiver grass roots could absorb Cu metal better than in the leaves. This plant can be stated to be able to absorb Cu better than Al. Liquid batik waste significantly ($p < 0.05$) affected most of the observed anatomical parameters, where concentrations of 75% and 100% were the most influential concentrations according to the DMRT test with a 95% confidence level. The histochemical analysis found that there was an increase in the distribution of lignin, phenolic compound, and terpenoids in the tissues composed of roots and leaves along with the increase in the concentration of the waste applied.

1. INTRODUCTION

Liquid batik waste is one type of textile waste that has an impact on the environment. This is due to the growth of batik industries in Indonesia, especially Java, after Batik was designated as a UNESCO World Heritage (Nurainun et al., 2008). However, this is incompatible with the environmentally friendly disposal of batik waste. According to Fajar et al. (2019), only about 0.6% of the batik industry in Pekalongan has a sewage treatment plant (IPAL), while the remaining liquid batik waste is discharged into water bodies (drainage channels or rivers). In the Special Region of Yogyakarta, especially in Kampung Batik Giriloyo, most batik producers do not dump waste into wells or directly into rivers without filtering (Muliasari and Widiastuti, 2010). This condition certainly causes risks to the environment and humans because the complexity of the molecules used in the batik production process, which consists of

heavy metals, makes batik waste difficult to degrade (Forgacs et al., 2004). Liquid batik waste has specific characteristic, thick color, alkaline pH, low in COD and BOD content (Mukimin et al., 2018), and also several heavy metals such as, Chromium (Cr), Copper (Cu), Iron (Fe), Cadmium (Cd), and Alumunium (Al) (Murti and Maryani, 2020).

There are several strategies to reduce the environmental impact of liquid batik waste, one of which is phytoremediation. Phytoremediation is an attempt to use plants to break down, stabilize, or remove pollutants from contaminated soil by leveraging the physiological properties of plants (Escoto et al., 2019). Plants that act as phytoremediation agents must show stronger growth properties than other plants: biomass, non-edible nutritional properties, complex root systems, ability to accumulate excess target pollutants, and specific mechanisms of tolerant stress (Prabakaran et al.,

2019). Adaptation mechanisms that occur in plants, especially phytoremediator plants are due to the ability of plants to develop a series of self-defense mechanisms, namely increased production of reactive oxygen species (ROS) and antioxidant compounds, physical defense through anatomical structural changes, and increased production of secondary metabolite defense compounds (Loix et al., 2017; He et al., 2018; Isah, 2019). Therefore, it is important to observe the response shown by plants after being stressed by liquid batik waste in phytoremediation efforts.

Vetiver grass is a gramineous plant species that meets these criteria. Vetiver grass is a non-invasive terrestrial plant species that has high biomass and has potential to grow on contaminated lands (Effendi et al., 2017; Effendi et al., 2020). Due to its strong root composition, this plant is intentionally planted with the aim of stabilizing the soil to prevent soil erosion (Mickovski et al., 2005). Vetiver grass is usually grown on the banks of rivers in border areas or in culture to extract the essential oils produced by this plant. Various studies have shown that vetiver grass can function as a phytoremediation agent in a variety of contaminated soils, including land contaminated with crude oil, heavy metals, tofu waste, and wood waste (Effendi et al., 2017; Gautam and Agrawal, 2017; Seroja et al., 2018; Rahmawan et al., 2019).

Plant defense strategies in the form of anatomical changes and distribution of secondary metabolites through histochemical techniques are the focus of this study. Anatomical changes that occur in plants are an excellent indicator for determining the effects of environmental stress on plants (Darmanti, 2015). This is the follow-up response that plants exhibit after the physiological response of the plant (Gratani, 2014). Detection of secondary metabolites by histochemical observations can be used to determine the distribution and localization of secondary metabolites that act as plant defense compounds from liquid batik waste stress. According to Badria and Aboelmaaty (2020), histochemical methods describe and track plant growth in ultra-fine-structured ways so that they can further explain the genetic basis of plant physiological and biochemical processes. Anatomical observations of changes in the structure and localization of secondary metabolites in tissues are considered indicators for assessing the ability of these plants to withstand environmental stress. Through this research, the effectiveness of vetiver grass in reducing liquid batik waste and the

responses exhibited by the plant are known, and it is hope that this plant can be used as an alternative in the phytoremediation process carried out by the community.

2. METHODOLOGY

2.1 Preparation and planting procedure

Vetiver grass (*Chrysopogon zizanioides* L. Roberty) is obtained from the Center for Agrotechnology Innovation (PIAT) UGM with a plant age of approximately 24 months and was cut to a leaf length of 20 cm to rejuvenate the plant. Geographically, the sampling location is at the coordinates of 7°7'47'1.3"S 110°27'48.8"E. The plant was planted in 2.5 kg of soil in the Greenhouse of the Sawitsari Research Station, Faculty of Biology, Universitas Gadjah Mada. The experimental design used a completely randomized design with five treatments and six replications. The liquid batik waste used in this study was obtained from the PC Batik Production House GKBI Medari, Sleman. Liquid batik waste was applied by watering for 60 days with as much as 200 ml with different waste concentrations, namely 0%, 25%, 50%, 75%, and 100% waste (P_0, P1, P_2, P_3, and P_4). The concentrations of heavy metals Cu, Cr, and Al in the liquid batik waste and planting media used were first measured in the laboratory of the Center for Environmental Health Engineering and Disease Control (BBTKLPP) in Yogyakarta. The results of measuring the concentration of batik waste applied in this study are presented in Table 1.

Table 1. Measurement results on the batik waste

Parameters	Unit	Results
Total Chrome (Cr)	mg/L	<0.0095
Copper (Cu)	mg/L	0.0130
Aluminium (Al)	mg/L	9.8040

2.2 Evaluation of the accumulation ability of Cu and Al metals in batik waste by vetiver grass

The process of observing the ability to accumulate metal in batik waste was carried out by measuring the metal concentrations of vetiver soil samples, roots and leaves. The plant samples and growth medium used for phytoremediation were 3 samples in each treatment group. Sample preparation was carried out by wet digestion method using (HNO_3 and $HClO_4$) (Ratnawati et al., 2019). The metal concentration in the filtrate was measured using AAS (Atomic Absorption Spectrophotometry) at BPTP

Yogyakarta. The efficiency level of heavy metal accumulation in the tissues was assessed using formula (1), and the rate of heavy metal transfer from roots to leaves (TF) was evaluated by the formula (2) (Takarina and Pin, 2017).

$$BCF = \frac{\text{Metal concentration in plant organ}}{\text{Metal concentration in soil}} \quad (1)$$

$$TF = \frac{\text{Root BCF value}}{\text{Leaf BCF value}} \quad (2)$$

2.3 Observation of anatomical and histochemical responses

The anatomical response data of vetiver grass was obtained through quantitative and qualitative observations on the anatomical structure of the roots and leaves of the plant after being treated with batik waste. Samples were prepared using the Embedding method according to Sutikno (2014) (Figure 1). Each root and leaf sample that had been cut approximately 0.5 cm long was fixed using FAA (Formaldehyde Alcohol Acetic Acid) solution for 24 h, then the sample was rinsed using 70% alcohol, followed by

graded dehydration using alcohol with a concentration of 80%, 95%, and 100% each for 30 min, then followed by the dealcoholization stage using alcohol, alcohol:xylol with different ratios, then carried out the infiltration stage using pure paraffin in an oven at 57°C for 24 h. The samples were then made into blocks using freshly pure paraffin for about one hour. The samples were then sliced using a rotary microtome with a thickness of 16 µm. The samples were then stained with a single stain of 1% safranin in 70% alcohol. The prepared anatomical slides were observed using a microscope equipped with Optilab and measured using Image Raster 3 software. The anatomical parameters of the roots observed in this study were root diameter, appearance of epidermal cells, exodermis thickness, cortex thickness, aerenchyma area (μm^2), endodermis thickness, endodermal cell wall thickness, stele diameter, metaxilem diameter, and number of metaxilem, while the leaf anatomical parameters observed were the thickness of upper and lower epidermis, mesophyll thickness, vascular bundle area (μm^2), number of bulliform cells, and bulliform cells area (μm^2).
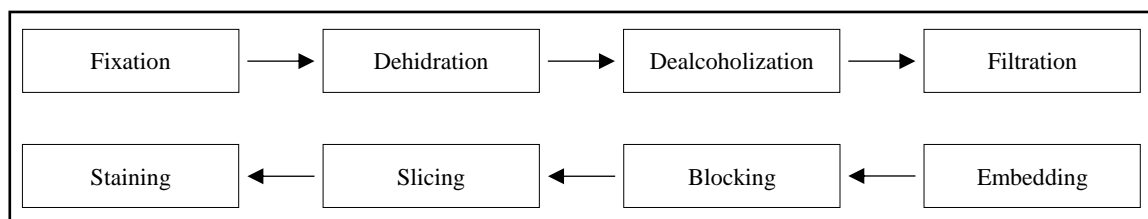

Figure 1. Flowchart of the embedding process carried out in this study.

The secondary metabolites of lignin, phenolic compounds, and terpenoids in the root and leaf tissues were observed histochemically using the free-hand section method. Phloroglucin-HCl reagent was used to observe lignin (Saulle et al., 2018), potassium dichromate (K_2CrO_4) to observe phenolic compounds (Badria and Aboelmaaty, 2020), and $CuSO_4$ 5% to detect terpenoids (Rahayu et al., 2021).

2.4 Data analysis

The observed data were tabulated using the Microsoft Excel application, then homogeneity and normality test were performed using the SPSS application for further analysis of variation (ANOVA) with a 95% confidence level. ANOVA was conducted to determine the effect of liquid batik waste in this study, then Duncan's Multiple Range Test (DMRT)

further test was conducted to determine the most influential treatment in this study.

3. RESULTS AND DISCUSSION
3.1 Heavy metals accumulation on soil and plant organ after application of liquid batik waste

The liquid batik waste used in this study did not significantly affect the Cu metal concentration in the vetiver grass soil and roots ($p > 0.05$). However, the difference in concentration of liquid batik waste treatment affected the plant's ability to translocate Cu from roots to leaves, where the increase in concentration of liquid batik waste was not accompanied by the ability to accumulate Cu in the leaves (Table 2). Vetiver can accumulate Cu much better in the roots than in the leaves. The higher BCF_{root} value than BCF_{leaf} in this study proves this.

The findings in the study Ghadiri et al. (2018) also showed that the roots of vetiver grass planted in polluted land accumulated higher Cu than in their leaves. The ability of Cu accumulation by vetiver grass was influenced by the Cu content in the soil and the duration of treatment, where the older plants were able to retain Cu in the roots better than the younger plants (Danh et al., 2012).

Table 2. Concentration of Cu and Al after batik waste treatment

Metal concentration in sample	Treatment				
	P_0	P_1	P_2	P_3	P_4
Cu					
Soil (mg/kg)	17.1±3.6[a]	18.0±1.6[a]	17.7±0.9[a]	18.3±1.4[a]	18.3±1.4[a]
Root (mg/kg)	17.4±3.5[a]	17.2±0.9[a]	17.7±1.1[a]	20.4±2.3[a]	20.3±4.7[a]
Leaf (mg/kg)	16.9±4.1[c]	12.7±0.9[b]	17.4±2.2[c]	6.3±0.8[a]	7.6±1.2[a]
BCF_{root} value	1.06	0.95	1.00	1.11	1.10
BCF_{leaf} value	1.05	0.71	0.99	0.35	0.42
TF value	0.99	0.75	0.99	0.32	0.38
Al					
Soil (mg/kg)	4475.1±167.4[c]	4286.6±113.1[bc]	4112.6±87.9[ab]	4004.1±144.3[a]	3912.1±33.3[a]
Root (mg/kg)	957.0±64.4[a]	1086.8±152.1[ab]	1194.4±102.6[ab]	1054.0±30.7[ab]	1418.9±451.3[b]
Leaf (mg/kg)	445.8±50.4[a]	453.1±40.2[a]	456.5±23.0[a]	489.6±35.0[a]	481.5±24.1[a]
BCF_{root} value	0.21	0.25	0.29	0.26	0.36
BCF_{leaf} value	0.10	0.11	0.11	0.12	0.12
TF value	0.48	0.44	0.38	0.46	0.33

Note: Similar letter notation shows no significant difference in DMRT's test with a significance level 5%. (P_0=control (0% concentration); P_1=25% concentration; P_2=50% concentration; P_3=75% concentration; P_4=100% concentration)

On the other hand, the soil and root Al concentrations of vetiver were significantly affected by the treatment of liquid batik waste ($p < 0.05$). As the concentration of batik waste increased, the concentration of Al in the roots increased. Increasing the concentration of batik waste lowers the pH of the soil, leading to the release of toxic Al^{3+} by H^+, making this form available to plants (Kinraide, 1997). The addition of complex metal species (Cd, Co, Cu, Pb, and Zn) with high concentrations in maize has been shown to reduce pH, therefore this condition affects the availability of Zn^{2+} and other metals dissolved in the soil so that their availability increases (Romdhane et al., 2021).

Plants can accumulate Al in high concentrations. Rahman et al. (2018), explained that woody plants were able to accumulate <1,000 mg/kg, while monocotyledonous plants such as *Oryza sativa*, *Glycine max*, and *Zea mays* were able to accumulate Al at high concentrations of <500 mg/kg. Likewise in this study, Al in the roots and leaves of the vetiver grass showed a high concentration compared to the Cu concentration (Table 2). Nevertheless, the ability of roots and leaves to accumulate Al, represented by BCF values, was very low, less than 1. Therefore, vetiver grass are excluders of Al metal in this study.

3.2 Anatomical responses

In general, the vetiver grass root anatomy is composed of single-cell epidermal tissue (Figure 2(a-e)), the cortex is composed of the exodermis, aerenchyma, and ordinary parenchyma cells, and the endodermis with 'U' thickening on the longitudinal wall. The central cylinder is composed of a layer of perisikel cells next to the endodermis, polyarch xylem type, phloem arranged between xylem elements, and pith cells which are isodiametrically shaped. The leaf anatomy (Figure 2(f-j)) consists of the abaxial epidermis tissue that has a smaller size and a more homogeneous/uniform shape compared to the adaxial epidermis. Bulliform cells are arranged in the center of the adaxial side of the leaf midrib. Mesophyll tissue is composed of parenchyma cells, where in the older leaves, the parenchyma tissue in the mesophyll forms a wide intercellular space so that aerenchyma is formed. Sclerenchyma tissue is located inside direction of the epidermis which is directly opposite the vascular tissue. Sclerenchyma also surrounds the transport tissue. Leaf stomata are scattered on the adaxial and abaxial surfaces.

The concentration of Cu and Al that accumulates more in the roots causes more pronounced anatomical changes than in the leaves.

The results of ANOVA showed that the applied liquid batik waste had a significant effect ($p<0.05$) on most of the root anatomical parameters except for the number of metaxylem parameters, as well as on most of the leaf anatomy parameters except for the number and bulliform cells area (Table 3). DMRT's further test with a significance value of 95% showed that the high concentration of waste treatment, namely 75% and 100%, was the concentration that had the most effect on increasing the measurement results of each anatomical parameter. Similar discoveries were found in the plant *Phragmites australis* (Cav.) Trin. Ex Steud. namely that the toxicity of various heavy metals (Mn, Zn, Cu, Pb, Cr, Ni, and Cd) causes degradation of the root epidermis, significant reduction in air space, and an increase in cell size in the endodermal tissue of these plants (Minkina et al., 2018).

The anatomical response indicated by the structure of vetiver grass roots is the form of defense to block the metal movement to the central cylinder and translocated to leaves, as also found in research by Gomes et al. (2011) in *Brachiaria decumbens*. The apoplastic barrier in the roots consisting of the epidermis, exodermis, and endodermis is the structure most affected by the occurrence of liquid batik waste stress in this study. Figure 3 shows the occurrence of damage to the cells that make up the epidermis accompanied by an increase in the thickness of the root exodermis. Figure 3(a) shows that at control treatment epidermal tissue is still exist, while in plants with high treatment concentrations (75% and 100%) it appears that there is a thickening of the exodermis as a compensation for the damage to the epidermal cells (Figure 3(b-c)). The location of the epidermis which is in direct contact with the environment allows the epidermal cells to experience oxidative stress, resulting in a thin cell wall that has the potential to damage the tissue (Gomes et al., 2011). Damage to epidermal cells is accompanied by thickening of the epidermal and endoderm cells, which act as a root apoplast barrier. Restricting the movement of toxic ions occurs by thickening these two structures (Lıska et al., 2016).
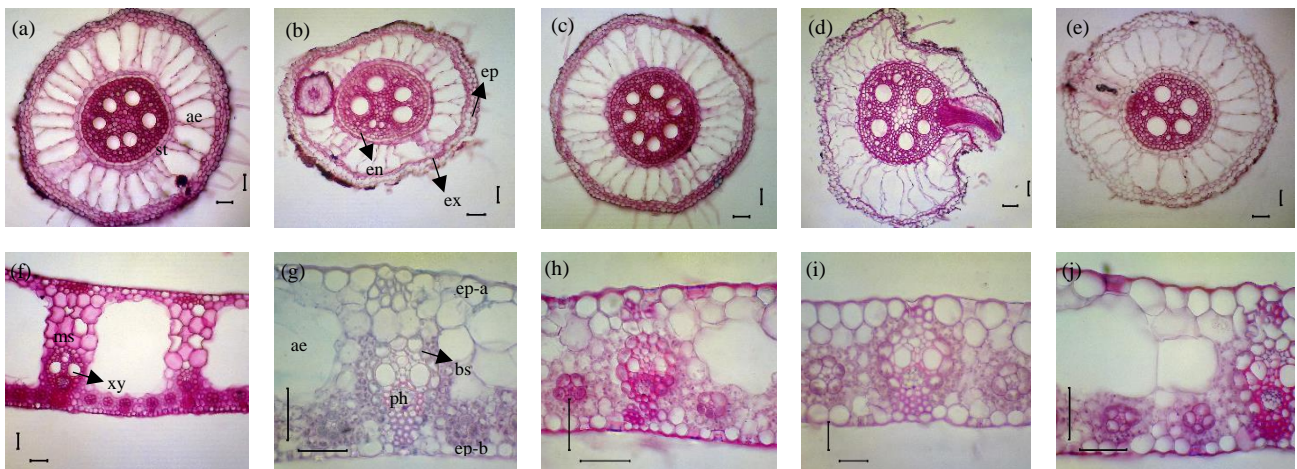

Figure 2. Cross section of roots (a-e) and leaves (f-j) of vetiver grass after treatment of batik waste for 60 days of observation. Desc: (a) P$_0$ (Control), (b) P$_1$ (Concentration 25%), (c) P$_2$ (Concentration 50%), (d) P$_3$ (Concentration 75%), and (e) P$_4$ (Concentration 100%). [ae=aerenchyma; st=stele; ep=epidermis; ex=exodermis; en=endodermis; ms=mesophyll; xy=xylem; ep-a=adaxial epidermis; ep-b=abaxial epidermis; ph=phloem; bs=bundle sheath] Bar=50 µm
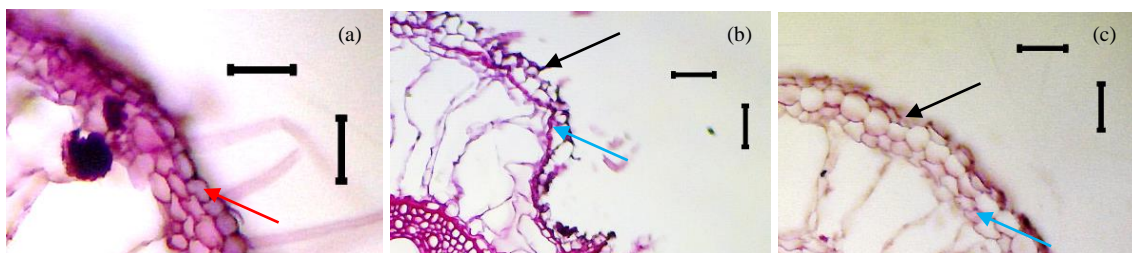

Figure 3. Comparison of appearance of epidermal cells after batik waste treatment. (a) P$_0$ (Control), (b) P$_3$ (Concentration 75%), and (c) P$_4$ (Concentration 100%). [Red arrow=epidermal cells; Blue arrow=exodermis cells; Black arrow=markers of epidermal cells have been degraded] Bar=50 µm

Table 3. Measurement results on the anatomical parameters of vetiver grass roots after batik waste treatment

Anatomical parameters	Measurement result (μm)				
	Treatment				
	P_0	P_1	P_2	P_3	P_4
Root					
Root diameter	604.59±77.80[b]	465.73±54.80[a]	518.75±76.00[a]	678.32±156.40[c]	683.52±18.00[c]
Exodermis thickness	11.26±3.20[a]	14.66±3.70[b]	15.44±4.20[bc]	18.35±5.90[cd]	21.21±3.70[d]
Cortex thickness	168.24±22.50[bc]	134.34±13.60[a]	147.31±17.80[ab]	195.11±53.30[d]	188.64±25.20[cd]
Aerenchyma area (μm^2)	4,689.67[b]	2,651.33[a]	4,644.07[b]	5,333.27[b]	6,375.40[c]
Endodermis thickness	14.74±1.50[bc]	10.84±1.60[a]	12.94±2.80[ab]	15.85±5.60[c]	12.68±4.40[ab]
Endodermal cell wall thickness	2.59±0.50[a]	2.54±0.40[a]	4.08±2.00[c]	3.44±1.00[bc]	3.20±0.90[ab]
Stele diameter	258.65±25.90[b]	212.37±27.20[a]	231.58±42.90[ab]	309.56±62.30[c]	305.48±26.10[c]
Metaxylem diameter	44.52±8.10[bc]	34.51±12.10[a]	37.82±5.40[ab]	55.22±11.50[d]	48.33±10.20[cd]
Number of metaxylem	9.0±7.2[a]	6.0±1.7[a]	6.0±2.8[a]	6.0±1.0[a]	6.0±2.6[a]
Leaf					
Adaxial epidermis thickness	13.32±2.90[b]	12.27±2.50[b]	10.89±1.60[a]	13.77±1.60[b]	12.13±4.50[a]
Abaxial epidermis thickness	17.02±6.30[a]	17.43±5.60[a]	19.01±2.50[a]	21.06±3.60[a]	18.61±7.50[a]
Mesophyll thickness	252.46±124.50[c]	167.75±28.34[b]	107.15±49.40[a]	111.69±40.20[a]	180.35±60.90[b]
Vascular bundle area (μm^2)	7,676.34[c]	5,313.97[b]	3,223.30[ab]	3,115.15[a]	5,155.85[ab]
Number of bulliform cells	9.0±0.0[a]	10.0±1.2[a]	9.0±1.5[a]	9.0±1.7[a]	9.0±1.2[a]
Bulliform cells area (μm^2)	6,650.76[a]	11,105.20[a]	12,493.89[a]	9,819.17[a]	10,677.06[a]

Note: Similar letter notation shows no significant difference in DMRT's test with a significance level 5%. (P_0=control (0% concentration); P_1=25% concentration; P_2=50% concentration; P_3=75% concentration; P_4=100% concentration)

The defense response of vetiver grass from liquid batik waste stress was also demonstrated by the intercellular space of aerenchyma along with the increase in waste water concentration. In vetiver grass, aerenchyma is a common structure found in the root cortex and leaf mesophyll tissue. Even so, stressful conditions allow aerenchyma development to be more intensive in aquatic and semi-aquatic plants (Rajhi and Mhadhbi, 2019). Aerenchyma development occurs influenced by programmed cell death (PCD) in cortical cells that are affected by ROS (Steffens et al., 2011).

The low concentration of Cu and Al that can accumulate in the leaves causes the response to anatomical changes that occur in the leaves is not so significant, where there is no damage to cells or tissues due to stress (Figure 2(f-j)). Changes occur in the form of an increase in the thickness of the adaxial and abaxial epidermis, as well as an increase in the area of vascular tissue in the leaves, and a decrease in the thickness of the mesophyll (Table 3). Similar findings also occurred in *Potamogeton* plants that were stressed by several heavy metals (Zn, Cu, Pb, and Cd) showing similar results to this study, such as a decrease in leaf thickness, an increase in adaxial and abaxial epidermal cell size (Al-Saadi et al., 2013). According to Thongchai et al. (2021), the increase in epidermal thickness is caused by the effect of growth medium,

which increases the amount of heavy metals that can be absorbed into the epidermal layer and then deposited on the epidermal cell wall.
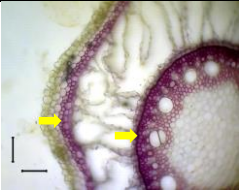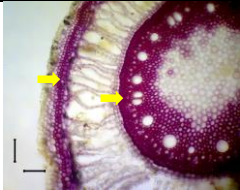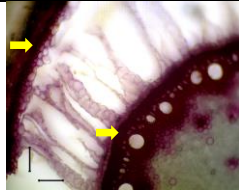
3.3 Histochemical observation
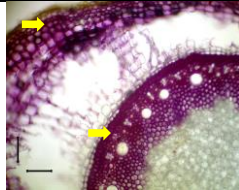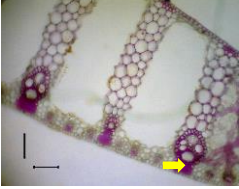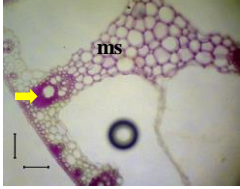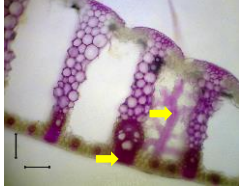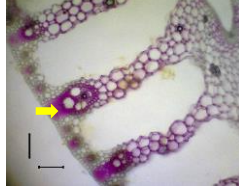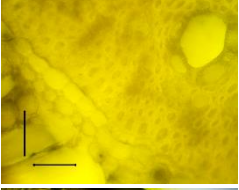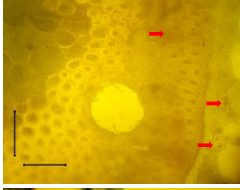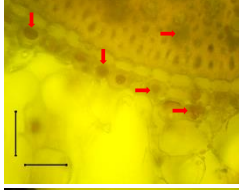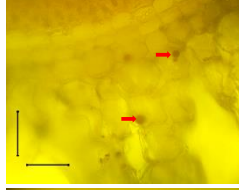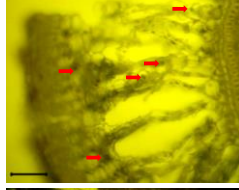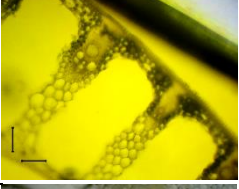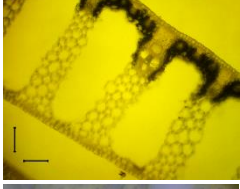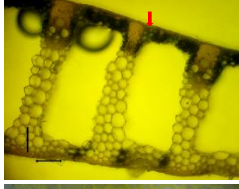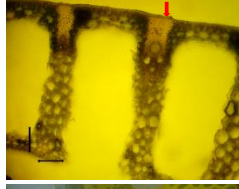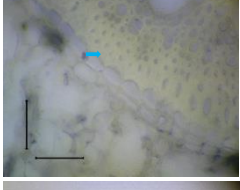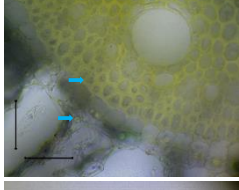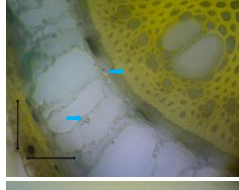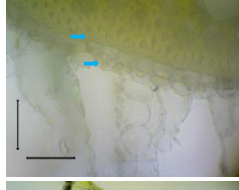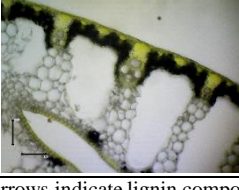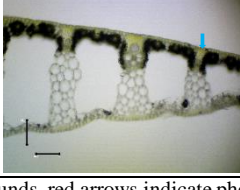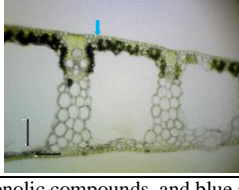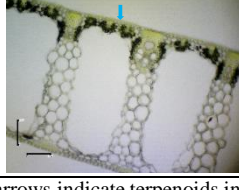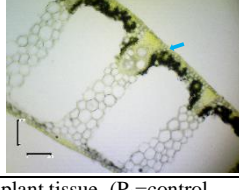
Secondary metabolites are compounds that have a role in plant adaptation to environmental stress. High levels concentrations of secondary metabolites can make plants more resilient to environmental stress (Mazid et al., 2011). Histochemical techniques allow for qualitative analysis of secondary metabolites related to plant tissue deposition. Table 4 shows the difference in the level of color density due to the distribution of secondary metabolites in the tissues that make up the roots and leaves and the reaction results with the reagents used. Liquid batik waste has an effect on the level of reaction color density and distribution of idioblasts as the concentration increases.

Lignin is a major compound that forms the secondary cell wall which plays a role in maintaining the strength and impermeability to water in plant tissues (Tao et al., 2009). Therefore, the reddish color change caused by the reaction with phloroglucin-HCl is seen in cells with thick cell walls, such as on root exodermis, endodermis, xylem cell wall in roots and leaves, as well as on sclerenchyma cell walls in leaves. Lignin is one of the product compounds of the

phenylpropanoid pathway, which is part of the shikimate pathway in the synthesis of phenolic compounds (Printz et al., 2016). Lignin deposit that have undergone a biosynthetic process are then polymerized on the cell wall by peroxidase and laccase (Alejandro et al., 2012). The production of lignin is strongly influenced by the activity of the enzyme Phenylalanine Ammonia-lyase/PAL, where its activity is strongly influenced by the environment, especially heavy metals. Research on the *Prosopis*

glandulosa plant from oxidative stress after exposure to heavy metals Cd and Cu (concentration of Cd^{2+} 0.001 M and Cu^{2+} 0.52 M) for 96 h, showed an increase in PAL enzyme activity in the phenylpropanoid pathway which caused an increase in the production of phenolic compounds and flavonoids which has a role as a non-enzymatic antioxidant and protects the plant (González-Mendoza et al., 2018). This qualitatively illustrates the effect of liquid batik waste on the lignin content of vetiver grass.

Table 4. Distribution of secondary metabolites in root and leaf tissue of vetiver grass after batik waste treatment

Type of secondary metabolites	Reaction on root and leaf tissue[2]				
	P_0	P_1	P_2	P_3	P_4
Lignin					
Phenolic compound					
Terpenoid					

Note: Yellow arrows indicate lignin compounds, red arrows indicate phenolic compounds, and blue arrows indicate terpenoids in plant tissue. (P_0=control (0% concentration); P_1=25% concentration; P_2=50% concentration; P_3=75% concentration; P_4=100% concentration)

The phenolic compounds in this study were observed by the reaction that occurred between these compounds and 5% potassium dichromate (K_2CrO_4) reagent and showed a brownish yellow color (Table 4). As a common reagent, potassium dichromate is capable of detecting phenolic compounds in tissues with different concentrations depending on the concentration of the target compound in the tissue (Badria and Aboelmaaty, 2019). The distribution and localization of phenolic compounds were more as idioblasts in the root cortex tissue and increased along with the increase in the concentration of liquid batik waste that was applied. This is related to the defense mechanism of these plants from liquid batik waste stress in this study. Research conducted by Melato et al. (2012), explained that there was an increase in the content of phenolic compounds in vetiver grass after receiving heavy metal stress Fe, Pb, Ni, As, Zn, Cu, and Cr which were measured quantitatively using spectrophotometry. It was further explained that this occurs because phenolic compounds are related to plant defense mechanisms against environmental stresses in the form of heavy metals and other stresses. Although no quantitative observations were made in this study, increased levels of color density and distribution of idioblast blasts explained high concentrations of phenolic compounds in tissues.

In line with observations on lignin and phenolic compounds, the distribution of terpenoids in vetiver grass was also affected by the applied liquid batik waste treatment. In addition to being found in the cell walls of the xylem constituents in roots and leaves, terpenoid compounds in roots are more commonly found in the form of idioblast structures distributed in the root cortex tissue. The same finding was also found in undifferentiated cells in *Cinchona ledgeriana* Moens culture which was observed for terpenoid compounds using 5% $CuSO_4$ reagent (Pratiwi et al., 2020). In leaves, terpenoids are also found in the leaf cuticle because the cuticle is composed of terpenoid and flavonoid compounds that are involved in defense mechanisms from biotic and abiotic (Singh et al., 2018; Ziv et al., 2018).

4. CONCLUSION

Vetiver grass was able to accumulate Cu metal better than Al contained in liquid batik waste used in this study, and its storage capacity was better in the roots than in the leaves. Therefore, the root structure shows a more pronounced anatomical response than the leaves. ANOVA showed that the treatment of batik waste significantly affected the anatomical response at most of the observed parameters ($p < 0.05$). The histochemically observed distribution and localization of secondary metabolites in the roots and leaves of vetiver showed an increase with increasing application concentration.

ACKNOWLEDGEMENTS

REFERENCES

Al-Saadi M, Al-Asaadi M, Al-Waheeb H. The effect of some heavy metals accumulation on physiological and anatomical characteristic of some *Potamogeton* L. plant. Journal of Ecology and Environmental Sciences 2013;4(1):100-8.

Alejandro S, Lee Y, Tohge T, Sudre D, Osorio S, Park J, et al. AtABCG29 is a monolignol ransporter involved in lignin biosynthesis. Current Biology 2012;22(13):1207-12.

Badria FA, Aboelmaaty WS. Plant Histochemistry: A versatile and indispensible tool in localization of gene expression, enzymes, cytokines, secondary metabolites and detection of plants infection and pollution. Acta Scientific Pharmaceutical Sciences 2019;3(7):88-100.

Badria FA, Aboelmaaty WS. Chemical, biochemical, genetics, and physiological role of secondary metabolites of medicinal plants via utilization of plant histochemical techniques. Asian Journal of Phytomedicine and Clinical Research 2020;8(1):12-28.

Danh LT, Truong P, Mammucari R, Pu Y, Foster N. Phytoremediation of soils contaminated by heavy metals, metalloids and radioactive materials using vetiver grass, *Chrysopogon zizanioides*. In: Anjum NA, Pereira ME, Iqbal A, Duarte AC, Umar S, Khan NA, editors. Phytotechnologies: Remediation of Environmental Contaminants. 1st ed. Boca Raton: CRC Press; 2012. p. 255-80.

Darmanti S. Xilem cell wall thickening of soybean plants (*Glycine max* L. Merr) Var. Grobogan due to double stress interference nut grass (*Cyperus rotundus* L.) and drought. Anatomy and Physiology Bulletin 2015;23(2):23-8. (in Indonesian).

Effendi H, Munawaroh A, Puspa AI. Crude oil spilled water treatment with *Vetiveria zizanioides* in floating wetland. Egyptian Journal of Aquatic Research 2017;43(3):185-93.

Effendi H, Widyatmoko, Utomo BA, Pratiwi NTM. Ammonia and orthophosphate removal of tilapia cultivation wastewater with *Vetiveria zizanioides*. Journal of King Saud University-Science 2020;32(1):207-12.

Escoto DF, Gayer MC, Bianchini MC, Pereira G da C, Roehrs R, Denardin EL. Use of *Pistia stratiotes* for phytoremediation of water resources contaminated by clomazone. Chemosphere 2019;227:299-304.

Fajar M, Mediani A, Finesa Y. Analysis of the role of wastewater treatments instalation in the strategy of handling batik industry

waste in Pekalongan City. Proceedings of the National Seminar on Geography 2019;84-90. (in Indonesian).

Forgacs E, Cserháti T, Oros G. Removal of synthetic dyes from wastewaters: A review. Environmental International 2004;30(7):953-71.

Gautam M, Agrawal M. Phytoremediation of metals using vetiver (*Chrysopogon zizanioides* (L.) Roberty) grown under different levels of red mud in sludge amended soil. Journal of Geochemical Exploration 2017;182:218-27.

Ghadiri S, Farpoor M, Mehrizi MH. Phytoremediation of soils polluted by heavy metals using Vetiver grass and Tall Fescue. Desert (Biaban) 2018;23(1):123-32.

Gomes MP, Marques TCLL de SM, Nogueira M de OG, de Castro EM, Soares ÂM. Ecophysiological and anatomical changes due to uptake and accumulation of heavy metal in *Brachiaria decumbens*. Scientia Agricola 2011;68(5):566-73.

González-Mendoza D, Troncoso-Rojas R, Gonzalez-Soto T, Grimaldo-Juarez O, Ceceña-Duran C, Duran-Hernandez D, et al. Changes in the phenylalanine ammonia lyase activity, total phenolic compounds, and flavonoids in prosopis glandulosa treated with cadmium and copper. Anais da Academia Brasileira de Cincias 2018;90(2):1465-72.

Gratani L. Plant phenotypic plasticity in response to environmental factors. Advances in Botany 2014;2014:1-17.

He M, He CQ, Ding NZ. Abiotic stresses: General defenses of land plants and chances for engineering multistress tolerance. Frontiers in Plant Science 2018;871:1-18.

Isah T. Stress and defense responses in plant secondary metabolites production. Biological Research 2019;52(1): Article No. 39.

Kinraide TB. Reconsidering the rhizotoxicity of hydroxyl, sulphate, and fluoride complexes of aluminium. Journal of Experimental Botany 1997;48(310):1115-24.

Lıska D, Martinka M, Kohanova J, Lux A. Asymmetrical development of root endodermis and exodermis in reaction to abiotic stresses. Annals of Botany 2016;118(4):667-74.

Loix C, Huybrechts M, Vangronsveld J, Gielen M, Keunen E, Cuypers A. Reciprocal interactions between cadmium-induced cell wall responses and oxidative stress in plants. Frontiers in Plant Science 2017;8:1-19.

Mazid M, Khan TA, Mohammad F. Role of secondary metabolites in defense mechanisms of plants. Biology and Medicine 2011;3:232-49.

Melato F, Regnier T, McCrindle R, Mokgalaka N. Impact of metals on secondary metabolites production and plant morphology in vetiver grass (*Chrysopogon zizanioides*). South African Journal of Chemistry 2012;65(1):178-83.

Mickovski SB, Van Beek LPH, Salin F. Uprooting of vetiver uprooting resistance of vetiver grass (*Vetiveria zizanioides*). Plant and Soil 2005;278(1-2):33-41.

Minkina T, Fedorenko G, Nevidomskaya D, Fedorenko A, Chaplygin V, Mandzhieva S. Morphological and anatomical changes of *Phragmites australis* Cav. due to the uptake and accumulation of heavy metals from polluted soils. Science of the Total Environmental 2018;636:392-401.

Mukimin A, Vistanty H, Zen N, Purwanto A, Wicaksono KA. Performance of bioequalization-electrocatalytic integrated method for pollutants removal of hand-drawn batik wastewater. Journal of Water Process Engineering 2018;21:77-83.

Muliasari IGAD, Widiastuti. Environmental carrying capacity related to batik waste processing in Giriloyo Batik Village,

Bantul Regency, Yogyakarta. Atrium 2010;6(2):131-9. (in Indonesian).

Murti VM, Maryani. Anatomical responses of marigold (*Tagetes erecta* L.) roots and stems to batik wastewater. AIP Conference Proceedings 2020;2260(1):Article No. 030018.

Nurainun, Heriyana, Rasyimah. Analysis of the Batik Industry in Indonesia. Economic Focus 2008;7(3):124-35. (in Indonesian).

Prabakaran K, Li J, Anandkumar A, Leng Z, Zou CB, Du D. Managing environmental contamination through phytoremediation by invasive plants : A review. Ecological Engineering 2019;138:28-37.

Pratiwi DR, Sulistyaningsih YC, Ratnadewi D. Localization of alkaloid and other secondary metabolites in *Cinchona ledgeriana* Moens: Anatomical and histochemical studies on fresh tissues and cultured cells. HAYATI Journal of Biosciences 2020;27(1):1-7.

Printz B, Lutts S, Hausman JF, Sergeant K. Copper trafficking in plants and its implication on cell wall dynamics. Frontiers in Plant Science 2016;7:1-16.

Rahayu T, Pratiwi RIA, Mubarakati NJ. Metabolite profile of kesambi leaves (*Schleichera oleosa*) based on histochemical and in silico analysis. Metamorfosa: Journal of Biological Sciences 2021;8(1):156-65. (in Indonesian).

Rahman MA, Lee SH, Ji HC, Kabir AH, Jones CS, Lee KW. Importance of mineral nutrition for mitigating aluminum toxicity in plants on acidic soils: Current status and opportunities. International Journal of Molecular Sciences 2018;19(10):1-28.

Rahmawan AJ, Effendi H, Suprihatin S. Potential of vetiver grass (*Chrysopongon zizanoides* L.) and water spinach (*Ipomoea aquatica* Forsk.) as phytoremediation agents for industrial wood waste. Journal Natural Resources and Environmental Management 2019;9(4):904-19. (in Indonesian).

Rajhi I, Mhadhbi H. Mechanisms of aerenchyma formation in maize roots. African Journal of Agricultural Research 2019;14(14):680-5.

Ratnawati NA, Prasetya AT, Rahayu F. Validation of the heavy metal lead (Pb) test method with wet destruction using FAAS in sediment of the West Semarang flood canal river. Indonesian Journal of Chemical Science 2019;8(1):60-8. (in Indonesian).

Romdhane L, Panozzo A, Radhouane L, Dal Cortivo C, Barion G, Vamerali T. Root characteristics and metal uptake of maize (*Zea mays* L.) under extreme soil contamination. Agronomy 2021;11(1):1-14.

Saulle CC, Raman V, Oliveira AVG, Maia BHL de NS, Meneghetti EK, Flores TB, et al. Anatomy and volatile oil chemistry of *Eucalyptus saligna* cultivated in South Brazil. Revista Brasileira de Farmacognisia 2018;28(2):Article No. 12534.

Seroja R, Effendi H, Hariyadi S. Tofu wastewater treatment using vetiver grass (*Vetiveria zizanioides*) and zeliac. Applied Water Science 2018;8(1):1-6.

Singh S, Das S, Geeta R. Role of cuticular wax in adaptation to abiotic stress: A molecular perspective. In: Abiotic Stress-Mediated Sensing and Signaling in Plants: An Omics Perspective. Springer Nature: 2018. p. 155-82.

Steffens B, Geske T, Sauter M. Aerenchyma formation in the rice stem and its promotion by H_2O_2. New Phytologist 2011;190(2):369-78.

Sutikno. Practical Guidance of Plant Microtechnique. Yogyakarta: Faculty of Biology Universitas Gadjah Mada; 2014. pp. 28-32. (in Indonesian).

Takarina ND, Pin TG. Bioconcentration factor (BCF) and Translocation factor (TF) of heavy metals in mangrove trees of Blanakan fish farm. Makara Journal of Science 2017;21(2):77-81.

Tao S, Khanizadeh S, Zhang H, Zhang S. Anatomy, ultrastructure and lignin distribution of stone cells in two *Pyrus* species. Plant Science 2009;176(3):413-9.

Thongchai A, Meeinkuirt W, Taeprayoon P, Chelong I. Effects of soil amendments on leaf anatomical characteristics of marigolds cultivated in cadmium-spiked soils. Scientific Report 2021;11(1):1-9.

Ziv C, Zhao Z, Gao YG, Xia Y. Multifunctional roles of plant cuticle during plant-pathogen interactions. Frontiers in Plant Science 2018;9:1-8.

Phosphorus Recovery and Bioavailability from Chemical Extraction of Municipal Wastewater Treatment's Waste Activated Sludge: A Case of Bangkok Metropolis, Thailand

Kay Thi Khaing[1,3], Chongchin Polprasert[1,3], Suwisa Mahasandana[1,3], Wanida Pimpeach[1,3], Withida Patthanaissaranukool[2,3], and Supawadee Polprasert[2,3*]

[1]Department of Sanitary Engineering Faculty of Public Health, Mahidol University, Rajvithee Road, Bangkok 10400, Thailand
[2]Department of Environmental Health Sciences, Faculty of Public Health, Mahidol University, Rajvithee Road, Bangkok 10400 Thailand
[3]Center of Excellence on Environmental Health and Toxicology (EHT), Ministry of Higher Education, Science, Research and Innovation, Bangkok 10400, Thailand

ARTICLE INFO

* Corresponding author:
E-mail:
supawadee.pol@mahidol.ac.th

ABSTRACT

This study evaluated the extractability and bioavailability of Phosphorus (P) recovered from waste activated sludge (WAS) so as to reduce dependence on the import of non-renewable P resources. P extraction was carried out using sulfuric acid (H_2SO_4). A response surface methodology was used to optimize conditions for the chemical leaching of WAS. The results showed the optimum condition for leaching WAS with 0.1 mol/L H_2SO_4 for 30 min, resulting in 97% P released. The efficiency of P recovery by P precipitation was associated with pH value and Mg:P. At pH 7, 9, and 11, P recovery was 92, 92, and 91% with uncontrolled Mg and 93, 93, and 92% with sea salt (Mg:P, 2:1), respectively. However, the yield of the produced struvite was much lower compared with that of added sea salt. From elemental analysis, the yield of struvite precipitated at pH 9 of Mg:P, 2:1 was about 26%, and the total P content of the precipitate was 12%. Available P was almost 80% after 35 days of operation, which was higher than that of commercial fertilizers. Results of this study are expected to provide fully comprehensive information to decision-makers regarding the suitability of implementing P-composite matter recovered from WAS. This will also help close the loop of the P cycle for food cultivation in the human ecosystem.

1. INTRODUCTION

Phosphorus (P) is an essential element for all living organisms and plays an important role as a fertilizing nutrient in agriculture. Moreover, P is one of the limited and nonrenewable resources and is required for food production (Withers et al., 2015). More than 85% of mined phosphate rock (PR), is used to produce P fertilizer (Geissler, 2015). Notably, the demand for P fertilizer for food production will increase significantly due to the growing world population, predicted to reach nine billion people in 2050 (Chen and Graedel, 2016; Geissler, 2015). PR is rapidly being depleted and is reserves are available in some geographical areas of the world such as Morocco, China and the USA (Van Vuuren et al., 2010). PR reserves are expected to dwindle in the next 50 to 100 years (Cordell and White,

2014). Consequently, P recovery from any P-rich residues has attracted considerable attention.

Among P-composite residues, domestic wastewater contains 5 to 20 g of P (in ortho-phosphates and organic compounds) in one cubic meter (Li et al., 2015). Biological nutrient removal is the most widely used technique to treat domestic wastewater. Phosphates are taken up in excess of normal metabolic requirements and then stored as intracellular bio-polymer polyphosphate (poly-P) within poly-P accumulating organisms (PAOs) (Chen et al., 2012; Wang et al., 2017). In the intervening time, PAOs are enriched by recirculating the waste activated sludge (WAS) (Kodera et al., 2013). Consequently, WAS, as a major byproduct derived from biological WWTP, accumulates a substantial amount of P leading to P

removal, in which over 90% of P is transferred to WAS (Balmer, 2004). Considering WAS is continuously produced in large amounts during biological nutrient removal (Wang et al., 2018; Xu et al., 2018; Zhao et al., 2017), P recovery from plentiful, inexpensive WAS has received increasing attention.

According to the work of Thitanuwat et al. (2016), P at the end of pipes in Bangkok Metropolitan Administration (BMA) was reported to come from domestic wastewater, septage sludge, and green garbage. Only 4% was recycled in public parks. In Bangkok, most solid wastes go directly to landfills, which are sinks for P resource and can potentially be used for P recycling. This constitutes 81% of discarded P. Moreover, an annual average of 2,116.7 t P is generated from domestic wastewater in the BMA. WAS is a major byproduct from WWTP in the BMA with 16.3 g P/kg or about 63% (456.1 t P/year) disposed in landfills. In addition, it also contains considerable amounts of P, about 356 mg P/L, together with components valuable for potential fertilizers such as Mg and Ca. WAS, on the other hand, is contaminated with human disease agents such as feces-borne coliform bacteria, viable helminth eggs, and active parasite cysts. Hence, fresh sewage sludge should not be disposed on land unless it has experienced pathogen diminishment (Sreesai et al., 2013). Therefore, direct application of WAS on agricultural fields is prohibited.

Although research on P recovery from sludge by struvite crystallization has been conducted, the method of effective P extraction from sludge requires further study. Finding economical and environmental-friendly methods to fully extract P from WAS is undoubtedly the first step to effectively recover P elements (Tong and Chen, 2009). Thus, many pretreatment processes of excess sludge have been developed. Wang et al. (2013) has reported that 92.8% of the P was recovered in the supernatant from electrochemical pretreatment (EPT) enhanced by anaerobic fermentation (AF) WAS. Leaching is the process of liquifying minerals to remove minerals from a solid. Leaching with acidic or alkaline solutions to recover P from sewage sludge ash and sewage sludge has been reported by (Fang et al., 2018; Shiba and Ntuli, 2017). Many different types of leaching agents include H_2SO_4 (Liang et al., 2019; Ottosen et al., 2013), HCl (Xu et al., 2012), HNO_3 (Gorazda et al., 2016; Sano et al., 2012), and oxalic acid (Liang et al., 2019). Among these extractants, H_2SO_4 is widely used because of its low cost and high efficiency

extraction yield. The factors affecting extraction of P by H_2SO_4 include reaction time, H_2SO_4 dosages, reaction temperature, and ratio of sludge/leachate (Fang et al., 2018; Shiba and Ntuli, 2017). Atienza-Martínez et al. (2014) used H_2SO_4 as the extraction agent, and the extraction yield of P from Sludge Incinerated Bottom Ash (SIBA) was 85% after 2 h reaction. Donatello et al. (2010) extracted P from SIBA with H_2SO_4 and obtained a P extraction yield of more than 80%. Based on these facts, H_2SO_4 was selected as the extraction agent in this study. Therefore, determining the effect of sludge chemical leaching methods on P recovery as struvite was necessary.

Recently, P recovery from wastewaters by chemical precipitation has been widely investigated. Struvite is a crystalline substance obtained from the input of chemicals including an alkali source for pH adjustment and an Mg source needed to achieve at least equimolar concentrations (1:1) of Mg^{2+} and PO_4^{3-} in the alkali pH solution. It could be used as P fertilizer or as a raw material for P-composite fertilizers (Rahman et al., 2014; Vaneeckhaute et al., 2017). Regardless of the total amount of P in the compost, the origin of the organic waste influences the type and fractions of P forms, which might alter P-bioavailability (Frossard et al., 2002). Due to the existence of low solubility P, struvite has been considered an excellent P fertilizer and is frequently described as a slow release fertilizer. (Ackerman et al., 2013; Talboys et al., 2016).

The aforementioned wastes comprise recoverable P, in which pre-treatment is needed to concentrate P from wastes prior to recovery process. However, very few studies in Thailand have been carried out to recover P before landfilling or incineration. Therefore, appropriate methods to recover P from such wastes to close the P cycle loop for production in the human ecosystem should be explored. Successful results of this study are expected to pave the way for implementing engineering processes for P recovery nationwide. These will help save the cost of imported fertilizer, and protect the environment from eutrophication, due to excessive P discharge. This study aimed (i) to evaluate the efficiency of chemical P extraction from WAS using sulfuric acid and study the feasibility of engineering and economic P recovery processes; (ii) to investigate speciation of P-composite materials obtained from precipitation of P-containing supernatants produced from chemical P extraction processes; and (iii) to

investigate the P-bioavailability from the recovered P product, in comparison with commercial fertilizers.

2. METHODOLOGY

2.1 Waste Activated Sludge (WAS)

The WAS used in this study was collected from the secondary sedimentation tank of Nong Khaem water quality control WWTP, BMA, Thailand. After collecting, the characteristics of WAS were measured, then stored in sealed plastic containers at 4°C, prior to use. The main characteristics of WAS are shown in Table 1, which demonstrates that the samples contained P, Ca, and Mg as major elements. The total solids (TS) content of WAS was diluted with distilled water to 3% of solid content, (w/v) which remains the average TS content found in general WAS (Zhang et al., 2020), to ensure consistency before acid leaching.

Table 1. Characteristics of waste activated sludge (WAS)

Parameter	Value	Unit
Total phosphorus (TP)	356.00±12.47	mg/L
Soluble phosphorus	48.05±0.37	mg/L
Chemical oxygen demand (COD)	16,304.00±10.30	mg/L
Magnesium (Mg)	155.37±0.06	mg/L
Ammonia (NH_3)	168.70±17.03	mg/L
Calcium (Ca)	226.93±2.00	mg/L
Total solids (TS)	35,100.00±24.30	mg/L
Percentage of volatile solids of total solids (VS)	52.28±3.40	%
Total suspended solids (TSS)	31,000.00±23.21	mg/L
Percentage of volatile suspended solids of total suspended solids (VSS)	53.72±2.27	%

2.2 Soil

The soil selected for this study was taken from the upper layer (depth 15 cm) of an agricultural field in Nakhon Pathom, Thailand. The soil was dried for 24 h at room temperature. The dried soil was sieved to obtain a fraction ≥1 cm. and P content was determined by the colorimetric method using vanadomolybdophosphoric acid and UV-spectrophotometer. The soil contained total P content of 0.005 mg/g dry weight.

2.3 Chemical leaching tests

In chemical leaching tests, 500 mL of WAS (3% of solids content) was mixed with H_2SO_4, to prepare four different concentrations of H_2SO_4 (0.01, 0.05, 0.10, and 0.50 mol/L). The mixture was stirred at 200 rpm using a Jar tester at ambient temperature (20 to 25°C). For P extraction, experiments were conducted in triplicate at varying reaction times (15, 30, 45, 60, 90, and 120 min). After leaching treatment, the mixture was separated using 10 µm filter paper (Whatman No. 93). Subsequently, the filtrates determined PO_4^{3-}, Mg, and Ca. The sludge residue was dried at 105°C for 24 h. After drying, it was used to analyze remaining P.

2.4 Optimization and prediction model

The response surface methodology (RSM) of Design Expert 13 Software licensed to the Faculty of Graduate Studies, Mahidol University was used to determine the optimum condition for the leaching process, which could be used to optimize the factors including reaction time and acid concentration (Anderson-Cook et al., 2009; Coetzer et al., 2018). The I-optimally with 16 runs was used. The interactions among the variables and responses to P extraction were determined from the analysis of variance (ANOVA). To quantify the quality of the quadratic prediction models, model terms statistical significance, coefficient of determination (R^2), probability (P-value) with 95% confidence level, and (t-test) at 5% significance level (Prob<0.05) were determined. Moreover, the 3D surface was created to identify the optimum region. Thus, a mathematical model was developed following a second order polynomial as shown in Equation (1).

$$Y = \beta_0 + \beta_i A + \beta_j B + \beta_{ii} A^2 + \beta_{jj} B^2 + \beta_{ij} AB \qquad (1)$$

Where; Y is percentage of P extraction response, β_0, β_i, β_j, β_{ii}, β_{jj}, and β_{ij} are constant, linear effect, quadratic effect, and interaction effect coefficients,

respectively; A and B represent the independent variables, viz., reaction time and acid concentration.

2.5 P precipitation

Precipitation tests were conducted for P recovery. The leachate obtained from the optimum condition of leaching process was used as the P-stock solution. In the experiment, two different Mg^{2+}:PO_4^{3-} molar ratios (1.07:1(uncontrolled) and 2:1 (sea salt addition)) were used. For Mg/P=2, sea salt was added as the external source of Mg. The pH of all cases was controlled at 7, 9, and 11 by dropwise addition of 50% sodium hydroxide solution at the beginning of each experiment. These experiments were conducted three times at ambient temperature. The stirring velocity was initially set at 3.33 Hz for 15 min, slow mixing at 1.25 Hz for 30 min, followed by settling for 1 h. After settling, the mixture was separated using a 10 µm filter (Whatman No. 93). Finally, the precipitates formed during this process were separated by filtration and oven dried at 103°C for 24 h. After that, the dried solid precipitates were determined for P-containing solids.

2.6 Phosphorus bioavailability procedures

Pot experiments were carried out to compare P-bioavailability of P-solids precipitates (PSP) obtained from this study with that of commercial fertilizers such as monophosphate (MP) and diammonium phosphate (DAP). The experiments were conducted in plastic pots (size 0.11 m × 0.005 m^2) filled with soil in triplicate for each experiment. Those three fertilizers were measured to 100 mg P per pot (15 g P/m^2). The control (blank) pot contained soil without added P fertilizer. The fertilizer in each pot and blank pot were dissolved with pH 6 tap water 90 mL daily equivalent to the amount of annual rainfall of the country. The experiments were generated until 35-day test duration. Samples were collected daily to analyze P content.

2.7 Analysis and calculations

The total Kjeldahl nitrogen (TKN), TS, VS, TSS, VSS, COD, and total ammonia nitrogen concentrations were measured according to standard methods (APHA, 2012). Mg and Ca were measured with an atomic adsorption spectrophotometer. Data were expressed using mean value and standard deviations (SD). Independent T test and One-way analysis of variance (ANOVA) were used to determine whether statistically significant differences existed among the leaching experiments, 16 runs for acid leaching of P recovery, P-bioavailability and

percentage P content in solids and liquids. All tests were performed using SPSS Software, 18.0 for Windows licensed to Mahidol University.

2.7.1 P recovery

The P recovery efficiency defined in Equation (2) was determined by the difference of initial and final PO_4^{3-} concentrations in experiments, as shown in Equation (2).

$$(\%) \ P_{recovery} = \left[\frac{[PO_4^{3-}-P]_{initial}-[PO_4^{3-}-P]_{final}}{[PO_4^{3-}-P]_{initial}}\right] \times 100 \qquad (2)$$

Where; $[PO_4^{3-} - P]_{initial}$ is the initial phosphate concentrations, mg/L and $[PO_4^{3-} - P]_{final}$ is final phosphate concentrations, mg/L.

2.7.2 Phosphorus crystal content

Phosphorus crystal content was calculated, following Equation (3).

$$P \ crystal \ content \ (\%) = \left[\frac{C_s \times MW \ of \ P \ crystal}{M}\right] \times 100 \qquad (3)$$

Where; Cs is the molar concentration of limiting ions (mol/L), the molecular weight of P crystal formed (g/mol) and M is the number of solids formed in the precipitation experiment (g/L).

2.7.3 P bioavailability

P bioavailability was computed, as shown in Equation (4).

$$\% \ P \ release \ efficiency = \frac{P_{mix,t} - Blank_t}{P_{initial}} \times 100 \qquad (4)$$

Where; $P_{mix,t}$ is the mixed concentrations of dissolved P from the pot at time=t, mg, $P_{initial}$ is start phosphorus concentrations (mg) in each fertilizer, Blank^t is dissolved P concentration of soil (Blank pot) at time=t (mg).

3. RESULTS AND DISCUSSION

3.1 Optimization of the extraction parameters by RSM and ANOVA

The results collected from these experiments were fitted in a quadratic polynomial model and regression coefficients obtained. To determine the best model for the response (%P extraction), standard deviations, the predicted sum of squares, and R-squared values were compared (Cornell et al., 2011; Iweka et al., 2021).

The resulting ANOVA data are shown in Table 2. It could be seen that the significant model terms

comprised time (A), acid concentration (B), the two-level interactions of time and acid concentration (A×B) and the quadratic effect of acid concentration (B^2) indicating that those terms greatly influenced %P extraction. Based on the mathematical calculations for a good-fit model, the amount of the variation in the response must be close to one (Onsekizoglu et al., 2010). According to the correlation coefficients (R^2) value obtained in this study for P extraction was 0.9889; a good fit between models and experimental data could be concluded. Moreover, the adjusted correlation coefficient, R^2 (adj) was 0.9833. F-tests for "lack of fit" were used to assess the model's suitability. The "lack of fit" in P extraction, was insignificant, with F-value of 0.7080 and p-value of 0.6430, respectively. This confirmed the model's suitability for explaining this process (Falowo et al., 2019). To make predictions about the response for given levels of each factor, an equation in terms of coded factors could be used. In other words, this equation is useful where identifying the relative influence of a factor is important and is accomplished through comparing the factor coefficients against one another. Effective mathematical models as functions of the coded variables for P extraction have been proposed as shown in Equation (5):

$$\%P \text{ extraction} = +121.25 + 32.20A + 285B - 1.38AB - 53.25A^2 - 1.6B^2 \quad (5)$$

Where; A is the reaction time (min), B is the acid concentration for chemical leaching (mol/L), for extraction P (min). This equation describes the created

model and gives solutions for the dependent variable based on the independent variable combinations, whether they are significant in the response. Optimization of the reaction parameters by response surface methodology (RSM) described by the regression model in Figure 1. Based on the above discussed, both time and acid concentration are important factors for the leaching efficiency of P. The Figure also shows that increasing acid concentration and time affected into increased %P extraction efficiency. However, the leaching efficiency decreases slightly when acid concentration increased above 0.45 (mol/L). As can be seen, this model forecast that optimum values to obtain the highest value of P extraction are: 30 min of reaction time and 0.1 (mol/L) of acid concentration.
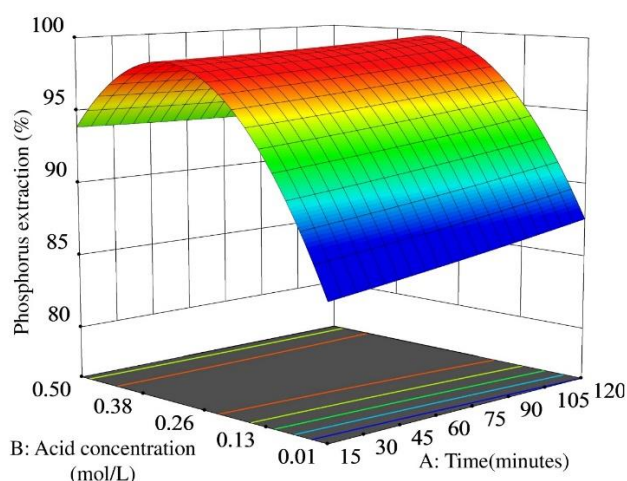
Figure 1. 3D-surface plot for P-extraction in respect to the most influential parameters, i.e., Time and acid concentration (ambient temperature).

Table 2. Analysis of variance table for P extraction

Source	Sum of squares	df	Mean square	F-value	p-value	
Model	6463.56	5	1292.71	177.39	<0.0001	Significant
A-Time	171.37	1	171.37	23.52	0.0007	
B-Acid concentration	5036.23	1	5036.23	691.10	<0.0001	
AB	39.54	1	39.54	5.43	0.0421	
A²	9.25	1	9.25	1.27	0.2861	
B²	3854.31	1	3854.31	528.91	<0.0001	
Residual	72.87	10	7.29			
Lack of Fit	30.21	5	6.04	0.7080	0.6430	Not significant
Pure Error	42.67	5	8.53			
Cor. Total	6536.44	15				
			R²	0.9889		
Std. Dev.	2.70		Adjusted R²	0.9833		
Mean	83.81		Predicted R²	0.9783		
C.V. %	3.22		Adeq. Precision	35.1792		

3.2 P recovery via precipitation and P-containing solids speciation

To confirm the feasibility of P recovery from WAS as magnesium ammonium phosphate (MAP) and hydroxyapatite (HAP), P crystallization from the leachate obtained from the optimum condition (0.1 mol/L, 30 min) followed by speciation of precipitates formed were conducted. The reactions of MAP and HAP and their solubility product constants are presented in Equations (6) and (7), respectively.

$$MgNH_4PO_4(s) \rightleftharpoons Mg^{2+}(aq) + NH_4^+(aq) + PO_4^{3-}(aq) \quad (6)$$

$$Ca_3(PO_4)_2(s) \rightleftharpoons 3Ca^{2+}(aq) + 2PO_4^{3-}(aq) \quad (7)$$
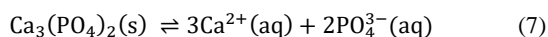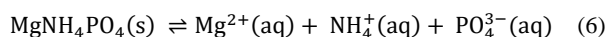
As illustrated in Figure 2, the efficiencies of P recovery from the WAS leachate under uncontrolled magnesium (Mg/P=1.07) were 92, 92, and 91% at pH 7, 9, and 11, respectively. Similarly, for sea salt addition (Mg/P=2), the P recovery efficiencies at pH 7, 9, and 11 were 93, 93, and 92%, respectively. These results indicate that both pH and molar ratio of Mg/P do not affect the %P extraction. However, it is obvious that efficiencies of P recovery for all cases decreased when using pH=11. Previous studies found that a wide range of molar ratios of Mg/P can be used for struvite precipitation (Khaita and Polprasert, 2019; Pinatha et al., 2020). In addition, P recovery efficiency was highly influenced by Mg/P ratios (Maekawa et al., 1995). Perera et al. (2007) reported that increasing the molar ratio of Mg/P increases supersaturation, resulting in more nucleation and crystal growth, but the final pH limits any further precipitation. Similarly,

the work of Beal et al. (1999) found that recovery P from swine waste as struvite could be increased with increasing of molar ratio of Mg/P from 0.25 to 1.1 using MgO addition with pH more than 8. Moreover, some studies showed that the Mg source is one factor affecting struvite precipitation. Barbosa et al. (2016) investigated the effect of different Mg sources on P crystallization efficiency from source separated urine, 99% P recovered as struvite was achieved when using MgO as Mg source. However, the different finding may be that the different type of supernatants used in P recovery.

The percentage of various types P-containing solids generated from this experiment also was calculated based on the proportion of P in each compound detected. Based on the results, the %MAP increased when sea salt addition was applied. The higher MAP% was found with sea salt addition (Mg/P=2) while the percentage of MAP were only 2 to 5% for uncontrolled Mg (Mg/P=1.07) at pH 7, 9, and 11. The highest MAP of 26% was found at pH 9 under addition of sea salt (Mg/P=2). This would mean that molar ratio of Mg/P affected to the formation of MAP in this study.

In case of %HAP, the results also show that %HAP under sea salt addition was higher than uncontrolled Mg condition, 8-12% of HAP for Mg/P=2 and 3-5% of HAP for Mg/P=1.07. As discussed above, pH 9 with the addition of sea salt was chosen to be an optimum condition for production of P-containing solids which was used in the P-bioavailability.

Figure 2. Speciation of P-composite precipitates recovered from WAS under different experimental conditions.
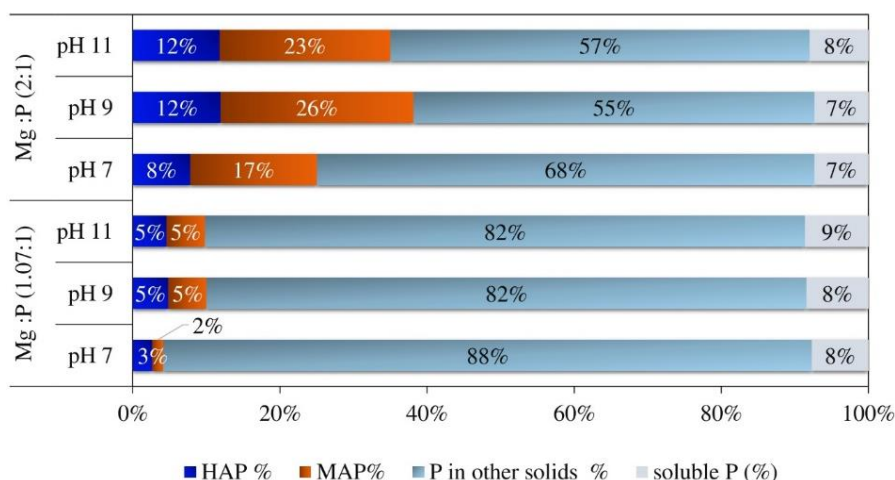
This paper was selected from the Environment and Natural Resources International Conference (ENRIC 2021) which was held during 16th December 2021 in Thailand

374

3.3 P recovery as different P fertilizer

The percentage of P content in the precipitates is an important measure for developing an alternative P fertilizer. Table 3 shows a comparison of the percent P content in the solids precipitated from this study and the commercial P fertilizers. The percent P content in the precipitates was in the range of 7-12% for both uncontrolled magnesium (Mg/P=1.07) and sea salt addition (Mg/P=2) with pH from 7 to 11. The highest %P in solids for all cases were found at pH 9, 11% P in solids for Mg/P=1.07 and 12% P in solids for Mg/P=2, which were higher than that of commercial superphosphate (SSP) fertilizer (8.8% P). Therefore, the P-containing solids obtained from both experiments can be used as an alternative P fertilizer. In addition, the precipitates from other experiments with P content less than 8.80% can be used as soil conditioner due to their good nutrient qualities, especially P (Lind et al., 2000). Hence, P-solids precipitates obtained from WAS can be effectively used to produce fertilizer for agricultural crops to achieve the sustainable P management helps to strengthen Thailand's food security.

Table 3. A comparison of P content in solid precipitate of this study and commercial P fertilizers

P recovery from WAS (This study)			Commercial P fertilizer			
Mg/P ratios	pH	%P content in solid precipitate (%dry wt.)	P fertilizer	Formula	%P_2O_5	%P
1.07	pH 7	8	Superphosphate	0-20-0	20	8.80
	pH 9	11	Triple super-phosphate	0-46-0	46	20.24
	pH 11	7	Diammonium phosphate	18-46-0	46	20.24
2	pH 7	11	Monoammonium phosphate	11-52-0	52	22.88
	pH 9	12				
	pH 11	9				

3.4 P bioavailability from WAS recovered product

Comparison of P-bioavailability of P-solids precipitates (PSP) obtained from WAS and commercial fertilizers including DAP and MP was determined by solubility of P compounds in water at pH 6.15 g P/m² of these P-fertilizers was dissolved in 90 mL of water for 35-day as shown in Figure 3. The results showed that the highest %P release (more than 5%) was found when DAP was applied. Moreover, %P release from DAP increased with increasing time of dissolution. However, it decreased after dissolution for one week. Compared with DAP, MP has lower %P dissolved efficiency (below 3%). It then slightly decreased after the fifth day. However, for PSP, the results showed that an increase in time provides high %P release efficiency. The highest %P dissolved (nearly 4%) from PSP was found at the middle of the experimental period (Day 17th) and it then dropped lower than 1%. The results indicate that P from both DAP and MP were fast-release fertilizers which is may be inappropriate for growth of plants. At the end of experiment, the amount of P released along with water dissolution (pH 6) was calculated so as to evaluate the amount of P that remained in the pot. The DAP, MAP, and P-precipitating solid were 47%, 31%, and 20% soluble into water after 35 days, respectively. The amount of P remaining in the soil is 7.92 g P/m² of DAP, 10.32 g P/m² of MP and 11.80 g P/m² of PSP which means that about 53%, 69%, and 80% of P in commercial fertilizers (DAP and MP) and PSP remained in the soil, respectively, indicating that PSP has the highest bioavailability for plant uptake.

3.5 Economic assessment

Finally, to complete the results of this study, the analysis of the costs of P recovery process and the possible gains from the sale of the resulting product have been calculated based on the method by Pinatha et al. (2020). Table 4 depicts the potential economic savings for P recovery from the leachate obtained at the optimum condition. The results showed that the highest P-containing precipitates of 0.23 kg P/m³ was found when using pH 9 with sea salt addition. It noted P-containing solids based on the amount of produced precipitates and %P content in solids. The results also found that the precipitates contained 8% and 7% P content were achieved at pH 7 and pH 11 with molar ratio of Mg:P=1.07:1.00. However, the higher amount of precipitates was obtained from pH 11. This resulted in the amount of P-containing solids at pH 7 was lower than pH 11 with the same Mg:P ratio (1.07:1.00). Chemical additions, especially sulfuric acid, are the

This paper was selected from the Environment and Natural Resources International Conference (ENRIC 2021) which was held during 16th December 2021 in Thailand

375

major costs of the process due to the extraction of P (pH lower than 1). This also resulted in the large amount of 50% NaOH used to adjust pH in the step of precipitation at pH 7 to 11. Therefore, when average costs in the unit of USD/kg P were compared with the market price of commercial fertilizers, the lowest average costs were found with the addition of sea salt

at pH 9. This indicates that sea salt addition can reduce the total costs that mostly came from acid addition by increasing both the production of precipitates and %P in solids. Thus, additional economic savings could also be possible when the market fertilizer price in the future is higher than the average costs obtained.
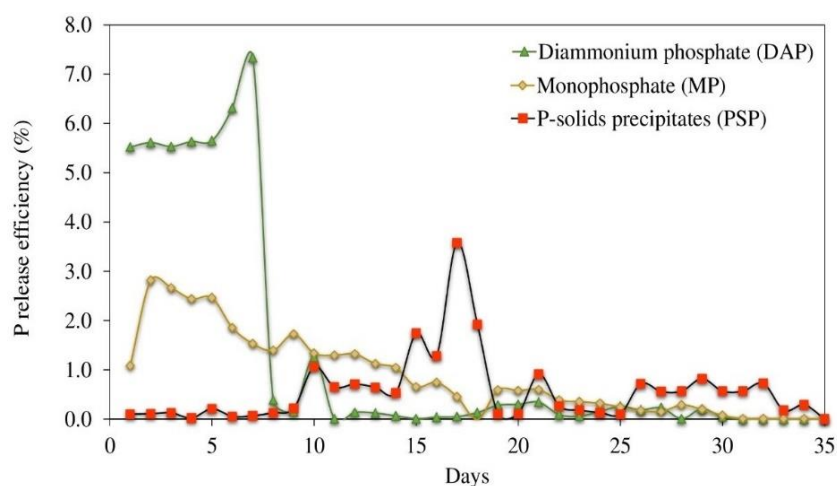
Figure 3. Percentage of P release efficiency for P-bioavailability test (%)

Table 4. Cost analysis of P recovery process using different pH and molar ratio of Mg/P.

Parameters	pH 7		pH 9		pH 11	
	(1.07:1)	(2:1)	(1.07:1)	(2:1)	(1.07:1)	(2:1)
Chemical additions (kg/m^3)						
Acid H_2SO_4	10.30	10.30	10.30	10.30	10.30	10.30
NaOH 50%	1.44	1.44	1.52	1.52	2.28	2.28
Sea salt	0.00	0.33	0.00	0.33	0.00	0.33
Material costs (USD/kg)						
Mg source (sea salt)[a]	0.06	0.06	0.06	0.06	0.06	0.06
50% NaOH[b]	0.20	0.20	0.20	0.20	0.20	0.20
Acid H_2SO_4[c]	0.18	0.18	0.18	0.18	0.18	0.18
Waste activated sludge	0.00	0.00	0.00	0.00	0.00	0.00
Energy consumption (kWh/m^3)						
Rapid mixing (15 min)	0.0626	0.0626	0.0626	0.0626	0.0626	0.0626
Slow mixing (30 min)	0.0013	0.0013	0.0013	0.0013	0.0013	0.0013
Electricity cost per unit (USD kW/h)[d]	0.12	0.12	0.12	0.12	0.12	0.12
Products produced (kg/m^3)						
Obtained solids from precipitation	1.03	1.30	1.11	1.88	1.20	1.60
%P content in solids precipitate	8.00	11.00	11.00	12.00	7.00	9.00
P-containing solids (kg P/m^3)	0.082	0.150	0.120	0.230	0.084	0.140
Total costs (USD/kg P)						
(1) Average costs	25.78	14.17	17.40	9.56	26.53	16.03
(2) Market fertilizer prize[e]	3.52±5.00	3.52±5.00	3.52±5.00	3.52±5.00	3.52±5.00	3.52±5.00
(2)-(1) Profit margin	-22±-21	-11±-9	-14±-12	-6±5	-23±-22	-13±-11

±Standard division

[a]Snowy Sky, Xuetian Salt Group Co., Ltd, China (https://www.alibaba.com)

[b]50% AMPS SODIUM SALT Solution, Shandong Kejian Chemical Co., China (https://www.alibaba.com)

[c]RCI LABSCAN LIMITED, Thailand (https://www.rcilabscan.com/product/sulfuric-acid-98-electropure/)

[d]Thailand's electricity cost from Metropolitan Electricity Authority (www.mea.or.th)

[e]OAE.go.th (Lowest price for N-P-K formula 18-46-0 and highest price for formula 16-16-8; P as P_2O_5 and K as K_2O).

4. CONCLUSION

P recovery from WAS, using chemical leaching and precipitation with sea salt addition, appears to be a promising method for recovering the limiting nutrient P. The optimum condition for P leaching (0.1 mol/L H_2SO_4, 30 min) found from RSM could achieved nearly 100% P extraction efficiency. The highest P recovery efficiency (%) was found at pH 9 with sea salt addition, resulting in 26% MAP formed. The precipitating solids contained about 12% P. Moreover, the percentage bioavailability of P uptake from WAS-recovered solid P was about 80%, which is much better than those of commercial fertilizers. This indicates that recovered P-solids from WAS is technically feasible to be utilized as fertilizing compound for plant cultivation and the sustainable P management helps to strengthen Thailand's food security. Therefore, the results found in this study will help understand P leaching and precipitating from WAS and guide decision-makers for its implementation. Consequently, this will lead to closing the loop of P-for-food management in the human ecosystem.

ACKNOWLEDGEMENTS

REFERENCES

Ackerman JN, Zvomuya F, Cicek N, Flaten D. Evaluation of manure-derived struvite as a phosphorus source for canola. Canadian Journal of Plant Science 2013;93(3):419-24.

American Public Health Association (APHA). Standard Methods for the Examination of Water and Waste Water. 22nd ed. Washington, DC, USA: APHA; 2012.

Anderson-Cook CM, Borror CM, Montgomery DC. Response surface design evaluation and comparison. Journal of Statistical Planning and Inference 2009;139(2):629-41.

Atienza-Martínez M, Gea G, Arauzo J, Kersten SR, Kootstra AMJJb. Phosphorus recovery from sewage sludge char ash. Bioenergy 2014;65:42-50.

Balmer P. Phosphorus recovery: An overview of potentials and possibilities. Water Science and Technology 2004;49(10):185-90.

Barbosa SG, Peixoto L, Meulman B, Alves MM, Pereira MA. A design of experiments to assess phosphorous removal and crystal properties in struvite precipitation of source separated urine using different Mg sources. Chemical Engineering Journal 2016;298:146-53.

Beal LJ, Burns RT, Stalder KJ. Effect of anaerobic digestion on struvite production for nutrient removal from swine waste prior to land application. Proceedings of the ASAE Annual International Meeting; 1999 July 18-21; Sheraton Centre: Canada; 1999.

Chen M, Graedel T. A half-century of global phosphorus flows, stocks, production, consumption, recycling, and environmental impacts. Global Environmental Change 2016;36:139-52.

Chen Y, Wang D, Zhu X, Zheng X, Feng L. Long-term effects of copper nanoparticles on wastewater biological nutrient removal and N_2O generation in the activated sludge process. Environmental Science and Technology 2012;46(22):12452-8.

Coetzer R, Joubert T, Viljoen C, Nel R, Strydom C. Response surface models for synthetic jet fuel properties. Applied Petrochemical Research 2018;8(1):39-53.

Cordell D, White S. Life's bottleneck: Sustaining the world's phosphorus for a food secure future. Annual Review of Environment and Resources 2014;39:161-88.

Cornell JA. Experiments with Mixtures: Designs, Models, and the Analysis of Mixture Data. Volume 403. John Wiley and Sons; 2011.

Donatello S, Freeman-Pask A, Tyrer M, Cheeseman CJC. Effect of milling and acid washing on the pozzolanic activity of incinerator sewage sludge ash. Composites Part C 2010;32(1):54-61.

Falowo OA, Oloko-Oba MI, Betiku E. Biodiesel production intensification via microwave irradiation-assisted trans-esterification of oil blend using nanoparticles from elephant-ear tree pod husk as a base heterogeneous catalyst. Chemical Engineering and Processing-Process Intensification 2019; 140:157-70.

Fang L, Li, Guo MZ, Cheeseman CR, Tsang DCW, Donatello S, et al. Phosphorus recovery and leaching of trace elements from incinerated sewage sludge ash (ISSA). Chemosphere. 2018;193:278-87.

Frossard E, Skrabal P, Sinaj S, Bangerter F, Traore O. Forms and exchangeability of inorganic phosphate in composted solid organic wastes. Nutrient Cycling in Agroecosystems 2002;62(2):103-13.

Geissler B, Mew MC, Weber O, Steiner G. Efficiency performance of the world's leading corporations in phosphate rock mining. Resources, Conservation and Recycling 2015;105:246-58.

Gorazda K, Tarko B, Wzorek Z, Nowak AK, Kulczycka J, Henclik AJOC. Characteristic of wet method of phosphorus recovery from polish sewage sludge ash with nitric acid. Open Chemistry 2016;14(1):37-45.

Iweka SC, Owuama K, Chukwuneke JL, Falowo OA. Optimization of biogas yield from anaerobic co-digestion of corn-chaff and cow dung digestate: RSM and python approach. Heliyon 2021;7(11):e08255.

Khaita C, Polprasert C. Effect of organic matter on struvite precipitation of phosphorus contained in tapioca-starch wastewater. Thai Environmental Engineering Journal 2019; 33(1):31-9.

This paper was selected from the Environment and Natural Resources International Conference (ENRIC 2021) which was held during 16th December 2021 in Thailand

Kodera H, Hatamoto M, Abe K, Kindaichi T, Ozaki N, Ohashi A. Phosphate recovery as concentrated solution from treated wastewater by a PAO- enriched biofilm reactor. Water Research 2013;47(6):2025-32.

Li WW, Yu HQ, Rittmann BE. Chemistry: Reuse water pollutants. Nature 2015;528:29-31.

Liang S, Chen H, Zeng X, Li Z, Yu W, Xiao K, et al. A comparison between sulfuric acid and oxalic acid leaching with subsequent purification and precipitation for phosphorus recovery from sewage sludge incineration ash. Water Research 2019; 159:242-51.

Lind B-B, Ban Z, Bydén S. Nutrient recovery from human urine by struvite crystallization with ammonia adsorption on zeolite and wollastonite. Bioresource Technology 2000;73(2):169-74.

Maekawa T, Liao CM, Feng XD. Nitrogen and phosphorus removal for swine wastewater using intermittent aeration batch reactor followed by ammonium crystallization process. Water Research 1995;29(12):2643-50.

Onsekizoglu P, Bahceci KS, Acar J. The use of factorial design for modeling membrane distillation. Journal of Membrane Science 2010;349(1-2):225-30.

Ottosen LM, Kirkelund GM, Jensen PE. Extracting phosphorous from incinerated sewage sludge ash rich in iron or aluminum. Chemosphere 2013;91(7):963-9.

Perera P, Han ZY, Chen YX, Wu WX. Recovery of nitrogen and phosphorous as struvite from swine waste biogas digester effluent. Biomedical and Environmental Sciences 2007; 20(5):343-50.

Pinatha Y, Polprasert C, Englande Jr AJ. Product and cost perspectives of phosphorus recovery from human urine using solid waste ash and sea salt addition: A case of Thailand. Science of the Total Environment 2020;713:Article No. 136514.

Rahman MM, Salleh MAM, Rashid U, Ahsan A, Hossain MM, Ra CS. Production of slow release crystal fertilizer from wastewaters through struvite crystallization: A review. Arabian Journal of Chemistry 2014;7(1):139-55.

Sano A, Kanomata M, Inoue H, Sugiura N, Xu KQ, Inamori YJC. Extraction of raw sewage sludge containing iron phosphate for phosphorus recovery. Chemosphere 2012;89(10):1243-7.

Shiba NC, Ntuli F. Extraction and precipitation of phosphorus from sewage sludge. Waste Management 2017;60:191-200.

Sreesai S, Peapueng P, Tippayamongkonkun T, Sthiannopkao S. Assessment of a potential agricultural application of Bangkok-digested sewage sludge and finished compost products. Waste Management and Research 2013;31(9):925-36.

Talboys PJ, Heppell J, Roose T, Healey JR, Jones DL, Withers PJ. Struvite: A slow-release fertiliser for sustainable phosphorus management? Plant and Soil 2016;401(1-2):109-23.

Thitanuwat B, Polprasert C, Englande Jr AJ. Quantification of phosphorus flows throughout the consumption system of Bangkok Metropolis, Thailand. Science of the Total Environment 2016;542:1106-16.

Tong J, Chen Y. Recovery of nitrogen and phosphorus from alkaline fermentation liquid of waste activated sludge and application of the fermentation liquid to promote biological municipal wastewater treatment. Water Research 2009; 43(12):2969-76.

Van Vuuren DP, Bouwman AF, Beusen AH. Phosphorus demand for the 1970-2100 period: A scenario analysis of resource depletion. Global Environmental Change 2010;20(3):428-39.

Vaneeckhaute C, Lebuf V, Michels E, Belia E, Vanrolleghem PA, Tack FM, et al. Nutrient recovery from digestate: Systematic technology review and product classification. Waste and Biomass Valorization 2017;8(1):21-40.

Wang Q, Li Js, Tang P, Fang L, Poon CS. Sustainable reclamation of phosphorus from incinerated sewage sludge ash as value-added struvite by chemical extraction, purification and crystallization. Journal of Cleaner Production 2018;181: 717-25.

Wang D, Fu Q, Xu Q, Liu Y, Ngo HH, Yang Q, et al. Free nitrous acid- based nitrifying sludge treatment in a two-sludge system enhances nutrient removal from low-carbon wastewater. Bioresource Technology 2017;244:920-8.

Wang X, Wang Y, Zhang X, Feng H, Li C, Xu T. Phosphate recovery from excess sludge by conventional electrodialysis (CED) and electrodialysis with bipolar membranes (EDBM). Industrial and Engineering Chemistry Research 2013;52(45):15896-904.

Withers PJ, Elser JJ, Hilton J, Ohtake H, Schipper WJ, Van Dijk KC. Greening the global phosphorus cycle: How green chemistry can help achieve planetary P sustainability. Green Chemistry 2015;17(4):2087-99.

Xu D-C, Zhong C-Q, Yin K-H, Peng S-H, Zhu T-T, Cheng G. Alkaline solubilization of excess mixed sludge and the recovery of released phosphorus as magnesium ammonium phosphate. Bioresource Technology 2018;249:783-90.

Xu H, He P, Gu W, Wang G, Shao L. Recovery of phosphorus as struvite from sewage sludge ash. Journal of Environmental Sciences 2012;24(8):1533-8.

Zhang L, Chen Y, Ma C, Liu L, Pan J, Li B, et al. Improving heavy metals removal, dewaterability and pathogen removal of waste activated sludge using enhanced chemical leaching. Journal of Cleaner Production 2020;271:Article No. 122512.

Zhao J, Gui L, Wang Q, Liu Y, Wang D, Ni BJ, et al. Aged refuse enhances anaerobic digestion of waste activated sludge. Water Research 2017;123:724-33.

Diversity and Antimicrobial Activity of Plant Growth Promoting Endophytic Actinomycetes Isolated from Thai Orchids

Nisachon Tedsree[1], Kittisak Likhitwitayawuid[2], Boonchoo Sritularak[2], and Somboon Tanasupawat[1*]

[1]*Department of Biochemistry and Microbiology, Faculty of Pharmaceutical Sciences, Chulalongkorn University, Bangkok 10330, Thailand*

[2]*Department of Pharmacognosy and Pharmaceutical Botany, Faculty of Pharmaceutical Sciences, Chulalongkorn University, Bangkok 10330, Thailand*

ARTICLE INFO

* Corresponding author:
E-mail: Somboon.T@chula.ac.th

ABSTRACT

Thirty-two endophytic actinomycetes isolated from 15 Thai orchids were taxonomically studied based on their phenotypic characteristics and 16S rRNA gene sequence analyses (98.97-100.00%). The isolates were identified as *Streptomyces* including *S. parvulus* (3 isolates), *S. tendae* (2 isolates), *S. ardesiacus* (2 isolates), *S. heilongjiangensis* (2 isolates), and each of *S. daghestanicus*, *S. antibioticus*, *S. malaysiensis*, *S. deserti*, *S. spiralis*, *S. thermoviolaceus* subsp. *apingens*, *S. globosus*, *S. collinus*, *S. olivaceus*, and *S. zaomyceticus*. *Micromonospora* including *M. humi* (2 isolates), *M. maritima* (2 isolates), and each of *M. tulbaghiae*, *M. schwarzwaldensis*, *M. chersina*, *M. chalcea M. citrea*, and *M. aurantiaca*; *Streptosporangium* (2 isolates) including *S. sandarakinum* and *S. pseudovulgare* and an isolate of *Actinomadura hibisca*. *Streptomyces* (7 isolates), *Micromonospora* (7 isolates), and *Streptosporangium* (1 isolate) exhibited antimicrobial activity against *Bacillus subtilis* ATCC 6633, *Kocuria rhizophila* ATCC 9341, *Staphylococcus aureus* ATCC 25923, *Escherichia coli* ATCC 25922, *Pseudomonas aeruginosa* ATCC 27853, and *Candida albicans* ATCC 10231. Indole-3-acetic acid (IAA) production of the isolates ranged from 0.04 to 67.30 µg/mL. Isolates DR10-1 and DR9-7 produced high amounts of IAA (58.03 and 67.30 µg/mL) and were selected for optimization. Maximum IAA values obtained were 284.87 and 132.35 µg/mL, using 0.4% L-tryptophan and pH 7 with incubation at 30°C for 13 days. These two isolates enhanced root length, shoot length, number of roots, and fresh weight of rice seedlings (*Oryza sativa* L. cv. RD49) compared to the control. Results indicated that actinomycetes from Thai orchids were promising sources of antimicrobial compounds and plant hormones for agricultural applications.

1. INTRODUCTION

Actinomycetes are Gram-positive filamentous bacteria having a high guanine (G) and cytosine (C) content in their genomic DNA (Stackebrandt et al., 1997). Research has demonstrated that they are generally safe and beneficial microorganisms in the pharmaceutical and agricultural industries as antimicrobials, antimalarials, anticancer, enzymes, pesticides, and plant growth hormones (Berdy, 2005; Flores-Gallegos and Nava-Reyna, 2019). Plant-associated microbes create substances with significant medicinal potential (Wu et al., 2021), while endophytes are commonly distributed in nature and maintain unique associations with host plants (Nair and Padmavathy, 2014), leading to the development of safer products for the environment and human health. Endophytic actinobacteria have been found in various plants, including the predominant *Streptomyces* and the genera *Micromonospora*, *Microbispora*, *Nocardia*, *Nocardioides,* and *Streptosporangium* (Shimizu, 2011), *Streptomyces platensis* 3-10 from healthy rice (Shakeel et al., 2016) and *Streptomyces* sp. KLBMP 5084 from healthy *Limonium sinense* (Qin et al., 2017).

Dendrobium, is the second largest genus of orchid in the family Orchidaceae (Puchooa, 2004)

which contains approximately 1,100 species. They are mainly distributed in the subtropical and tropical regions of Asia and Oceania (Xiang et al., 2013). Since ancient times, many *Dendrobium* plants have been used as ingredients for nutraceutical beverages and food products (Bao et al., 2001). Orchids have been shown to generate a wide range of bioactive substances including antibiotics, anticancer, antitumor, antioxidant, and anti-infection agents, demonstrating a crucial impact on drug discovery. The methanol extract from the whole plant of *Dendrobium harveyanum* had a high anti-lipase effect (Maitreesophone et al., 2022), while the crude extract from *D. venustum* showed antimalarial and anti-herpetic activities (Sukphan et al., 2014). The gigantol from *Dendrobium draconis* exhibited pharmacological activity (Charoenrungruang et al., 2014), while moscatilin, gigantol, lusianthridin, and dendroflorin from *D. brymerianum* (Klongkumnuankarn et al., 2015) showed cytotoxicity against human lung cancer cell lines. Dendroparishiol, a new compound from *D. parishii*, has shown high antioxidant activities (Kongkatitham et al., 2018). Recently, orchid-associated microorganisms have been found on orchid roots. They assist plants to solubilize important nutrients, create a variety of metabolites and control phytopathogenic fungi (Herrera et al., 2022). The endophytic bacterium strain PVL1 isolated from the leaf of the orchid *Vanda cristata* promoted the growth of *Cymbidium aloifolium* by IAA (Shah et al., 2021), while fungal endophytes isolated from *Dendrobium officinale* (Wu et al., 2016) and *D. devonianum* (Xing et al., 2011) were great sources for the prevention and treatment of harmful fungi and bacteria.

Plant-microbial interactions have been extensively researched. However, the variety and functional activity of orchid-associated bacteria are little understood. In Thailand, orchid species rich in fungi and endophytic organisms established in the tissues of terrestrial orchids have been found to follow a seasonal rhythm (Chutima et al., 2011). Investigation of endophytic actinomycetes might lead to the discovery of new species, their biological activity and secondary metabolites. In this study, endophytic actinomycetes were isolated from selected Thai orchids and characterized based on their phenotypic, chemotaxonomic and genetic characteristics. Their antibacterial activity and the plant growth promoting IAA production were also evaluated.

2. METHODOLOGY
2.1 Sampling and isolation

Endophytic actinomycetes were isolated from the roots of fifteen species of Thai orchids: *Dendrobium christyanum*, *D. formosum*, *D. kentrophyllum*, *D. findlayanum*, *D. chrysanthum*, *Calanthe cardioglossa*, *D. friedericksianum*, *D. chrysotoxum*, *D. crumenatum*, *D. heterocarpum*, *Coelogyne lawrenceana*, *Eria ornate*, *Cleisostoma rostratum*, *Coelogyne assamica*, and *Pinalia globulifera*. All endophytic actinomycete isolates were characterized based on their phenotypic, chemotaxonomic, and genetic characteristics, as well as their antibacterial activity and indole-3-acetic acid (IAA) production. The orchid roots were prepared according to Tedsree et al. (2021). The suspension of bacteria was serially diluted ten times. Each diluted suspension was applied to a different medium including gellan gum, Gause synthetic No.1 (Gause et al., 1983), glycerol arginine (Arai, 1975), and starch casein (Küster and Williams, 1964) supplemented with nalidixic acid (25 µg/mL) and cycloheximide (50 µg/mL). All the plates were incubated at 30°C for 20 to 30 days. The purified isolates were preserved on ISP 2 and freeze-dried for long-term preservation.

2.2 Characterization of endophytic actinomycetes

Morphological and cultural characteristics of isolates were observed on ISP 2 agar as described previously (Shirling and Gottlieb, 1966). The NBS/IBCC color system was used to determine the colors of aerial mycelia, substrate mycelia and diffusible pigment (Kelly, 1964). Physiological characteristics, including growth at different temperatures (20-45°C), NaCl concentrations (0-10%, w/v), and pH range 4-12 (at intervals of 1 pH unit) were evaluated in ISP 2 broth at 30°C for 14 days. Carbon utilization on ISP 9 supplemented with 1% (w/v) carbon sources, starch hydrolysis, nitrate reduction, milk coagulation and peptonization, and gelatin liquefaction were examined as described by Arai (1975). The method of Staneck and Roberts (1974) was used to analyze the isomers of diaminopimelic acid.

Genomic DNAs of the isolates were generated following the technique of Kudo et al. (1998). The 16S rRNA gene sequence was amplified as reported by Suriyachadkun et al. (2009) and sequenced on a DNA sequencer (Macrogen) using universal primers, 27F forward (5'-AGAGTTTGATCMTGGCTCAG-3') and 1492R reverse (5'-TACGGYTACCTTGTTAC

GACTT-3'). Sequence similarity values between the isolates and their related neighbors were calculated using the EzBiocloud service (Yoon et al., 2017) and the Kimura-2-parameter (Kimura, 1980) was used to create a phylogenetic distance matrix. A phylogenic tree was constructed through the neighbor-joining (NJ) technique (Saitou and Nei, 1987) using MEGA 7.0 (Kumar et al., 2016) based on 1000 replications of bootstrap value.

2.3 Evaluation of antimicrobial activity

The culture was cultivated in 10 mL of seed medium No. 301 (2.4% starch, 0.3% peptone, 0.1% glucose, 0.5% yeast extract, 0.3% meat extract, and 0.3% $CaCO_3$, pH 7.0), on a shaker (180 rpm) incubated at 30°C for 3 days. The seed culture of each isolate was inoculated into 10 mL of three production media as ISP 2 (0.4% yeast extract, 1.0% malt extract, 0.4% glucose), medium No. 30 (0.3% peptone, 0.1% glucose, 0.5% yeast extract, 0.3% meat extract, 0.3% $CaCO_3$, 2.4% starch), and 5 mL/L of trace elements containing 1.0 g/L of $FeSO_4 \cdot 7H_2O$, $MnCl_2 \cdot 4H_2O$, $ZnSO_4 \cdot 7H_2O$, $CuSO_4 \cdot 5H_2O$, and $CoCl_2 \cdot 6H_2O$, and medium No. 57 (0.5% peptone, 2% glucose, 0.5% meat extract, 0.3% dry yeast, 0.5% NaCl, and 0.3% $CaCO_3$). After 14 days, each fermentation broth was extracted with 10 mL of 95% ethanol and shaken at 180 rpm for 2 h before centrifugation at 7,000 rpm for 10 min. The supernatant was collected and 50 µL was applied to each paper disk (6 mm).

A paper disk diffusion technique was used to determine antimicrobial activity (Mearns-Spragg et al., 1998) against *Staphylococcus aureus* ATCC 25923, *Kocuria rhizophila* ATCC 9341, *Bacillus subtilis* ATCC 6633, *Escherichia coli* ATCC 25922, *Pseudomonas aeruginosa* ATCC 27853, and *Candida albicans* ATCC 10231. Muller-Hinton agar (MHA) and potato dextrose agar (PDA) were used to cultivate the tested bacteria (1×10^8 cells/mL) and yeast (1×10^6 cells/mL), which were incubated for 24 h at 37°C and 30°C, respectively. The inhibition zone (mm) was measured and reported as an antibacterial activity index. All experiments were carried out in triplicate.

2.4 Evaluation of IAA production

All isolates were streaked on ISP 2 agar plates and incubated at 30°C. After seven days, the agar discs containing actinomycete mycelia were transferred to ISP 2 broth (0.2% L-tryptophan, pH 7.0) and incubated at 30°C for seven days with 180 rpm shaking. The culture was centrifuged at 6,500 rpm for

five minutes, and the supernatant was used to determine the amount of IAA production. One mL of supernatant was added to two mL of Salkowski reagent (0.5 M of $FeCl_3$ in 35% $HClO_4$ in a proportion of 1:50 (v/v)) and kept in the dark for 30 min (Sameera et al., 2018). A UV-Vis spectrophotometer was used to detect IAA at absorbance 530 nm. The uninoculated medium with reagent was used as a control. The amount of IAA produced per milliliter of culture broth was calculated based on the calibration curve of IAA obtained from standard IAA at different concentrations (0-100 µg/mL). The amount of IAA in the culture was expressed as µg/mL.

2.5 Optimization of IAA production

The potent isolates of IAA production were optimized based on the effects of incubation time, temperature, pH, and L-tryptophan level. Isolates that produced high amounts of IAA were chosen for optimization. The chosen isolates were grown in a 500 mL flask with 100 mL of ISP 2 medium plus 0.2% L-tryptophan with shaking at 180 rpm. Salkowski's method was used to evaluate IAA production. The same cultural conditions as mentioned before were employed. The influence of incubation period on IAA production was investigated at 48 h intervals for 15 days. Results of the concentration of L-tryptophan (0.1, 0.2, 0.3, 0.4, 0.5, 1.0, and 1.5%), pH (4, 5, 6, 7, 8, 9, and 10), temperature (25, 30, 35, 37, and 40°C) were performed for seven days. The one-factor-at-a-time (OFAT) method was used to optimize all experiments (Czitrom, 1999).

2.6 Plant growth-promoting activity of the isolates

To investigate the impact of IAA produced by the isolates DR9-7 and DR10-1 on seed germination and root elongation in rice (*Oryza sativa* L. cv. RD49), surface sterilization of rice seeds was performed by soaking in 10% sodium hypochlorite (NaOCl) for one minute and 95% ethanol for three minutes, followed by thorough washing in sterile distilled water. The treatment was carried out by soaking rice seeds in a standard IAA solution containing 50 µg/mL and supernatant culture of DR9-7 and DR10-1 with an IAA concentration of 50 µg/mL. The control group was soaked in sterile distilled water. Seeds were placed in sterilized Petri dishes coated with two sheets of filter paper and soaked with 10 mL of sterile distilled water (three replicates, ten seeds/plate). All the Petri dishes were incubated in a chamber with light at 30°C for 16 h daily. Seed germination, root length,

shoot length, number of roots, fresh weight, and dry weight were measured after 7 days.

2.7 Statistical analysis

Data were statistically analyzed by one- way analysis of variance (ANOVA) using the SPSS software package (SPSS 28 for Windows). The grouping was performed by Duncan's multiple range tests at p<0.05 on each of the significant variables measured. Data were expressed as mean values of triplicates±standard deviation.

3. RESULTS AND DISCUSSION

3.1 Isolation and identification of isolates

Thirty-two endophytic actinomycetes were recovered from the roots of Thai orchids. All isolated actinomycetes revealed 4, 12, 8, and 8 isolates from gellan gum, starch casein, glycerol arginine, and Gause No. 1, respectively (Table 1). Based on 16S rRNA gene sequence analysis and phenotypic characteristics, the isolates were classified into four taxa (Table 2) including, *Streptomyces* (Group I, 19 isolates), *Micromonospora* (Group II, 10 isolates), *Streptosporangium* (Group III, 2 isolates), and *Actinomadura* (Group IV, 1 isolate). Most of the Group I isolates (59.5%) had LL-DAP, whereas the remaining 13 isolates (40.6%) carried *meso*-DAP (Williams and Cross, 1971). Similarities of all isolates and closely related isolates ranged between 98.97 and 100%. The NJ-phylogenetic tree based on 16S rRNA gene sequences is shown in Figure 1. The 16S rRNA gene sequences of the isolates were deposited at the NCBI database, with accession numbers listed in Table 1.

Group I contained 19 isolates. The isolates produced spiral spore chains with pale blue to greenish gray on ISP 2 agar after 7 days of incubation (Table 1). The isolates, DR2-3, DR5-2, and DR7-6 were closely related to *S. parvulus* NBRC 13193^T (99.40-99.85% similarity); DR3-5 and CC1-3 were closely related to *S. tendae* ATCC 19812^T (99.93-99.70%); CC1-1 and DR9-7 were closely related to *S. ardesiacus* NRRL B-1773^T (99.92-99.93%); CL1-6 and EO1-13 were closely related to *S. heilongjiangensis* NEAU-W2^T (99.78-99.93%). The isolates DR1-1, DR2-2, DR8-9, DR9-4, DR9-5, DR10-1, DR10-6, DR10-8, CL1-8, and EO1-10 were closely related to *S. daghestanicus* NRRL B-5418^T (99.32%), *S. antibioticus* NBRC 12838^T (99.70%), *S. malaysiensis* NBRC 16446^T (99.92%), *S. deserti* C63^T (99.41%), *S. spiralis* NBRC 14215^T (99.98%), *S. thermoviolaceus*

subsp. *apingens* DSM 41392^T (98.97%), *S. globosus* LMG 19896^T (99.93%), *S. collinus* NBRC 12759^T (99.93%), and *S. olivaceus* NRRL B-3009^T (99.85%), *S. zaomyceticus* NBRC 13348^T (99.48%), respectively (Table 1).

Group II contained ten isolates. They produced single spores on mycelium substrate. Colonies on ISP 2 agar were dark purplish red to greenish black. Based on the 16S rRNA gene sequences, the two isolates DR4-1 and CA1-5 were closely related to *M. humi* DSM 45647^T (99.33-99.47%); two isolates, CR1-1 and CA1-9 were closely related to *M. maritima* D10-9-5^T (99.93-100.00%); and isolates DR6-8, CA1-1, YG1-1, YG1-7, YG1-8, and EO1-8 were closely related to *M. tulbaghiae* DSM 45142^T (99.75%), *M. schwarzwaldensis* HKI0641^T (99.92%), *M. chersina* DSM 44151^T (99.85%), *M. chalcea* DSM 43026^T (99.85%), *M. citrea* DSM 43903^T (99.77%), and *M. aurantiaca* ATCC 27029^T (99.49%), respectively (Table 1).

Group III consisted of two isolates, DR9-9 and YG1-5. They produced spherical sporangia in the aerial mycelium. On ISP 2 agar, the isolates were pale purple-pink (Table 1). The isolates DR9-9 and YG1-5 were closely related to *S. sandarakinum* GW-12028^T and *S. pseudovulgare* DSM 4318^T, based on 16S rRNA gene sequence similarity (99.32 and 99.93%), respectively (Table 1).

Group IV contained one isolate, CL1-5. This isolate formed straight chain spores on the tip of aerial mycelium and colonies and was vivid reddish-orange on ISP2 agar plate. Based on 16S rRNA gene sequence analysis, the isolate CL1-5 was 99.85% closely related to *A. hibisca* NBRC 15177^T (Table 1).

In this study, nineteen *Streptomyces* isolates were associated with the eleven orchids *D. christyanum*, *D. polyanthum*, *D. formosum*, *D. kentrophyllum*, *D. findlayanum*, *D. chrysanthum*, *C. cardioglossa*, *D. friedericksianum*, *D. chrysotoxum*, *C. lawrenceana,* and *E. ornate*. Ten *Micromonospora* isolates were found in the six orchids, *D. crumenatum*, *D. heterocarpum*, *C. rostratum*, *C. assamica*, *P. globulifera*, and *E. ornate*. Two *Streptosporangium* isolates were distributed in the two orchids *D. friedericksianum* and *P. globulifera*, and one *Actinomadura* isolate was found in *Coelogyne lawrenceana*. The isolates DR2-3, DR5-2, and DR6-6, all closely related to *S. parvulus* NBRC 13193^T, were found in *D. polyanthum*, *D. kentrophyllum*, and *D. findlayanum*, while the isolates DR3-5 and CC1-3

Table 1. Source, isolate number, cultural characteristics, and the nearest isolate species based on 16S rRNA gene sequence similarity (%)

Group	Plant	Isolate No.	Cultural characteristics		% Similarity	Accession No.	Nearest species
			Upper color	Reverse color			
I	Dendrobium christyanum	DR1-1[b]	Greenish gray	Light yellow	99.32	LC667376	S. daghestanicus NRRL B-5418[T]
	Dendrobium polyanthum	DR2-3[b]	Pale blue	Light yellow	99.84	LC667377	S. parvulus NBRC 13193[T]
	Dendrobium polyanthum	DR2-2[b]	Brilliant greenish blue	Light yellow	99.70	LC667378	S. antibioticus NBRC 12838[T]
	Dendrobium formosum	DR3-5[b]	Greenish gray	Moderate olive brown	99.70	LC667379	S. tendae ATCC 19812[T]
	Dendrobium kentrophyllum	DR5-2[b]	Pale blue	Light yellow	99.40	LC667380	S. parvulus NBRC 13193[T]
	Dendrobium findlayanum	DR7-6[b]	Pale blue	Light yellow	99.85	LC667381	S. parvulus NBRC 13193[T]
	Dendrobium chrysanthum	DR8-9[b]	Bluish gray	Light yellow	99.92	LC667382	S. malaysiensis NBRC 16446[T]
	Calanthe cardioglossa	CC1-1[b]	Olive gray	Light olive brown	99.93	LC667383	S. ardesiacus NRRL B-1773[T]
	Calanthe cardioglossa	CC1-3[b]	Greenish gray	Moderate olive brown	99.93	LC667384	S. tendae ATCC 19812[T]
	Dendrobium friedericksianum	DR9-4[b]	Greenish gray	Yellowish gray	99.41	LC667385	S. deserti C63[T]
	Dendrobium friedericksianum	DR9-5[a]	Light olive gray	Yellowish gray	98.98	LC667386	S. spiralis NBRC 14215[T]
	Dendrobium friedericksianum	DR9-7[a]	Olive gray	Light olive brown	99.92	LC667387	S. ardesiacus NRRL B-1773[T]
	Dendrobium chrysotoxum	DR10-1[a]	Grayish olive green	Light olive gray	98.97	LC667388	S. thermoviolaceus subsp. apingens DSM 41392[T]
	Dendrobium chrysotoxum	DR10-6[d]	Moderate yellow	Light yellow	99.93	LC667389	S. globosus LMG 19896[T]
	Dendrobium chrysotoxum	DR10-8[d]	Bluish white	Brownish gray	99.93	LC667390	S. collinus NBRC 12759[T]
	Coelogyne lawrenceana	CL1-6[c]	Bluish gray	Dark bluish gray	99.93	LC667391	S. heilongjiangensis NEAU-W2[T]
	Coelogyne lawrenceana	CL1-8[c]	Greenish gray	Moderate olive	99.85	LC667392	S. olivaceus NRRL B-3009[T]
	Eria ornata	EOI-10[b]	Pale blue	Grayish greenish yellow	99.48	LC667393	S. zaomyceticus NBRC 13348[T]
	Eria ornata	EOI-13[b]	Greenish gray	Moderate olive brown	99.78	LC667394	S. heilongjiangensis NEAU-W2[T]
II	Dendrobium crumenatum	DR4-1[c]	Greenish black	Greenish black	99.33	LC666836	M. humi DSM 45647[T]
	Dendrobium heterocarpum	DR6-8[c]	Moderate olive brown	Moderate olive brown	99.75	LC666837	M. tulbaghiae DSM 45142[T]
	Cleisostoma rostratum	CR1-1[c]	Grayish red	Grayish red	100.00	LC666838	M. maritima D10-9-5[T]
	Coelogyne assamica	CA1-1[c]	Dark olive brown	Dark olive brown	99.92	LC666839	M. schwarzwaldensis HKI0641[T]
	Coelogyne assamica	CA1-5[c]	Greenish black	Greenish black	99.47	LC666840	M. humi DSM 45647[T]
	Coelogyne assamica	CA1-9[a]	Dark grayish red	Dark grayish red	99.93	LC666841	M. maritima D10-9-5[T]
	Pinalia globulifera	YGI-1[d]	Greenish black	Greenish black	99.85	LC666842	M. chersina DSM 44151[T]
	Pinalia globulifera	YGI-7[d]	Very dark purplish red	Very dark purplish red	99.85	LC666843	M. chalcea DSM 43026[T]
	Pinalia globulifera	YGI-8[d]	Brownish black	Brownish black	99.77	LC666844	M. citrea DSM 43903[T]
	Eria ornata	EOI-8[d]	Deep reddish brown	Deep reddish brown	99.49	LC666845	M. aurantiaca ATCC 27029[T]

All isolates grew well on ISP 2 agar medium. [a]gellan gum; [b]starch casein gellan gum; [c]glycerol arginine gellan gum; [d]gauze synthetic No.1,

Table 1. Source, isolate number, cultural characteristics, and the nearest isolate species based on 16S rRNA gene sequence similarity (%) (cont.)

Group	Plant	Isolate No.	Cultural characteristics		% Similarity	Accession No.	Nearest species
			Upper color	Reverse color			
III	*Dendrobium friedericksianum*	DR9-9[d]	Pale pink	Pinkish gray	99.32	LC667395	*S. sandarakinum* GW-12028[T]
	Pinalia globulifera	YG1-5[d]	Pale purple pink	Pale purple pink	99.93	LC667396	*S. pseudovulgare* DSM 4318[T]
IV	*Coelogyne lawrenceana*	CL1-5[c]	Very deep red	Very deep red	99.85	LC667397	*A. hibisca* NBRC 15177[T]

All isolates grew well on ISP 2 agar medium. [a] gellan gum; [b] starch casein gellan gum; [c] glycerol arginine gellan gum; [d] gauze synthetic No.1,

Table 2. Differential phenotypic characteristics of the isolates

Characteristic	*Streptomyces*	*Micromonospora*	*Streptosporangium*	*Actinomadura*
	I	II	III	IV
No. of isolates	19	10	2	1
Temperature range, °C	20-37	20-37	25-37	25-37
pH range	5-10	5-8	5-10	5-10
NaCl tolerance				
• 4%	+	-(+4)	w	+
• 6%	+(-3)	-(+2)	-	-
• 8%	-(+8)	-	-	-
Starch hydrolysis				
• Coagulation	-(+3)	-	-	-
• Peptonization	-(+4)	-(+3)	-	-
• Nitrate reduction	-(+5)	-(+4)	+	+
• Gelatin liquefaction	-(+5)	-(+4)	-	-
Utilization of				
• D-Glucose	+(w1)	+(-1)	+	+
• Sucrose	+(w5)	+(-1, w1)	+	+
• Lactose	+	+(-1, w1)	+	+
• Dextrose	+	+(-1, w2)	+	+
• Maltose	+	+(w5)	+	+
• D-Mannitol	+	-(+2, w3)	+	+
• D-Xylose	+	+(-1, w3)	+	w
• Sorbitol	-(+4, w3)	+(-1)	w	+

Note: + positive reaction; w weakly positive reaction; – negative reaction. Numbers in parentheses indicate numbers of isolates showing positive, weak and negative reactions.
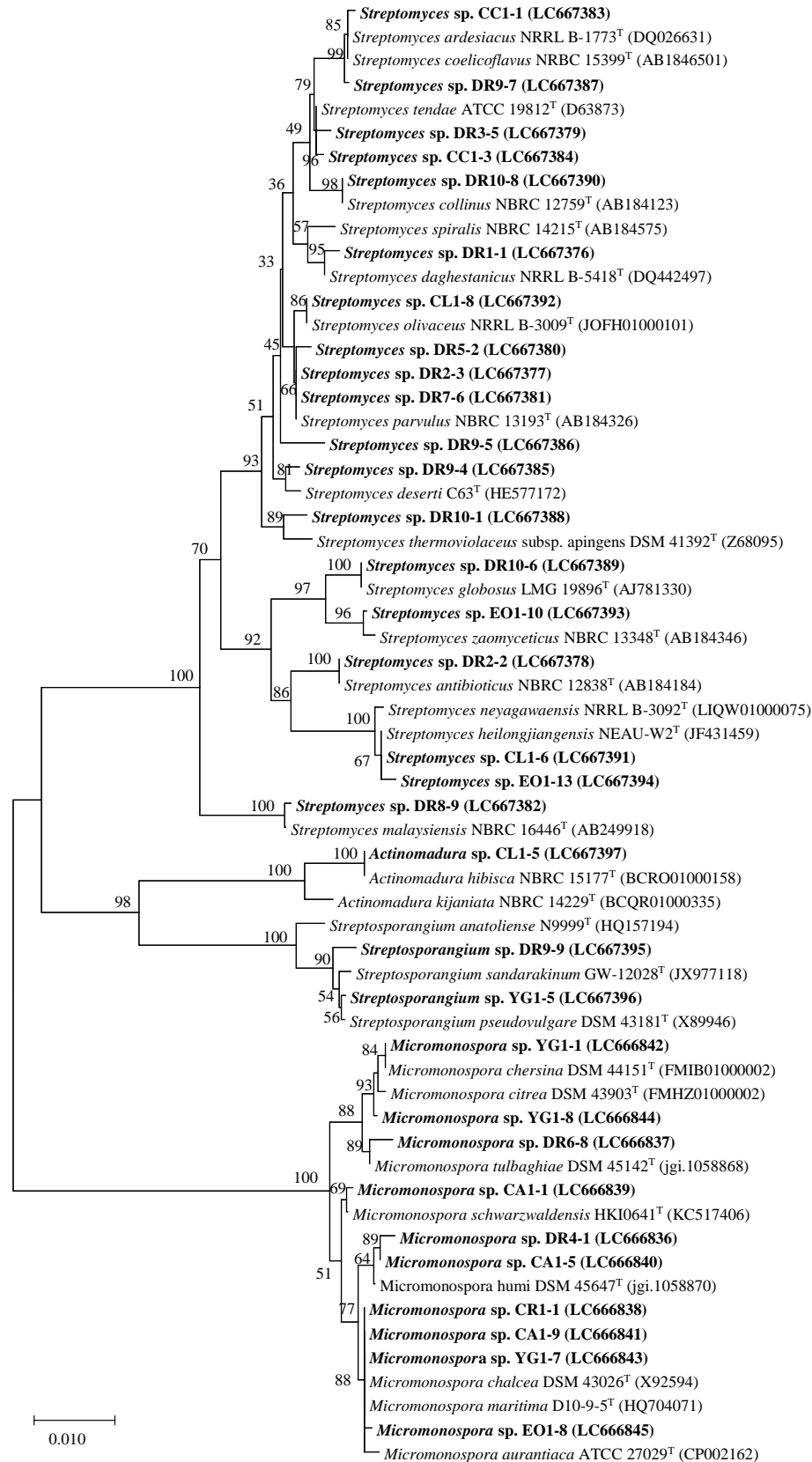
Figure 1. Neighbor-joining phylogenetic tree based on 16S rRNA gene sequences showing relationships between the 32 isolates and related type strains. Numbers at branch nodes indicate bootstrap percentages derived from 1000 replications. Bar, 0.01 substitutions per nucleotide position.

closely related to *S. tendae* ATCC 19812^T were presented in *Dendrobium* and *Calanthe*. *Streptomyces* and *Micromonospora* isolates were found in *E. ornate*, while *Streptomyces* and *Streptosporangium* isolates were found in *D. friedericksianum*. These results indicated that various associated bacteria were extensively distributed among the host plants.

Most of the isolates (59.38%) belonged to the genus *Streptomyces*, previously identified as a dominating organism in sugar cane roots (Sinma et al., 2015), *Citrus reticulata* L. (Shutsrirung et al., 2013), and *Acacia auriculiformis* (Bunyoo et al., 2009) in Thailand. Our result was similar to previous research that found *Streptomyces* strains in plant roots (Taechowisan and Lumyong, 2003; Gangwar et al., 2012; Shan et al., 2018). Actinobacteria were prominent in the roots and stems of *Neottia ovata* (50.02 and 48.47%, respectively) and in the seeds of *Spiranthes spiralis* (48.95%) (Alibrandi et al., 2020). Endophytic actinomycetes were distributed in plant roots, where water and nutrients were absorbed (Passari et al., 2015). Many plant species had diverse strains of *Microbispora* (Bunyoo et al., 2009) and *Micromonospora* (Kuncharoen et al., 2019), including novel species of *Amycolatopsis dendrobii* from the root of *Dendrobium heterocarpum* Lindl. (Tedsree et al., 2021) and *Streptomyces radicis* from the roots of plants (Kuncharoen et al., 2022).

3.2 Antimicrobial activity

Fifteen isolates (46.87%) showed antimicrobial activity against at least one of the six tested bacteria (Table 3). Five isolates of *Streptomyces* and five isolates of *Micromonospora* inhibited *S. aureus* ATCC 25923 when cultivated in all production media. The isolate DR8-9 presented the highest antimicrobial activity against *S. aureus* ATCC 25923 (24.32±1.01 mm) when cultivated in 57 media. Four isolates of *Streptomyces*, five isolates of *Micromonospora*, and one isolate of *Streptosporangium* inhibited *K. rhizophila* ATCC 9341. Isolate DR6-8 showed the highest activity (24.91±0.94 mm), while isolates DR2-2 and DR4-1 showed 22.76±0.58 and 19.65±0.58 mm, respectively. Five isolates of *Streptomyces* and four of *Micromonospora* were active against *B. subtilis* ATCC 6633 when grown in all media. Isolate DR7-6, which was closely related to *S. parvulus* NBRC 13193^T, showed the highest activity (20.00±0.58 mm) in medium No. 30. Isolates DR8-9 and DR1-1 inhibited *C. albicans* ATCC 10231 in all production

media, including DR2-2 in ISP 2 medium. The isolate DR1-1 was closely related to *S. daghestanicus* NRRL B-5418^T and showed the highest activity against *C. albicans* ATCC 10231 (21.90±0.77 mm) on medium no.30. Three isolates DR1-1, DR2-2, and DR8-9 were active against the gram-negative bacteria *P. aeruginosa* ATCC 27853, while isolate DR2-2 inhibited this bacterium when cultivated on all production media. Interestingly, DR2-2 was closely related to *S. antibioticus* NBRC 12838^T and inhibited all indicator organisms, including *Escherichia coli* ATCC 25922 (Table 3).

Endophytic actinomycetes have been reported for their antibacterial activity against pathogenic bacteria (Taechowisan and Lumyong, 2003; Passari et al., 2015). In this study, both *Streptomyces* and *Micromonospora* isolates inhibited *S. aureus*, *B. subtilis*, and *K. rhizophila*. Our results concurred with Musa et al. (2020) who discovered that 54 of 126 endophytic actinobacteria strains were resistant to at least one or more indicator species. Notably, the majority of *Streptomyces* strains exhibited antagonistic activities. Rao et al. (2015) found that all *Streptomyces* strains from *Combretum latifolium* showed significant antimicrobial activity against both bacterial and fungal pathogens. This study reported on the incidence of possible endophytic actinomycetes that suppress pathogenic bacteria.

3.3 Indole-3-acetic acid production

Twenty-two isolates (68.75%) were able to produce indole-3-acetic acid (IAA) (Table 4). In Group I *Streptomyces*, 15 isolates produced IAA ranging from 10.59±0.45 to 67.30±1.00 µg/mL. Isolate DR10-1 was closely related to *S. thermoviolaceus* subsp. *apingens* DSM 41392^T and produced the highest IAA (67.30±1.00 µg/mL), followed by DR9-7 closely related to *S. ardesiacus* NRRL B-1773^T and DR2-2 closely related to *S. antibioticus* NBRC 12838^T at 58.03±0.16 and 52.39±0.89 µg/mL, respectively. Five of ten isolates of Group II *Micromonospora* produced between 18.22±0.84 and 44.77±0.54 µg/mL of IAA. Isolate CA1-5 closely related to *M. humi* DSM 45647^T showed the highest IAA production (44.77±0.54 µg/mL) followed by isolate YG1-7 closely related to *M. chalcea* DSM 43026^T (30.91±0.80 µg/mL). Only one Group III *Streptosporangium*, DR9-9, closely related to *S. sandarakinum* GW-12028^T produced maximum IAA of 43.97±0.30 µg/mL (Table 4).

Table 3. Antimicrobial activities (inhibition zone, mm in diameter) of Group I *Streptomyces*, Group II *Micromonospora*, and Group III *Streptosporangium* isolates cultivated in ISP 2, 30, and 57 media.

Isolate No.	S. aureus ATCC 25923			K. rhizophila ATCC 9341			B. subtilis ATCC 6633			P. aeruginosa ATCC 27853			C. albicans ATCC 10231		
Medium	ISP 2	30	57	ISP 2	30	57	ISP 2	30	57	ISP 2	30	57	ISP 2	30	57
Group I															
DR1-1	-	-	-	-	-	-	-	-	-	18.79±0.56a	-	-	20.60±0.58a	21.90±0.77	20.37±1.00
DR2-2	16.98±0.57c	16.43±1.00c	17.98±0.58b	21.18±1.00b	21.43±1.01b	22.76±0.58b	16.66±1.00b	18.47±0.57b	18.25±0.58a	9.13±1.00c	9.57±0.67	10.08±0.66	17.23±0.61b	-	-
DR5-2	15.24±1.00d	14.98±1.00c	9.84±0.50de	11.23±1.01f	15.89±1.00d	16.95±1.01d	16.51±0.79b	17.84±0.86b	13.85±1.00c	-	-	-	-	-	-
DR7-6	21.22±1.00b	19.11±1.00b	18.01±1.00b	-	-	-	19.87±1.01a	20.00±0.58a	18.80±0.57a	-	-	-	-	-	-
DR8-9	22.64±0.75a	21.79±0.57a	24.32±1.01a	15.66±0.57d	15.35±1.00de	18.52±1.00c	14.53±0.67c	14.35±0.76c	15.95±0.99b	-	-	9.36±0.58	12.76±0.59c	13.01±0.57	12.37±0.57
DR9-5	11.56±1.00e	12.44±0.61c	12.46±1.01c	-	-	-	-	-	-	-	-	-	-	-	-
DR10-1	-	-	-	8.07±0.58g	8.17±0.81g	7.97±0.84h	9.55±0.61d	9.62±1.01ef	10.74±1.00d	-	-	-	-	-	-
Group II															
DR4-1	8.39±0.56fg	9.54±0.58d	9.79±1.00de	19.65±0.58c	19.11±0.57c	17.77±0.58cd	9.90±0.57d	11.68±1.01d	11.94±0.99d	8.28±0.60c	-	-	-	-	-
DR6-8	9.67±0.58f	9.90±0.58d	10.42±0.62de	24.91±0.94a	24.91±1.53a	24.24±0.99a	10.36±0.58d	10.78±0.85de	11.29±0.72d	-	-	-	-	-	-
CR1-1	9.46±0.57f	9.47±0.53d	11.20±0.58cd	10.45±0.88f	11.36±1.00f	12.34±1.00f	-	-	-	14.55±1.02b	-	-	-	-	-
CA1-1	-	-	-	-	-	-	-	-	-	9.72±0.53c	-	-	-	-	-
CA1-5	7.88±0.99g	8.63±0.75d	9.39±0.60e	15.79±0.99d	16.60±0.79d	16.75±0.73d	9.06±0.58d	8.84±0.56f	9.06±0.99e	-	-	-	-	-	-
YG1-1	17.91±0.58c	17.92±0.58b	18.87±0.59b	13.86±1.00e	13.91±0.58e	14.68±0.57e	7.32±1.00e	8.23±1.00f	7.84±1.00e	-	-	-	-	-	-
YG1-8	-	-	-	7.85±0.50g	7.46±1.00g	-	-	-	-	-	-	-	-	-	-
Group III															
DR9-9	-	-	-	10.32±0.57f	10.15±0.58f	9.85±1.01g	-	-	-	-	-	-	-	-	-

Group IV *Actinomadura*, CL1-5, did not exhibit antimicrobial activity.
All isolates exhibited no antimicrobial activity to *E. coli* ATCC 25922 except for isolate DR2-2 that showed 16.41±0.58, 17.26±0.53, and 18.52±0.52 when cultivated in ISP 2, 30, and 57 media, respectively.
Data are expressed as mean±standard deviation (SD), including the disc diameter (6 mm).
Different superscripts in the same row indicate significant differences (p<0.05).

Table 4. IAA production of Group I *Streptomyces*, Group II *Micromonospora*, Group III *Streptosporangium*, and IV *Actinomadura* isolates.

Group	Isolate No.	IAA (µg/mL)
I	DR1-1	22.04±0.89[i]
	DR2-3	52.36±0.86[c]
	DR2-2	52.39±0.89[c]
	DR3-5	19.67±1.00[j]
	DR5-2	51.54±0.84[c]
	DR7-6	45.94±0.67[d]
	DR8-9	6.95±0.65[q]
	CC1-1	10.59±0.45[o]
	CC1-3	11.92±0.79[m]
	DR9-4	32.61±0.68[f]
	DR9-5	15.62±0.72[l]
	DR9-7	58.03±0.16[b]
	DR10-1	67.30±1.00[a]
	DR10-6	2.30±0.16[st]
	DR10-8	6.47±0.16[q]
	CL1-6	8.72±0.28[p]
	CL1-8	0.78±0.24[wx]
	EO1-10	14.17±0.33 [m]
	EO1-13	18.45±0.37[k]
II	DR4-1	29.13±0.47[h]
	DR6-8	0.04±0.36[x]
	CR1-1	18.22±0.84[k]
	CA1-1	7.33±0.84[q]
	CA1-5	44.77±0.54[e]
	CA1-9	21.54±0.78[i]
	YG1-1	1.63±0.70[tu]
	YG1-7	30.91±0.80[g]
	YG1-8	2.84±0.73[s]
	EO1-8	4.80±0.54[r]
III	DR9-9	43.97±0.30[e]
	YG1-5	1.13±0.90[v]
IV	CL1-5	14.48±0.83[m]

Different superscripts indicate significantly different (p<0.05) mean±SD.

In this study, *Streptomyces* showed the highest IAA production. Several previous studies demonstrated that IAA production of actinomycetes from different crops differed by species and strains. *Streptomyces* sp. En-1 from *Taxus chinensis* (Lin and Xu, 2013) and *S. rochei* ERY1 from *Eryngium foetidum* L. showed the ability to produce IAA (Suwitchayanon et al., 2018).

3.4 Optimization of IAA production

The two isolates DR9-7 and DR10-1 showed the highest IAA production after the screening was optimized at different factors. IAA production of isolates DR9-7 and DR10-1 started after three days and peaked at 106.32±2.04 and 298.12±4.19 µg/mL after 13 days (Figure 2 (a)). *S. atrovirens* ASU14 exhibited the maximum IAA value when optimization at 30°C for 13 days (Abd-Alla et al., 2013). Maximum IAA production of the two isolates was observed in medium containing 0.4% L-tryptophan (Figure 2 (b)). When the concentration of L-tryptophan increased from 0.1 to 0.4%, IAA production of DR9-7 and DR10-1 increased to maximum levels at 94.35±1.56 and 123.14±4.17%, respectively. Results indicated that different amounts of L-tryptophan had variable influence on IAA production, with tryptophan as an important element in increasing IAA production.

Highest concentration of IAA was obtained from isolate DR10-1 at pH 7 (82.76±1.22 µg/mL) and DR9-7 cultivated at pH 7 and 8 at 54.08±0.59 and 54.71±0.25 µg/mL, respectively. IAA levels of DR9-1 and DR10-1 decreased when the pH value was less than 6 and greater than 8, (Figure 2 (c)). *Streptomyces* and other actinomycete strains grew slowly in acidic or basic environments; therefore, pH levels are important for IAA synthesis (Shirokikh et al., 2007). Our findings concurred with Goudjal et al. (2013), who showed that pH 7 was optimal for IAA production of *Streptomyces* sp. PT2 . Isolates DR9-7 and DR10-1 produced the highest IAA when grown at 30°C (Figure 2 (d)). However, there was no significant change in IAA generation of DR10-1 at 35°C compared to 30°C. When temperature exceeded 30°C, IAA production of DR9-7 and DR10-1 decreased. A temperature of 30°C was found to be optimal for this investigation. *Streptomyces* sp. CMU H009 produced the largest IAA when cultivated at 30°C (Khamna et al., 2010). Accordingly, OFAT optimization experiments showed that the highest IAA production required cultivation in ISP 2 broth with 0.4% L-tryptophan, pH 7 at 30°C for 13 days. Maximum IAA values of DR10-1 and DR9-7 were 284.87±8.24 and 132.35±9.39 µg/mL, respectively.

3.5 Plant growth-promoting activity of the isolates

The effects of IAA in DR9-7 and DR10-1 supernatant cultures on rice seed germination, root length, and shoot length were determined. Rice seeds soaked under various conditions exhibited significant differences in root lengths and quantity of roots compared to the controls (Table 5). Treatments with supernatant DR9-7 had the greatest influence on seedling root length, with no significant differences

identified between supernatant DR10-1 and standard IAA. Supernatant of isolate DR10-1 showed the highest number of roots, whereas other treatments showed no significant differences. Fresh and dry weight of seedlings after treatment with DR9-7, DR10-1 and standard IAA were significantly different compared to the control. However, all treatments had no effect on seed germination. Our study results related to root growth of the host plants, as reported by

Etesami et al. (2015). IAA-producing bacteria isolated from orchid rhizoplanes of *Dendrobium moschatum* (Tsavkelova et al., 2007) and *Cymbidium eburneum* (Faria et al., 2013) improved symbiotic seed germination. Our isolates indicated the presence of IAA production as a good option for use as plant growth enhancement in both economic and agricultural systems.
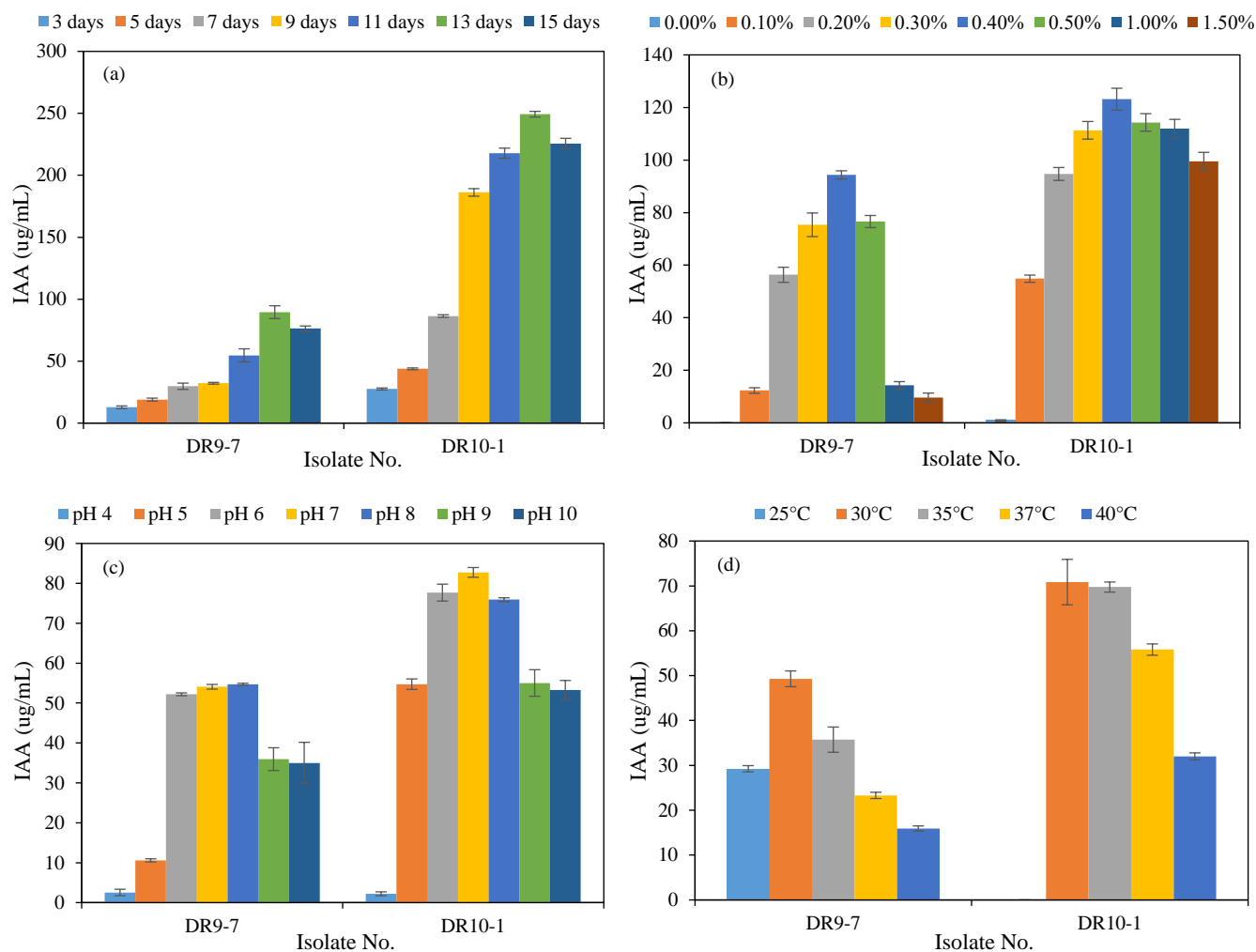

Figure 2. (a) Effect of incubation time (day), (b) Effect of L-tryptophan concentrations, (c) Effect of pH, and (d) Effect of temperature on IAA production by the selected isolates. Vertical bars represent standard deviation from triplicate experiments.

Table 5. Effect of isolates DR9-7 and DR10-1 on the growth of rice (*Oryza sativa*)

Isolate No.	Growth parameters of actinomycetes treated rice					
	Root length (cm)	Shoot length (cm)	Number of roots	Seedling fresh weight (g)	Seedling dry weight (g)	% Seed germination
DR9-7	6.90±0.52[a]	3.55±0.96[c]	3.00±1.05[b]	0.93±0.07[a]	0.33±0.03[a]	100
DR10-1	4.85±0.34[b]	6.25±0.81[a]	4.30±0.82[a]	0.81±0.07[a]	0.30±0.05[ab]	100
IAA	4.85±0.24[b]	3.85±0.94[c]	3.40±0.52[b]	0.78±0.08[a]	0.31±0.06[ab]	100
Control	3.30±1.27[c]	4.95±0.65[b]	3.20±0.63[b]	0.56±0.07[b]	0.27±0.04[b]	100

Different superscripts indicate significantly different (p<0.05) mean±SD.

4. CONCLUSION

Endophytic actinomycetes are mainly distributed in the root system and xylem tissues of host plants. The major role of these bacteria is to improve the health and growth of the host plant by producing beneficial metabolites to control plant infections from pathogens and promote the growth of host plants. This study concluded that 19 *Streptomyces* isolates were associated with the roots of the Thai orchid species *D. christyanum*, *D. polyanthum*, *D. formosum*, *D. kentrophyllum*, *D. findlayanum*, *D. chrysanthum*, *C. cardioglossa*, *D. friedericksianum*, *D. chrysotoxum*, *C. lawrenceana*, and *E. ornate*. Ten *Micromonospora* isolates were associated with *D. crumenatum*, *D. heterocarpum*, *C. rostratum*, *C. assamica*, *P. globulifera*, and *E. ornate*, while 2 *Streptosporangium* isolates were found in *D. friedericksianum* and *P. globulifera* and an *Actinomadura* isolate was found in *C. lawrenceana*. Our *Streptomyces, Micromonospora* and *Streptosporangium* isolates exhibited significant antimicrobial activities against *Bacillus subtilis* ATCC 6633, *Kocuria rhizophila* ATCC 9341, *Staphylococcus aureus* ATCC 25923, *Escherichia coli* ATCC 25922, *Pseudomonas aeruginosa* ATCC 27853, and *Candida albicans* ATCC 10231. Only *Streptomyces antibioticus* DR2-2 inhibited all tested pathogens, while two endophyte isolates DR10-1 and DR9-7 showed high IAA activity that promoted the number of roots, shoot length, root length and fresh weight of rice seedlings. This is the first report on the diversity, antimicrobial and plant-growth-promoting properties of endophytic actinomycetes associated with the root of Thai orchids.

REFERENCES

Abd-Alla MH, El-Sayed E-SA, Rasmey A-HM. Indole-3-acetic acid (IAA) production by *Streptomyces atrovirens* isolated from rhizospheric soil in Egypt. Journal of Biology and Earth Sciences 2013;3(2):182-93.

Alibrandi P, Schnell S, Perotto S, Cardinale M. Diversity and structure of the endophytic bacterial communities associated with three terrestrial orchid species as revealed by 16S rRNA gene metabarcoding. Frontiers in Microbiology 2020;11: Article No. 604964.

Arai T. Culture Media for Actinomycetes. Tokyo, Japan: The Society for Actinomycetes Japan; 1975.

Bao X, Shun Q, Chen L. The Medicinal Plants of *Dendrobium* (Shi-Hu) in China. A Coloured Atlas. Shanghai, Chaina: Press of Fudan University and Press of Shanghai Medical University; 2001.

Berdy J. Bioactive microbial metabolites. The Journal of Antibiotics 2005;58(1):1-26.

Bunyoo C, Duangmal K, Nuntagij A, Thamchaipenet A. Characterisation of endophytic actinomycetes isolated from wattle trees (*Acacia auriculiformis* A. Cunn. ex Benth.) in Thailand. Genomics and Genetics 2009;2(2):155-63.

Charoenrungruang S, Chanvorachote P, Sritularak B, Pongrakhananon V. Gigantol, a bibenzyl from *Dendrobium draconis*, inhibits the migratory behavior of non-small cell lung cancer cells. Journal of Natural Products 2014;77(6): 1359-66.

Chutima R, Dell B, Vessabutr S, Bussaban B, Lumyong S. Endophytic fungi from *Pecteilis susannae* (L.) Rafin (Orchidaceae), a threatened terrestrial orchid in Thailand. Mycorrhiza 2011;21(3):221-9.

Czitrom V. One-factor-at-a-time versus designed experiments. The American Statistician 1999;53(2):126-31.

Etesami H, Alikhani HA, Hosseini HM. Indole-3-acetic acid (IAA) production trait, a useful screening to select endophytic and rhizosphere competent bacteria for rice growth promoting agents. MethodsX 2015;2:72-8.

Faria DC, Dias ACF, Melo IS, de Carvalho Costa FE. Endophytic bacteria isolated from orchid and their potential to promote plant growth. World Journal of Microbiology and Biotechnology 2013;29(2):217-21.

Flores-Gallegos AC, Nava-Reyna E. Plant growth-promoting microbial enzymes. In: Kuddus M, editor. Enzymes in Food Biotechnology. Elsevier; 2019. p. 521-34.

Gangwar M, Rani S, Sharma N. Diversity of endophytic Actinomycetes from wheat and its potential as plant growth promoting and biocontrol agents. Journal of Advanced Laboratory Research in Biology 2012;3(1):13-9.

Gause GF, Preobrazhenskaya TP, Sveshnikova MA, Terekhova LP, Maximova TS. A Guide for the Determination of Actinomycetes. Genera *Streptomyces, Streptoverticillium*, and *Chainia*. Moscow, Russia: Nauka; 1983.

Goudjal Y, Toumatia O, Sabaou N, Barakate M, Mathieu F, Zitouni A. Endophytic actinomycetes from spontaneous plants of Algerian Sahara: Indole-3-acetic acid production and tomato plants growth promoting activity. World Journal of Microbiology and Biotechnology 2013;29(10):1821-9.

Herrera H, Fuentes A, Soto J, Valadares R, Arriagada C. Orchid-associated bacteria and their plant growth promotion capabilities. In: Mérillon JM, Kodja H, editors. Orchids Phytochemistry, Biology and Horticulture: Fundamentals and Applications. Switzerland: Springer; 2022. p. 175-200.

Kelly KL. Inter-Society Color Council-National Bureau of Standard Color Name Charts Illustrated with Centroid Colors. Washington DC, USA: Government Printing Office; 1964.

Khamna S, Yokota A, Peberdy JF, Lumyong S. Indole-3-acetic acid production by *Streptomyces* sp. isolated from some Thai

medicinal plant rhizosphere soils. EurAsian Journal of BioSciences 2010;4:23-32.

Kimura M. A simple method for estimating evolutionary rates of base substitutions through comparative studies of nucleotide sequences. Journal of Molecular Evolution 1980;16(2):111-20.

Klongkumnuankarn P, Busaranon K, Chanvorachote P, Sritularak B, Jongbunprasert V, Likhitwitayawuid K. Cytotoxic and antimigratory activities of phenolic compounds from *Dendrobium brymerianum*. Evidence-Based Complementary and Alternative Medicine 2015;2015:1-9.

Kongkatitham V, Muangnoi C, Kyokong N, Thaweesest W, Likhitwitayawuid K, Rojsitthisak P, et al. Anti-oxidant and anti-inflammatory effects of new bibenzyl derivatives from *Dendrobium parishii* in hydrogen peroxide and lipopolysaccharide treated RAW264. 7 cells. Phytochemistry Letters 2018;24:31-8.

Kudo T, Matsushima K, Itoh T, Sasaki J, Suzuki K-I. Description of four new species of the genus Kineosporia: *Kineosporia succinea* sp. nov., *Kineosporia rhizophila* sp. nov., *Kineosporia mikuniensis* sp. nov., and *Kineosporia rhamnosa* sp. nov., isolated from plant samples, and amended description of the genus *Kineosporia*. International Journal of Systematic and Evolutionary Microbiology 1998;48(4):1245-55.

Kuncharoen N, Fukasawa W, Mori M, Shiomi K, Tanasupawat S. Diversity and antimicrobial activity of endophytic actinomycetes isolated from plant roots in Thailand. Microbiology 2019;88(4):479-88.

Kuncharoen N, Yuki M, Kudo T, Ohkuma M, Booncharoen A, Mhuantong W, et al. Comparative genomics and proposal of *Streptomyces radicis* sp. nov., an endophytic actinomycete from roots of plants in Thailand. Microbiological Research 2022;254:Article No. 126889.

Kumar S, Stecher G, Tamura K. MEGA7: Molecular evolutionary genetics analysis version 7.0 for bigger datasets. Molecular Biology and Evolution 2016;33(7):1870-4.

Küster E, Williams S. Selection of media for isolation of *Streptomycetes*. Nature 1964;202(4935):928-9.

Lin L, Xu X. Indole-3-acetic acid production by endophytic *Streptomyces* sp. En-1 isolated from medicinal plants. Current Microbiology 2013;67(2):209-17.

Maitreesophone P, Khine HEE, Nealiga JQL, Kongkatitham V, Panuthai P, Chaotham C, et al. α-Glucosidase and pancreatic lipase inhibitory effects and anti-adipogenic activity of dendrofalconerol B, a bisbibenzyl from *Dendrobium harveyanum*. South African Journal of Botany 2022;146:187-95.

Mearns-Spragg A, Bregu M, Boyd K, Burgess J. Cross-species induction and enhancement of antimicrobial activity produced by epibiotic bacteria from marine algae and invertebrates, after exposure to terrestrial bacteria. Letters in Applied Microbiology 1998;27(3):142-6.

Musa Z, Ma J, Egamberdieva D, Mohamad OAA, Abaydulla G, Liu Y, et al. Diversity and antimicrobial potential of cultivable endophytic actinobacteria associated with the medicinal plant *Thymus roseus*. Frontiers in Microbiology 2020;11:Article No. 191.

Nair DN, Padmavathy S. Impact of endophytic microorganisms on plants, environment and humans. The Scientific World Journal 2014;2014:1-11.

Passari AK, Mishra VK, Saikia R, Gupta VK, Singh BP. Isolation, abundance and phylogenetic affiliation of endophytic actinomycetes associated with medicinal plants and screening for their in vitro antimicrobial biosynthetic potential. Frontiers in Microbiology 2015;7(6):Article No. 273.

Puchooa D. Comparison of different culture media for the *in vitro* culture of *Dendrobium* (Orchidaceae). International Journal of Agriculture and Biology 2004;6(5):884-8.

Qin S, Feng W-W, Wang T-T, Ding P, Xing K, Jiang J-H. Plant growth-promoting effect and genomic analysis of the beneficial endophyte *Streptomyces* sp. KLBMP 5084 isolated from halophyte *Limonium sinense*. Plant and Soil 2017;416(1):117-32.

Rao HY, Rakshith D, Satish S. Antimicrobial properties of endophytic actinomycetes isolated from *Combretum latifolium* Blume, a medicinal shrub from Western Ghats of India. Frontiers in Biology 2015;10(6):528-36.

Saitou N, Nei M. The neighbor-joining method: A new method for reconstructing phylogenetic trees. Molecular Biology and Evolution 1987;4(4):406-25.

Sameera B, Prakash HS, Nalini MS. Actinomycetes from the coffee plantation soils of Western Ghats: diversity and enzymatic potentials. International Journal of Current Microbiology and Applied Sciences 2018;7(8):3599-611.

Shah S, Chand K, Rekadwad B, Shouche YS, Sharma J, Pant B. A prospectus of plant growth promoting endophytic bacterium from orchid (*Vanda cristata*). BMC Biotechnology 2021; 21(1):1-9.

Shakeel Q, Lyu A, Zhang J, Wu M, Chen S, Chen W, et al. Optimization of the cultural medium and conditions for production of antifungal substances by *Streptomyces platensis* 3-10 and evaluation of its efficacy in suppression of clubroot disease (*Plasmodiophora brassicae*) of oilseed rape. Biological Control 2016;101:59-68.

Shan W, Zhou Y, Liu H, Yu X. Endophytic actinomycetes from tea plants (*Camellia sinensis*): Isolation, abundance, antimicrobial, and plant-growth-promoting activities. BioMed Research International 2018;2018:1-12.

Shimizu M. Endophytic actinomycetes: Biocontrol agents and growth promoters. In: Maheshwari DK, editor. Bacteria in Agrobiology: Plant Growth Responses. Berlin Heidelberg, Germany: Springer; 2011. p. 201-20.

Shirling ET, Gottlieb D. Methods for characterization of *Streptomyces* species1. International Journal of Systematic and Evolutionary Microbiology 1966;16(3):313-40.

Shirokikh I, Zenova G, Merzaeva O, Lapygina E, Batalova G, Lysak L. Actinomycetes in the prokaryotic complex of the rhizosphere of oats in a soddy-podzolic soil. Eurasian Soil Science 2007;40(2):158-62.

Shutsrirung A, Chromkaew Y, Pathom-Aree W, Choonluchanon S, Boonkerd N. Diversity of endophytic actinomycetes in mandarin grown in northern Thailand, their phytohormone production potential and plant growth promoting activity. Soil Science and Plant Nutrition 2013;59(3):322-30.

Sinma K, Nurak T, Khucharoenphaisan K. Potentiality of endophytic actinomycetes isolated from sugar cane. Current Applied Science and Technology 2015;15(2):88-97.

Staneck JL, Roberts GD. Simplified approach to identification of aerobic actinomycetes by thin-layer chromatography. Applied Microbiology 1974;28(2):226-31.

Stackebrandt E, Rainey FA, Ward-Rainey NL. Proposal for a new hierarchic classification system, *Actinobacteria* classis nov. International Journal of Systematic and Evolutionary Microbiology 1997;47(2):479-91.

Sukphan P, Sritularak B, Mekboonsonglarp W, Lipipun V, Likhitwitayawuid K. Chemical constituents of *Dendrobium venustum* and their antimalarial and anti-herpetic properties. Natural Product Communications 2014;9(6):825-7.

Suriyachadkun C, Chunhametha S, Thawai C, Tamura T, Potacharoen W, Kirtikara K, et al. *Planotetraspora thailandica* sp. nov., isolated from soil in Thailand. International Journal of Systematic and Evolutionary Microbiology 2009;59(5):992-7.

Suwitchayanon P, Chaipon S, Chaichom S, Kunasakdakul K. Potentials of *Streptomyces rochei* ERY1 as an endophytic actinobacterium inhibiting damping-off pathogenic fungi and growth promoting of cabbage seedling. Chiang Mai Journal of Science 2018;45:692-700.

Taechowisan T, Lumyong S. Activity of endophytic actinomycetes from roots of *Zingiber officinale* and *Alpinia galanga* against phytopathogenic fungi. Annals of Microbiology 2003;53(3):291-8.

Tedsree N, Tanasupawat S, Sritularak B, Kuncharoen N, Likhitwitayawuid K. *Amycolatopsis dendrobii* sp. nov., an endophytic actinomycete isolated from *Dendrobium heterocarpum* Lindl. International Journal of Systematic and Evolutionary Microbiology 2021;71(7):Article No. 004902.

Tsavkelova EA, Cherdyntseva TA, Botina SG, Netrusov AI. Bacteria associated with orchid roots and microbial production of auxin. Microbiological Research 2007;162(1):69-76.

Williams ST, Cross T. Actinomycetes. In: Booth C, editor. Methods in Microbiology. London, UK: Academic Press; 1971. p. 295-334.

Wu LS, Jia M, Chen L, Zhu B, Dong HX, Si JP, et al. Cytotoxic and antifungal constituents isolated from the metabolites of endophytic fungus DO14 from *Dendrobium officinale*. Molecules 2016;21(1):Article No. 0014.

Wu W, Chen W, Liu S, Wu J, Zhu Y, Qin L, et al. Beneficial relationships between endophytic bacteria and medicinal plants. Frontiers in Plant Science 2021;12:Article No. 646146.

Xiang XG, Schuiteman A, Li DZ, Huang WC, Chung SW, Li JW, et al. Molecular systematics of Dendrobium (Orchidaceae, Dendrobieae) from mainland Asia based on plastid and nuclear sequences. Molecular Phylogenetics and Evolution 2013;69(3):950-60.

Xing YM, Chen J, Cui JL, Chen, XM, Guo SX. Antimicrobial activity and biodiversity of endophytic fungi in *Dendrobium devonianum* and *Dendrobium thyrsiflorum* from Vietnam. Current Microbiology 2011;62(4):1218-24.

Yoon S-H, Ha S-M, Kwon S, Lim J, Kim Y, Seo H, et al. Introducing EzBioCloud: A taxonomically united database of 16S rRNA gene sequences and whole-genome assemblies. International Journal of Systematic and Evolutionary Microbiology 2017;67(5):1613-7.

Alternative Feed Sources for Vermicompost Production

Sophoanrith Ro[1*], Vimean Long[1], Rathana Sor[1], Sambo Pheap[1], Raby Nget[1], and Jared William[2]

[1]Faculty of Agronomy, Royal University of Agriculture, Dangkor District, Phnom Penh, P.O. Box 2696, Cambodia
[2]Department of Applied Plant Science, Brigham Young University-Idaho, Rexburg ID 83460, USA

ARTICLE INFO

* Corresponding author:
E-mail: rsophoanrith@rua.edu.kh

ABSTRACT

Locally-available materials could be used to address soil fertility constraints. Vermicomposting is a promising technology where various organic materials are converted into processed compost by earthworms. This study evaluated local feed sources and their potential for vermicompost production. The vermicompost production was carried out in the plastic container under a roofed and net-sided production house. The plot design was laid out in Completely Randomized Design (CRD) with nine replications. Vermiculture feedstock treatments were cow manure (CM) and three cow manure and alternative feed stock treatments (75:25 on a dry basis) that included water hyacinth (WH), used coffee grounds (coffee), or Azolla. The results showed that cow manure combined with Azolla tended to produce more vermicompost after four weeks, but post-harvest earthworm weight was lower. The cow manure treatment produced higher earthworm weights. However, the earthworm population was not influenced by feed sources. The chemical characteristics of vermicompost were not different among feed source ratios or combination. A comparison of the feed stock material before and after vermiculture composting show that EC and total P increased in the compost, total K, organic C and the C:N ratio decreased, but pH and Total N remained constant.

1. INTRODUCTION

Low-fertility tropical soils are common (Razakatiana et al., 2020) and combined nitrogen (N) and phosphorus (P) deficiencies are a widespread problem in tropical soils (Smithson and Giller, 2002). For Cambodia, some production areas are characterized as having soils with low fertility, specifically Cambodia's commonly found sandy soils which have low nutrient levels and low SOM/SOC (Seng et al., 2001). These soils have low specific surface areas with low activity clay fraction, resulting in low nutrient and water retention. The use efficiency of applied mineral fertilizers is very low. The low economic return is an additional concern for farmers. Locally available materials could be used to address the soil fertility constraints of Cambodian soils. Local organic materials may consist of crop residues, farmyard manure, cow manure, kitchen waste, leguminous crop rotation, and other compostable feedstocks (Palm et al., 2001). Moreover, mineral fertilizers are not affordable for many small-scale farmers. Therefore, the sole reliance on mineral fertilizers is not plausible for long-lasting sustainable soil management.

The trend of urban farming, such as small-scaled home garden and pot-based cultivation, are increasing in popularity and need organic materials. Thus, composting is preferable over mineral fertilizer as it is perceived as environmentally friendly. Proper handling and use of compost may reduce environmental pollution (Dolliver et al., 2008). Compost can help recycling of farm wastes, but the decomposition and composting process can take a long time to get the final product (Ayilara et al., 2020). Vermicomposting is an innovative technology in which various organic materials are converted into processed compost by earthworms (Blouin et al., 2019). Cow manure is commonly used as a feedstock for earthworms, and it is commonly used by many farmers as a nutrient source. In vermicompost production, cow manure is the only feed source that cannot be avoided (Yuvaraj et al., 2021). However, the

future availability of cow manure in Cambodia is decreasing because of the reduced use of cattle for draft power. Yuvaraj et al. (2021) reported that cow manure can be combined with other biowastes in vermicompost production. Therefore, there is a need to reduce sole reliance on cow manure as a feedstock for vermiculture and find supplementary local feedstocks such as aquatic fern Azolla, used coffee grounds, water hyacinth, or other plant biproducts. The effects of various feedstocks on vermicompost quality have been reported by other researchers (Amouei et al., 2017; Ansari and Rajpersaud, 2012; Karmegam et al., 2019; Kumari et al., 2020; Nath et al., 2009; Ramnarain et al., 2019).

The objective of this study was to evaluate the effect of various earthworm feedstocks on production and chemical characteristics of vermicompost. It is hypothesized that locally-available feed sources such as Azolla, used coffee grounds, water hyacinth can partially replace cattle manure which is decreasing. It will also pave the way to conduct in-depth study to maximize the alternative feed sources to cow manure in future studies.

2. METHODOLOGY
2.1 Experimental condition and design
The experiment was conducted under a production house with a size of 3 m × 6 m × 3 m (height×length×width). The house was sided by net to allow air flow inside. The plot design was laid out in Completely Randomized Design (CRD) with nine replications. Feedstock treatments were placed in black round plastic containers with a bottom diameter of 43 cm, surface diameter of 43 cm and a height of 13 cm. Cow manure (CM100%) was used as a standard feedstock for earthworm rearing and was treated as the control. Cow manure (CM) was supplemented at a ratio of 75:25 (dry basis) with three types of earthworm feedstocks that included water hyacinth (CM75%+WH25%), Azolla (CW75% +Azolla25%) and used coffee grounds (CM75% +Coffee25%).

2.2 Earthworm and feed preparation
The mass culture of the African earthworm, *Eudrilus engeniae* was carried out by feeding in partially decomposed cowdung (CD) substrate. Cow manure was air-dried for 10 days. The dried cow manure was soaked in water for four days. The water hyacinth was ground chopped by a machine into approximate 2-3 cm length, then water hyacinth, used

coffee grounds and Azolla were subjected to initial decomposition in separate plastic boxes for four weeks when the heat is lower before feeding them to the earthworms.

Containers were filled with 4 kg of feedstock materials on an oven-dry weight basis. The cow manure and supplementary feedstocks were homogenously mixed before filling the containers to a level of 3 to 5 cm below the container's edge. The earthworms were placed in each container at a rate of 234 earthworms per container, which was approximately 250 g of earthworm biomass.

2.3 Feedstock maintenance and vermicompost harvest
The feedstocks were kept moist by spraying water daily at a rate of 550 mL per container until two days prior to the vermicompost harvesting. Pests were controlled by manually removing them from the feedstock. Vermicompost harvesting was performed twice at two and four weeks after earthworms were introduce to the feedstock treatments.

2.4 Data collection
The temperature was recorded twice: two and four weeks after earthworms were introduced to the feedstock treatments. The number and weight of earthworms per container were determined after four weeks following the final harvesting. The productivity of vermicompost (%) was calculated by weight of harvested vermicompost divided by initial total mass of feedstock on a dry weight basis per container (Ramnarain et al., 2019). The vermicompost in each container was harvested by removing the earthworms that were longer than 5 cm and sieving the vermicompost with a 5 mm-sieve. The vermicompost were weighed and its moisture was recorded. The chemical characteristics of vermicompost was analyzed in the soil laboratory of Faculty of Agronomy, Royal University of Agriculture.

2.5 Statistical analysis
The data were analyzed using analysis of variance (ANOVA) to detect the significance among treatments. Means comparison testing was carried out using Tukey's HSD (Honestly Significant Difference) test at an appropriate level of significance. Both ANOVA and mean comparison were determined using Statistix 8 (Version 8.0, Analytical Software, 1985-2003).

3. RESULTS

3.1 Vermicompost production and earthworm population

The data analysis using ANOVA showed a significant difference in total vermicompost harvest among the feedstock treatments (Figure1). The cow manure and Azolla treatment (CM75%+Azolla25%) showed the highest production of vermicompost but was not significantly different from the CM100% earthworm feedstock treatment. The CM75%+ Coffee25% and CM75%+WH25% treatments produced the least amount of vermicompost.

The amount of vermicompost expressed on a dry weight biomass basis showed that replacing 25% of the cow manure with 25% used coffee grounds (CM100%+Coffee25%) resulted in a lower amount of vermicompost (1.82 kg per container) (Table 1). The CM75%+Azolla25% treatment produced a greater amount of vermicompost (2.18 kg per container), but it was not significantly different from either the CM100% or CM75%+WH25% treatments. The production of vermicompost using 75% cow manure and 25% Azolla 25% indicated higher productivity

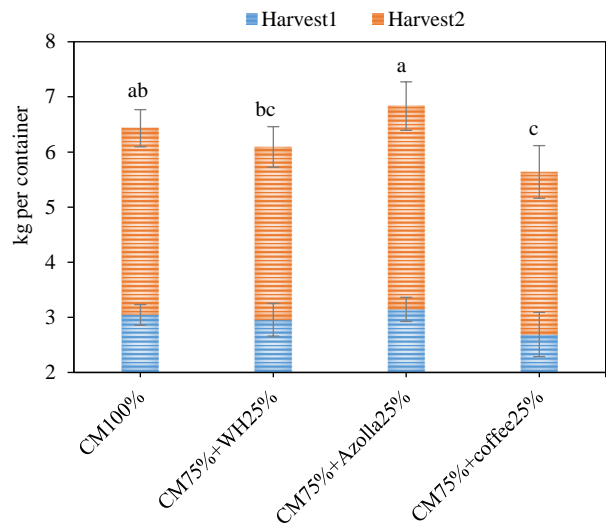than the use of cow 75% manure and 25% used coffee grinds (54.50% Vs 45.59%).

Figure 1. 1st harvest, 2nd harvest and total production of vermicompost per container with different feedstock combinations. Different letters on the bars denote significant difference at p<0.05 by Tukey HSD's test. The error bars represent±standard deviation.

Table 1. Total harvest and productivity of vermicompost

Treatments	Total mass of feed initially (kg, dried basis)	Total harvest vermicompost (kg, dried basis)	Productivity (%)
CM100%	4	2.05[ab]±0.27	51.14[ab]±6.75
CM75%+WH25%	4	1.98[ab]±0.13	49.59[ab]±3.16
CM75%+Azolla25%	4	2.18[a]±0.07	54.50[a]±1.71
CM75%+coffee25%	4	1.82[b]±0.23	45.59[b]±5.82
P-value		0.00**	0.00**

Value is the mean±standard deviation (SD); Different letters in a column denote significant difference at p<0.05 by Tukey HSD's (Honestly Significant Difference) test.

Earthworm population and moisture at the 4-week harvest were not significantly different among the feedstock treatments (Table 2). Earthworm weight (>5 cm length) was significantly different among the feedstock treatments at the 4-week harvest. The feedstock with only cow manure (CM100%) indicated the highest weight value at 407.31 g per container, but

this was not statistically different from the CM75%+WH or CM75%+Coffee25% feedstock treatments. The lowest weight of earthworm (362.06 g per container) was observed in the CW75%+Azolla25% treatment. The temperature measured from week 2 to week 4 showed a drop in temperature from 0.6 to 2 degree Celsius (Figure 2).

Table 2. Earthworm weight and population, temperature and moisture at harvest per container

Treatments	Earthworm weight (g)	Earthworm population (> 5 cm length)	Temperature at harvest (°C)	Moisture at harvest (%)
CM100%	406.31[a]±15.50	217±21	32.56[a]±0.56	68.27±3.38
CM75%+WH25%	387.25[ab]±40.66	220±15	32.26[a]±0.86	67.33±3.17
CM75%+Azolla25%	362.06[b]±34.49	221±14	33.09[ab]±0.34	67.93±3.09
CM75%+coffee25%	394.63[ab]±13.47	220±16	32.66[b]±0.18	67.63±3.75
P-value	0.01*	0.96[ns]	0.00**	0.99[ns]

Value is the mean±standard deviation (SD); Different letters in a column denote significant difference at p<0.05 by Tukey HSD's (Honestly Significant Difference) test.
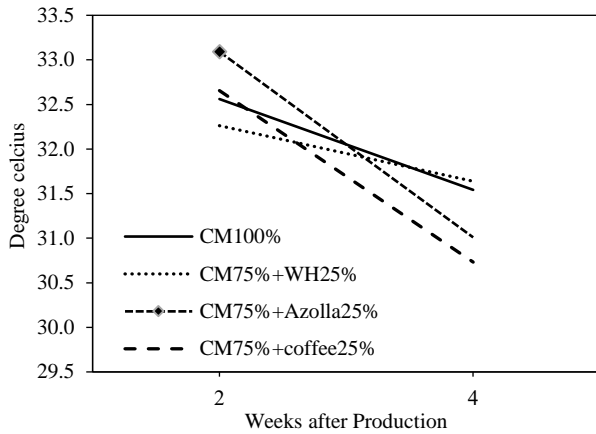
Figure 2. Changes in temperature 2 and 4 weeks after feeding

3.2 Chemical characteristics of vermicompost

There were no significant differences in chemical characteristics among the different vermicompost feedstock treatments (Table 3). The combined treatment mean pH and EC were 7.16 and 582.75 μS/cm, respectively (Table 2). The harvested vermicompost had combined treatment macronutrient means of 1.47% N, 4.77% P, and 1.82% K (Table 2). The combined treatment mean for total Ca was 1.02% and total Mg was 1.80%. The combined treatment ratio of carbon to nitrogen was 27.66.

The changes of final vermicompost product from initial cow manure were observed in some parameters while pH and total N had minor changes (Figure 3). Electrical conductivity, total P and total Mg increased by 24, 28 and 35%, respectively. The large decrease was observed for total Ca, total K and C:N ratio by 412, 167, 14%, respectively.

Table 3. Chemical characteristics of vermicompost for different feedstock treatments

Treatments	pH 1:10 H$_2$O	EC (μS/cm)	Organic C (%)	Total N (%)	Total P (%)
CM100%	7.22±0.10	582.67±87.32	40.40±1.86	1.47±0.14	4.66±1.29
CM75%+WH25%	7.12±0.07	638.00±71.14	40.18±0.54	1.47±0.12	4.27±0.79
CM75%+Azolla25%	7.13±0.15	510.67±67.17	40.04±1.38	1.49±0.23	5.14±1.10
CM75%+coffee25%	7.18±0.08	563.00±53.22	40.86±1.58	1.46±0.21	5.34±0.81
Mean	7.16	582.75	40.37	1.47	4.77
P-value	0.68^{ns}	0.62^{ns}	0.90^{ns}	0.99^{ns}	0.23^{ns}
Treatments	Total K (%)	Total Ca (%)	Total Mg (%)	C:N ratio	
CM100%	1.68±0.44	1.09±0.23	1.84±0.26	27.55±1.49	
CM75%+WH25%	1.82±0.35	1.05±0.10	1.77±0.73	27.55±2.69	
CM75%+Azolla25%	1.86±0.22	1.16±0.22	1.75±0.51	27.14±3.57	
CM75%+coffee25%	1.92±0.54	0.78±0.54	1.85±0.56	28.38±4.30	
Mean	1.82	1.02	1.80	27.66	
P-value	0.90^{ns}	0.26^{ns}	0.99^{ns}	0.97^{ns}	

Value is the mean±standard deviation (SD). "ns" indicates non-significant difference.
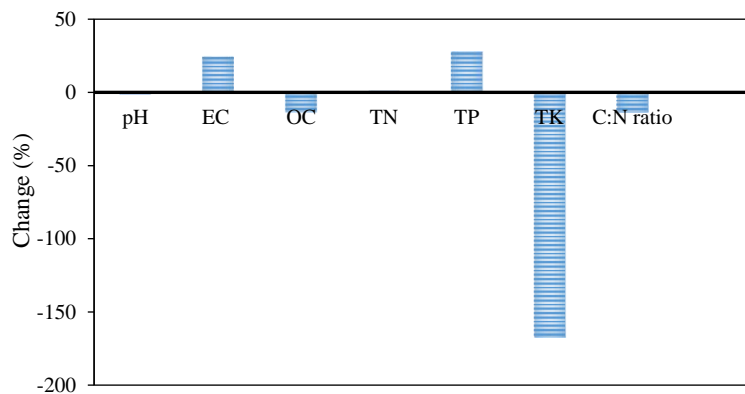

Figure 3. Changes in chemical characteristics of vermicompost products compared to initial cow manure

4. DISCUSSION

The final harvest of fresh and dried vermicompost product for the cow manure and Azolla combination tended to be higher, compared to other feedstocks used in this study. Feedstocks were pre-composted, which likely increased the rate of decomposition fed to earthworms. Azolla has the potential to decompose in 8-10 days and processed into a powder (Setiawati et al., 2018). Used coffee grounds typically decompose at a slower rate due to its lipid fraction and recalcitrant decomposable structural protein-N content (Kitou and Okuno, 1999), which may take several months for microbes to breakdown.

The weight of earthworms from CM75% +Azolla25% treatment collected after harvest seemed to be less, compared to the CM100% treatment. This implied, that even though the population of earthworm was not significantly different among the four feedstocks, cow manure is probably the main food source for the earthworms and could be used as substrate for mass culture and the alternative feedstocks used in this study did not harm the earthworm. The decrease in number of earthworms during the study period may be due to the decline in C/N ratio during the decomposition process (Amouei et al., 2017). The temperature dropped slightly from week 2 to week 4 and was below 35ºC. Although this temperature is out of the optimum temperature range for adult earthworms (Juarez et al., 2011), it did not notably affect the earthworms in this study. The daily watering may have stabilized the temperature for earthworm growth, and the decrease in temperature may have been a result of microbial degradation and dynamics.

The analysis of chemical properties of the feedstock treatments showed no significant difference among the treatments. The modification of only 25% of the feedstock with alternative sources (water hyacinth, Azolla, and used coffee grounds) may have been too small to make changes in their chemical characteristics. The lack of difference of total N among the treatments contrasts with other studies (Ramnarain et al., 2019; Amouei et al., 2017) which reported higher total N in the vermicompost end product. The reason for the difference in total N may be due to the different composting production durations, initial feeds and conditions. This study showed a decline in total K in vermicompost, which has been reported in other studies (Ramnarain et al., 2019). The C/N ratio of vermicompost in this study was 27, which is higher than previously reported to be

smaller than 22 (Karmegam et al., 2019; Deepthi et al., 2021). The drop in C/N ratio compared to initial cow manure was probably due to the use of carbon as energy source during the composting process (Ansari and Rajpersaud, 2012; Ramnarain et al., 2019), leading to low C in the final production and resulting in a low C:N ratio. The reduction of C/N after vermicompost was also reported by Deepthi et al. (2021) and Wang et al. (2022). The decomposition rate in this study ranged from 46 to 55% over a month period. The composting rate of feedstock by earthworms in this study was twice as fast as composting studies that did not include earthworms. The lack of differences observed in the chemical properties before and after composting including pH were also observed by Karmegam et al. (2019). The average pH of final product was around neutral (7.16), which was in a similar range reported by Ramnarain et al. (2019) and Kumari et al. (2020). Additionally, the pH range of the vermicompost in this study is consider a normal vermicomposting product pH (Suthar, 2008; Nath et al., 2009). However, Wako (2021) found the variation of vermicompost pH was dependent on initial feedstock. For instance, the use of soybean and maize feedstock could raise the pH up to between 8.1-8.4, which could be harmful to the earthworms and affect composting rates. Thus, the feedstocks used in this study (cow manure, water hyacinth, Azolla, used ground coffee) are not limiting the earthworm's ability to compost the feedstock based on pH. Karmegam et al. (2019) reported an increase of EC and total P. This study did not show a difference in EC or total P among the feedstock treatments, but EC and total P did increase over the 4-week composting period. The increase in total P is a result of phosphatase in the earthworm's gut (Parthasarathi et al., 2016; Ramnarain et al., 2019; Wako, 2021). The increase of EC during composting showed the role of earthworm to enhance EC in vermicompost and may indicate the release of plant nutrients for mineral salts (Nath et al., 2009). The solubility of mineralized compounds may have increased, leading to the increase in EC (Amouei et al., 2017). However, the EC in this study was less than 8 ds/m or 8,000 µS/cm, which is harmful to most earthworms and plants.

The decrease in organic C in the final product is a result of organic matter degradation, mineralization and respiratory activity of earthworms and other microorganisms, leading to the loss of carbon in the form of CO_2 (Karmegam et al., 2019; Amouei et al., 2017). The reduction of organic carbon and organic

matter content in vermicompost was also reported by Wang et al. (2022) and Jayakumar et al. (2022).The decline of total K and total Mg was also reported by (Ramnarain et al., 2019).

5. CONCLUSION

The ratio of different combinations in feedstocks may affect the rate of vermicomposting decomposition. A combination of cow manure and Azolla tended to produce higher vermicompost productivity, but lower earthworm weights following final vermicompost harvest. The use of cow manure only as feedstock produced the highest earthworm weights. However, the earthworm population was not influenced by the different feedstocks used in this study. Azolla could be used with cow manure to increase vermicompost production. However, cow manure can be used without Azolla as standard medium for earthworm rearing. The chemical characteristics of vermicompost were not difference among the different feedstock ratios and combinations used in this study. However, there was a change in chemical characteristics between the feedstocks and the resulting vermicompost in which pH, total N remained constant while EC and total P increased after vermicompost process. Total K was observed to have reduced significantly in the vermicompost as compared to the feedstock and organic C and C:N ratio also decreased, but to a lesser degree. Future research should focus on other potential feedstocks, which can replace or be used with cow manure to increase the vermicompost quality.

ACKNOWLEDGEMENTS

REFERENCES

Amouei AI, Yousefi Z, Khosravi T. Comparison of vermicompost characteristics produced from sewage sludge of wood and paper industry and household solid wastes. Journal of Environmental Health Science and Engineering 2017; 15:Article No. 5.

Ansari AA, Rajpersaud J. Physicochemical changes during vermicomposting of water hyacinth (*Eichhornia crassipes*) and grass clippings. International Scholarly Research Notices 2012;2012:Article No. 984783.

Ayilara MS, Olanrewaju OS, Babalola OO, Odeyemi O. Waste Management through composting: Challenges and Potentials. Sustainability 2020;12(11):Article No. 4456.

Blouin M, Barrere J, Meyer N, Lartigue S, Barot S, Mathieu J. Vermicompost significantly affects plant growth: A meta-analysis. Agronomy Sustainable Development 2019;39(4): Article No. 34.

Deepthi MP, Kathireswari P, Rini J, Saminathan K, Karmegam N. Vermitransformation of monogastric *Elephas maximus* and ruminant *Bos taurus* excrements into vermicompost using *Eudrilus eugeniae*. Bioresource Technology 2021;320:Article No. 124302.

Dolliver H, Gupta S, Noll S. Antibiotic degradation during manure composting. Journal of Environmental Quality 2008;37:1245-53.

Juarez PDA, Fuente JL, Paulin RV. Vermicomposting as a process to stabilize organic waste and sewage sludge as an application for soil. Tropical and Subtropical Agroecosystems 2011; 14:949-63.

Jayakumar M, Emana AN, Subbaiya R, Ponraj M, Ashok Kumar KK, Muthusamy G, et al. Detoxification of coir pith through refined vermicomposting engaging *Eudrilus eugeniae*. Chemosphere 2022;291:Article No. 132675.

Karmegam N, Vijayan P, Prakash M, Paul JA. Vermicomposting of paper industry sludge with cowdung and green manure plants using *Eisenia fetida*: A viable option for cleaner and enriched vermicompost production. Journal of Cleaner Production 2019; 228:718-28.

Kitou M, Okuno S. Decomposition of coffee residue in soil. Journal of Soil Science and Plant Nutrition 1999;45:981-5.

Kumari V, Paul S CH, Singh M, Kumar A, Pradhan AK. Quality characterisation of vermicompost produced from crop residue and cow dung. International Journal of Current Microbiology and Applied Science 2020;9:776-82.

Nath G, Singh K, Singh D. Chemical analysis of vermicomposts/vermiwash of different combinations of animal, agro and kitchen wastes. Journal of Basic and Applied Science 2009;3:3671-6.

Palm CA, Gachengo CN, Delve RJ, Cadisch G, Giller KE. Organic inputs for soil fertility management in tropical agroecosystems: Application of an organic resource database. Agriculture, Ecosystems and Environment 2001;83:27-42.

Parthasarathi K, Balamurugan M, Prashija KV, Jayanthi L, Ameer Basha S. Potential of *Perionyx excavatus* (Perrier) in lignocellulosic solid waste management and quality vermifertilizer production for soil health. International Journal Recycline Organic Waste Agriculture 2016;5:65-86.

Ramnarain YI, Ansari AA, Ori L. Vermicomposting of different organic materials using the epigeic earthworm *Eisenia foetida*. International Journal of Recycling Organic Wastes in Agriculture 2019;8:23-36.

Razakatiana ATE, Trap J, Baohanta RH, Raherimandimby M, Le Roux C, Duponnois R, et al. Benefits of dual inoculation with arbuscular mycorrhizal fungi and rhizobia on *Phaseolus vulgaris* planted in a low-fertility tropical soil. Pedobiologia 2020;83:Article No. 150685.

Wako RE. Preparation and characterization of vermicompost made from different sources of materials. Open Journal of Plant Science 2021;6(1):42-8.

Seng V, Ros C, Bell RW, White PF, Hin S. Nutrient requirements of rainfed lowland rice in Cambodia. Proceedings of an

International Workshop; 2001 Oct 30-Nov 2; Vientiane: Laos; 2001.

Setiawati MR, Damayani M, Herdiyantoro D, Suryatmana P, Anggraini D, Khumairah FH. The application dosage of *Azolla pinnata* in fresh and powder form as organic fertilizer on soil chemical properties, growth and yield of rice plant. Proceedings of the 1st International Conference and Exhibition on Powder Technology Indonesia; 2017 Aug 8-9; Jatinangor: Indonesia; 2018.

Smithson PC, Giller K. Appropriate farm management practices for alleviating N and P deficiencies in low-nutrient soils of the tropics. In: Adu-Gyamfi JJ, editor. Food Security in Nutrient-Stressed Environments: Exploiting Plants' Genetic Capabilities. Dordrecht, Netherlands: Springer; 2002. p. 277-88.

Suthar S. Development of a novel epigeic-anecic-based polyculture vermireactor for efficient treatment of municipal sewage water sludge. International Journal of Environment and Waste Management 2008;2:84-101.

Wang F, Miao L, Wang Y, Zhang M, Zhang H, Ding Y, et al. Using cow dung and mineral vermireactors to produce vermicompost for use as a soil amendment to slow Pb^{2+} migration. Applied Soil Ecology 2022;170:Article No. 104299.

Yuvaraj A, Thangaraj R, Ravindran B, Chang SW, Karmegam N. Centrality of cattle solid wastes in vermicomposting technology: A cleaner resource recovery and biowaste recycling option for agricultural and environmental sustainability. Environmental Pollution 2021;268:Article No. 115688.

Simulation of PM$_{2.5}$ Concentrations around the Proposed Yangon Outer Ring Road (Eastern Section) in Myanmar Using CALINE 4 Model

Shwe Sin Ko Ko[1], Ranjna Jindal[1*], Win Trivitayanurak[2], Kraichat Tantrakarnapa[3], and Nawatch Surinkul[1]

[1]*Department of Civil and Environmental Engineering, Faculty of Engineering, Mahidol University, Nakhon Pathom 73170, Thailand*
[2]*Department of Environmental Engineering, Faculty of Engineering, Chulalongkorn University, Bangkok 10330, Thailand*
[3]*Department of Social and Environmental Medicine, Faculty of Tropic al Medicine, Mahidol University, Bangkok 10400, Thailand*

ARTICLE INFO

* Corresponding author:
E-mail: ranjna.jindal@gmail.com

ABSTRACT

An increase in traffic volume has resulted in the deterioration of environmental quality and human health in Yangon as well as in the surrounding areas that are connected to the city via several road links. The Yangon Outer Ring Road Construction (YORR) (Eastern Section) is a priority project for solving traffic-related problems. This study aimed to simulate the current levels of PM$_{2.5}$ concentration around the proposed YORR (Eastern Section) area using the CALINE 4 model and to evaluate the model's performance. Air quality measurements of PM$_{2.5}$ were carried out in five townships around the proposed road construction area-for one week at each monitoring location-from January 24th to March 2nd, 2021 using the Haz-Scanner Environmental Perimeter Air Station. When compared to the ambient air quality guidelines of Myanmar, the International Finance Corporation, and the World Health Organization, the observed PM$_{2.5}$ concentrations were found to be usually high at all locations, except in Kyauktan township. Statistical analysis indicated that the CALINE 4 model performed satisfactorily with a coefficient of determination of 0.85-0.90, fractional bias of 0.03-0.50, and normalized mean square error of 0.001-0.100. It is crucial that mitigation measures, including policies regarding the use of low PM emission vehicles and road-side barriers, be implemented by regulatory authorities during and after the YORR construction.

1. INTRODUCTION

Rapid growth in traffic volume has resulted in deterioration of environmental quality and human health. Evidently, an increase in traffic volume-as a result of a newly constructed roads-is an additional source of particulate matter (PM) in the surrounding environment of the new roads (Chuang et al., 2020). PM exposure leads to a risk of developing diseases and health conditions, such as nonfatal heart attacks, irregular heartbeat, aggravated asthma, decreased lung function, and increased respiratory symptoms such as coughing or difficulty breathing, and premature death in people with existing heart or lung diseases (Kim et al., 2015). Particulate matter that is 2.5 µm or smaller in size (PM$_{2.5}$) not only causes health problems but also seriously affects the chemical processes in the atmosphere and influences climate change (Kumar et al., 2010).

The development of roads for transportation plays an important role in a country's economic growth as it facilitates a continuous supply of goods and services. The proposed Yangon Outer Ring Road Construction (YORR) (Eastern Section) has a total length of approximately 49 km, including a 1.28 km-long bridge across the Bago River and frontage roads; it is approximately 20 km from the downtown area and is a priority project for solving traffic problems (JICA, 2015). The project site is located near five townships: Hlegu, East Dagon, Dagon Seikkan, Thanlyin, and Kyauttan. In view of sustainable development goals, such projects must focus on the environment, including air quality.

Several air quality models have been developed to evaluate roadside air quality (Gokhale and Khare, 2004). However, several of these models are complex, given the poor availability of meteorological and traffic data. The modified general finite line source model of particulates, as well as CALINE 3 and CAL3QHC models have been used to evaluate vehicle-derived airborne particulate mass emissions (Gokhale and Raokhande, 2008). Other models that have been widely used to evaluate the dispersion of air pollutants at roadsides (Ghanshyam, 2018) include a series of California Line Source Dispersion Models. CALINE 4 is the most recent version in the CALINE series, which has been used extensively worldwide and is claimed to perform better than other line source models (Dhyani et al., 2013; Goud et al., 2015; Muneeswaran and Chandrasekaran, 2015; Sharma et al., 2013).

In view of the proven negative effects of new road construction on air quality, forecasting $PM_{2.5}$ concentration is important to control air pollution in the study area, as no such research has been conducted to date. The objective of this study was to simulate the current levels of $PM_{2.5}$ concentration in the proposed YORR (Eastern Section) area using the CALINE 4 model. Overall, this study aimed to lay the foundation for further research into the impacts of the YORR (Eastern Section) on the $PM_{2.5}$ concentrations.

2. METHODOLOGY

2.1 Study area

The Yangon Outer Ring Road (YORR) (Eastern Section) project in Yangon-a former capital city and now the biggest commercial center of Myanmar-was chosen as the study area. Based on the 2014 census, the total population of the five townships in the YORR project area was approximately 1,039,328 (city population, 2022). The climate of Yangon is mainly characterized by tropical monsoon (Weatherbase, 2022). The main contributors of $PM_{2.5}$ in the study area include traffic, domestic fuel consumption, industrial activities, and natural dust. Air quality was monitored at one location in each of the five townships, represented as Point-1, Point-2, Point-3, Point-4, and Point-5. A map of the study area with the air quality monitoring locations is presented in Figure 1.
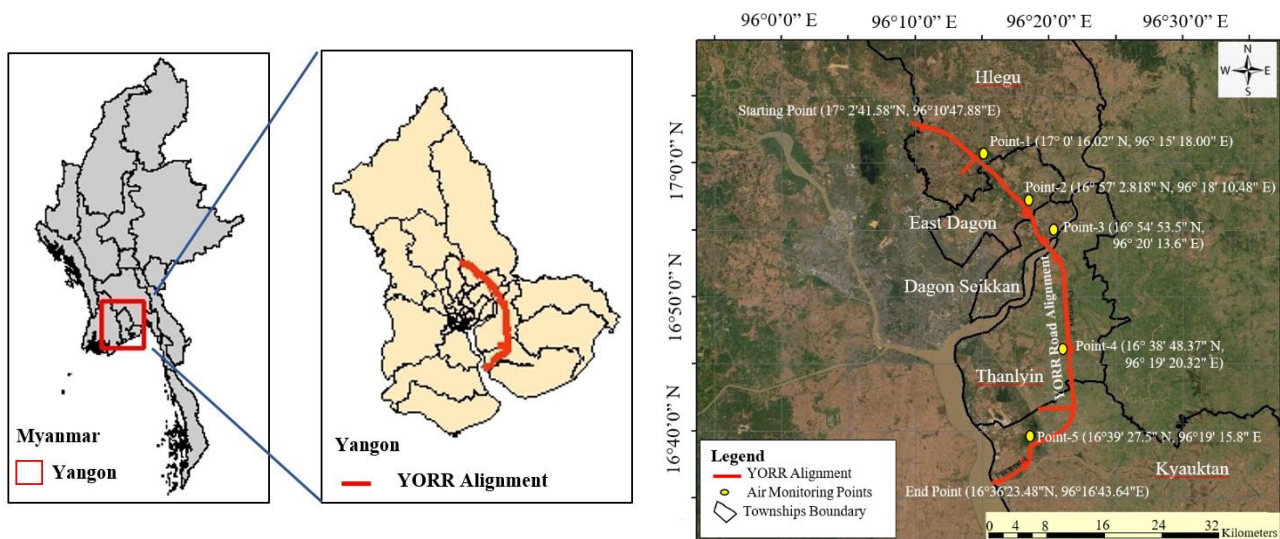

Figure 1. Map of Yangon Outer Ring Road (Eastern section) showing the air quality monitoring locations (location of YORR (Eastern section) in Yangon is shown in the top panel)

2.2 Data collection

$PM_{2.5}$ measurements were carried out from January 24th to March 2nd, 2021, at the five locations surrounding the proposed road construction area (Table 1) using the portable wireless Haz-Scanner Environmental Perimeter Air Station (HAZS-CANNER™ EPAS). The Haz-Scanner is equipped with a variety of gas, $PM_{2.5}$, temperature, and humidity sensors, which can detect different variables ranging

from 1 to 20,000 μg/m^3. The $PM_{2.5}$ sensor is equipped with a high-precision laser sensor that detects the number and diameter of particles through the laser scattering method, and accurately calculates the $PM_{2.5}$ concentration. An anemometer (Vantage Pro2 Console) was installed on top of the monitoring station (2.5 m above ground level) and connected to HAZSCANNER™ EPAS instrument. Due to limited availability of instruments, simultaneous monitoring

at all five locations could not be performed. In addition, the weekly variability and long-range transport events were not considered.

2.3 CALINE 4 model

CALINE 4 is a Gaussian dispersion model specifically used to simulate the level of air pollution adjacent to roadways by estimating the vehicular pollutant concentration at source receptor distances of tens to hundreds of meters (Pournazeri et al., 2013).

The CALRoads View model Version 6.2.5 form of CALINE 4, developed by Lakes Environmental Software, Canada in 2008, was used for this study (Mishra, 2016).

Table 1. Air quality monitoring locations and schedule

Location	Description	Monitoring date
Point-1	Hlegu Township (~0.8 km from centerline of road alignment)	24-30 January 2021
Point-2	East Dagon Township (~0.24 km from centerline of road alignment)	31 January - 6 Febuary 2021
Point-3	Dagon SeikKan Township, (~1.9 km from centerline of road alignment)	7-13 Febuary 2021
Point-4	Thanlyin Township, (~0.7 km from centerline of road alignment)	15-21 Febuary 2021
Point-5	Kyaut Tan Township, (~0.51 km from centerline of road alignment)	23 Febuary - 1 March 2021

2.3.1 Inputs for CALINE 4 model

"Multirun" was chosen as the CALINE 4 model run type to calculate the eight-hourly average $PM_{2.5}$ concentration at the receptor points - because of the time limitations - to observe the fluctuations during different periods of the day. The five monitoring points were set as discrete receptor points.

The important input variables required for the CALINE 4 model included traffic volume (number of vehicles per hour), meteorological parameters (wind speed, wind direction, ambient temperature, mixing height, and stability class), composite emission factors (CEFs), road geometry (road width, median width, and road elevation), type of terrain (rural or urban), background concentration of pollutants (ppm or $\mu g/m^3$), and pre-identified receptor locations along the road alignment (Dhyani et al., 2013). The input parameters used in the model are listed in Table 2.

Meteorological data of the observation periods, including wind direction, wind speed, and temperature at the monitoring stations, were obtained through on-site measurements. The CALINE 4 model cannot predict input wind speeds of less than 1 m/s and automatically selects a speed of 0.5 m/s as the default value (Dhyani and Sharma, 2017).

Table 2. Input parameters used in the CALINE 4 model

No	Input data	Units	Source
1	Meteorological data		
	- Wind direction	Degree	On-site measurement
	- Wind speed	m/s	On-site measurement
	- Atmospheric stability class (Pasquill (P-G) stability class)	A (1) to G (7)	Based on on-site measurement of wind speed
	- Wind degree standard deviation	Degree	Based on on-site measurement of wind direction
	- Mixing height	Meters (m)	Benson, 1984 (recommended value)
	- Temperature	°C	On-site measurement
2	Road link information		
	- Link type	At-grade	Physically observed
	- Link height (at-great option assumes roadway to be at ground level)	Meters (m)	
	- Mixing zone width (carriage width+3 on both sides)	Meters (m)	Google map
	- Link geometry Beginning (17° 2'41.58" N, 96°10'47.88" E) and Ending coordinates (16°36'23.48" N, 96°16'43.64" E)	-	Google map

Table 2. Input parameters used in the CALINE 4 model (cont.)

No	Input data	Units	Source
3	Road link activity		
	- Hourly traffic volume	vehicles/h	Calculated based on the secondary data with the assumed percent fraction for the existing road networks JICA, 2015 MJTD, 2016
	- Composite emission factor	g/vehicle-km	JICA, 2016 ARAI, 2008 for PM$_{2.5}$
4	Background concentration	µg/m^3	Calculated based on on-site measurement of wind direction and observed concentrations at the nearest monitoring points

Hourly atmospheric stability classes in the study area, which were based on the Pasquill-Gifford classification, were estimated using wind speed, incoming solar radiation, and cloud cover (daytime and night-time) (Turner, 1994). The study area was either sunny or slightly cloudy during the monitoring period. Typically, the temperature fluctuated between 30 and 38°C during the daytime; the amount of incoming solar radiation was assumed to be moderate. Clear skies and a temperature drop to 16°C were recorded at night-time (Weather Spark, 2022). According to the classification of Pasquill-Gifford, atmospheric stability in the study area was classified as A (extremely unstable) at daytime and F (moderately stable) at night-time. The wind degree standard deviation of the horizontal wind direction (σθ) was based on the atmospheric stability classification (NRC, 1980). The meteorological parameters used in the CALINE 4 model are presented in Table 3.

Table 3. Meteorological parameters used in CALINE 4 model

Townships (monitoring Points)	Temperature (°C)		Wind speed (m/s)		Predominant wind direction	Predominant atmospheric stability class	
	Max	Min	Max	Min		Daytime	Nighttime
Hlegu (Point-1)	37.3	18.3	5	0	*NNE	A	F
East Dagon (Point-2)	36.9	17.2	2	0	*NE	A	F
Dagon Seikkan (Point-3)	35.9	16.9	4	0	*E	A	F
Thanlyin (Point-4)	36.2	19.5	7	0	*S	A	F
Kyauk Tan (Point-5)	37.6	17.3	2	0	*SE	A	F

*NNE- North East, *NE- North East, E-East, S- South, SE-South East

The mixing height was set to 1,000 m, except for very severe nocturnal inversions; this is the recommended value for all normal atmospheric occurrences (Benson, 1984; Chen et al., 2008; USEPA, 1995). Mixing height rarely affects the predicted concentration, especially under perpendicular wind conditions (Sahlodin et al., 2007). Some studies have reported negligible effects of mixing height on the predicted concentrations (Batterman et al., 2010; El-Fadel et al., 2000).

Road link information: The road geometry, used as the input parameter for the model, was obtained from the YORR project information. Based on physical observations, all road link types for the existing road networks were at-grade. Therefore, all road links were assumed to be zero.

The mixing zone was considered to be an area of uniform emissions and turbulence. Mixing zone width is defined as the width of the travelled way (traffic lanes not including shoulders) plus 3 m (horizontal dispersion adjustment) on each side. Google Map measurements were applied to the carriageway width of the roads.

Road link activity: Hourly traffic volumes were taken from a study conducted at the Bago and Yangon-Thanlyin bridges in 2013 (JICA, 2015) to obtain hourly distribution factors. Subsequently, the hourly traffic volume (vehicles/h) recorded in 2015 on Than Lyin-Thilawa and Thilawa roads near the study area (MJTD, 2016) were used to calculate the hourly traffic volume based on hourly traffic volume distribution factors (vehicles/h) obtained from a previous study

(JICA, 2015). Furthermore, the total traffic volume in the study area for 2021 was calculated using future annual average daily traffic formula (Horowitz, 1999; Dixon, 2004). The traffic volumes in the vicinity of the monitoring points were obtained using mass balance and after adjusting the percentage fraction based on the location and direction of the roads in the existing road networks in each township.

The CEF represented the source strength by the average emission rate of all vehicle types in the local vehicle kilometer (g/v-km). The weighted emission factor was obtained based on the vehicle distribution by type, age, and operation mode. Information on the distribution of vehicle types was collected from the Bago River Bridge EIA report (JICA, 2016). $PM_{2.5}$ emission factors for different vehicle types were obtained from the Automotive Research Association of India, assuming a similar traffic pattern in developing countries (ARAI, 2008). The evaluated average CEFs for different vehicle types were used in the CALINE 4 model for simulations.

The background concentrations for each simulation were estimated according to the hourly concentrations observed at the nearest monitoring points. Based on the wind directions and distance between the two points, the background concentrations at the receptor location were assumed to be 70% and 50% of the observed concentration at

the nearest monitoring points for dominant and non-dominant wind directions, respectively. For example, at Point-4, the predominant wind direction during the observation period was from the south, and the closest observation location was point-5, which was situated 12.6 km away at the south-south-west region of Point-4. Therefore, the background concentrations at Point-4 were assumed to be 70% and 50% of the observed concentrations at Point-5 for the dominant and nondominant wind directions, respectively.

Five simulation domains were set up to represent the emission sources from the existing road networks in each of the five townships located near the new YORR alignment. As the CALRoads View Model could be used for a maximum of 62 links, domains were set up considering this limitation.

Model performance evaluation was conducted by regression analysis of observed and simulated $PM_{2.5}$ concentrations, including coefficient of determination (r^2), normalized mean square error (NMSE), and fractional bias (FB), as recommended by the U.S. Environmental Protection Agency (Hanna et al., 1993).

3. RESULTS AND DISCUSSION
3.1 Meteorological results

Wind rose diagrams displaying the distribution of wind directions and wind speeds for each township are presented in Figure 2.
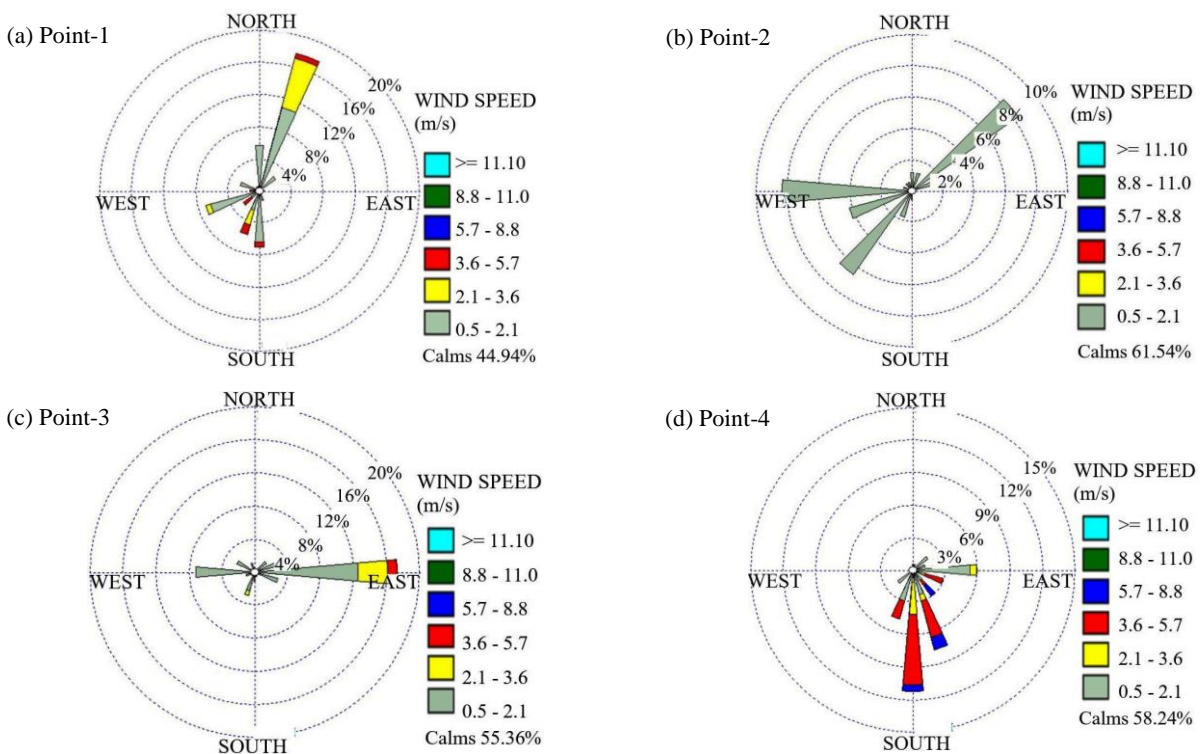

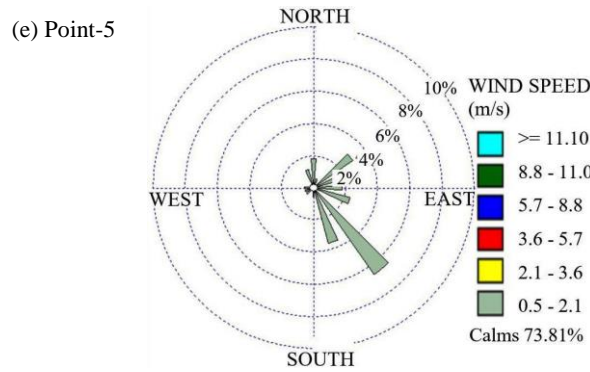**Figure 2.** Wind directions and wind speeds at each monitoring station during the respective monitoring periods

Figure 2. Wind directions and wind speeds at each monitoring station during the respective monitoring periods (cont.)

3.2 Observed and simulated results

Based on the hourly $PM_{2.5}$ concentrations observed at each monitoring station for seven days, the maximum concentration observed at Point-1 was 176.76 μg/m³. This could be due to dust erosion from nearby unpaved roads, vehicular emissions, or domestic fuel consumption. In Myanmar, the ambient air quality standard for the daily average concentrations of $PM_{2.5}$, as prescribed in the National Environmental Quality (Emission) Guidelines, is 25 μg/m³; this is similar to the value prescribed by the General Environmental Health and Safety Guidelines (ECD, 2015; IFC, 2007). The WHO released the updated air quality guidelines in September 2021, which significantly reduced the maximum allowable safe levels of daily average $PM_{2.5}$ concentration to 15 μg/m³. In this study, the daily average concentrations of $PM_{2.5}$ were generally higher than the value specified in the new WHO guidelines, except at Point-4 and Point-5 on certain days (Figure 3). The WHO estimates approximately 7 million premature deaths every year due to the effects of air pollution. However, 80% of the deaths attributed to $PM_{2.5}$ exposure can be avoided if countries attain their annual air quality level for $PM_{2.5}$ (WHO, 2021).
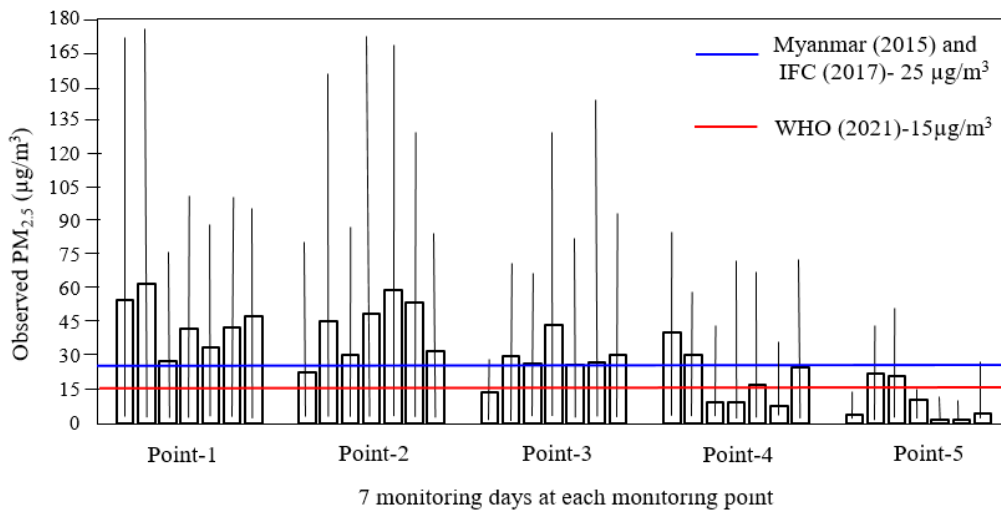
Figure 3. Range and daily average concentrations of $PM_{2.5}$ during the 7-day observation period at all receptor locations

A recent study conducted in seven townships of Yangon City, reported the highest $PM_{2.5}$ concentration observed in the morning (164±52 μg/m³) followed by the second highest concentration in the evening (100±35 μg/m³) and the lowest concentrations in the afternoon (31±15 μg/m³) in the Hlaingtharyar Township (Yi et al., 2018). Another study conducted in Mingaladon, one of the most crowded townships of Yangon, observed the daily average $PM_{2.5}$ concentrations in residential and commercial areas to be 23.60±10.13 μg/m³ and 33.40±10.64 μg/m³, respectively. It was observed that 61% of the observed $PM_{2.5}$ concentrations exceeded the previous guideline (25 μg/m³) of the WHO. Tun et al. (2017) concluded that $PM_{2.5}$ concentration reached its peak between 3:00 and 5:00 am, and after 9:00 pm

at traffic congestion locations in Mingaladon Township, Yangon. In this study, 74% of the observed $PM_{2.5}$ concentrations exceeded the new WHO guideline (15 $\mu g/m^3$), while 60% of the observed results exceeded the old guideline (25 $\mu g/m^3$). Overall, the $PM_{2.5}$ concentrations in the present study were lower than those in other studies conducted in the Yangon area because the townships around the YORR were outside the city and the traffic congestion in downtown area of Yangon was acceptable.

The average of eight-hour interval concentrations of $PM_{2.5}$ at each of the five monitoring stations obtained during the seven monitoring days

were compared with the simulated concentrations by the CALINE 4 model (Figure 4).

As shown in Figure 4, the highest eight-hourly average $PM_{2.5}$ concentration was 99.65 $\mu g/m^3$ at Point-1 (Hlegu Township). In general, the model slightly underpredicted $PM_{2.5}$. Most of the observed eight-hourly concentrations of $PM_{2.5}$ were close to the simulated results (difference of less than 10 $\mu g/m^3$), except at some points during a few monitoring periods. Differences increased with varying wind directions at the monitoring point. For example, wind directions on day-1 (5:00-1:00 am) at Point-1 was from several directions; therefore, the simulated results had a higher difference (26.03 $\mu g/m^3$).

(a) Observed and simulated concentration of $PM_{2.5}$ at Hlegu Township- (Point-1)
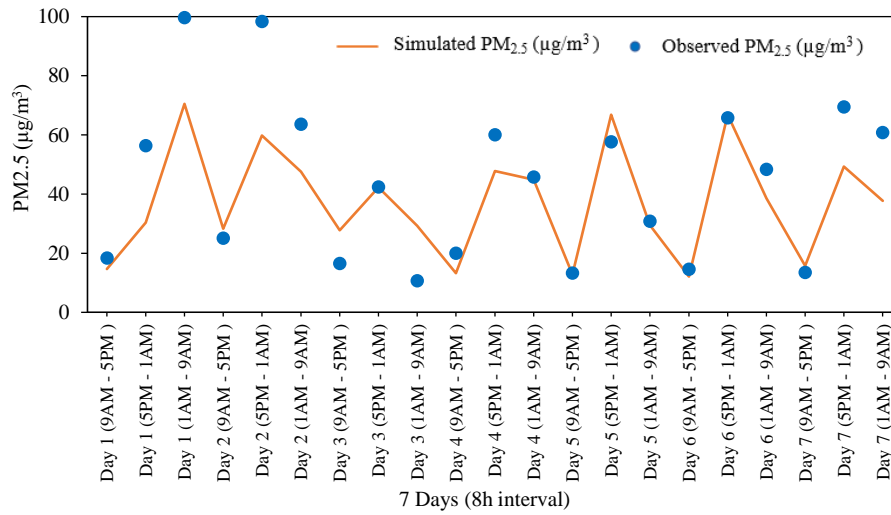
(b) Observed and simulated concentration of $PM_{2.5}$ at East Dagon Township- (Point- 2)
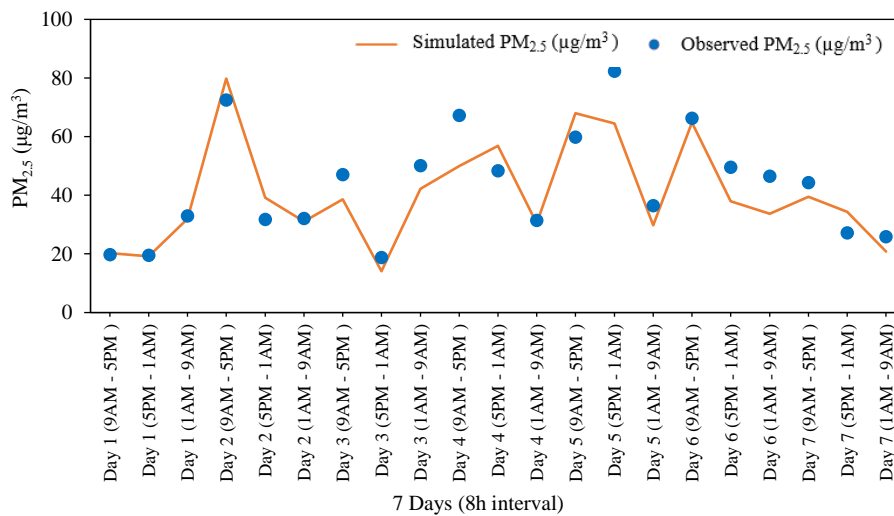
Figure 4. Observed and simulated $PM_{2.5}$ concentrations at five monitoring stations during the seven-day observation period

(c) Observed and simulated concentration of PM₂.₅ at Dagon Seikkan Township- (Point-3)
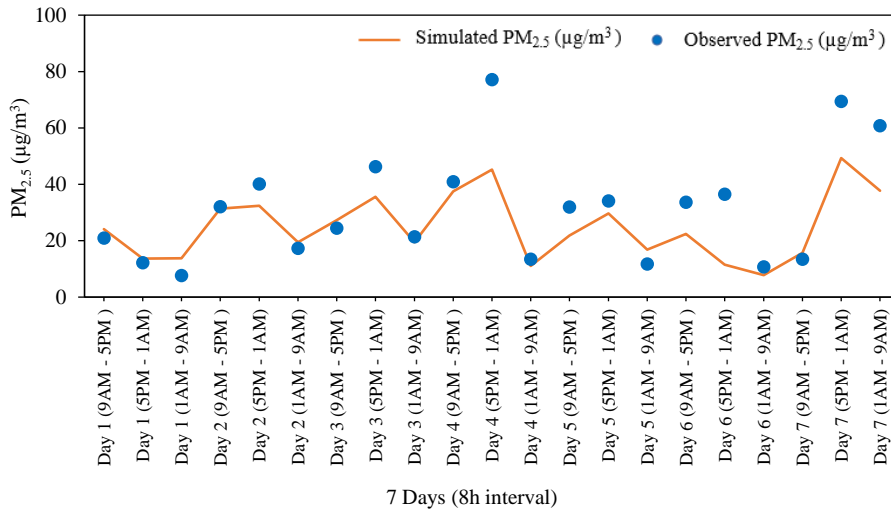
(d) Observed and simulated concentration of PM₂.₅ at Thanlyin Township- (Point-4)
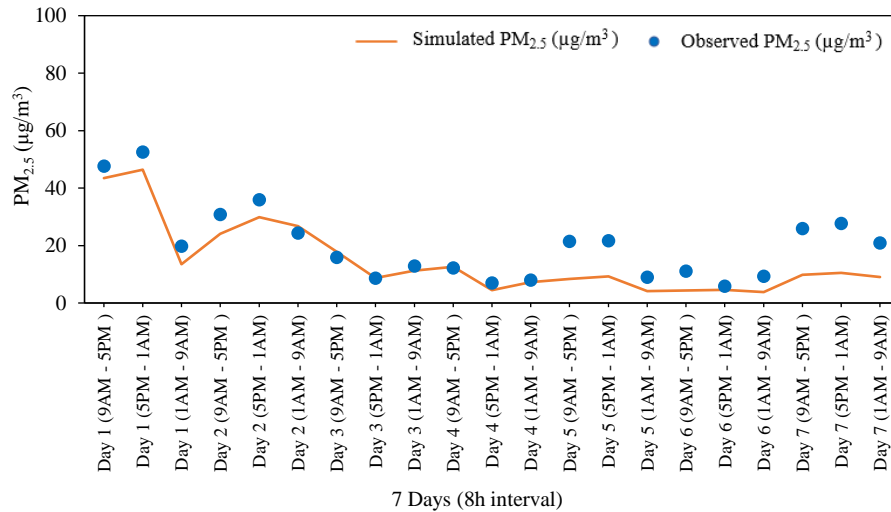
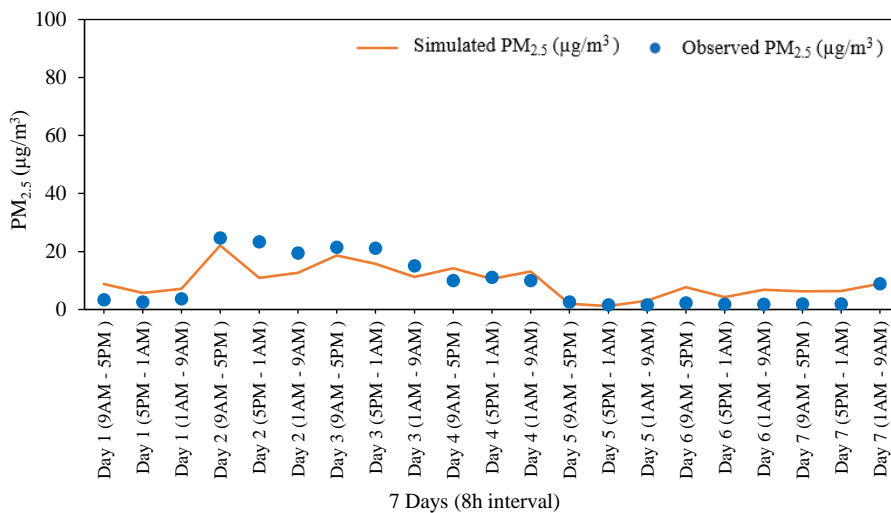(e) Observed and simulated concentration of PM₂.₅ at Kyauktan Township- (Point-5)

Figure 4. Observed and simulated PM₂.₅ concentrations at five monitoring stations during the seven-day observation period (cont.)

3.3 Performance evaluation of the model

Scatter plots of the observed versus simulated concentrations during the monitoring period are presented in Figure 5.

Performance evaluation parameters, r^2, NMSE, and FB, which are based on the regression analysis of observed and simulated $PM_{2.5}$ concentrations, are shown in Table 4.
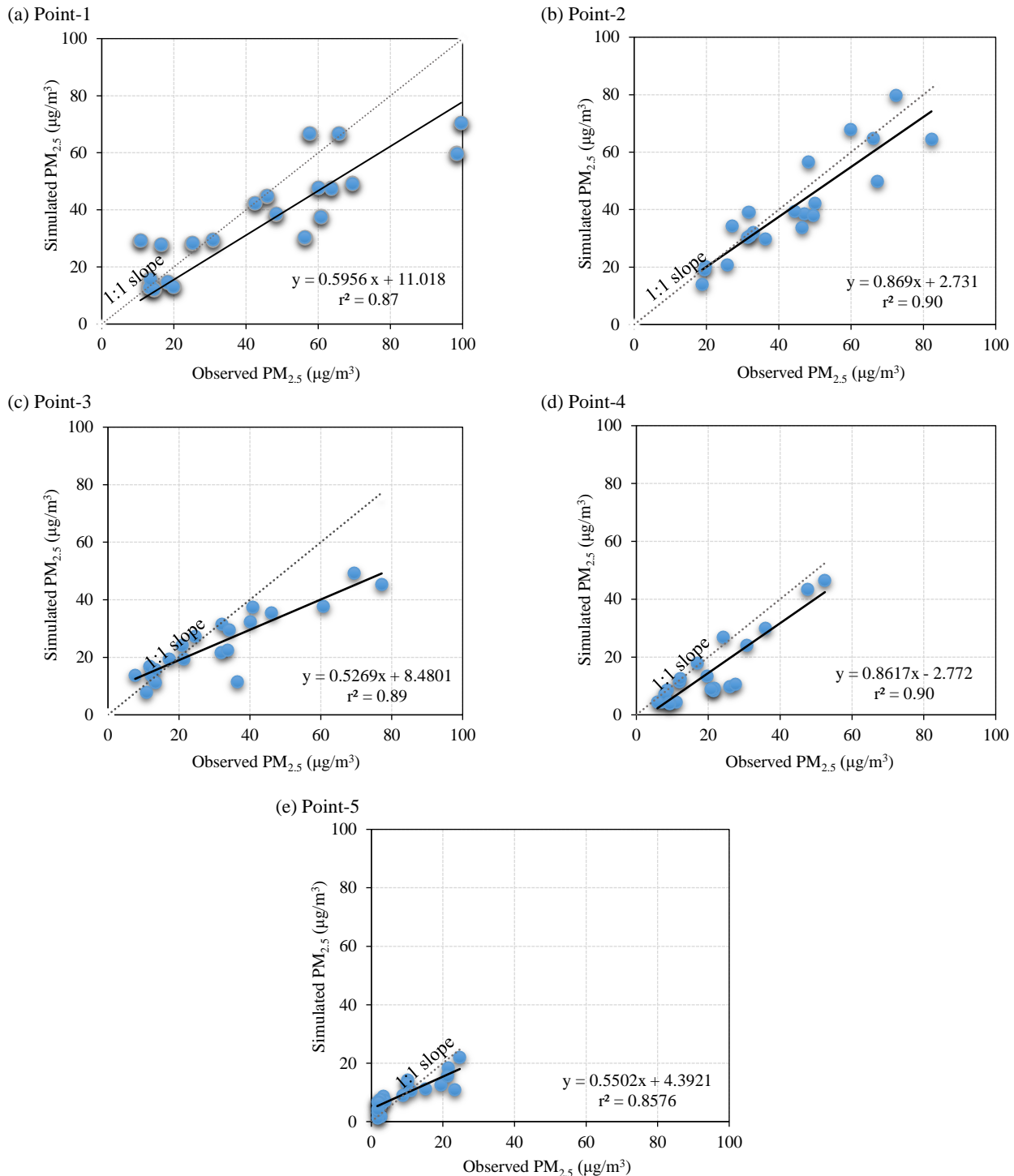
Figure 5. Model performance for 8 h mean concentration at five receptor locations during the seven-day observation period

Correlation between the observed and simulated $PM_{2.5}$ concentrations for all the receptor points was higher than 0.85, which was better than the result obtained by Yu et al. (2021) at 0.51. However, higher values of correlation between the observed and simulated $PM_{2.5}$ concentrations (0.95 and 0.89) with and without background concentrations have been reported in other studies (Chen et al., 2008; Chen et

al., 2009). As shown in Table 4, the values of the correlation coefficient, FB, and NMSE were within the acceptance limits. Hence, the CALINE 4 model performed satisfactorily in simulating the $PM_{2.5}$.

Table 4. Model performance evaluation

	Model performance					Acceptance value
	Point-1	Point-2	Point-3	Point-4	Point-5	
Correlation (r^2)	0.8714	0.9020	0.8873	0.9007	0.8576	close to 1
Fractional bias (FB)	0.3760	0.0373	0.5000	0.0442	0.4367	$-0.5 < FB < 0.5$
Normalized mean square error (NMSE)	0.0287	0.0050	0.0510	0.1038	0.0010	$NMSE \leq 0.5$

The CALINE 4 model can be effectively used to estimate the concentrations of other air pollutants in the YORR (Eastern Section), such as $PM_{2.5}$ CO, and NO_2, and compare with pre-project conditions. This can aid in the vehicular pollution management of new road projects.

4. CONCLUSION

Based on the hourly $PM_{2.5}$ concentrations during the seven days at each monitoring station, the highest concentration observed at Point-1 was 176.76 $\mu g/m^3$. This could be due to dust erosion from nearby unpaved village roads. When compared with the ambient air quality guidelines of Myanmar, International Finance Corporation (IFC), and WHO, $PM_{2.5}$ concentrations were generally high at all locations, except at Point-4 and Point-5 on certain days.

The observed 8-hourly average $PM_{2.5}$ concentrations (for seven days) were compared with the simulated concentrations for all five receptor locations. The slopes of the regression lines between the observed (Y-axis) and simulated concentrations (X-axis) were less than the ideal 1:1 line. Therefore, model slightly underestimated $PM_{2.5}$. Based on statistical analysis, r^2, NMSE, and FB were well within the prescribed limits. Therefore, the performance of the CALINE 4 model was considered acceptable.

Mitigation measures, such as transportation policies regarding the use of low PM emission fuels and roadside barriers, need to be implemented by regulatory authorities.

ACKNOWLEDGEMENTS

REFERENCES

Automotive Research Association of India (ARAI). Emission Factor Development for Indian Vehicles as A Part of Ambient Air Quality Monitoring and Emission Source Apportionment Studies. Pune, India: ARAI; 2008. p. 1-89.

Batterman SA, Zhang K, Kononowech R. Prediction and analysis of near-road concentrations using a reduced-form emission/dispersion model. Environmental Health 2010;9:1-18.

Benson PE. CALINE 4: A Dispersion Model for Predicting Air Pollutant Concentrations near Roadways. California, USA: Department of Transportation; 1984.

Chen H, Bai S, Eisinger D, Niemeier D, Claggett M. Modeling Uncertainties and Near-Road $PM_{2.5}$: A Comparison of CALINE 4, CAL3QHc and AERMOD [dissertation]. Department of Civil and Environmental Engineering, University of California; 2008.

Chen H, Bai S, Eisinger D, Niemeier D, Claggett M. Predicting near-road $PM_{2.5}$ concentrations: Comparative assessment of CALINE4, CAL3QHC, and AERMOD. Transportation Research Record: Journal of the Transportation Research Board 2009;2123:26-37.

Chuang KJ, Lin LY, Ho KF, Su CT. Traffic-related $PM_{2.5}$ exposure and its cardiovascular effects among healthy commuters in Taipei, Taiwan. Atmospheric Environment 2020;7:Article No. 100084.

City Population. MYANMAR: Administrative Division [Internet]. 2022 [cited 2022 Mar 23]. Available from: https://www.citypopulation.de/en/myanmar/admin/.

Dhyani R, Sharma N. Sensitivity analysis of CALINE4 model under mix traffic conditions. Aerosol and Air Quality Research 2017;17:314-29.

Dhyani R, Singh A, Sharma N, Gulia S. Performance evaluation of CALINE 4 model in a hilly terrain: A case study of highway corridors in Himachal Pradesh (India). International Journal of Environment and Pollution 2013;52:244-62.

Dixon M. The Effects of Errors in Annual Average Daily Traffic Forecasting: Study of Highways in Rural Idaho. Moscow, Russia: National Institute for Advanced Transportation Technology (NIATT); 2004.

El-Fadel M, Najm MA, Sbayti H. Air quality assessment at a congested urban intersection. Journal of Transportation and Statics September 2000;3:86-102.

Environmental Conservation Department (ECD). National Environmental Quality (Emission) Guidelines. Naypyitaw, Myanmar: ECD; 2015. p. 1-72.

Ghanshyam. CALINE 4 model validation in the nearfield of Bahadur Shah Zafar Marg, New Delhi, India. Ghanshyam Journal of Engineering Research and Application 2018;8:1-6.

Gokhale S, Khare M. A review of deterministic, stochastic and hybrid vehicular exhaust emission models. International Journal of Transport Management 2004;2:59-74.

Gokhale S, Raokhade N. Performance evaluation of air quality models for predicting PM_{10} and $PM_{2.5}$ concentrations at urban traffic intersection during winter period. Science of the Total Environment 2008;394:9-24.

Goud BS, Savadatti S, Prathibha D. Application of CALINE 4 model to predict $PM_{2.5}$ concentration at central silk board traffic intersection of Bangalore City. International Journal of Civil Engineering and Technology 2015;6:191-200.

Hanna SR, Strimaitis DG, Chang JC. Hazard Response Modeling Uncertainty (A Quantitative Method).Volume 1: User's Guide for Software for Evaluating Hazardous Gas Dispersion Models. Massachusetts, USA: Sigma Research Corporation; 1993.

Horowitz A. Guidebook on Statewide Travel Forecasting. Washington, DC, USA: Federal Highway Administration; 1999

International Finance Corporation (IFC). Environmental, Health, and Safety Guidelines. Air Emissions and Ambient Air Quality. Washington, DC, USA: World Bank Group; 2007. p. 4-17.

Japan International Cooperation Agency (JICA). Bago River Bridge Environmental Impact Assessment Report. Yangon, Myanmar: Ministry of Construction; 2016. p. 9-81.

Japan International Cooperation Agency (JICA). Project for Comprehensive Urban Transport Plan of the Greater Yangon (YUTRA) Data Collection Survey for the Yangon Urban Expressway (YUEX) Project. Yangon, Myanmar: JICA; 2015. p. 19-140.

Kim KH, Kabir E, Kabir S. A review on the human health impact of airborne particulate matter. Environment International 2015;74:136-43.

Kumar P, Robins A, Vardoulakis S, Britter R. A review of the characteristics of nanoparticles in the urban atmosphere and the prospects for developing regulatory controls. Atmosphere Environment 2010;44:5035-52.

Mishra AK. Analysis and modeling of air pollutants along a link road in Mumbai City. International Journal of Innovative Research in Science and Engineering 2016;2:287-92.

Muneeswaran S, Chandrasekaran R. Ambient air quality modelling near busy road junctions in Coimbatore City using CALINE 4 model. International Journal of Engineering Research and Technology 2015;3:1-10.

Myanmar Japan Thilawa Development (MJTD). Environmental Impact Assessment for Industrial Area of Zone B, EIA Report. Yangon, Myanmar: MJTD; 2016. p. 23-332.

Nuclear Regulatory Commission (NRC). Meteorological Monitoring Programs for Nuclear Power Plants, Regulatory Guide 1.23, Proposed Revision 1. Washington, DC, USA: Nuclear Regulatory Commission; 1980. p. 1-16.

Pournazeri S, Gazollo B, Princevac M. Development of an air dispersion model to study near-road exposure. Journal of the Air and Waste Management Association 2013;1:38-40.

Sahlodin AM, Sotudeh-Gharebagh R, Zhu Y. Modeling of dispersion near roadways based on the vehicle-induced turbulence concept. Atmospheric Environment 2007;41:92-102.

Sharma N, Gulia S, Dhyani R, Singh A. Performance evaluation of CALINE 4 dispersion model for an urban highway corridor in Delhi. Journal of Scientific and Industrial Research 2013;72:521-30.

Tun SNL, Aung TH, Mon AS, Kyaw PH, Siriwong W, Robson M, et al. Assessment of ambient dust pollution status at selected point sources (residential and commercial) of Mingaladon Area, Yangon Region, Myanmar. Journal of Health Research 2017;32:60-8.

Turner DB. Workbook of Atmospheric Dispersion Estimates an Introduction to Dispersion Model. 2nd Ed. Florida, USA: International Lewis Publishers; 1994.

United State Environmental Protection Agency (USEPA). User's Guide to CAL3QHC Version 2.0: A Modeling Methodology for Predicting Pollutant Concentrations Near Roadway Intersections. North Carolina, USA: Environmental Protection Agency; 1995. p. 7-24.

Weather Spark. February Weather in Yangon [Internet]. 2022 [cited 2022 Mar 22]. Available from: https:// weatherspark.com/m/112503/2/Average-Weather-in-February-in-Yangon-Myanmar-(Burma).

Weatherbase. Yangon, Myanmar: Weather [Internet]. 2022 [cited 2022 Mar 19]. Available from: https://www.weatherbase.com/ weather/weather-summary.php3?s=69084.

World Health Organization (WHO). WHO Global Air Quality Guidelines. Particulate Matters ($PM_{2.5}$ and PM_{10}), Ozone, Nitrogen Dioxide, Sulphur Dioxide and Carbon Monoxide. Bonn, Germany: European Center for Environment and Health; 2021. p. 73-139.

Yi EEPN, Nway NC, Aung WY, Thant Z, Wai TH, Hlaing KK, et al. Preliminary monitoring of concentration of particulate matter ($PM_{2.5}$) in seven townships of Yangon City, Myanmar. Environmental Health and Preventive Medicine 2018;23:1-8.

Yu S, Chang TC, Ma CM. Simulation and measurement of air quality in the traffic congestion area. Sustainable Environment Research 2021;21;1-18.

Optimization Removal of COD and Nitrogen at Different Hydraulic Retention Times in Biocord-Integrated Fixed-Film Activated Sludge System

Nguyen Thi Tuyet Nhi[1], Phan Thi Thuy Van[1], Nguyen Thi Thao[1], Nguyen Thi Thanh Truc[1], Tran Le Truong Khanh Hung[1], Do Thi Ngoc Tay[1], Huynh Tan Nhut[1*], and Nguyen Trung Hiep[2]

[1]*Faculty of Environment and Natural Resources, Nong Lam University-Ho Chi Minh City, Linh Trung Ward, Thu Duc City, Ho Chi Minh City 700000, Vietnam*

[2]*Research Institute for Sustainable Development, Ho Chi Minh University of Natural Resources and Environment, 236B Le Van Sy, Ward 1, Tan Binh District, Ho Chi Minh City 700000, Vietnam*

ARTICLE INFO

* Corresponding author:
E-mail:
tannhut.env@hcmuaf.edu.vn

ABSTRACT

Although conventional activated sludge has been demonstrated to be a feasible approach for extracting nitrogenous chemicals and organic pollutants from wastewater, it still has a number of drawbacks. In this research, a pilot-scale biocord-integrated fixed-film activated sludge (Biocord-IFAS) reactor fed with actual domestic wastewater was operated to examine the effect of varying hydraulic retention time (HRT) on the COD and nitrogen removal. The type of material employed in this study is fibrous polypropylene (biocord), which is a major difference. The contribution of the Biocord-IFAS to COD removal efficiency reached 94.2% at HRT of 8 h and gradually decreased to 82.9% when HRT was reduced to 4 h. During the investigation period, a slight decrease in nitrification was found at a shorter HRT. The NH_4^+-N removal efficiencies at HRTs of 10, 8, 6, and 4 h were 97.8%, 98.7%, 97.1%, and 96.3%, respectively. The average effluent nitrate concentration was 5.3 mg/L with HRTs from 10 to 6 h, but over 30 mg/L with an HRT of 4 h. The SEM analysis results show that microorganisms have formed on the biocord surface. The results of this research have demonstrated the potential application of IFAS reactors in bioremediation procedures employing biocord material with great processing efficiency.

1. INTRODUCTION

Hitherto, biofilm methods are rapidly being used in wastewater treatment due to their advantages, such as reduced reactor sizes, ease of operation, less demanding solids separation needs, and improved specialization of attached biomass. The integrated fixed-film activated sludge (IFAS) method is one of these technologies. This process is an integration process that includes both suspended and attached growth (Kim et al., 2010; Mahendran et al., 2012; Malovanyy et al., 2015). By adding a fixed media to a suspended growth basin, the IFAS system boosts the microbial population and accelerates the biodegradation of organic compounds, making it one of the most common modified activated sludge processes (Kim et al., 2010). The biomass attached to the bio-carriers is kept within the system, which is a

fundamental advantage of the IFAS method over traditional activated sludge procedures. The IFAS system is a viable alternative for upgrading activated sludge systems, particularly if land is limited. (Eslami et al., 2018). In comparison to ordinary activated sludge, the IFAS process has a higher COD and nutrient removal efficiency.

Previous studies have shown that the IFAS system is effective in removing nitrogen from wastewater (Onnis-Hayden et al., 2007; Shao et al., 2017). Furthermore, the IFAS process has exhibited consistent nitrification at much lower mixed liquor contents than the standard activated sludge process can produce. As is well known, nitrification is divided into two steps: In the first, ammonium is used by autotrophic ammonia-oxidizing bacteria (AOB) to make nitrite, and in the second, nitrite is oxidized to

nitrate by nitrite-oxidizing bacteria (NOB) (Xu et al., 2014). A high COD promotes heterotrophic growth and increases competition for space and oxygen between heterotrophs and autotrophic nitrifying bacteria (Bassin et al., 2012; Kim et al., 2011; Onnis-Hayden et al., 2011). This has affected the nitrification efficiency negatively. Bio-carriers are added to conventional activated sludge reactors in the IFAS design to provide surface area for microorganism attachment and growth. The support media in the IFAS reactor can also provide longer sludge retention time (SRT) than the traditional activated sludge process, allowing slow-growing nitrifying growth and promoting nitrification (Shreve and Brennan, 2019). As a result, combining the properties of suspended and attached growth processes by using specifically designed biomass carriers for simultaneous COD and nitrogen removal is more appealing.

However, because IFAS is a new technology, there are still some studies in the literature that are limited. There is a knowledge gap regarding the impact of several operational variables on removal performance and bio-carrier activity characteristics. The goal of this study was to see how different HRT parameters influenced the performance of a biocord-IFAS reactor in the short term. The purpose of this study was to assess the treatability of COD and nitrogen in real home wastewater utilizing an IFAS reactor system with bio-cords as bio-carriers.

2. METHODOLOGY
2.1 Characteristics of wastewater
The raw wastewater was collected from the storage tank of Co May dormitory in Vietnam. The characteristics of the dormitory wastewater are shown in Table 1.

Table 1. Characteristics of influent wastewater used in the research

Parameter	Unit	Range (n=3)
pH	-	6.9±0.3
SS	mg/L	195±5
DO	mg/L	0.4±0.1
BOD_5	mg/L	201.6±2.5
COD	mg/L	335.9±4.1
$N-NO_3^-$	mg/L	0.30±0.01
$N-NH_4^+$	mg/L	70.4±1.2
TP	mg/L	4.9±0.9

2.2 Experimental apparatus
The pilot-scale Biocord-IFAS system employed had a similar design as previously described in Nhut et al. (2020). Figure 1 shows the Biocord-IFAS reactor which is composed of transparent glass sheets with a thickness of 8 mm and a useful volume of 27 L. The Biocord media used in this research was made of a polypropylene fibrous bundle with a specific surface area of 1.6 m²/m (commercial code: MK-PP50, Bishop Water Technologies, Canada). The total 2 m length of Biocord was installed in an IFAS tank. In detail, the wastewater was fed into the reactor from the sewage tank by a peristaltic pump. The bioreactor was operated at various HRT of 10, 8, 6, and 4 h. The sludge retention time (SRT) was 10 days. The organic loading rate (OLR) was from 0.5 to 1.5 kg COD/m³/day. The return activated sludge (RAS) rates were chosen from 1 to 1.5Q. The average DO concentration was maintained at 5.5±0.5 mg/L.
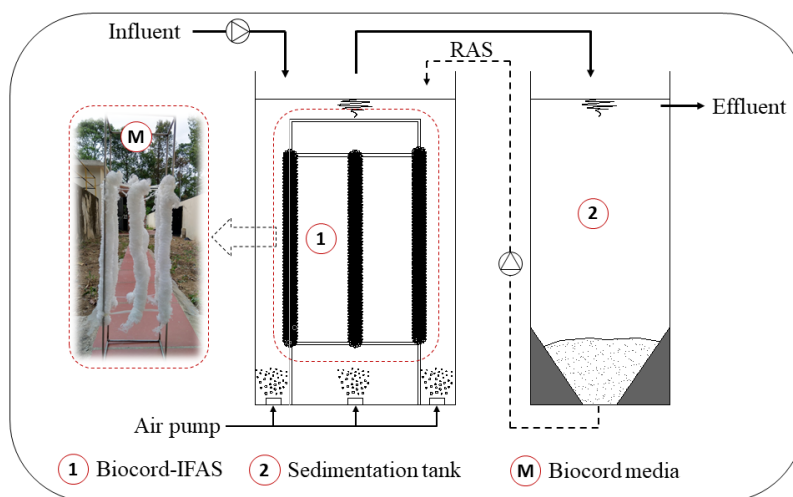

Figure 1. Diagram of the Biocord-IFAS system.

2.3 Analysis methods

In this research, the "Standard methods for examining water and wastewater" (Baird et al., 2017) was used for the determination of BOD$_5$ (5210B), COD (5220D), nitrate (4500-NO$_3^-$), nitrite (4500-NO$_2^-$), ammonium (4500-NH$_3$), suspended solids (2450B), and total phosphorus (4500-P). DO and pH were directly tested by Water Quality Checker WQC-22A (DKK-TOA, Japan). Moreover, Scanning Electron Microscopy (SEM, S-4800, HI-9039-0006, Hitachi, Japan) was used to prepare images of the biofilm. In addition, this study utilized the most common statistical descriptive parameters such as mean and standard deviations (±SD). The data were analyzed by the SPSS 22 software package for Windows (SPSS Inc., Chicago, IL, USA).

3. RESULTS AND DISCUSSION
3.1 Overall performance of start-up phase

The start-up test operated for 15 days with a hydraulic retention time (HRT) of 10 h. The average efficiencies, as well as influent and effluent quality, are presented in Table 2. The COD and ammonium removal efficiencies were 79.5±3.3% and 86.2±0.9%, respectively, in Biocord-IFAS reactors. Additionally, attached biomass growth also achieved a steady state. The MLSS concentration of mixed liquor was steady at 2,675±150.4 mg/L. For the biocord, the biofilm was mainly developed on the outer surface of the carrier. However, the biocord possesses a large surface area that microorganisms can attach in the cords, and then develop over surface areas.

Table 2. Performance of treatment during the start-up test

Parameter	Influent (mg/L)	Effluent (mg/L)	Efficiency (%)
COD	230.1±15.8	46.7±5.6	79.5±3.3
N-NH$_4^+$	53.9±2.5	7.4±0.2	86.2±0.9
SS	115.7±6.2	27.7±1.1	76.0±1.7

3.2 COD removal

The removal of COD in the Biocord-IFAS system was evaluated at different HRT as illustrated in Figure 2. The removal efficiency of COD ranged between 82.9% and 94.2% with HRT ranging from 4 to 10 h. The average effluent of COD concentration was 37.2±14.4 mg/L for the operated HRTs. A similar observation was reported by Dang et al. (2020), who suggested the effluent COD from loofah sponges as a bio-carriers in the IFAS system for the treatment of municipal wastewater was maintained at a level of 35.2±18.9 mg/L, despite a change in the HRT from 3 to 7 h. The COD removal was maintained at 92.2±2.5%, 94.2±1.6%, and 91.7±2.9% at HRT of 10, 8, and 6 h, respectively, but was 82.9±3.0% at an HRT of 4 h, which indicates that the HRT affects the COD efficiency removal. This result agreed with Singh et al. (2015), who reported that the IFAS maintained an average removal rate of ~92% for COD at HRT of 6.9 h. In addition, Eslami et al. (2018) reported the best removal efficiency of COD was 92.52±4.33% at HRT of 10.8 h.

The effluent COD concentration not only complies with the Vietnam National Technical Regulation on Industrial Wastewater, QCVN 40:2011/BTNMT (75 mg COD/L, column A), but also reaches the Vietnam National Technical Regulation for surface water quality, QCVN 08:2008/BTNMT (50 mg COD/L, column B2). Furthermore, the organic content in the effluent was removed to an acceptable level for reuse such as park irrigation, flushing a toilet, or aquaculture recirculation.

3.3 Nitrogen removal

The variation of NH$_4^+$-N and NO$_3^-$-N in the dormitory wastewater treated using Biocord-IFAS are shown in Figure 3. During the investigation period, the NH$_4^+$-N removal efficiencies at HRTs of 10, 8, 6, and 4 h were 97.8±1.1%, 98.7±1.1%, 97.1±1.7%, and 96.3±0.8%, respectively, which implies a slight decrease in nitrification at a shorter HRT. This result agreed with Sriwiriyarat et al. (2008), who reported the IFAS system with a 0.6 m^2 of 2.54 cm Bioweb media could always maintain ammonium removal efficiencies greater than 95% at HRT of 6-10 h. Furthermore, the effluent NH$_4^+$-N concentration throughout the study period remained low, averaging 1.0±1.1 mg/L, which complies with the Vietnam National technical regulation on domestic wastewater, QCVN 14:2008/BTNMT (5 mg NH$_4^+$-N/L, column A). Notably, there were a few days when the ammonia concentration in the effluent was lower than detectable (less than 0.4 mg/L), indicating that nitrification had occurred completely.
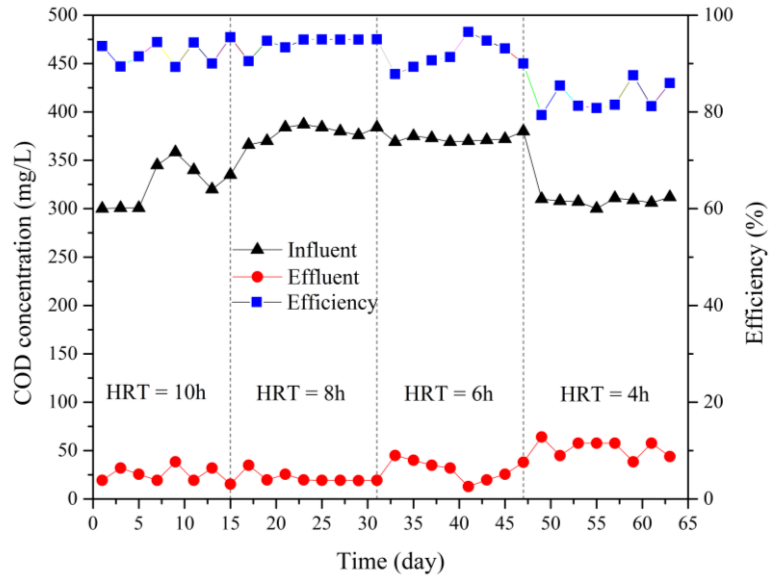
Figure 2. Variation of COD concentration at different HRTs

The average effluent nitrate concentration was 5.3±2.0 mg/L with HRTs from 10 to 6 h, but over 30 mg/L with an HRT of 4 h. At short HRT, the denitrification process is not efficient because the organic carbon source is not sufficient for the metabolic heterotrophic microorganisms. One possible explanation was that low COD concentrations inhibited the bioactivities of heterotrophic denitrifiers. On average about 3.4% of nitrate was denitrified at

HRT of 4 h. The effluent nitrite concentrations generally remained at less than 0.5 mg/L (data not shown) across all HRTs illustrating that there was no nitrite accumulation in the IFAS tank. This suggested that very short HRT was unconducive to the contact between pollutants degradations and the biofilm. Meanwhile, residual organics in wastewater inhibited the activity of nitrifying bacteria, which eventually led to an inefficient nitrogen removal.
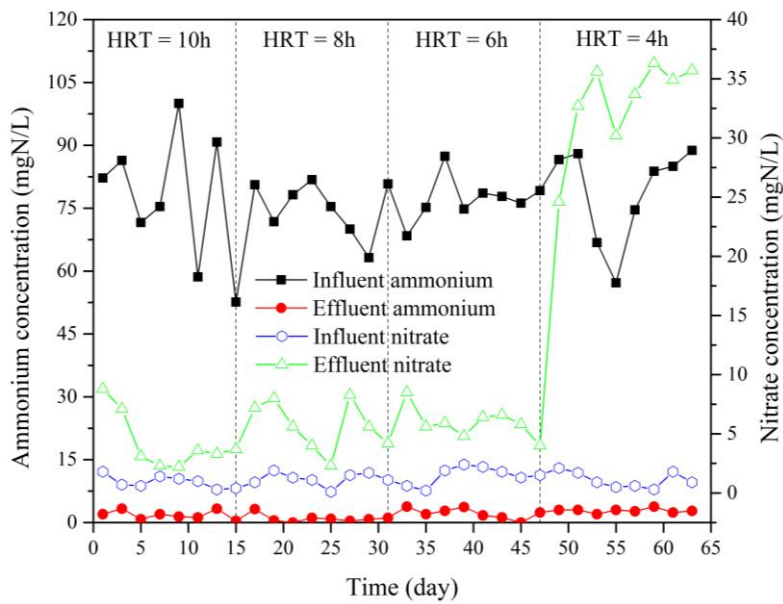
Figure 3. Variation of nitrogen concentration at different HRTs

3.4 Biofilm formation on the bio-carriers

After over 60 days of use in experiments, bio-carriers in the IFAS reactor were removed to observe biofilm formation. Figure 4 shows the SEM image before and after biofilm formation on the surface biocord in the IFAS reactor. Many gaps between the polypropylene fibrous bundle can be seen in Figure 4 (a), providing a highly porous surface area for the adhesion and trapping of microbial cells. For bio-carrier materials, the important parameters affecting microbial colonization are the surface area and the ability to adhere. Figure 4 (c and d) show the formation and development of microorganisms on the biocord surfaces. These biofilms as surface-associated communities of microorganisms could play a great role in the bio-oxidation of organic pollutants especially in the IFAS by means of a large surface area for biomass accumulation. Indeed, Kim et al. (2011) also showed that in the IFAS system, the ammonium removal rate was better than that of conventional activated sludge.
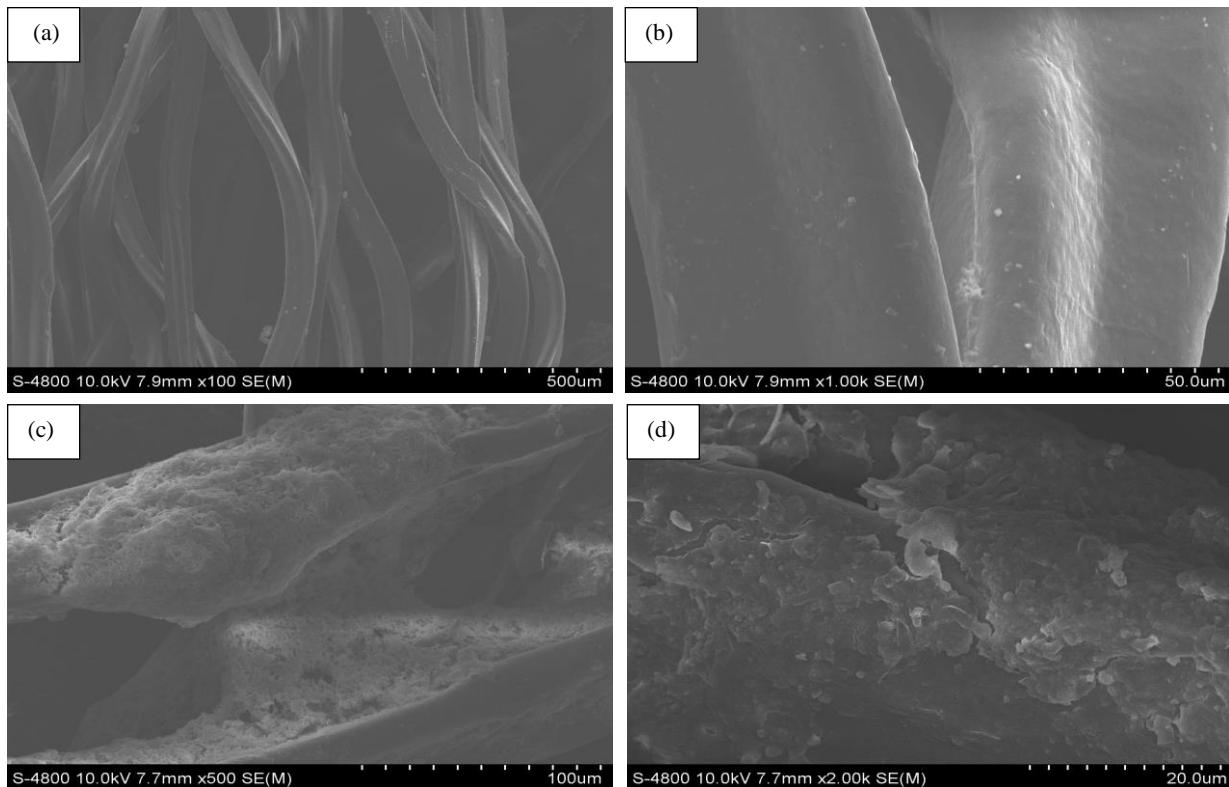
Figure 4. SEM images from biocord within IFAS reactor, (a, b) before biofilm formation, (c, d) after biofilm formation

3.5 Comparison of domestic wastewater treatment performance between IFAS technologies

Table 3 shows a summary of IFAS performance for domestic wastewater treatment between different studies. As shown in Table 3, a variety of materials have been used as carrier media. They are loofah sponge, non-woven polyester, PE, plastic, and biocord. According to the report of Lariyah et al. (2016), the material of carrier media was vital and affected the microbial ecosystem. Furthermore, the filling ratio is important to control microbial activity. It ranges from 10% to 50% selected as a function of IFAS configuration (Table 3). On the other hand, Leyva-Díaz et al. (2017) indicated the filling ratio affects the HRT and SRT (from a few hours to a few days) because of the volume occupied by the media. Under a high filling ratio, IFAS can accomplish high nutrient removals due to higher SRT and higher biofilm amount. The notable difference in this study is the type of material used, which is fibrous polypropylene (biocord). With outstanding properties such as large surface area, high biocompatibility, high durability and large size, it will limit washout in the outlet stream. This has shown the potential application of biocord material with high processing efficiency in bioremediation processes.

Table 3. Summary of IFAS technology for treatment of domestic wastewater

Type of reactor	DO (mg/L)	HRT (h)	SRT (day)	Type of carrier	Media filling ratio (%)	Performance	References
Pilot-scale IFAS	7	4-10	10	Biocord MK-PP50	10*	COD removal >95%, NH_4^+-N removal >95%	This study
Pilot-scale IFAS	NA	12.5	13.5	Acrylic fiber	20	COD removal >80%, NH_4^+-N removal >95%	Xu et al. (2021)
Pilot-scale IFAS	NA	3-7	NA	Loofah sponge	30	COD removal 83%, TN removal 71%	Dang et al. (2020)
Pilot-scale IFAS	2.2-6.3	24	4-10	BMX1	43	COD removal >90%, effluent NH_4^+-N 1 mg/L	Moretti et al. (2018)
Lab-scale SNAD-IFAS	0.4-0.6	18	20	Non-woven polyester ring	40	COD removal 64.8%, TN removal 45-70% (71.4-79.4 mg/L), TOC removal 44.7-91.4%	Wang et al. (2018)
Lab-scale IFAS-SFD-MBR	2-4	8	30	PE carrier	19	COD 26.0±3.5 mg/L (>90%), TN 28.7±5.0 mg/L, NH_4^+-N <1 mg/L, NO_3^--N 28.4±4.4 mg/L, TP 7.2±1.5 mg/L	Vergine et al. (2018)
Lab-scale IFAS-SBR	7-8	12.8	NA	Bioflow 9	50	COD 10-20 mg/L (98.6±1.5%) and NH_4^+-N <0.1 mg/L (99.93±0.004%)	Shao et al. (2017)
Lab-scale IFAS-SBR	NA	6.5	NA	Cubic sponge	25	COD removal 85% (57 mg/L), TN removal 85%	Gu et al. (2017)
Lab-scale IFAS	0.7-1.5	18-58.8	NA	AnoxKaldnes K1	40	TN removal 70±4% at sCOD/NH_4^+-N 1.8±0.2, effluent ammonium 9.2 mg/L, nitrogen removal rate 55±6 g N/(m³/day)	Malovanyy et al. (2015)
Full-scale IFAS	3-5	NA	4.8	AnoxKaldnes K3	50	TN 9.95 mg/L (75.1%), NH_4^+-N 1.6 mg/L, NO_3^--N 8.4 mg/L	Regmi et al. (2011)

Note: NA-not available; (*) SRT for activated sludge without Biocord

4. CONCLUSION

According to the results above, it is obvious that using the Biocord-IFAS reactor can effectively remove nitrogenous compounds and organic contaminants from domestic wastewater. Meanwhile, the HRT plays a key role in the system, and the optimized solution was an HRT of 8 h. Under such conditions, the removal efficiency of COD and ammonium were 94.2±1.6% and 98.7±1.1%, respectively. Analysis of the SEM images also showed the development of microorganisms on the biocord surfaces. These surface-associated communities of microorganisms could play a great role in the bioreactors. The effluent concentration not only complies with the Vietnam National technical regulation on domestic wastewater, QCVN 14:2008/BTNMT, but also reaches the Vietnam National Technical Regulation for surface water quality, QCVN 08:2008/BTNMT and the Vietnam National Technical Regulation on Industrial Wastewater, QCVN 40:2011/BTNMT. Thus, the use of the biocord as a biofilm carrier in an IFAS reactor can be an effective wastewater treatment alternative to activated sludge.

ACKNOWLEDGEMENTS

REFERENCES

Baird RB, Eaton AD, Rice EW. Standard Methods for the Examination of Water and Wastewater. Washington, DC: American Public Health Association (APHA); American Water Works Association (AWWA); Water Environment Federation (WEF); 2017.

Bassin J, Kleerebezem R, Rosado A, van Loosdrecht MM, Dezotti M. Effect of different operational conditions on biofilm development, nitrification, and nitrifying microbial population in moving-bed biofilm reactors. Environmental Science and Technology 2012;46(3):1546-55.

Dang HT, Dinh CV, Nguyen KM, Tran NT, Pham TT, Narbaitz RM. Loofah sponges as bio-carriers in a pilot-scale integrated fixed-film activated sludge system for municipal wastewater treatment. Sustainability 2020;12(11):Article No. 4758.

Eslami H, Ehrampoush MH, Falahzadeh H, Hematabadi PT, Khosravi R, Dalvand A, et al. Biodegradation and nutrients removal from greywater by an integrated fixed-film activated sludge (IFAS) in different organic loadings rates. AMB Express 2018;8(1):1-8.

Gu J, Xu G, Liu Y. An integrated AMBBR and IFAS-SBR process for municipal wastewater treatment towards enhanced energy recovery, reduced energy consumption and sludge production. Water Research 2017;110:262-9.

Kim HS, Gellner JW, Boltz JP, Freudenberg RG, Gunsch CK, Schuler AJ. Effects of integrated fixed film activated sludge media on activated sludge settling in biological nutrient removal systems. Water Research 2010;44(5):1553-61.

Kim HS, Schuler AJ, Gunsch CK, Pei R, Gellner J, Boltz JP, et al. Comparison of conventional and integrated fixed-film activated sludge systems: Attached-and suspended-growth functions and quantitative polymerase chain reaction measurements. Water Environment Research 2011;83(7):627-35.

Lariyah M, Mohiyaden H, Hayder G, Hussein A, Basri H, Sabri A, et al. Application of moving bed biofilm reactor (MBBR) and integrated fixed activated sludge (IFAS) for biological river water purification system: a short review. Proceedings of the IOP Conference Series: Earth and Environmental Science; 2016 Feb 23-25 ;Putrajaya: Malaysia; 2016.

Leyva-Díaz J, Martín-Pascual J, Poyatos J. Moving bed biofilm reactor to treat wastewater. International Journal of Environmental Science and Technology 2017;14(4):881-910.

Mahendran B, Lishman L, Liss SN. Structural, physicochemical and microbial properties of flocs and biofilms in integrated fixed-film activated sludge (IFFAS) systems. Water Research 2012;46(16):5085-101.

Malovanyy A, Trela J, Plaza E. Mainstream wastewater treatment in integrated fixed film activated sludge (IFAS) reactor by partial nitritation/anammox process. Bioresource Technology 2015;198:478-87.

Moretti P, Choubert JM, Canler JP, Buffière P, Pétrimaux O, Lessard P. Dynamic modeling of nitrogen removal for a three-stage integrated fixed-film activated sludge process treating municipal wastewater. Bioprocess and Biosystems Engineering 2018;41(2):237-47.

Nhut HT, Hung NTQ, Sac TC, Bang NHK, Tri TQ, Hiep NT, et al. Removal of nutrients and organic pollutants from domestic wastewater treatment by sponge-based moving bed biofilm reactor. Environmental Engineering Research 2020;25(5): 652-8.

Onnis-Hayden A, Dair D, Johnson C, Schramm A, Gu AZ. Kinetics and nitrifying populations in nitrogen removal processes at a full-scale integrated fixed-film activated sludge (IFAS) plant. Proceedings of the Water Environment Federation 2007;15:3099-119.

Onnis-Hayden A, Majed N, Schramm A, Gu AZ. Process optimization by decoupled control of key microbial populations: Distribution of activity and abundance of polyphosphate-accumulating organisms and nitrifying populations in a full-scale IFAS-EBPR plant. Water Research 2011;45(13):3845-54.

Regmi P, Thomas W, Schafran G, Bott C, Rutherford B, Waltrip D. Nitrogen removal assessment through nitrification rates and media biofilm accumulation in an IFAS process demonstration study. Water Research 2011;45(20):6699-708.

Shao Y, Shi Y, Mohammed A, Liu Y. Wastewater ammonia removal using an integrated fixed-film activated sludge-sequencing batch biofilm reactor (IFAS-SBR): Comparison of suspended flocs and attached biofilm. International Biodeterioration and Biodegradation 2017;116:38-47.

Shreve MJ, Brennan RA. Trace organic contaminant removal in six full-scale integrated fixed-film activated sludge (IFAS) systems treating municipal wastewater. Water Research 2019;151:318-31.

Singh NK, Kazmi AA, Starkl M. Environmental performance of an integrated fixed-film activated sludge (IFAS) reactor treating actual municipal wastewater during start-up phase. Water Science and Technology 2015;72(10):1840-50.

Sriwiriyarat T, Pittayakool K, Fongsatitkul P, Chinwetkitvanich S. Stability and capacity enhancements of activated sludge process by IFAS technology. Journal of Environmental Science and Health, Part A 2008;43(11):1318-24.

Vergine P, Salerno C, Berardi G, Pollice A. Sludge cake and biofilm formation as valuable tools in wastewater treatment by coupling integrated fixed-film activated sludge (IFAS) with

self forming dynamic membrane bioreactors (SFD-MBR). Bioresource Technology 2018;268:121-7.

Wang C, Liu S, Xu X, Zhang C, Wang D, Yang F. Achieving mainstream nitrogen removal through simultaneous partial nitrification, anammox and denitrification process in an integrated fixed film activated sludge reactor. Chemosphere 2018;203:457-66.

Xu S, Wu D, Hu Z. Impact of hydraulic retention time on organic and nutrient removal in a membrane coupled sequencing batch reactor. Water Research 2014;55:12-20.

Xu X, Liu G-h, Li Q, Wang H, Sun X, Shao Y, et al. Optimization nutrient removal at different volume ratio of anoxic-to-aerobic zone in integrated fixed-film activated sludge (IFAS) system. Science of the Total Environment 2021;795:Article No. 148824.

Color Removal of Pulp and Paper Mill Wastewater Using Residual Eucalyptus Wood

Kanjana Yupin[1,2], Thanakrit Neamhom[1,2], Chatchawal Singhkant[1,2], Siranee Sreesai[1,2], and Supawadee Polprasert[1,2*]

[1]*Department of Environmental Health Sciences, Faculty of Public Health, Mahidol University, 420/1 Rajvithi Road, Bangkok 10400, Thailand*

[2]*Center of Excellence on Environmental Health and Toxicology (EHT), Ministry of Higher Education, Science, Research and Innovation (MHESI), Bangkok 10400, Thailand*

ARTICLE INFO

* Corresponding author:
E-mail:
supawadee.pol@mahidol.ac.th

ABSTRACT

This study investigated the color removal efficiency of pulp and paper mill wastewater using residual eucalyptus wood as a method to minimize the solid wastes generated from pulp and paper processes. The activated carbon used in this study as the color adsorbent was produced from residual eucalyptus wood. The carbon was activated with phosphoric acid and carbonized in a furnace at 500°C for 60 min. Effects of types and amounts of activated carbon on color removal efficiency were evaluated. Three types of solid wastes, consisting of wood chip, bark, and mixed wood (wood chip:bark, 1:1), were investigated at a loading of 1, 3, 5, and 7 g/100 mL under contact times of 30, 60, 90, and 120 min. The results showed that 7 g of wood chip activated carbon/100 mL under all contact times gave color removal efficiency of 94-97%. However, the highest adsorption capacity of 216 ADMI/g occurred at 1 g of adsorbent used. Freundlich isotherms were satisfactorily fitted to experimental data for the best condition with high correlation coefficients. The color removal efficiency depended on surface area, pore volume, structure, and characteristics of the activated carbon.

1. INTRODUCTION

At present, Thailand has a high rate of paper use leading to increasing waste in the paper industry. The paper industry requires large volumes of processed water of high purity and generates large amounts of wastewater from digestion, lignin extraction, and bleaching processes, which are highly colored. Approximately 20 m^3 of fresh water are required to process 1 ton of eucalyptus wood for producing pulp and paper. Moreover, one ton of eucalyptus wood can produce about 0.534 ton of paper and generate solid waste such as bask, wood chip and dust of about 0.074 ton, 0.43 ton, and 0.018 ton, respectively. The pulp and paper production generates a significantly large amount of pollutants characterized by high concentrations of suspended solids (SS), COD, toxicity, and biochemical oxygen demand (BOD) (Pokhrel and Viraraghavan, 2004). Pulp and paper mill wastewater is a dark brown colored liquid known as 'black liquor' (Kumar et al., 2021). The pulp and paper mill effluent color is largely due to lignin derivatives and polymerized tannins removed during pulping and bleaching processes, which are resistant to degradation due to the presence of carbon-to-carbon biphenyl linkages (El-Bestawy et al., 2008). The color of paper mill wastewater is one of the major environmental problems because of the difficulty of treating by conventional methods. Production of various types of paper has been defined as a business that is harmful to health because it produces color and toxic substances from the production process (Armstrong et al., 1998). Color not only causes bad aesthetical effects but also reduces the self-purification capacity of rivers by inhibiting photosynthetic production of oxygen and direct destruction of aquatic communities (Chooaksorn, 2012). Due to these risks, the Department of Industrial Works of Thailand provides water quality standard values for controlling the color of effluent from the industry. The effluent standard of color is 600 ADMI

for pulp production and 350 ADMI for paper production (MNRE, 2018). Meeting the regulatory discharge standards for pulp and paper mill wastewater has become more difficult because of its recalcitrant and colored dissolved organic matter (DOM) (Shi et al., 2016). The effluent is normally treated by biological process such as aerated lagoon and activated sludge processes. The biological processes are very effective for removing the nonsettleable colloidal solids and to stabilize the organic matter, but are unsuitable for removing the color (Yadav et al., 2012).

Many processes are available to remove color from pulp and paper wastewater. Activated carbon has a well known high adsorption capacity and can absorb both color and odor. The activated carbon prepared from prickly pear seed cake by phosphoric acid activation is effective for removing cationic and anionic dyes such as methylene blue and methyl orange from aqueous solution (El maguana et al., 2020). Moreover, a maximum reduction of dying effluent in color and COD of 91.84% and 75.21% was observed using bamboo-based activated carbon (Ahmad and Hameed, 2009). Additionally, the performance of oat hull activated carbon was studied and the results showed that COD and color removal from landfill leachate were up to 90% (Ferraz and Yuan, 2020). Therefore, the color removal efficiency of pulp and paper effluent using residual eucalyptus wood as activated carbon absorbent was investigated in this study.

2. METHODOLOGY

The pulp and paper wastewater was collected from the effluent of wastewater treatment plants at the mixed tank after being treated with the secondary clarifier process by grab sampling. The parameters of pH, color, COD, TSS, TDS, and TKN were investigated. The residual eucalyptus wood generated from pulp and paper processes was used as activated carbon for the color adsorbent. The characteristics of pulp and paper wastewater used in the study are described in Table 1. The BOD and COD ratio was low at about 0.15 because the effluent was already treated with biological processes. Therefore, adsorption proved an attractive alternative process to treat the color of the effluent after biological treatment. The carbon was activated with 85% phosphoric acid (wt:vol, 1:1) and soaked for 60 min. Activated carbon was then washed with deionized water several times

until pH returned to neutral and dried at 105°C for 4 h (Patnukao and Pavasant, 2008; Kongsuwan et al., 2009), then carbonized in a furnace at 500°C for 60 min. (Kongsuwan et al., 2009). The activated carbon was crushed and filtered using a sieve to a particle size of 0.71 mm. (Chuyingsakuntip and Tangsathitkulchi, 2013). The physical characteristics of the residual eucalyptus wood and activated carbon are shown in Figures 1, 2, and 3.

Table 1. Characteristics of pulp and paper effluent used in this study

Parameter	Unit	Value
pH	-	7.8-8.2
BOD	(mg/L)	13-17
COD	(mg/L)	96-102
TSS	(mg/L)	10-13
TDS	(mg/L)	1,362-1,370
Color	ADMI (pH-Original)	379-384
	ADMI (pH-Adjust)	338-345
Conductivity	(µs/cm)	2,560-2,620
TKN	(mg/L)	3.24-3.86

Experiments were carried out to investigate the color removal efficiency in batch experiments. The experimental design comprised a 3×4×4 factorial design with 4 replications. The studied factors included the type of eucalyptus wood (wood chip, bark, and mixed wood), amount of activated carbon (1, 3, 5, and 7 g) and contact times (30, 60, 90, and 120 min) to determine the optimum condition of color removal efficiency. A 250 mL Erlenmeyer flask was used as an adsorption reactor with 100 mL working volume. The amount of each type of activated carbon was added according to the experimental design, and the sample was shaken at 120 rpm for 30, 60, 90, and 120 min. The color concentration was analyzed using a spectrophotometer following the ADMI method (Kumar et al., 2021; Azha and Ismail, 2021). The isotherms of Langmuir and Freundlich adsorption were also studied to evaluate the adsorption pattern.

3. RESULTS AND DISCUSSION
3.1 Effect of type and amount of activated carbon

Regarding the three types of activated carbon investigated, the maximum color removal efficiency was obtained from wood chips due to their physical properties such as porosity and surface area. Bark differs from wood chips in terms of its anatomical structure, properties and chemical composition as

Figure 1. Physical structure: eucalyptus wood chips (a); eucalyptus bark (b); eucalyptus wood chips after carbonization (c); and eucalyptus bark after carbonization (d)
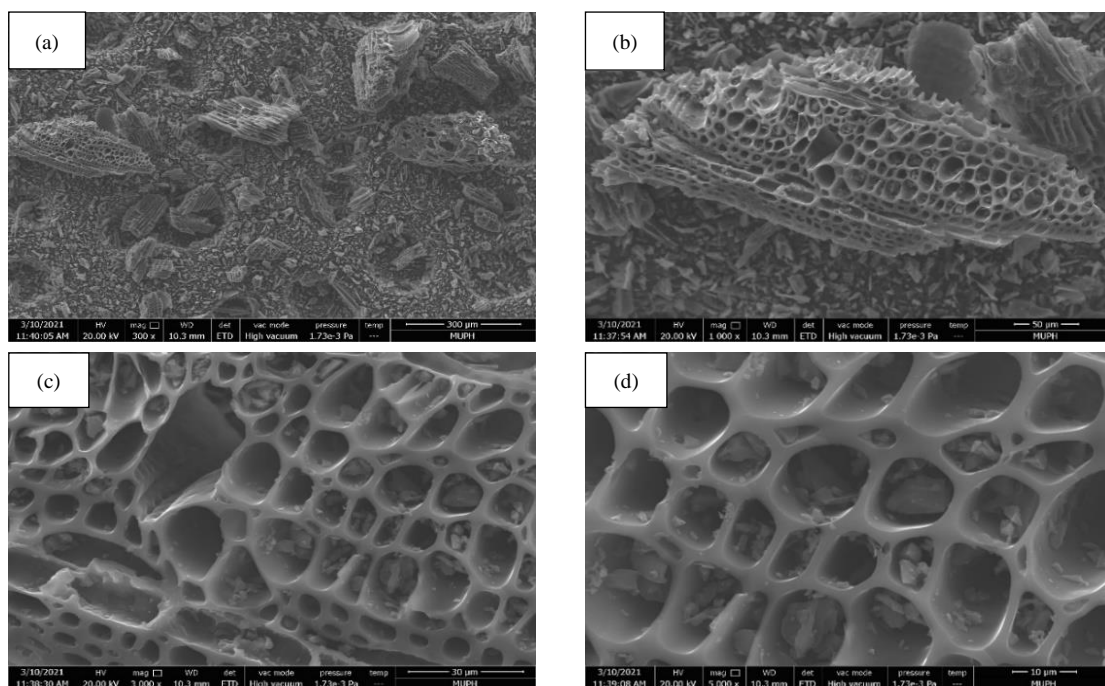

Figure 2. Physical characterization of wood chip activated carbon with SEM photographs of wood chip activated carbon: wood chips 500X (a); wood chips 1000X (b); wood chips 3000X (c); and wood chips 5000X (d)

shown in Figure 1. The physical structure of wood and bark AC are illustrated in Figures 2 and 3, respectively. The eucalyptus wood chip AC is mainly composed of tube structures, which should promote the velocity of liquid diffusion for the adsorption process. However, bark AC consists of xylem and phloem and is a narrow layer of tissue. The pore size of wood chip AC was larger than bark AC and exhibited nonuniform pore size from 3.597 µm to 23.89 µm, while bark AC had similar pore size from 8.467 µm to 14.75 µm as shown in Figure 4. The fixed carbon in bark was higher than in wood chips, namely,

13.10% in bark and 16.42% in wood chips. The volatile matter content of wood chips and bark was 83.23% and 75.05%, respectively. The ash in bark was approximately four times higher than that of others, namely, 0.5% in wood and 1.35% in bark. (Kiatgrajai et al., 1994; Kongsuwan et al., 2009; Borgesa et al., 2019). Moreover, the results showed that when using wood chips of 7 g/100 mL, the highest color removal efficiency of 97% was obtained, as shown in Figure

5(a). Moreover, TDS decreased from 1,370 mg/L to 713 mg/L and conductivity also decreased from 2,620 µs/cm to 1,220 µs/cm as illustrated in Table 2. However, the highest adsorption capacity of 216 ADMI/g occurred at 1 g of adsorbent used. When using bark and mixed wood of 7 g/100 mL, the highest color removal efficiencies of 84 and 89% were obtained, as shown in Figures 5(b) and 5(c), respectively.
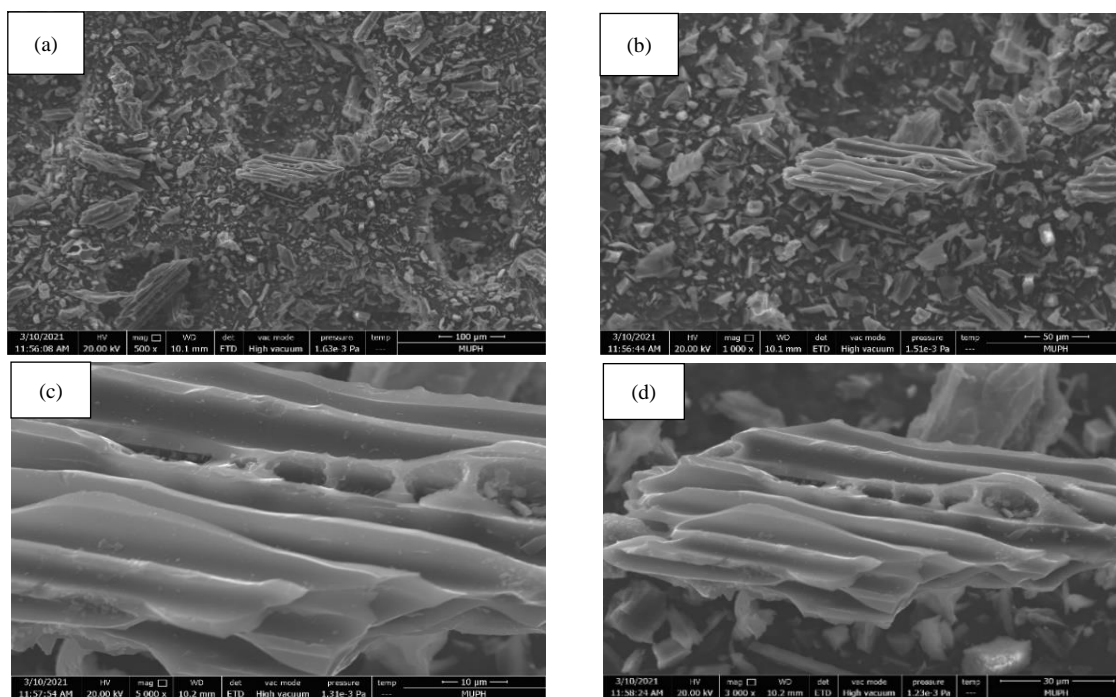
Figure 3. Physical characterization of bark activated carbon with SEM photographs of bark activated carbon: bark 500X (a); bark 1000X (b); bark 3000X (c) and bark 5000X (d)
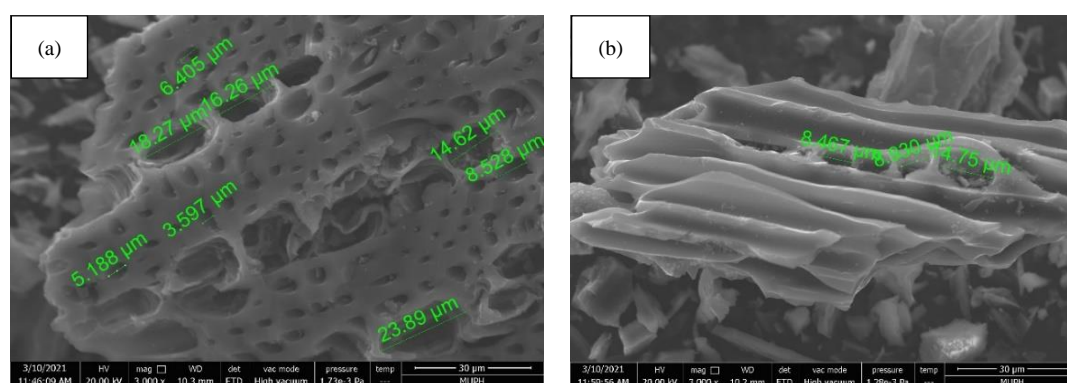
Figure 4. Surface characteristics and pore sizes of wood chip AC (a), and bark AC (b)

3.2 Effect of contact time

The effect of contact time was determined on color removal in batch experiments. Regarding the three types of activated carbon from loading at 1, 3, 5, and 7 g/100 mL for a contact time of 30, 60, 90, and

120 min, the efficiency of adsorption increased with increasing contact time. However, color adsorption rapidly increased in the first period. After that, the color adsorption gradually decreased.

(a)

(b)

(c)
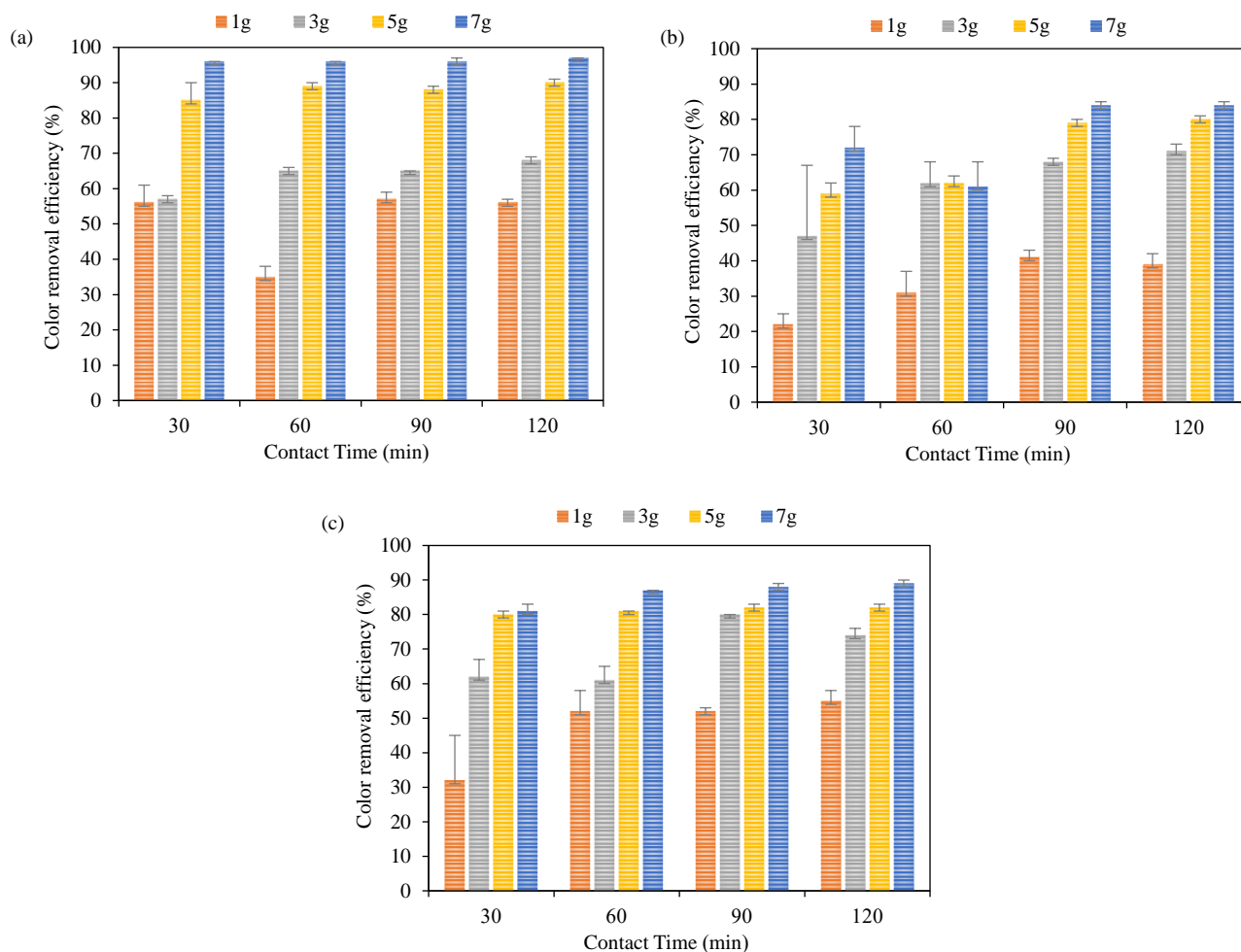
Figure 5. Color removal efficiency using eucalyptus wood chips (a); using eucalyptus bark (b); and using mixed wood (c) at activated carbon loading 1, 3, 5, and 7 grams for contact times of 30, 60, 90, and 120 min

Table 2. Characteristics of pulp and paper effluents after adsorption using wood chips AC for 120 min

Parameter	Unit	Amount of wood chips AC (g)			
		1 g	3 g	5 g	7 g
COD	(mg/L)	84-91	73-80	45-56	28-37
TSS	(mg/L)	7.6-8.2	5.8-6.6	5.6-6.4	4.6-5.4
TDS	(mg/L)	1,320-1,360	1,190-1,210	984-998	698-728
Color	ADMI (pH-Original)	158-171	117-128	35-43	10-11
	ADMI (pH-Adjust)	138-151	71-78	39-58	15-30
Conductivity	(µs/cm)	2,140-2,160	1,910-1,940	1,620-1,680	1,220-1,280

In addition, the highest color removal efficiency of 97% was obtained from wood chips loading at 7 g/100 mL for contact times of 120 min. This result was similar to that of El maguana et al. (2020) reporting that the adsorbed amount increased with contact time at the initial stage of adsorption and reached equilibrium in 120 min. Obviously, a specific period is desired for using a high amount of wood chip activated carbon. When the contact time increased to 120 min, the color removal efficiency significantly

differed from that of 30 min. The highest color removal efficiency of 84% was observed when using 7 g/100 mL of bark-activated carbon as an adsorbent for 90 min. However, the highest color removal efficiency of about 89% was achieved using 7 g of mixed wood for 120 min as shown in Figures 5(a), 5(b), and 5(c). The effluent after adsorption had characteristics within the effluent standard of color according to the regulation of the Ministry of Industry. Freundlich isotherms were supposed to be

satisfactorily fitted to these experimental data for the best condition of wood chip AC because of high correlation coefficients as shown in Table 3 and Figure 6. When comparing the R^2 values, the Freundlich equation represented a better fit of equilibrium experimental data than that of the Langmuir. Therefore, the color adsorption process of the wood chip activated carbon could be described more appropriately using the Freundlich isotherm, indicating the multilayer adsorption on the heterogeneous surface (Rajahmundry et al., 2021).

When contact time increased, the ability of adsorption also increased until equilibrium was achieved. In the first period, the fast initial adsorption occurred because the concentration gradient in the solution and the surface space of the adsorbent remained plentiful. After that, the ability of adsorption reduced until equilibrium was attained because the spaces had been fully absorbed with color and other substances (Srimoon, 2016). The fixed carbon contents and pore size of activated carbon were factors influencing the color removal efficiency (Okeola et al., 2012). Moreover, TDS concentration and conductivity decreased with increasing amount of adsorbent and contact time. To predict the mechanisms of the color adsorption process on different types of eucalyptus wood activated carbon, the Freundlich isotherm model described the adsorption process with a high coefficient of determination R^2 better than the Langmuir isotherm model.

Table 3. Langmuir and Freundlich's adsorption isotherm parameters

Activated carbon	pH	Langmuir adsorption isotherm			Freundlich's adsorption isotherm		
		Q_m (mg/g)	$K_L=b$ (L/mg)	R^2	$1/n$	Kf (L/g)	R^2
Wood chips	pH original	11.86	0.070	0.4956	2.106	1.2990	0.6131
	pH adjust	14.22	0.024	0.7021	1.436	0.4976	0.8588
Bark	pH original	141.29	0.00057	0.9761	1.221	0.1801	0.9659
	pH adjust	-117.32	-0.00062	0.9721	1.009	0.0803	0.9751
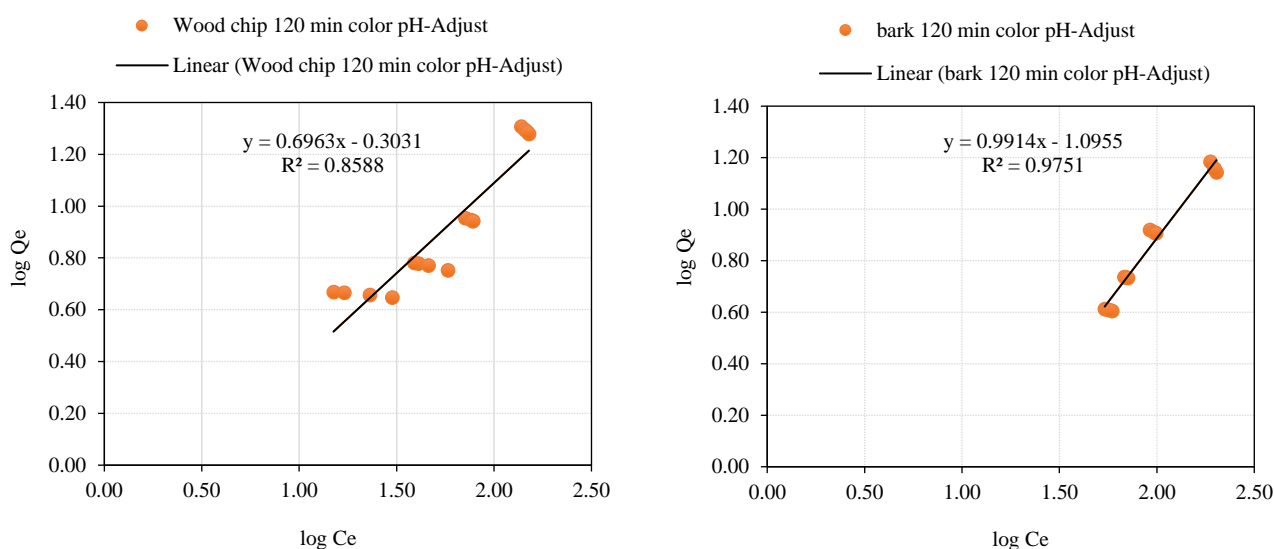
Figure 6. Freundlich isotherms of eucalyptus wood chip AC (a) and bark AC (b) for 120 min contact time

4. CONCLUSION

The use of activated carbon prepared from residual eucalyptus wood using phosphoric acid and carbonized in a furnace at 500°C for the removal of color of pulp and paper mill wastewater has been studied. The adsorption efficiency of wood chip AC was higher than bark and mixed wood due to its physical characteristics. The color removal efficiencies were slightly increased by increasing the amount of activated carbon from 1 to 7 g per 100 mL of wastewater. The adsorption process occurred rapidly on the surface of the adsorbent when using a large amount of the adsorbent because more surface area of the adsorbent was obtained. Moreover, the ability of absorbent increased with increasing contact time from 30 to 120 min. When contact time increased, the ability of adsorption also increased until equilibrium was achieved. Therefore, a shorter contact

time was sufficient when using a higher amount of adsorbent. Regarding the experimental data, the eucalyptus wood chip activated carbon gave the highest color removal efficiency due to higher fixed carbon content and nonuniform pore sizes because of tube structure variation. The activated carbon can be regenerated with appropriate methods. If the activated carbon cannot be economically regenerated, it must be treated and disposed in an approved landfill. Therefore, the economical regeneration of activated carbon and other alternative biomass substances should be studied.

ACKNOWLEDGEMENTS

REFERENCES

Ahmad AA, Hameed BH. Reduction of COD and color of dyeing effluent from a cotton textile mill by adsorption onto bamboo-based activated carbon. Journal of Hazardous Materials 2009;172:1538-43.

Ministry of Natural Resources and Environment (MNRE). Announcement of the Ministry of Natural Resources and Environment: Establishing Standards for Controlling the Drainage of Pulp and Paper Factories. Thailand: Ministry of Natural Resources and Environment; 2018. p. 13-6.

Armstrong AD, Bentley KM, Galeano SF, Olszewski RJ, Smith GA, Smith JR. The Pulp and Paper Industry. In: The Ecology of Industry. Washington, DC: National Academy Press; 1998. p. 101-41.

Azha SF, Ismail S. Feasible and economical treatment of real hand-drawn batik/textile effluent using zwitterionic adsorbent coating: Removal performance and industrial application approach. Journal of Water Process Engineering 2021; 41:Article No. 102093.

Borgesa ACP, Onwudilib JA, Andradec HMC, Alves CT, Ingram

A, Vieira de Melo SAB, et al. Catalytic supercritical water gasification of eucalyptus wood chips in a batch reactor. Journal of Fuel 2019;255:Article No. 115804.

Chooaksorn W. Color removal technology in industrial wastewater. Burapha Science Journal 2012;17:181-91.

Chuyingsakuntip S, Tangsathitkulchi C. Adsorption of natural aluminium dye complex from silk-dyeing effluent using eucalyptus wood activated carbon. American Journal of Analytical Chemistry 2013;4:379-86.

El maguana Y, Elhadiri N, Benchanaa M, Chikri R. Activated carbon for dyes removal: Modeling and understanding the adsorption process. Journal of Chemistry 2020;2020:Article No. 2096834.

El-Bestawy E, El-Sokkary I, Hussein H, Keela AFA. Pollution control in pulp and paper industrial effluents using integrated chemical-biological treatment sequences. Journal of Industrial Microbiology and Biotechnology 2008;35:1517-29.

Ferraz FM, Yuan Q. Performance of oat hulls activated carbon for COD and color removal from landfill leachate. Journal of Water Process Engineering 2020;33:Article No. 101040.

Kiatgrajai P, Laohathai B, Sangkul S. Charcoal Briquette from river red gum. Thai Journal Forestry 1994;13:38-49.

Kongsuwan A, Patnukao P, Pavasant P. Binary component sorption of Cu (II) and Pb (II) with activated carbon from *Eucalyptus camaldulensis Dehn* bark. Journal of Industrial and Engineering Chemistry 2009;15:465-70.

Kumar A, Srivastava NK, Gera P. Removal of color from pulp and paper mill wastewater-methods and techniques: A review. Journal of Environmental Management 2021;298:Article No. 113527.

Okeola O, Odebunmi E, Ameen O. Comparison of sorption capacity and surface area of activated carbon prepared from prepared from *Jatropha curcas* fruit pericarp and seed coat. Chemical Society of Ethiopia 2012;26(2):171-80.

Patnukao P, Pavasant P. Activated carbon from *Eucalyptus camaldulensis Dehn* bark using phosphoric acid activation. Journal of Bioresource Technology 2008;99:8540-43.

Pokhrel D, Viraraghavan T. Treatment of pulp and paper mill wastewater: A review. Science of the Total Environment 2004;333:37-58.

Rajahmundry GK, Garlapati C, Ponnusamy, Kumar S, Alwi RS, Vo DN. Statistical analysis of adsorption isotherm models and its appropriate selection. Chemosphere 2021;276:Article No. 130176.

Shi X, Xu C, Hu H, Tang F, Sun L. Characterization of dissolved organic matter in the secondary effluent of pulp and paper mill wastewater before and after coagulation treatment. Water Science and Technology 2016;74(6):1346-53.

Srimoon R. Dyes treatment in wastewater using adsorption processes. Khon Kaen University Science Journal 2016; 44(3):419-34.

Yadav R, Upadhyay K, Maru S. Colour removal from paper mill effluent using activated carbon. Journal of Industrial Pollution Control 2012;28(1):45-50.

This paper was selected from the Environment and Natural Resources International Conference (ENRIC 2021) which was held during 16th December 2021

Mapping Degraded Area for Tropical Peatland Revegetation Using Forest Canopy Density Model Landsat 8 OLI-TIRS in Central Kalimantan, Indonesia

Yusuf Aguswan[1*], Sulmin Gumiri[2], Raden Mas Sukarna[1], and Indrawan Permana[3]

[1]*Department of Forestry, Faculty of Agriculture, University of Palangka Raya, Kampus UPR Tunjung Nyaho, Yos Sudarso Street, Kotak Pos 2/PLKUP 73111, Palangka Raya, Central Kalimantan, Indonesia*

[2]*Department of Fisheries, Faculty of Agriculture, University of Palangka Raya, Kampus UPR Tunjung Nyaho, Yos Sudarso Street Kotak Pos 2/PLKUP 73111, Palangka Raya, Central Kalimantan, Indonesia*

[3]*Department of Architecture, Faculty of Engineering, University of Palangka Raya, Kampus UPR Tunjung Nyaho, Yos Sudarso Street, Kotak Pos 2/PLKUP 73111, Palangka Raya, Central Kalimantan, Indonesia*

ARTICLE INFO

ABSTRACT

Peatland rehabilitation in Indonesia has been massively carried out since 2016 following a huge fire event in 2015. Rehabilitation efforts have so far focused only on burned areas, although non-forested areas and areas with a limited number of juveniles must also be considered for natural regeneration. Spatial mapping can identify areas that need revegetation so that resources can be used more effectively and efficiently. This study aims to map potential areas for peatland rehabilitation by determining the distribution of tree canopy cover using the Forest Canopy Density (FCD) model from Landsat 8 OLI. The area selected for study was Ex-Mega Rice Project (MRP) area in Pulang Pisau district and Palangka Raya city, which burns almost every year. The study identifies eight areas with different levels of Forest Cover Density (FCD). Our field observation confirms that the eight different areas have different levels of natural revegetation. When forest cover is 1-30% of the FCD model, natural regeneration is insufficient and revegetation is required. This study found that 34,543.3 ha or 22.1% of the area of the MRP needs to be rehabilitated. This result provides information on which areas can be naturally revegetated and which areas need to be rehabilitated. This information is important to develop a peat restoration strategy and increase the likelihood of success.

1. INTRODUCTION

Despite covering a relatively small portion of the global land area (Andriesse, 1988; Page et al., 2011; Xu et al., 2018), peatland provides numerous benefits both for the global and local community (Usup et al., 2021). About 3.1% or 13.43 million ha of the world's peatlands are in Indonesia (Anda et al., 2021), and especially widespread on the three largest islands, namely Sumatra (5.8-7.2 million ha), Kalimantan (4.5-5.6 million ha) and Papua (about 3.8 million ha) (Anda et al., 2021; Ministry of Agriculture, 2011; Page et al., 2011; Wahyunto et al., 2005). In Kalimantan region, peatlands in Central Kalimantan Province accounted for 2,659,234 ha or 55.6% of the total peat in the island (Ministry of Agriculture, 2011).

Peatlands are a unique and fragile ecosystem. This ecosystem habitat consists of peat with depths that vary from 25 cm to more than 15 m. This ecosystem also has a distinctive richness of flora and fauna and has a high economic value. The peat swamp ecosystem also plays an important role in maintaining the climate and environmental balance, both as a reservoir of water and as a carbon storage (Daryono, 2009).

Peat forests in Central Kalimantan have been degrading as a result of logging activities, agricultural land extensification, and forest fires. In the 1980s, there were approximately 200 forest concession units (HPH) in peatland areas, with a total area reaching 13 million ha. These concession companies have the right to cut down various woods in the peat swamp forests,

and the destruction of the peat forests had begun at this time (Cattau et al., 2016). In the 1990s, there were more than 50 forest concessions exploiting peat swamp forests in Central Kalimantan. The exploitation and degradation of peat swamp areas was further exacerbated by the Mega Rice Project (MRP), which was implemented under Presidential Decree No. 82 of 1995. This project was intended to support food production by using one million hectares of peat forest in Central Kalimantan to create agricultural land (Government of Indonesia, 1995; Surahman et al., 2018). The project (PLG) then built approximately 4,533 km of drainage canals as necessary infrastructure for agriculture in the peat swamp area. The combination of forest clearing and canal construction resulted in the peatland being over-drained and prone to fire. As a result, the 2015 fire was one of the worst fires in the history of forest and land fires in Indonesia in the last 18 years. More than 2.6 million ha of forest and land burned from June to November 2015. These fires triggered dense smog and caused a national problem. Economic losses from these fires were estimated at $16.1 billion (Glauber et al., 2016). This fire event also released an estimated 800 megatons to 1.6 giga tons of carbon dioxide equivalent (Peat Restoration Agency, 2016; Glauber et al., 2016). The Indonesian government stated that 33% of the burned area in 2015 was peatland (Peat Restoration Agency, 2016).

Degraded peatlands need to be rehabilitated to restore their functions and benefits. The rehabilitation of peatlands is also critical to ensure the sustainability of ecosystem services. From an ecological perspective, peatlands provide habitat for enormous endemic species, maintain hydrological balance, and contribute to climate change mitigation. In addition to their ecological importance, peatlands also support the livelihoods and basic needs of local communities. Peatlands provide fresh water, food, medicinal plants, building materials, fuelwood, and are also a source of their culture (Cheyne and Macdonald, 2011; Wich et al., 2008). In order to restore and maintain the function of peatlands, degraded peatlands must be revegetated. Revegetation of degraded peatlands is intended to complement natural revegetation. Revegetation of degraded peatlands generally uses endemic species that adapt well to flooding and high acidity (Graham et al., 2017).

The Peat Restoration Agency (Badan Restorasi Gambut or BRG) is one of the Indonesian government agencies that has implemented revegetation programs such as (a) planting endemic and adaptive seeds on open peatlands, (b) enriching plantings in degraded peat forest areas, and (c) improving and implementing seed dispersal techniques to promote peat vegetation regeneration. The revegetation activities focused on the areas burned in 2015. The target revegetation areas were classified into three forest classes: dense, medium, and sparse. This classification was based on the 2017 land cover map, which was re-verified with Landsat and the spot image using the on-screen digitizing method.

The main obstacles to the re-vegetation of peatlands include the large area to be worked and the difficulty of access. Therefore, revegetation of degraded peatlands should be well planned to increase the probability of success, use resources efficiently, and reduce costs. Spatial mapping can help identify areas that need revegetation. In this way, allocation of resources (e.g., time, effort, and cost) can be more effective and efficient. This study aims to map degraded peatland by using the distribution of tree canopy cover from the Forest Canopy Density (FCD) model of Landsat 8 OLI to identify areas that need revegetation. This spatial mapping is further able to provide recommendations for areas that need to be revegetated, existing natural regeneration, and vegetation structure and composition in the study area.

2. METHODOLOGY
2.1 Study area
This study is located in the Ex-Mega Rice Project (MRP) area in Pulang Pisau regency and Palangka Raya city (Figure 1). The Ex-MRP area is tropical peatland that has been degraded due to deforestation, and the construction of canals that over-drain the peat and make it susceptible to fires. The study area, which is part of Pulang Pisau administration, covers an area of approximately 131,200 ha and is inhabited by communities in seven villages: Henda, Jabiren, Pilang, Sakakajang, Simpur, Tanjung Taruna, and Tumbang Nusa. On the other hand, the study area in Palangka Raya administrative area covers an area of approximately 24,500 ha, which includes eight villages: Langkai, Panarung, Bereng Bengkel, Kalampangan, Kameloh Baru, Kereng Bangkirai and Sabaru.

The research site reflects a tropical peat swamp area that is severely threatened by land conversion for agricultural purposes, construction of canals and roads, fires, and pressure from population growth. Agricultural land converted from peatlands usually

causes fires during the dry season, the effects of which are also felt in neighboring countries such as Singapore and Malaysia. The research site is a peat dome that is prone to fires. The success of revegetation at this site will have a major impact on reducing carbon emissions from agriculture, forestry, and other land use (AFOLU).

The local communities in the study area are predominantly subsistence communities that are highly dependent on natural resources and forests. Their main sources of livelihood are rubber cultivation, fishing,

artisanal mining, and collection of non-timber forest products. The peat swamp forests provide latex, building materials, honey, and livestock to meet the basic needs of the local people (Suwito et al., 2020).

2.2 Data acquisition

The basic canopy cover map was obtained from Landsat 8 OLI imagery from the United States Geological Survey (USGS) with the January 2020 Path/Row 118/62 acquisition.
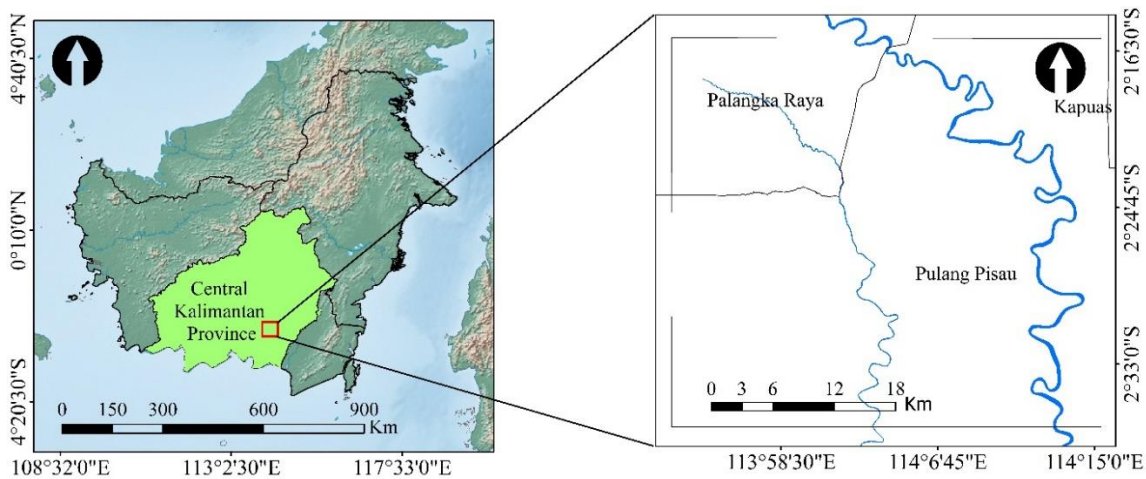
Figure 1. Map of research site in Palangka Raya City and Pulang Pisau Regency

2.3 Correction and normalization image

To obtain a better image of tree canopy cover, the basemap is then corrected to reduce spectral disturbances such as thin clouds, water, shadows, and atmospheric disturbances. The correction was performed using Forest Canopy Density Mapper V.2 software. The generated image was then processed with the Digital Earth Map of Indonesia with datum World Geodetic System (WGS) 1984 using Quantum GIS 3.16 software to improve the geometry.

2.4 Image processing in FCD

The tree canopy cover map was then analysed to differentiate the spectral data from the Landsat image using FCD models (Rikimaru, 1996; Rikimaru and Miyatake, 1997; Chandrashekhar et al., 2005; Roy et al., 1997; Sukarna et al., 2021), with the following descriptions:

- Advanced vegetation index: $AVI = ((NIR + 1) \times (256 - Red) \times (NIR\ Red))^{1/3}$
- Bare soil index: $BI = \frac{(SWIR + Red) - (NIR + Blue)}{(SWIR + Red) + (NIR + Blue)} \times 100 + 100$

- Shadow index: $SI = ((256 - Blue) \times (256 - Green) \times (256 - Green))^{1/3}$
- Temperature index: $TI \rightarrow L = (L.\min + (L.\max - L.\min))255 \times Q$

Landsat's spectral bands consist of 8 OLI/TIRS band colors comprising of Blue Band, Green Band, Red Band, Near Infra-Red (NIR) Band, Short Wave Infra-Red (SWIR) Band, L (Thermal infrared radiance), and Q is the digital number of the images.

The analysis included four indices of analysis. The advanced vegetation index (AVI) was used to calculate and evaluate changes in green vegetation density. The bare soil index (BI) was used to examine open areas. The shadow index (SI) was used to analyse forest cover conditions, and the thermal index (TI) was used to determine the differences in micro temperature in each land cover unit. Based on these four indices, the value of forest canopy density is estimated using the following equation (Rikimaru and Miyatake, 1997):

$$Forest\ Canopy\ Density\ ;\ FCD = (VD \times SSI + 1)^{1/2} - 1$$

2.5 Field survey in tropical peatland

The field survey was conducted to validate the result of the FCD analysis and to calculate the number of natural regeneration of seedlings, saplings, poles, and trees on each hectare. The field survey was conducted using the purposive sampling method. Field survey sampling was conducted for each canopy cover class generated from the Forest Canopy Density (FCD) model (8 classes). Each FCD class consisted of four graded plots with two replicates replications. A 2×2 m^2 plot was used for seedling regeneration observations, a 5×5 m^2 plot was used for sapling regeneration observations, a 10×10 m^2 plot was used for pole regeneration observations, and a 20×20 m^2 plot was used for tree regeneration observations (reference). A total of 64 plots were observed in this study, evenly distributed among eight classes of tree canopy cover in the FCD model.

2.6. Assessment of sufficiency of natural re-generation

Data obtained from field observation were analysed by calculating density (stem/hectare). Whether an area is vegetated or not is determined by assessing the sufficiency of natural regeneration. The assessment of sufficient natural regeneration was based on the standards issued by Ministry of Forestry (1994) and Wyatt-Smith and Panton (1995). The criteria for adequate natural regeneration from the two

standards are 1,000 seedlings/ha, 240 saplings/ha, 75 poles/ha and 25 young trees/ha.

2.7. Classification result test

The classification results are tested for accuracy using the confusion matrix method. Classification results are compared to existing field conditions. The confusion matrix provides data on the accuracy of the classification results in terms of overall accuracy (%), producer accuracy (%) and user accuracy (%).

3. RESULTS AND DISCUSSION
3.1 Forest Canopy Density (FCD) processing

The first process is the elimination of water disturbances and the reduction of cloud disturbances. The result of this process is images that are free of water disturbances and thin clouds. Standing water, light clouds, and thin clouds must be removed to obtain the optimal coverage class of the Landsat 8 OLI. To eliminate water and thin clouds, the threshold value is inserted into the curve. The larger the value, the more water will be removed by the software. A similar method is then used in image normalization for cloud and shadow noise. The vegetation index (RVI) and bare soil index (BI) were calculated after the process of reducing cloud, water, and shadow disturbances was complete (Figure 2). Next, the thermal index (TI) and shadow index (SI) are calculated using the FCD mapper (Figure 3).
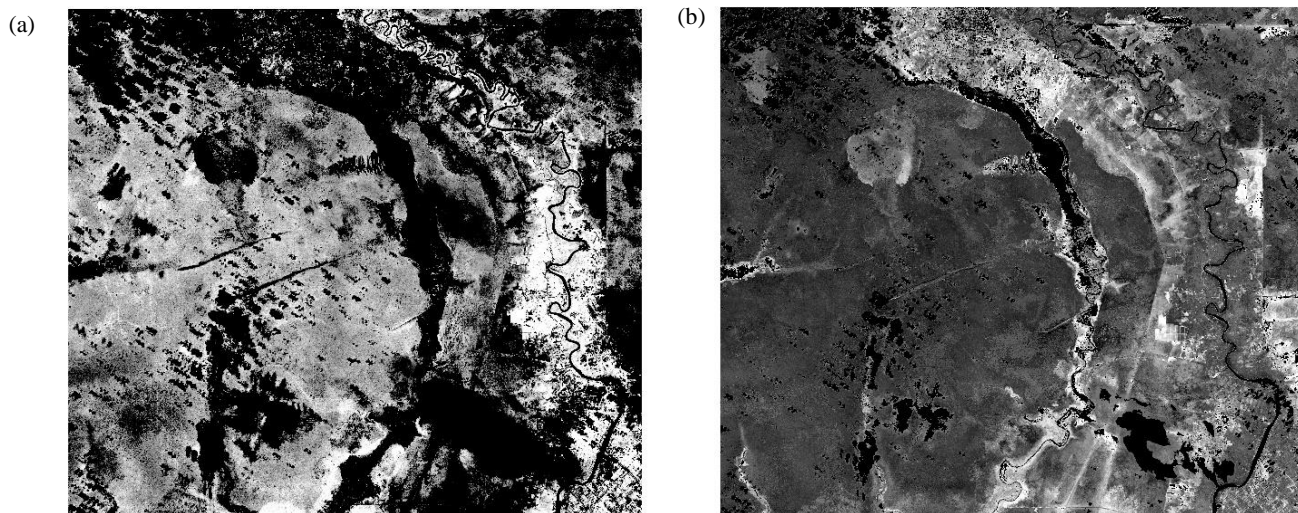

Figure 2. The results of the calculation of the vegetation index (a) and the bare soil index (b) in the Forest Canopy Density (FCD) mapper software
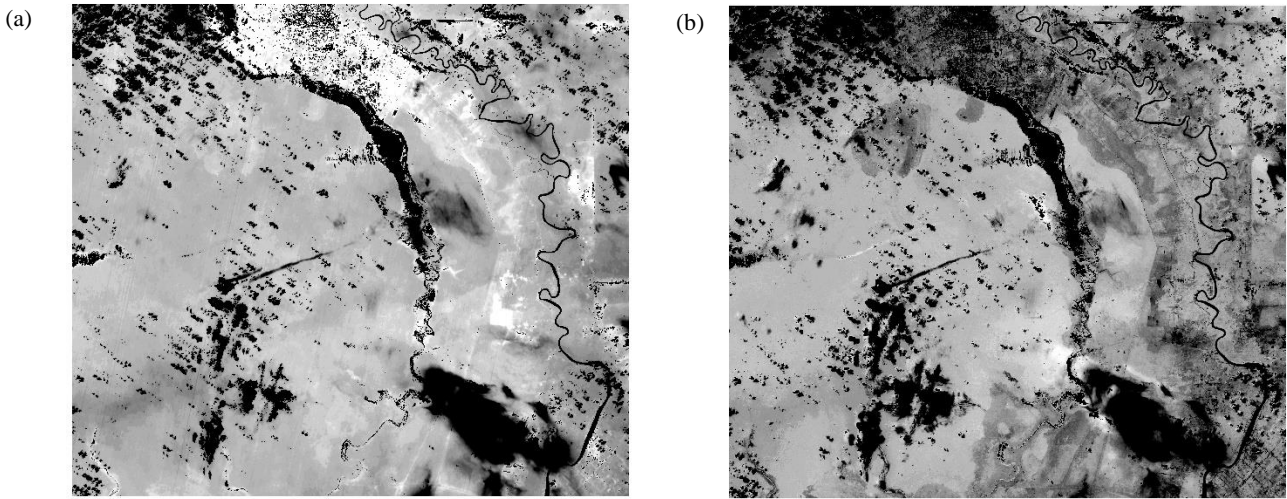
Figure 3. The results of the calculation of the thermal index (a) and the shadow index (b) in the Forest Canopy Density (FCD) mapper software

The next important process in creating canopy cover from the Forest Canopy Density (FCD) model is index integration. The first index combination is the combination of vegetation index (VI) and bare soil index (BI). The result of combining these two indices is vegetation density index (VD) (Figure 4(a)). The second index is a combination of shadow index (SI) and thermal index (TI). The combination of these two indices results in the scaled shadow index (SSI) (Figure 4(b)).

The final process in the series of creating tree canopy coverage in the Forest Canopy Density (FCD) mapper is the combination of the vegetation density index (VD) with the shadow scale index (SSI). The result of combining this index is new data called the Forest Canopy Density model/FCD model, as shown in Figure 5.
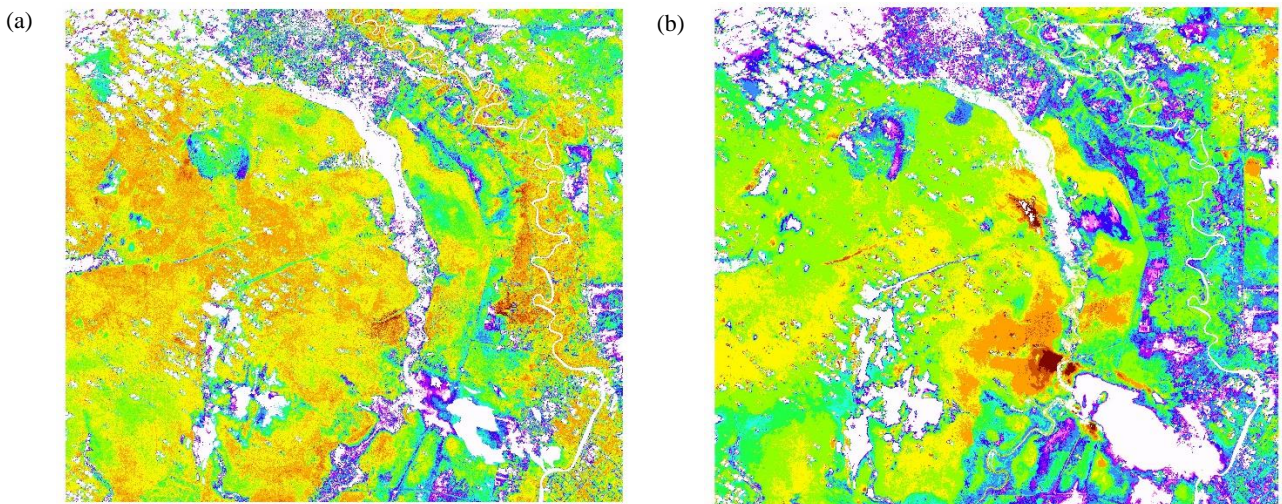
Figure 4. The vegetation density index (VD) is the result of the combination of the vegetation index (VI) and bare soil index (BI) (a) and the shadow scale index (SSI) as a result of the shadow index (SI) and thermal index (TI) (b) in Forest Canopy Density (FCD) mapper

3.2. Classification test results and field survey

The test of classification results was performed by comparing the classification results of the FCD model with the field data. The test results using the confusion matrix give an overall accuracy (89.7%), a producer accuracy (89.8%), and a user accuracy (89.9%). The FCD accuracy rate exceeds the value of 85%, which is the most acceptable standard in remote sensing research (Foody, 2008).
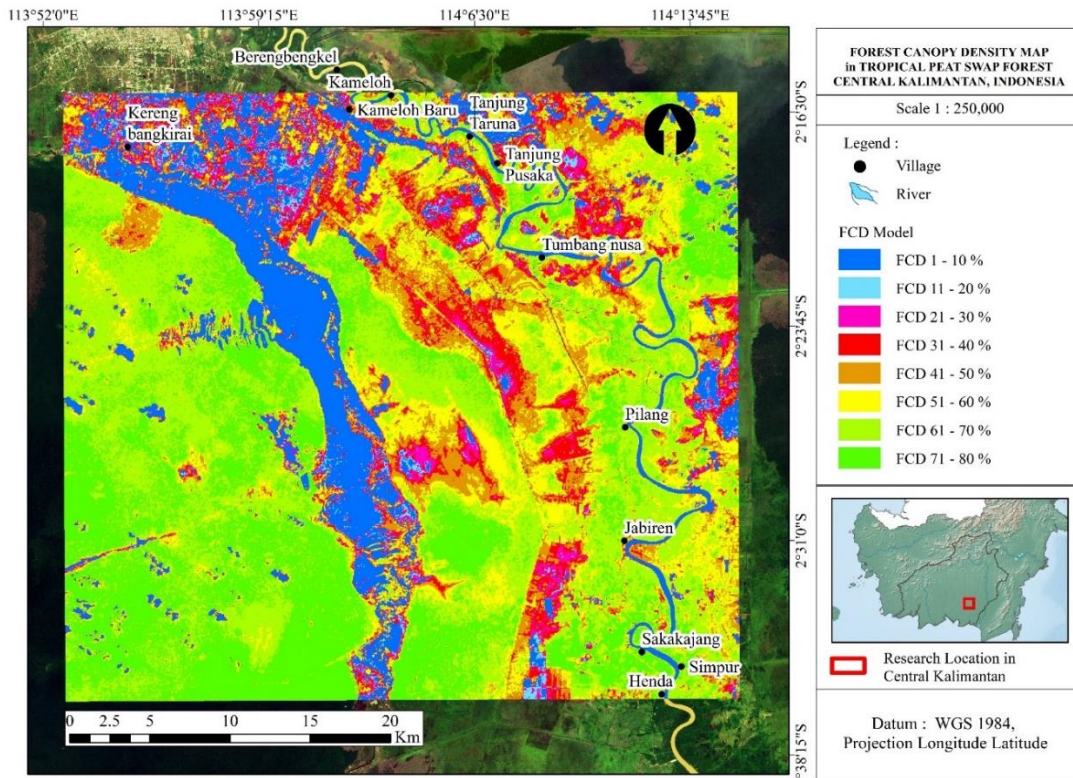
Figure 5. Forest Cover Density (FCD) class

This is consistent with Azadeh et al. (2017), Himayah et al. (2017), Mann et al. (2019), Rikimaru (1996), and Rikimaru and Miyatake (1997) who found that the Forest Canopy Density (FCD) model is very good at differentiating forest cover. FCD is also appropriate when applied with Landsat imagery and in tropical countries. The application of the revegetation space model in tropical peat swamp areas using the FCD model has only been applied to this study.

The results of the confusion matrix analysis show that the software has weaknesses in mapping forest structures in tropical peat swamps. The weakness is that whenever there is still a large puddle of peat swamp water, the software shows higher values than the facts on the ground (overestimation).

3.3. Field survey results in tropical peatland

The results of the field study on eight classes of canopy revealed three main landscapes: (a) Degraded tropical peat swamp forest; (b) Semi-degraded tropical peat swamp forest; and (c) Non-degraded tropical peat swamp forest. In general, the area is classified as non-degraded tropical peat swamp forest with an area of 68,477 ha or 44% of the study area. The field study also shows the area of degraded tropical peat swamp forest with an area of 34,543.3 ha or 22.2% of the study area (Table 1).

Degraded tropical peat swamp forests (FCD 1-30%) show that most of the areas that require revegetation are burned areas with FCD below 30%. This is consistent with the 2015 spatial study by the Ministry of Environment and Forestry (KLHK) for spatial study in 2017, 2019, and 2020, which shows that a large number of burned peat swamp areas in the study area need rehabilitation. The study area is severely degraded due to over-drainage and deforestation. Dianti et al. (2018) stated that excessive drainage is the cause of peatland water mass loss. Hirano et al. (2009) stated that loss of peat moisture in the surface layer is also a factor that can trigger fires. The loss of water in the peat due to drainage that divides the "hummock" makes the peat swamp area susceptible to fires (Hirano et al., 2009; Susilo et al., 2013).

The results of the study also show that the area required for rehabilitation spread at the area accessible by both roads and rivers/canals. This result is consistent with the findings of Rachmanadi et al. (2017) which stated that the closer the accessibility, the fewer species and vegetation density. The loss of tree species diversity is also due to logging as a result of easy accessibility to the field. The vegetation found in the study area such as Purun (*Lepironia articulata*) and Patanak (*Elaeocarpus* sp.) and various species of young trees such as Tumeh (*Combretocarpus*

rotundatus) and Geronggang (*Cratoxylon arborescens*). Dohong et al. (2017), Tonks et al. (2017), and Cattau et al. (2016) noted that degradation of peatlands in Southeast Asia occurs through deforestation, conversion to industrial plantations, drainage, and repeated fires.

Table 1. Forest canopy class based on FCD Model in study area

Symbol	FCD model	Field appearance	Landscape description	Hectare	%
	FCD 1-10%		Degraded tropical peat swamp forest. Most of this area consists of a new burn scar area. Natural revegetation from all classes (seedling, sapling, pole, and tree) is rare. Located at the area with high access such as river bank, near the village road and the canal.	24,430.7	15.7
	FCD 11-20%			3,221.9	2.1
	FCD 21-30%			6,890.7	4.4
	FCD 31-40 %		Semi degraded tropical peat swamp forest. In general, this area includes the relatively old burn scar area. Natural regeneration occurs at an early stage, so seedlings and saplings dominate. The area is easily accessible by small rivers, unused canals, or small trails.	11,628.7	7.5
	FCD 41-50%			16,517.6	10.6

Table 1. Forest canopy class based on FCD Model in study area (cont.)

Symbol	FCD model	Field appearance	Landscape description	Hectare	%
	FCD 51-60 %			24,581.2	15.8
	FCD 61-70 %		Non degraded tropical peat swamp forest the majority of this area consists of ex-logging areas. The succession process in this area almost reaches the natural state. There are no signs of burned areas. The vegetation in this area exhibits all stages of growth (seedling, sapling, pole, and tree). Natural regeneration in the form of trees and poles is abundant in this area. This type of area is located in a remote area, far from accesses or has no access.	49,182.4	31.6
	FCD 71-80 %			19,294.6	12.4
Total				155,747.8	100.0

3.4. Assessment of sufficiency of natural re-generation

The results of the field survey on 64 field measurement plots show that the FCD has insufficient natural regeneration at canopy cover levels of 1-30%. The lack of natural regeneration at the 1-30% canopy cover level of the FCD model can be seen in the regeneration of seedlings, saplings, pole and trees (Figures 6, 7, 8, and 9).

Figure 6 shows that it is difficult to find seedlings when canopy cover is 0-30%. Canopy cover 0-30% is a burned area in 2015 and 2019. Forest and bog fires eliminate almost all seeds in the study area. In the regions with canopy cover 31-40%, the number of seeds increased sharply, reaching about 12,500 stems/ha. The field survey showed that canopy cover of 41-50% was the most common canopy cover that had a sufficient number of seedlings.

Figure 7 shows that the amount of saplings in the remaining burned areas of the 2015 and 2019 fires is relatively low. Sapling density is estimated to be between 11-13 stems/ha at 0-30% of canopy cover. This sapling density is still far from the sufficient level, which is 240 stems/ha. The field survey found that stem density is highest at 41-50% canopy cover.

The absence of poles in FCD 0-30% indicates that no tree survived the large wildfire in 2015 and 2019. Tree density begins to reach sufficient level at 31-80% FCD. The field survey indicated that the most abundant tree natural regeneration is found at 51-60% FCD, which equates to 25 stems/ha. The trees in this area are more diverse compared to the other FCD level.
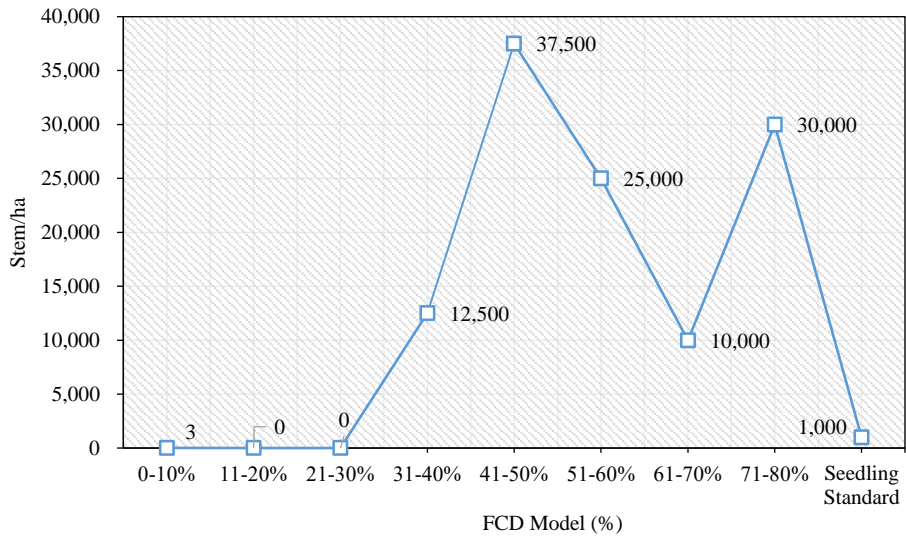
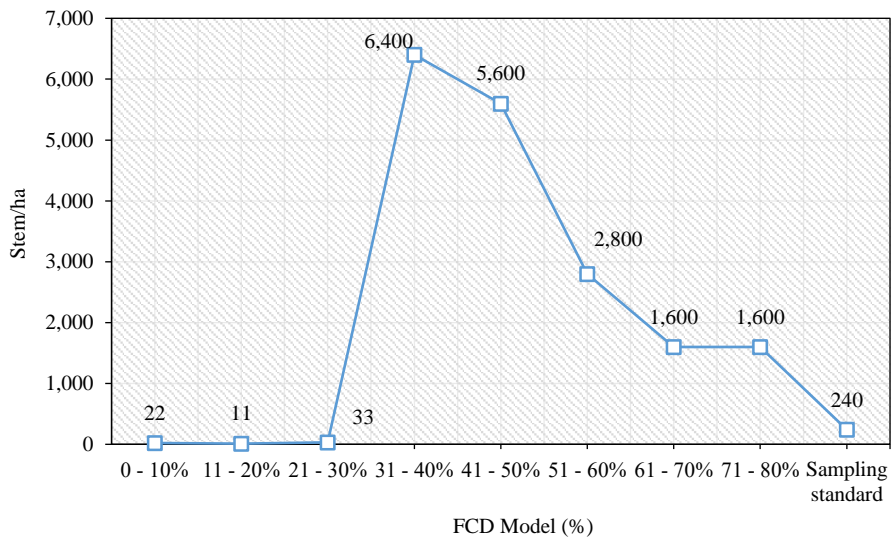**Figure 6.** Sufficiency of natural regeneration at the seedling level at the tropical peat swamp research sit

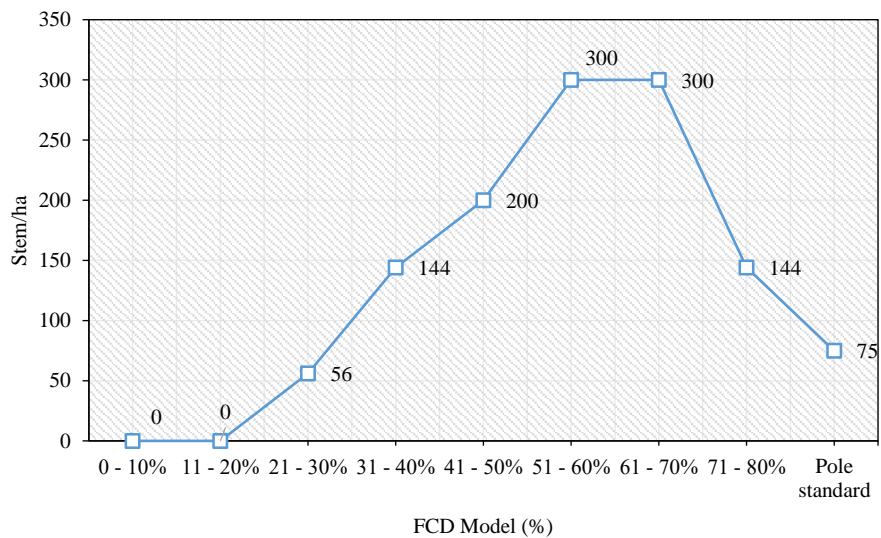**Figure 7.** Sufficient level of sapling natural regeneration at the tropical peat swamp research site

Figure 8. The density of pole in various forest cover density (FCD) in peat tropical forest
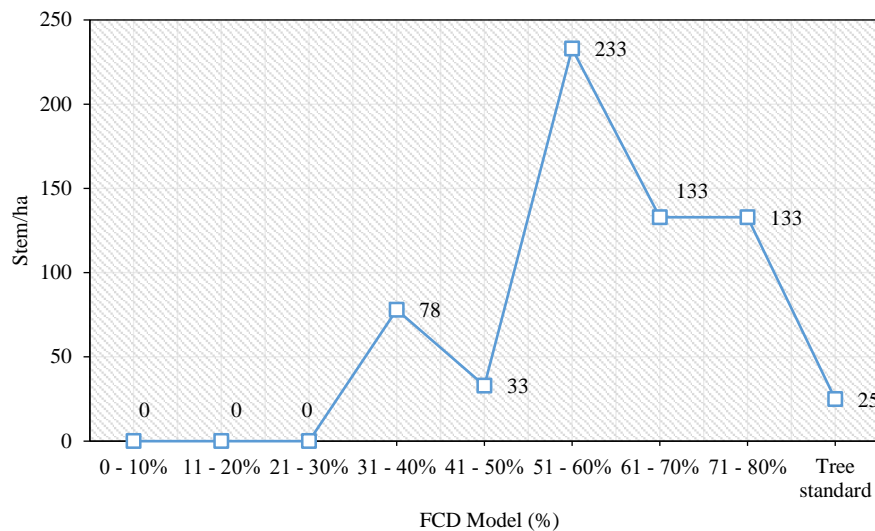
Figure 9. The density of trees in various forest cover densities (FCD) in peat tropical forest

Figure 9 shows the loss of young trees in the remaining areas burned in the 2015 and 2019 fires. Tree density begins to reach sufficient levels at FCD 31-80%. The field survey found that the highest stem density is achieved at 51-60% canopy cover. Referring to the asessment of the sufficiency of natural regeneration using the standards issued by Ministry of Forestry of Indonesia (Ministry of Forestry, 1994) and the Manual of Malayan Silviculture for Inland Forest (Wyatt-Smith and Panton, 1995), then FCD 1-30% means that the area needs to be revegetated. The field conditions in the canopy cover of FCD 1-30% show a wide and deep burned area, showing the loss of all types of growth from seedlings to young trees. Yuningsih et al. (2018) found that no tree seedlings could grow at the burn site three years after the fire.

3.5. Landscape of Revegetation Areas in Tropical Peat Swamps

From the results of the field observations, it appears that the landscape that needs to be revegetated contains areas that are often flooded for a very long period of time, even in the dry season. The flooded areas are the Klaru and Sebangau landscapes. Long-term flooded peat swamps without drainage require different revegetation techniques (Figure 10). The paludiculture technique is recommended for rehabilitation of these types of landscapes (Tata and Susmianto, 2019; Tan et al., 2020). Jessup et al. (2020) and Ramdhan and Siregar (2018) stated that a landscape approach that is carried out in a participatory manner and involves the community around the site is an appropriate approach for peatland restoration.

The results show that the frequently flooded areas for revegetation represent about 21,589.9 ha or 13.8% of the studied area. These flooded areas are generally located to the left and right of the river and in areas that have subsided after fire (Table 2). This is consistent with the findings of Ohkubo et al. (2021) and Anshari et al. (2021) that puddling and subsidence of peat soils occur after fires.

Table 2. Distribution of revegetation area according to species resistance to flooding

Symbol	Landscape description	Hectare	%
	Non degraded area	121,204.5	77.8
	Area requires revegetation with peat swamp forest vegetation	12,974.4	8.3
	Long period flooded area requires revegetation with flood resistence species	21,568.9	13.8
Total		155,747.8	100.0

4. CONCLUSION

Our spatial mapping of the ex-mega rice project identifies eight areas with different levels of FCD. Field observations revealed that these eight different areas have different levels of natural revegetation. When forest cover is 1-30% of the FCD model, natural regeneration is insufficient and revegetation is required. This study shows that 34,543 ha or 22.1%
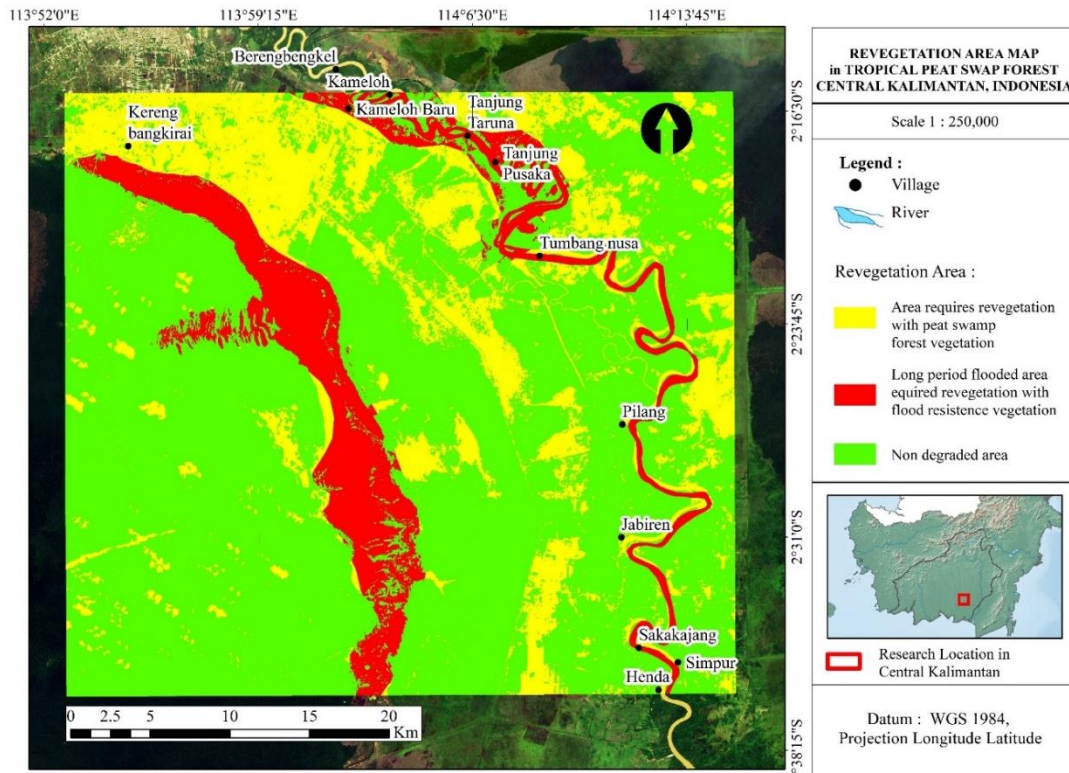
Figure 10. Spatial distribution of revegetation areas in the study locations of tropical peat swamps in Central Kalimantan by species resistance to flooded

of the area of the Ex-Mega Rice Project needs rehabilitation. The results of this survey provide information regarding the natural revegetation in the study area and which areas require rehabilitation. This information is essential to develop a peatland rehabilitation strategy and increase the likelihood of success. Tropical peat swamp areas that are always flooded during the rainy season and for several months afterward interfere with the analysis in the FCD. The water puddles cause the FCD mapper to overestimate forest structure in the prediction. To avoid this, it is better if the mapping is done with the FCD mapper using Landsat 8 OLI on the peak dry season image.

ACKNOWLEDGEMENTS

REFERENCES

Anda M, Ritung S, Suryani E, Sukarman, Hikmat M, Yatno E, et al. Revisiting tropical peatlands in Indonesia: Semi-detailed mapping, extent and depth distribution assessment. Geoderma 2021;402:Article No. 115235.

Andriesse JP. Nature and Management of Tropical Peat Soils. Rome, Italy: Soil Resources, Management and Conservation Service, FAO Land and Water Development Division; 1988.

Anshari GZ, Gusmayanti E, Novita N. The use of subsidence to estimate carbon loss from deforested and drained tropical peatlands in Indonesia. Forests 2021;12(6):Article No. 732.

Azadeh A, Dimitrios P, Peter S. Forest canopy density assessment using different approaches: Review. Journal of Forest Science 2017;63(3):107-16.

Cattau ME, Harrison ME, Shinyo I, Tungau S, Uriarte M, De Fries R. Sources of anthropogenic fire ignitions on the peat-swamp landscape in Kalimantan, Indonesia. Global Environmental Change 2016;39:205-19.

Chandrashekhar MB, Saran S, Raju PLN, Roy PS. Forest canopy density stratification: How relevant is biophysical spectral response modelling approach? Geocarto International 2005; 20(1):15-21.

Cheyne SM, Macdonald DW. Wild felid diversity and activity patterns in Sabangau peat-swamp forest, Indonesian Borneo. Oryx 2011;45(1):119-24.

Daryono H. Potentials, problems and policies required in sustainable management of forests and peat swamps. Jurnal Analisis Kebijakan Kehutanan 2009;6(2):71-101. (in Indonesian).

Dianti A, Ratnasari NG, Palamba P, Nugroho Y. Effect of rewetting on smouldering combustion of a tropical peat. E3S Web of Conferences 2018;67:Article No. 02042.

Dohong A, Aziz AA, Dargusch P. A review of the drivers of tropical peatland degradation in South-East Asia. Land Use Policy 2017;69:349-60.

Foody GM. Harshness in image classification accuracy assessment. International Journal of Remote Sensing 2008;29(11):3137-58.

Government of Indonesia. Presidential Decree No. 82/1995 Concerning Peatland Development for Food Crops

Agriculture in Central Kalimantan. Jakarta, Indonesia: Government of Indonesia; 1995. (in Indonesian).

Glauber AJ, Moyer S, Adriani M, Gunawan I, Mileva E, Harimurti P, et al. Losses from Forest Fires, Economic Impact Analysis and the 2015 Fire Crisis. Jakarta, Indonesia: Indonesia Sustainable Landscape Knowledge; 2016. (in Indonesian).

Graham LLB, Giesen W, Page SE. A common-sense approach to tropical peat swamp forest restoration in Southeast Asia. Restoration Ecology 2017;25(2):312-21.

Himayah S, Hartono H, Danoedoro P. Utilization of multitemporal Landsat 8 imagery and Forest Canopy Density (FCD) model for analysis of changes in forest canopy density in the Faculty of Geography, Gadjah Mada University, Gunung Kelud, East Java. Majalah Geografi Indonesia 2017;31(1):65-72. (in Indonesian).

Hirano T, Jauhiainen J, Inoue T, Takahashi H. Controls on the carbon balance of tropical peatlands. Ecosystems 2009; 12(6):873-87.

Jessup T, Segah H, Silvius M, Applegate G, Jagau Y. An integrated landscape approach for socially inclusive peatland restoration. Journal of Wetlands Environmental Management 2020;8(1):77-84.

Mann D, Agrawal G, Joshi PK. Spatio-temporal forest cover dynamics along road networks in the Central Himalaya. Ecological Engineering 2019;127:383-93.

Ministry of Agriculture. Peatland Map of Indonesia 1:250.000 Scale. Jakarta, Indonesia: Ministry of Agriculture; 2011. (in Indonesian).

Ministry of Forestry. Decree of the Indonesian Ministry of Forestry No. 200/Kpts-II/1994 Concerning Criteria for Unproductive Natural Production Forest. Jakarta, Indonesia: Ministry of Forestry; 1994. (in Indonesian).

Ohkubo S, Hirano T, Kusin K. Influence of fire and drainage on evapotranspiration in a degraded peat swamp forest in Central Kalimantan, Indonesia. Journal of Hydrology 2021;603: Article No. 126906.

Page SE, Rieley JO, Banks CJ. Global and regional importance of the tropical peatland carbon pool. Global Change Biology 2011;17(2):798-818.

Peat Restoration Agency. Initiating Indonesian Peat Restoration. Jakarta, Indonesia: Peat Restoration Agency (BRG); 2016. (in Indonesian).

Rachmanadi D, Faridah E, Van Der Meer PJ. Diversity of vegetation regeneration potential in peat swamp forest: A case study in a special purpose forest area (KHDTK) Tumbang Nusa, Central Kalimantan. Jurnal Ilmu Kehutanan 2017; 11(2):224-38. (in Indonesian).

Ramdhan M, Siregar ZA. Management of peat areas through empowerment of coastal village communities in the Katingan River and Mentaya River Peat Hydrological Areas, Central Kalimantan Province. Jurnal Segara 2018;4(3):145-57. (in Indonesian).

Rikimaru A. Landsat TM data processing guide for forest canopy density mapping and monitoring model. Proceedings of the ITTO Workshop on Utilization of Remote Sensing in Site Assessment and Planting of Logged-over Forest; 1996 Jul 30-Aug 1; Bangkok: Thailand; 1996.

Rikimaru A, Miyatake S. Development of forest canopy density mapping and monitoring model using indices of vegetation, bare soil and shadow. Proceedings of the 18th Asian Conference on Remote Sensing; 1997 Oct 20-24; Kuala Lumpur: Malaysia; 1997.

Roy PS, Rikimaru A, Miyatake S. Biophysical spectral response modeling approach for forest density stratification. Proceedings of the 18th Asian Conference on Remote Sensing; 1997 Oct 20-24; Kuala Lumpur: Malaysia; 1997.

Sukarna RM, Birawa C, Junaedi A. Mapping above-ground carbon stock of secondary peat swamp forest using Forest Canopy Density model Landsat 8 OLI-TIRS: A case study in Central Kalimantan Indonesia. Environment and Natural Resources Journal 2021;19(2):165-75.

Surahman A, Soni P, Shivakoti GP. Are peatland farming systems sustainable? Case study on assessing existing farming systems in the peatland of Central Kalimantan, Indonesia. Journal of Integrative Environmental Sciences 2018;15(1):1-9.

Susilo GE, Yamamoto K, Imai T. Modeling groundwater level fluctuation in the tropical peatland areas under the effect of El Nino. Procedia Environmental Sciences 2013;17:119-28.

Suwito D, Suratman, Poejirahajoe E. Peat swamp forest-firesimpacts on local livelihoods: A case study in Kapuas Kahayan Protected Forest Management Unit, Central Kalimantan, Indonesia. IOP Conference Series: Earth and Environmental Science 2020;451(1):Article No. 012097.

Tan ZD, Lupascu M, Wijedasa LS. Paludiculture as a sustainable land use alternative for tropical peatlands: A review. Science of the Total Environment 2020;753:Article No. 142111.

Tata HL, Susmianto A. The Prospect of Paludiculture in Indonesia's Peat Ecosystem. Jakarta, Indonesia: Forda; 2019. (in Indonesian).

Tonks AJ, Aplin P, Beriro DJ, Cooper H, Evers S, Vane CH, et al. Impacts of conversion of tropical peat swamp forest to oil palm plantation on peat organic chemistry, physical properties and carbon stocks. Geoderma 2017;289:36-45.

Usup A, Afentina A, Aguswan Y. Climate change mitigation through forest fire prevention and peatland rewetting programs in Central Kalimantan Indonesia. Journal of Ecological Engineering 2021;22(11):230-8.

Wahyunto, Ritung S, Suparto, Subagjo H. Distribution of Peat and Carbon Content in Sumatra and Kalimantan. Jakarta, Indonesia: Climate Change Project, Forests and Peatlands in Indonesia; 2005. (in Indonesian).

Wich SA, Meijaard E, Marshall AJ, Husson S, Ancrenaz M, Lacy RC, et al. Distribution and conservation status of the orang-utan (*Pongo* spp.) on Borneo and Sumatra: How many remain? Oryx 2008;42(03):329-39.

Wyatt-Smith J, Panton W. Manual of Malayan Silviculture for Inland Forest. Kuala Lumpur, Malaysia: Forest Research Institute; 1995.

Xu J, Morris PJ, Liu J, Holden J. PEATMAP: Refining estimates of global peatland distribution based on a meta-analysis. Catena 2018;160:134-40.

Yuningsih L, Bastoni, Yulianty T, Harbi J. Vegetation analysis on Burnt Peat Forest Land in Ogan Komering Ilir (OKI) District, South Sumatra Province. Sylva 2018;7(2):58-67. (in Indonesian).

INSTRUCTION FOR AUTHORS

Publication and Peer-reviewing processes of Environment and Natural Resources Journal

Environment and Natural Resources Journal is a peer reviewed and open access journal that is published twice a year (January-June and July-December). Manuscripts should be submitted online at https://ph02.tci-thaijo.org/ index.php/ennrj/about/submissions by registering and logging into this website. Submitted manuscripts should not have been published previously, nor be under consideration for publication elsewhere (except conference proceedings papers). A guide for authors and relevant information for the submission of manuscripts are provided in this section and also online at: https://ph02.tci-thaijo.org/index.php/ennrj/author. All manuscripts are refereed through a **double-blind peer-review** process.

Submitted manuscripts are reviewed by outside experts or editorial board members of **Environment and Natural Resources Journal**. This journal uses double-blind review, which means that both the reviewer and author identities are concealed from the reviewers, and vice versa, throughout the review process. Steps in the process are as follows:
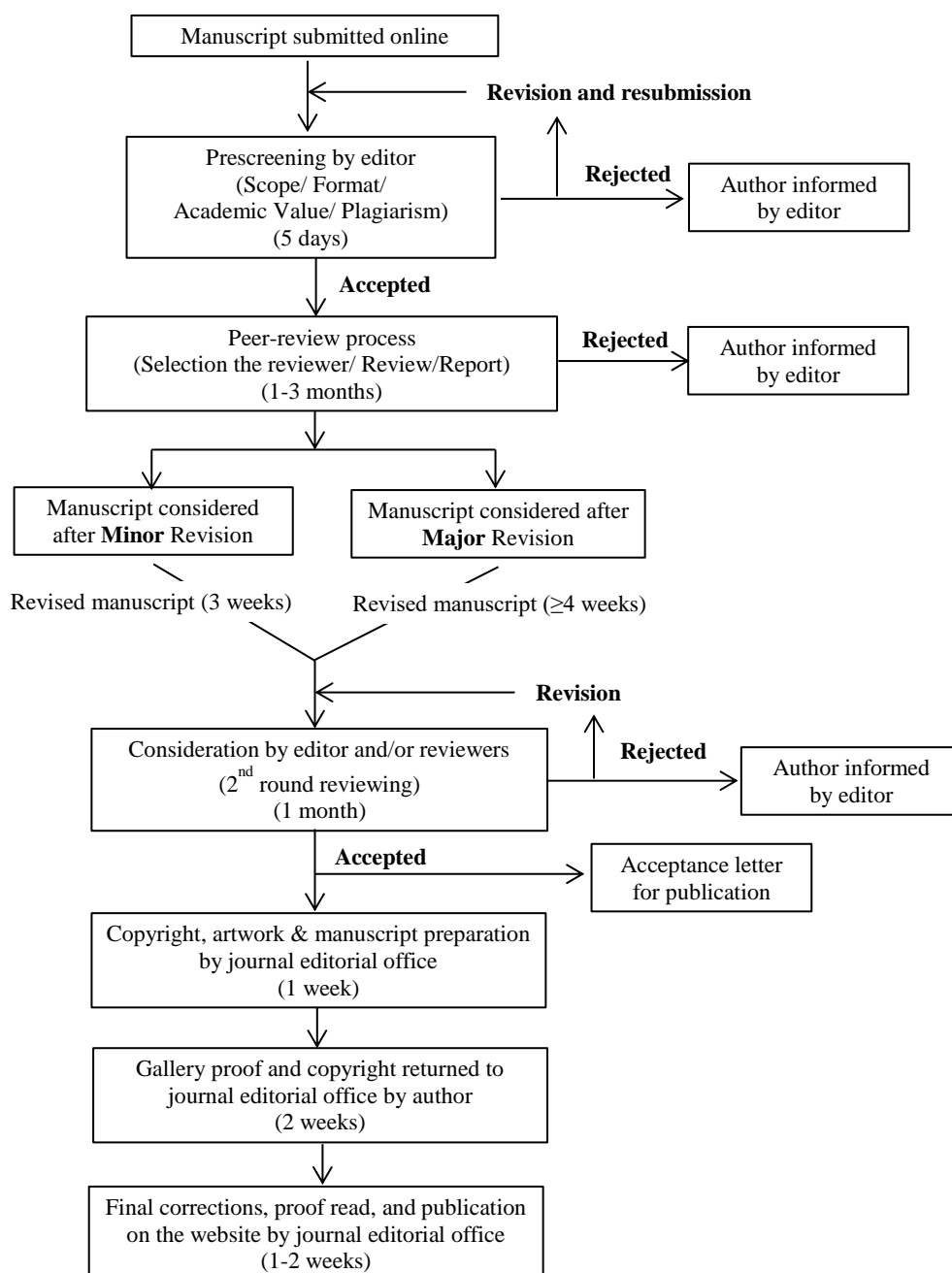
The Environment and Natural Resources Journal (EnNRJ) accepts 2 types of articles for consideration of publication as follows:

- *Original Research Article:* Manuscripts should not exceed 3,500 words (excluding references).
- *Review Article (by invitation):* This type of article focuses on the in-depth critical review of a special aspect in the environment and also provides a synthesis and critical evaluation of the state of the knowledge of the subject. Manuscripts should not exceed 6,000 words (excluding references).

Submission of Manuscript

Cover letter: Key points to include:

- Statement that your paper has not been previously published and is not currently under consideration by another journal
- Brief description of the research you are reporting in your paper, why it is important, and why you think the readers of the journal would be interested in it
- Contact information for you and any co-authors
- Confirmation that you have no competing interests to disclose

Manuscript-full: Manuscript (A4) must be submitted in Microsoft Word Files (.doc or .docx). Please make any identifying information of name(s) of the author(s), affiliation(s) of the author(s). Each affiliation should be indicated with superscripted Arabic numerals immediately after an author's name and before the appropriate address. Specify the Department/School/Faculty, University, Province/State, and Country of each affiliation.

Manuscript-anonymized: Manuscript (A4) must be submitted in Microsoft Word Files (.doc or .docx). Please remove any identifying information, such as authors' names or affiliations, from your manuscript before submission and give all information about authors at title page section.

Reviewers suggestion *(mandatory)*: Please provide the names of 3 potential reviewers with the information about their affiliations and email addresses. *The recommended reviewers should not have any conflict of interest with the authors. Each of the reviewers must come from a different affiliation and must not have the same nationality as the authors.* Please note that the editorial board retains the sole right to decide whether or not the recommended potential reviewers will be selected.

Preparation of Manuscript

Manuscript should be prepared strictly as per guidelines given below. The manuscript (A4 size page) must be submitted in Microsoft Word (.doc or .docx) with Times New Roman 12 point font and a line spacing of 1.5. *The manuscript that is not in the correct format will be returned and the corresponding author may have to resubmit.* The submitted manuscript must have the following parts:

Title should be concise and no longer than necessary. Capitalize first letters of all important words, in Times New Roman 12 point bold.

Author(s) name and affiliation must be given, especially the first and last names of all authors, in Times New Roman 11 point bold.

Affiliation of all author(s) must be given in Times New Roman 11 point italic.

Abstract should indicate the significant findings with data. A good abstract should have only one paragraph and be limited to 250 words. Do not include a table, figure or reference.

Keywords should adequately index the subject matter and up to six keywords are allowed.

Text body normally includes the following sections: 1. Introduction 2. Methodology 3. Results and Discussion 4. Conclusions 5. Acknowledgements 6. References

Reference style must be given in Vancouver style. Please follow the format of the sample references and citations as shown in this Guide below.

Unit: The use of abbreviation must be in accordance with the SI Unit.

Format and Style

Paper Margins must be 2.54 cm on the left and the right. The bottom and the top margin of each page must be 1.9 cm.

Introduction is critically important. It should include precisely the aims of the study. It should be as concise as possible with no sub headings. The significance of problem and the essential background should be given.

Methodology should be sufficiently detailed to enable the experiments to be reproduced. The techniques and methodology adopted should be supported with standard references.

Headings in Methodology section and Results and Discussion section, no more than three levels of headings should be used. Main headings should be typed (in bold letters) and secondary headings (in bold and italic letters). Third level headings should be typed in normal and no bold, for example;

2. Methodology
2.1 Sub-heading
    2.1.1 Sub-sub-heading

Results and Discussion can be either combined or separated. This section is simply to present the key points of your findings in figures and tables, and explain additional findings in the text; no interpretation of findings is required. The results section is purely descriptive.

Tables Tables look best if all the cells are not bordered; place horizontal borders only under the legend, the column headings and the bottom.

Figures should be submitted in color; make sure that they are clear and understandable. Please adjust the font size to 9-10, no bold letters needed, and the border width of the graphs must be 0.75 pt. *(Do not directly cut and paste them from MS Excel.)* Regardless of the application used, when your electronic artwork is finalized, please 'save as' or convert the images to TIFF (or JPG) and separately send them to EnNRJ. The images require a resolution of at least 300 dpi (dots per inch). If a label needed in a figure, its font must be "Times New Roman" and its size needs to be adjusted to fit the figure without borderlines.

All Figure(s) and Table(s) should be embedded in the text file.

Conclusions should include the summary of the key findings, and key take-home message. This should not be too long or repetitive, but is worth having so that your argument is not left unfinished. Importantly, don't start any new thoughts in your conclusion.

Acknowledgements should include the names of those who contributed substantially to the work described in the manuscript but do not fulfill the requirements for authorship. It should also include any sponsor or funding agency that supported the work.

References should be cited in the text by the surname of the author(s), and the year. This journal uses the author-date method of citation: the last name of the author and date of publication are inserted in the text in the appropriate place. If there are more than two authors, "et al." after the first author' name must be added. Examples: (Frits, 1976; Pandey and Shukla, 2003; Kungsuwas et al., 1996). If the author's name is part of the sentence, only the date is placed in parentheses: "Frits (1976) argued that . . ."

Please be ensured that every reference cited in the text is also present in the reference list (and vice versa).

In the list of references at the end of the manuscript, full and complete references must be given in the following style and punctuation, arranged alphabetically by first author's surname. Examples of references as listed in the References section are given below.

Book
Tyree MT, Zimmermann MH. Xylem Structure and the Ascent of Sap. Heidelberg, Germany: Springer; 2002.

Chapter in a book
Kungsuwan A, Ittipong B, Chandrkrachang S. Preservative effect of chitosan on fish products. In: Steven WF, Rao MS, Chandrkachang S, editors. Chitin and Chitosan: Environmental and Friendly and Versatile Biomaterials. Bangkok: Asian Institute of Technology; 1996. p. 193-9.

Journal article
Muenmee S, Chiemchaisri W, Chiemchaisri C. Microbial consortium involving biological methane oxidation in relation to the biodegradation of waste plastics in a solid waste disposal open dump site. International Biodeterioration and Biodegradation 2015;102:172-81.

Published in conference proceedings
Wiwattanakantang P, To-im J. Tourist satisfaction on sustainable tourism development, amphawa floating marketSamut songkhram, Thailand. Proceedings of the 1st Environment and Natural Resources International Conference; 2014 Nov 6-7; The Sukosol hotel, Bangkok: Thailand; 2014.

Ph.D./Master thesis

Shrestha MK. Relative Ungulate Abundance in a Fragmented Landscape: Implications for Tiger Conservation [dissertation]. Saint Paul, University of Minnesota; 2004.

Website

Orzel C. Wind and temperature: why doesn't windy equal hot? [Internet]. 2010 [cited 2016 Jun 20]. Available from: http://scienceblogs.com/principles/2010/08/17/wind-and-temperature-why-doesn/.

Report organization:

Intergovernmental Panel on Climate Change (IPCC). IPCC Guidelines for National Greenhouse Gas Inventories: Volume 1-5. Hayama, Japan: Institute for Global Environmental Strategies; 2006.

Remark
    * *Please be note that manuscripts should usually contain at least 15 references and some of them must be up-to-date research articles.*
    * *Please strictly check all references cited in text, they should be added in the list of references. Our Journal does not publish papers with incomplete citations.*

Changes to Authorship
This policy of journal concerns the addition, removal, or rearrangement of author names in the authorship of accepted manuscripts:

Before the accepted manuscript

For all submissions, that request of authorship change during review process should be made to the form below and sent to the Editorial Office of EnNRJ. Approval of the change during revision is at the discretion of the Editor-in-Chief. The form that the corresponding author must fill out includes: (a) the reason for the change in author list and (b) written confirmation from all authors who have been added, removed, or reordered need to confirm that they agree to the change by signing the form. Requests form submitted must be consented by corresponding author only.

After the accepted manuscript

The journal does not accept the change request in all of the addition, removal, or rearrangement of author names in the authorship. Only in exceptional circumstances will the Editor consider the addition, deletion or rearrangement of authors after the manuscript has been accepted.

Copyright transfer
The copyright to the published article is transferred to Environment and Natural Resources Journal (EnNRJ) which is organized by Faculty of Environment and Resource Studies, Mahidol University. The accepted article cannot be published until the Journal Editorial Officer has received the appropriate signed copyright transfer.

Online First Articles
The article will be published online after receipt of the corrected proofs. This is the official first publication citable with the Digital Object Identifier (DOI). After release of the printed version, the paper can also be cited by issue and page numbers. DOI may be used to cite and link to electronic documents. The DOI consists of a unique alpha-numeric character string which is assigned to a document by the publisher upon the initial electronic publication. The assigned DOI never changes.

Mahidol University

Wisdom of the Land